THE DEVELOPMENT OF A PROGRAMMABLE WAVE GENERATOR FOR THE SIMULATION OF SEA STATE

C. D. CHRISTIAN

SEPTEMBER 1973

ABSTRACT

FACULTY OF ENGINEERING AND APPLIED SCIENCE
CIVIL ENGINEERING

Doctor of Philosophy

THE DEVELOPMENT OF A PROGRAMMABLE WAVE GENERATOR FOR THE SIMULATION OF SEA STATE
by Colin Douglas Christian

A programmable wave generator suitable for the modelling of a variety of sea states was developed and used to simulate prototype and theoretical wave spectra.

Prototype wave records from different locations were analysed in order to determine the spectral form for typical coastal conditions. Different methods were used in certain cases to show how the spectral shape varied with changes in the computation process.

The wave generator, which was developed, consisted of a piston type paddle suspended from a carriage running on linear bearings. Motivation was provided by a double-acting hydraulic ram. A closed loop control circuit was employed to control the motion of the paddle. A purpose-built punched tape interface, incorporating sequencing logic and digital-to-analogue conversion, provided the command signal for the programmed waves.

The command tapes were generated on a digital computer by filtering random numbers using a fast Fourier transform method. The filter shape was determined by considering the desired spectral shape and the paddle amplitude to wave amplitude relationship predicted by small amplitude theory.

The overall performance of the system was assessed by simulating the spectra derived from the prototype records and the Moskowitz spectrum.

ACKNOWLEDGEMENTS

The Author is grateful to Mr. N. B. Webber for his advice and encouragement throughout the project. Dr. T. S. Durrani is also to be thanked for his advice on electronic matters. Many thanks are also due to Mr. R. F. Porter for his invaluable practical assistance. The Author would also like to thank his wife for her patience in typing the manuscript.

The Science Research Council are gratefully acknowledged for providing financial support for the study and the Department of Civil Engineering for providing the facilities.

CONTENTS

1. INTRODUCTION

1.1 The Problem

Increasing activity in the construction of offshore structures has highlighted the need for a better understanding of sea waves and their interaction with the structures and environment. The use of analytical methods in determining the response of even simple structures to periodic waves is not exact. Numerical methods have, in a number of cases, proved useful, but rarely account for the non-linear effects so often encountered with the problem. As a result, the physical model is still a viable design tool to solve such problems as wave overtopping, breakwater stability and structural efficiency.

This thesis is concerned with the development of suitable equipment to provide an economical method of producing a realistic model of sea waves. For a number of years, model tests have been conducted in regular waves produced by the simple harmonic motion of a wave generator, the height and period of the waves being scaled values of significant wave height and period. Even to the casual observer of a stormy sea the lack of uniformity will be evident, although in some cases (swell, for example), the approximation may be quite good. Thus, in order to achieve more realistic models, attention has been focussed upon the use of irregular waves for model testing. The difference of experimental results conducted in regular and irregular waves has been demonstrated, amongst others, by Kraai (1969).

The civil engineer is concerned with coastal waves which may be loosely defined as waves with periods between thirty seconds and two seconds occurring in water depths of less than 200 m. At this stage, it is useful to introduce the concept of a sea state as a description of wave conditions at a given time and place and to make use of the power spectral density function or spectrum as a means of describing the sea state. A coastal sea state may contain a variety of wave lengths, from shallow water to deep water waves. This complicates the modelling process and raises theoretical questions which will be dealt with later.

The problem, then, is to provide a programmable one-dimensional wave generator capable of producing a realistic sea state model of coastal waves.

1.2 Description of a "Sea State"

Before modelling any phenomena it is necessary to assign values to certain parameters in order to assess the degree of success of the simulation. In the case of sea waves, these parameters may be, say, wave height and spectral width. The choice of parameters may be critical, and in order to achieve a better understanding of prototype conditions, wave record analysis was studied in detail.

A sea state is characterised by four main physical quantities - a measure of height, length, direction and time. It is not yet feasible to resolve wave properties in terms of direction on a routine basis, and consequently, this thesis assumes that the waves are uni-directional.

The earliest method of analysing waves consisted of estimating by eye the wave heights, and timing the passing crests as a measure of period. The direction was given approximately (e.g. North-West) and the length was sometimes estimated, otherwise the period was taken as a measure of length. With the introduction of wave recording instruments (such as the Wave Staff) it was possible to produce a chart record of the waves at a single point. Thus, the wave heights could be measured directly from the record. However, this posed problems in interpreting exactly what was meant by wave height. For example, should the wave height be defined as the difference in level of a crest and preceding trough, or should an approach based on zero upcrossings be used? When the wave heights had been measured, should they be averaged and if so, should the average be the root mean square value or the average height of the highest third waves?

The introduction of sophisticated wave recorders and subsequent use of computer-orientated recording techniques has resulted in the treatment of the time history of the water surface elevation as a stochastic process. From this, the concept of describing a sea state by its power spectral density function developed. The relationship between the spectral density and wave heights (see Section 2) is important when relating tests in regular waves and those in programmed waves.

1.3 The Hardware for Wave Models

Conventionally, there are two approaches to creating a laboratory sea state which is hydraulically similar to a prototype condition. The actual mechanism of wave generation may be modelled by the use of a fan placed above the flume in such a manner as to create an artificial wind over the water surface. The wave conditions are thus limited by the fetch length and, since prototype fetches for fully arisen seas may be of the order of two hundred nautical miles, any reasonably scaled model will require a very long channel. Consequently, it is customary to use a mechanical disturbance to produce a regular wave and use the wind to provide an irregular motion.

Alternatively, the irregular profile may be produced entirely by the motion of a mechanical wave generator. The three basic types of mechanical wave generator in common use are:-

(i) piston or flap

(ii) pneumatic

(iii) plunger.

The principle of operation of these generators is different, but they all produce waves as a result of a physical disturbance to the water. Because of its simplicity and common usage, only the first type will be considered in detail. The velocities induced in the water as a result of the generating motion have a theoretical bearing on the question of similitude.

For the model to accurately predict the performance of the prototype, the two systems must be hydraulically similar. This implies

(i) geometric similarity, (ii) kinematic similarity and (iii) dynamic similarity.

Geometric similarity implies that any corresponding physical dimensions of model and prototype are in a constant ratio. Streamline patterns and velocity directions should be the same for kinematic similarity. The third criterion is usually the prime consideration. Dynamic similarity results if the force polygons at corresponding points in model and prototype are similar and in the same ratio. The criterion for dynamic similarity depends upon the type of forces which exert influence on the system. It is well known that certain dimensionless numbers must be equal in model and prototype for dynamic similarity, and that when attempting to model two or more predominant forces inconsistent scale factors are obtained from each number. The motion of water waves are generally assumed to be dominated by gravitational forces and the Froude Law is the scaling criterion. In extreme cases, other forces may be equally dominant, although in general, the results of model tests indicated that the choice of the Froude number is justified. Thus, if the model is to be hydraulically similar to the prototype, the water surface elevation and velocity distributions must be consistent with Froude Law scaling. This requirement has an important bearing on the type of wave generator used.

From the Airy theory of wave motion, the velocity distributions vary with wave length and hence, frequency. For waves in deep water (with respect to length) the motion may be approximated by circular orbits decreasing in radius rapidly with depth. The motion

in shallow waters is similar with the orbits being ellipses and decreasing in magnitude exponentially with depth. In this case, there is appreciable motion at the bed. It is, therefore, natural to design a wave generator which imparts this motion to the water particles, but despite many ingenious attempts, this does not seem feasible. The nearest approximation to this motion is achieved by the rigid flap hinged at the bed for long waves, and the piston type for shallow water waves. A double-acting paddle which may be capable of both rotational and translational motion would appear to be the best solution to the problem. However, from Biesel (1951) it may be argued that at a distance of several wave lengths from the wave generator, the waves lose any abnormal properties inherited from the generation processes.

Early experiments in the mechanical generation of water waves made use almost exclusively of simple harmonic wave forms generated by means of a connecting rod between the paddle and an eccentric fly wheel on an electric motor.

With the introduction of oil hydraulic control systems, several wave generators were built to provide irregular waves. The National Physical Laboratory (see Ewing (1962)) constructed a harmonic signal generator, which combined 16 sine waves of fixed frequencies with adjustable amplitude and phase, to control a plunger-type wave generator. Berg and Traetteberg (1969) describe a piston-type generator which is controlled by a signal from a magnetic tape recording. The signal being prepared by electronically filtering white noise to produce the desired spectrum. A double-acting flap

is described by D'Angremond and van Oorschot (1969), the rotational and translational motions being controlled by separate servocontrol mechanisms. The control signal was produced either by filtering white noise or from actual wave records by means of punch tape. A fan was also provided to generate wind waves simultaneously with the irregular waves. The Hydraulics Research Station, Wallingford, (see Annual Report 1971) have been using a plane-faced wedge which slides up and down a slope. A special digital synthesiser has been built to produce an irregular wave train and is described by Thompson and Shuttler (1972). Several similar systems have been developed in the United States, notably at the Massachusetts Institute of Technology (see Ippen and Eagleson 1964) although the trend there is to use large flumes with wind-generated waves.

All the methods mentioned have advantages and disadvantages, but all have been shown to produce realistic waves in the laboratory. The wave generator described in this thesis is an attempt to provide a simple, low-cost method of modelling sea state and to provide a versatile research tool.

2. ANALYSIS OF WAVE RECORDS

2.1 Introduction

Before building models or performing any design calculations it is necessary to be able to quantify the particular phenomena. During the 19th Century, the analysis of waves in a fluid such as water was primarily concerned with obtaining analytic solutions in classical hydrodynamic terms. It was thought that the randomness of the real sea state was beyond analytical description so that average values were assigned to wave heights, wave lengths, etc. and the classical laws applied to these. It is interesting to note that the theory of Fourier analysis existed but recording instruments were not sophisticated enough to make this a useful approach.

The interest in the statistical breakdown of waves was accelerated during the Second World War. Sverdrup and Monk (1947) introduced another average, the average of the third highest waves which was known as the significant wave height, and is still the most common method of describing a sea state. Rice (1944) in a series of papers on the analysis of random noise in communications developed a stochastic model of a time series with which he investigated the relation between power spectral density and the statistics of the noise.

Longuet-Higgins (1952) and Cartwright (1958) extended the work of Rice and presented it in terms of a wave record, enabling the averaged quantities of wave height to be related to the spectrum. Meanwhile, Deacon (1949), Klebba (1946), Birkhoff and Kotik (1952)

and Pierson and Marks (1952) had been measuring power spectra for various wave records. Following the realisation that the sea state could be described by the power spectral density function, attempts were made to determine a theoretical form for this.

Before considering the spectral and statistical analysis of it, it is pertinent to examine the average wave heights and periods mentioned so far. If the section of record shown in Fig. 2.1 is taken as an example, the definition of a wave may be approached from either the crest-to-trough method or the zero upcross method.

The former was used for visual observation and a wave is defined as the time history between two successive maxima. Associated with this is the apparent period $\tilde{T}$ and a wave height which is defined as either the average of the difference in elevation of the trough and the two maxima H^* or as the difference in elevation between the trough and the preceding crest $\hat{H}$ depending on the reference consulted. This method is illustrated in Fig. 2.1 showing six crest-to-trough waves. The zero upcross method defines a wave as the time history between two successive zero upcrossings, associated with this is the zero crossing period T_z and a wave height which is the difference in elevation between the maximum and minimum of that wave. Fig. 2.1 shows examples of zero upcross waves, noting that in this case there are only four waves. The zero crossing approach to defining waves has many advantages over the crest-to-trough method especially when used with modern wave recorders. Since significant wave heights may be measured using both methods, care should be taken to avoid ambiguity, especially

when dealing with old records or papers. A further parameter which is often used is the significant wave period, this being defined as the wave period associated with the significant wave height. However, this parameter should be treated cautiously since it is not statistically well-founded.

2.2 Theory of Spectral Analysis

The essence of the spectral analysis of sea waves is to treat the time history of the water surface elevation as a simple time series making only basic assumptions about its nature in order to analyse it. However, it is necessary to consider the general classification of any time series or stochastic process before treating specific wave records.

Time series in general may be subdivided into deterministic or random data. Deterministic data is that which has a specific value at a given time, the value being determined from a mathematical relationship. Deterministic data may be subdivided into periodic and non-periodic. Periodic data may be represented, for example, by finite Fourier expressions. Non-periodic data comprises such classes as almost-periodic and transient data.

Random data may also be subdivided, and the subdivision into which specific time histories fall determines to a large extent the ease with which they may be analysed. The two important properties utilised in this classification are stationarity and ergodicity. Stationarity implies that the time series possess properties which are invariant with respect to time. Ergodicity

implies stationarity together with properties which are independent of which sample is selected for analysis. This fact that the time history of the water surface elevation is assumed to be an ergodic stochastic process is important since it implies that the time averaged properties of the process are equal to the corresponding ensemble averages, and it is for this reason that the properties of stationary random processes may be measured properly from a single time history observed at a single point.

To illustrate this, consider a large number of time histories of water surface elevation taken at single points. If the i^{th} time history is denoted by $\eta_i(t)$ then the collection $\eta_1(t), \eta_2(t) \ldots\ldots \eta_n(t)$ is known as the 'ensemble' of time histories of the water surface elevation. At a fixed time $t = t_1$, then the values $\eta_i(t)$ have the probability distribution $p\{\eta(t_1)\}$. If the time axis may be shifted without the probability distribution changing from then the process is said to be stationary since the property is independent of t . Ideally, an infinite number of infinitely long records should be considered in the ensemble. The process is said to be 'ergodic' if for each record the probability distribution is equal to $p\{\eta(t_1)\}$. This statement implies the equivalence of time averages and ensemble averages.

In practice, in order that the water surface elevation may be regarded as ergodic, it is necessary to restrict the ensemble to a local area (a sheltered inlet will not be in the same ensemble as the open sea) and to relatively short time histories since obviously the sea state changes from day to day. In fact, both these restrictions

are viable since it is only necessary to make wave records of 15 - 20 minutes duration.

Much of the spectral analysis approach to the description of time histories is based upon the Fourier transform $F(f)$ of a time function $f(t)$. When dealing with these transforms caution is needed because there may be discrepancies between various texts over factors of 2π and the sign of the exponential.

The form of Fourier transform used in this case is:

$$F(f) = \int_{-\infty}^{\infty} f(t) \exp(-j2\pi f t)\, dt \qquad (2.1)$$

$$f(t) = \int_{-\infty}^{\infty} F(f) \exp(j2\pi f t)\, dt \qquad (2.2)$$

Much useful information may be gained by considering the complex expansions of the above equations.

$$F(f) = F_1(f) + j F_2(f) \qquad f(t) = f_1(t) + j f_2(t)$$

$$F(f) = \int_{-\infty}^{\infty} \left[f_1(t) \cos 2\pi f t + f_2(t) \sin 2\pi f t \right] dt - j \int_{-\infty}^{\infty} \left[f_1(t) \sin 2\pi f t - f_2(t) \cos 2\pi f t \right] dt \qquad (2.3)$$

$$f(t) = \int_{-\infty}^{\infty} \left[F_1(f) \cos 2\pi f t - F_2(f) \sin 2\pi f t \right] df + j \int_{-\infty}^{\infty} \left[F_1(f) \sin 2\pi f t + F_2 \cos 2\pi f t \right] df \qquad (2.4)$$

Of particular interest is the case of the real time function, from 2.4 it is obvious that for $f_2(t) = 0$ $\int_{-\infty}^{\infty} [F_1(f) \sin 2\pi ft + F_2(f) \cos 2\pi ft]\, df$ must be zero and since sine $2\pi ft$ is an odd function and cos $2\pi ft$ an even function, then $F_1(f) = F_1(-f)$, $F_2(f) = -F_2(-f)$. So for a real function $F(-f) = \overset{*}{F}(f)$ where $\overset{*}{F}(f)$ is the complex conjugate of $F(f)$.

This result is very important in both analysis and synthesis of wave records.

$F(f)$ can also be expressed as $A(f)e^{j\phi(f)}$ where $A(f)$ is the Fourier spectrum of $f(t)$ and $\phi(f)$ its phase angle. Now the energy spectrum of $f(t)$ is $A^2(f)$. This last fact is a consequence of Parseval's theorum.

$$\int_{-\infty}^{\infty} |f(t)|^2 \, dt = \int_{-\infty}^{\infty} A^2(f)\, d(f) \qquad (2.5)$$

The left-hand of the above equation is proportional to the total energy in the process. Also of significance is the result of the convolution theorum.

$$\int_{-\infty}^{\infty} f(t)\, e(t-\tau)\, d\tau \longleftrightarrow F(f) \cdot E(f)$$

If $e(t) = f(t)$ the convolution theorum may be written as

$$\int_{-\infty}^{\infty} f(t)\, f(t-\tau)\, d\tau \longleftrightarrow F(f)^2 \qquad (2.6)$$

Equations 2.5 and 2.6 prompt the introduction of the Power Spectral Density Function (PSD function) and a discussion of its physical meaning and mathematical derivation. The PSD function,

otherwise known as the "spectrum", "power spectrum" or "energy spectrum", is defined as the amount of statistical variance per increment of frequency. Thus, the area under the power spectral density function is proportional to the total energy of the phenomena.

Now consider the energy in a wave as defined by Airy theory as being equal to $\rho g H^2 L/8$ for unit width of crest per wave. Thus, for unit surface area this is $\rho g H^2/8$ or $\rho g \sigma^2$ for the assumed sine wave component. Now σ^2 is the time averaged mean square of the zero mean process $x(t)$

$$\sigma^2 = \lim_{T\to\infty} \frac{1}{T} \int_{-T/2}^{T/2} x^2(t)\, dt \qquad (2.7)$$

Now if we define a PSD $G(f)$ such that

$$\sigma^2 = \int_{-\infty}^{\infty} G(f)\, df \qquad (2.8)$$

$G(f)$ is a two-sided power spectral density function and as such has finite values for negative frequency. This is useful when deriving theoretical relationships but it poses problems when trying to interpret such spectra in a physically meaningful way. In presenting wave spectra a one-sided PSD $S(f)$ will be defined such that

$$\sigma^2 = \int_{0}^{\infty} S(f)\, df \qquad (2.9)$$

A rigourous mathematical definition of the power spectral density function is:

$$S(f) = \lim_{\Delta f \to 0} \lim_{T \to \infty} \frac{1}{\Delta f T} \int_0^T x^2(t, f, \Delta f)\, dt \qquad (2.10)$$

where $x(t, f, \Delta f)$ is the portion of $x(t)$ in the frequency range f, to $f + \Delta f$.

Equations 2.5 and 2.6 are the key to the estimation of power spectra since σ^2 is simply the time average of the left-hand side of Equation 2.5. Thus the PSD may be computed as a time average of the square of the Fourier spectrum. An alternative method is shown by Equation 2.6 since the left-hand side, if taken as a time average, is the auto-correlation function. Thus, another method of computing the PSD is to Fourier transform the autocorrelation function. The autocorrelation function is difficult to interpret physically but can provide useful information about the nature of the phenomena.

The implementation of the above equations will be treated later. Having determined the power spectral density function it is possible to compute two important properties. Firstly, the spectral width defined by Longuet-Higgins (1958) as:

$$\varepsilon^2 = \frac{m_0 m_4 - m_2^2}{m_0 m_4} \qquad (2.11)$$

where $m_n = \int_0^\infty S(f) f^n\, df$

Secondly, the peakedness of the spectrum Q_p is

$$Q_p = \frac{2\int_0^\infty f\, S^2(f)\, df}{\left[\int_0^\infty S(f)\, df\right]^2} \qquad (2.12)$$

This is similar to that described by Goda (1970) but not the same as that used by Tucker (1963).

The computation of the power spectral density function is discussed in detail in Appendix 2.

2.3 Statistical Analysis of Wave Records

In addition to the spectral decomposition of a wave train it is also of importance to be able to determine statistical properties of the water surface, wave heights etc. Wave heights and periods are the most important features of a sea state to a practicing engineer faced with a design problem, since much of the present design approaches are based upon significant wave heights and periods.

The random nature of ocean waves are usually examined by assuming that the time series given by the surface elevation at a given point in space may be represented by a stationary Gaussian process. The surface elevation is, over a long period of time, assumed to follow the distribution:

$$p(\eta) = \frac{1}{\sqrt{2\pi}\,\sigma} \exp\left[-\eta^2/2\sigma^2\right] \qquad (2.13)$$

where σ^2 is the variance of $\eta(t)$ and the mean value of $\eta(t)$ (the still water level) is taken as zero.

The moments of any probability distribution are a fundamental property of that distribution. The n^{th} moment about the origin is defined as:

$$\mu_n = \int_{-\infty}^{\infty} p(\eta)\,\eta^n\,d\eta \qquad (2.14)$$

The $zero^{th}$ moment by definition is unity and the first moment is the mean. The central moments are defined:

$$\mu_n' = \int_{-\infty}^{\infty} p(\eta)\,(\eta-\mu_1)^n\,d\eta \qquad (2.15)$$

The $zero^{th}$ central moment is unity, the second moment is the variance. Two useful ratios of these moments are the skewness and kurtosis. The skewness of a probability distribution is defined as:

$$\beta_1 = \mu_3'/\sigma^3$$

and the kurtosis as:

$$\beta_2 = \mu_4'/\sigma^4$$

The kurtosis is a measure of the clipping of a signal and the skewness describes the deviation of a probability distribution away from the Gaussian.

For a Gaussian process the following values are characteristic:

$\mu_0 = 1$ $\qquad$ $\mu_1 =$ mean value

$\mu_2' = \sigma^2$ $\qquad$ $\beta_1 = 0.0$

$\beta_2 = 3.0$

And for a sinewave of amplitude a

$$\mu_0 = 1 \qquad \mu_1 = 0.0$$

$$\mu_2' = a^2/2 \qquad \beta_1 = 0.0$$

$$\beta_2 = 1.5$$

The Gaussian distribution of surface elevation is an approximation and Kinsman (1964) has reported a skewness of between 0.045 and 0.168, and the Chi-square test also fails to support the fitness of the Gaussian assumption.

The deviation from the Guassian is, however, not great and histograms of sampled surface elevations are close to that described by Equation 2.13.

In considering the spectral analysis of the record no form of equation was assumed for the surface elevation. However, in order to examine the statistical properties it is necessary to write $\eta(t)$ explicitly. If the Gaussian distribution is assumed then the waves can be thought of as a sum of an infinite number of wavelets with infinitesimal amplitudes and random phases. Thus,

$$\eta(t) = \sum_{n=1}^{\infty} a_n \cos(2\pi f_n t + \phi_n) \qquad (2.16)$$

where a_n is the amplitude of the n^{th} wave, f_n the frequency, and ϕ_n the phase. The amplitude a_n is related to the one-sided power spectral density by

$$\sum_{f}^{f+\delta f} \frac{a_n^2}{2} = S(f)\,df \qquad (2.17)$$

Hence, the surface elevation may be represented by a pseudo integral.

$$\eta(t) = \sqrt{2} \int_0^\infty \sqrt{S(f)\,df}\, \cos(2\pi f_n t + \phi_n) \qquad (2.18)$$

The variance can then be obtained as:

$$\sigma^2 = \frac{1}{T}\int_0^T \eta^2(t)\,dt = \int_0^\infty S(f)\,df \qquad (2.19)$$

Using this type of simulation for the surface elevation the statistics have been examined by several authors, notably Longuet-Higgins (1952) and Cartwright and Longuet-Higgins (1959) and Putz (1953). Whilst others, such as Pierson (1955), Goda (1970) and Wiegel (1965) have summarised these results and extended their interpretation.

Longuet-Higgins (1952) firstly, by considering a wave composed of two sine waves with almost identical frequencies super-imposed on each other, and then by use of a narrow band spectrum, examined the statistical distribution of the heights of sea waves. He showed that for this case the distribution of wave peaks η_{max} was a Rayleigh distribution.

$$p(\eta_{max})\,d\eta_{max} = \frac{\eta_{max}}{\sigma^2} \exp\left[-\frac{\eta_{max}^2}{2\sigma^2}\right] d\eta_{max} \qquad (2.20)$$

The mean value of η_{max} is obtained from the above

$$\bar{\eta}_{max} = \int_{-\infty}^{\infty} \eta_{max}\, p(\eta_{max})\,d\eta_{max} = \sqrt{\frac{\pi}{2}}\,\sigma \qquad (2.21)$$

In this case of a narrow band spectrum the wave height is twice the maximum surface elevation $H=2\zeta_{max}$. A distribution of wave heights may be defined thus:

$$p(H)\,dH = \frac{1}{4}\frac{H}{\sigma^2}\exp\left[-\frac{H^2}{8\sigma^2}\right]dH \qquad (2.22)$$

Using the mean wave height we may write

$$p(H)\,dH = \frac{\pi}{2}\left(\frac{H}{\bar{H}}\right)\exp\left[-\frac{\pi}{4}\left(\frac{H}{\bar{H}}\right)^2\right]d\left(\frac{H}{\bar{H}}\right) \qquad (2.23)$$

Longuet-Higgins calculated the mean value a^r of those a's that are greater than r by:

$$\frac{a^r}{\bar{a}} = \frac{r}{\bar{a}} + \exp\left(\frac{r^2}{\bar{a}^2}\right)\int_r^\infty e^{-r^2/\bar{a}^2}\,\frac{dr}{\bar{a}} \qquad (2.24)$$

where r is defined by $p(r)\,dr = e^{-r^2/\bar{a}^2}$

The results of this give $H_{1/10} = 5.09$

$H_{1/3} = 4.004$ $\qquad H_{1/3} = 1.415\,H_{rms}$

The expected value of the maximum wave height in a sample of N waves also results from this analysis and is given by

$$\frac{\bar{H}_{max}}{2\sigma} = \sqrt{2\ln N} + \frac{\gamma}{2\ln N} + O\left[(\ln N)^{-3/2}\right] \qquad (2.25)$$

$$\gamma = 0.5772$$

Goda (1970) uses expression 2.24 to obtain a few more interesting relationships.

The mode or most frequent value is given by $H_{mode} = 2\sigma$

The root mean square wave height is given by $H_{rms} = 2.828\,\sigma$

The standard deviation of the wave height from the mean wave height is:

$$\sigma(H) = \sqrt{H_{rms}^2 - \bar{H}^2} = 1.309\,\sigma \qquad (2.26)$$

Thus, by use of these expressions it is possible to work in wave height or amplitude and relate the two for a narrow spectrum.

Wave periods were assumed by Bretschneider (1959) to follow a Rayleigh distribution, or rather the square of the wave period did.

$$p(T)\,dT = 2.7\,\frac{T^3}{\bar{T}^4}\,\exp\left[-0.675\left(\frac{T}{\bar{T}}\right)^4\right]dt \qquad (2.27)$$

The standard deviation away from the mean is thus:

$$\sigma(T) = 0.281\,\bar{T} \qquad (2.28)$$

The distribution of η_{max} for waves with a broad frequency spectrum has been investigated by Cartwright and Longuet-Higgins (1956). An expression for the statistical distribution of η_{max} was derived as:

$$p(x) = \frac{1}{\sqrt{2\pi}}\left[\varepsilon\,\exp\left[\frac{-x^2}{2\varepsilon^2}\right] + \sqrt{1-\varepsilon^2}\,x\exp\left[\frac{-x^2}{2}\right] \times \int_{-\infty}^{x\sqrt{1-\varepsilon^2}/\varepsilon} \exp\left[-\frac{t^2}{2}\right] dt\right] \qquad (2.29)$$

$$x = \eta_{max}/\sigma$$

The so-called spectral width parameter ε varies between 0 and 1. For the limiting cases:

(a) $\varepsilon \longrightarrow 0$ An infinitely narrow spectrum results

$$p(x) = x \exp\left[-x^2/2\right], \quad x \geq 0$$

$$= 0, \quad x < 0$$

This is the Rayleigh distribution.

(b) $\varepsilon \longrightarrow 1$

$$p(x) = \frac{1}{\sqrt{2\pi}} \exp\left[-\frac{x^2}{2}\right]$$

which is recognisable as a Gaussian or Normal distribution.

In the latter case maxima occur above and below the mean with equal frequency. The intermediate values of ε lead to probabilities as shown in Fig. 3.2. The mean and standard deviation of the variable x were calculated as functions of ε.

$$\bar{x} = \sqrt{\frac{\pi}{2}(1-\varepsilon^2)} \tag{2.30}$$

$$\sigma_x = \sqrt{1-\left(\frac{\pi}{2}-1\right)(1-\varepsilon^2)} \tag{2.31}$$

These, together with the third moment are shown in Fig. 2.3.

The cumulative probability $q(x)$ of x exceeding a given value is given by:

$$q(x) = \int_x^\infty p(x)\,dx \tag{2.32}$$

and this is found to be (substituting from 2.29)

$$q(x) = \frac{1}{\sqrt{2\pi}} \left\{ \int_{x/\varepsilon}^{0} e^{-t^2/2}\,dt + (1-\varepsilon^2)^{1/2} e^{-x^2/2} \times \int_{-\infty}^{x\sqrt{1-\varepsilon^2}/\varepsilon} e^{-t^2/2}\,dt \right. \tag{2.33}$$

when $\varepsilon \longrightarrow 0$ $\quad q(x) = 1 \quad , \quad x \leq 0$

$$= e^{-\frac{x^2}{2}} \quad , \quad x \geq 0$$

and when $\varepsilon \longrightarrow 1$

$$q(x) = \frac{1}{\sqrt{2\pi}} \int_x^\infty e^{-t^2/2} \, dt$$

These results lead to the examination of the highest $1/n^{th}$ waves. The highest $1/n^{th}$ maxima correspond to those values of x greater than x' say, where:

$$q(x') = \int_{\eta'}^\infty p(\eta) \, d\eta = \frac{1}{n} \tag{2.34}$$

Hence, $x^{1/n}$ the average value of x for these maxima:

$$x^{1/n} = n \int_{x'}^\infty p(x) \, dx \tag{2.35}$$

Common values of n have been used in plotting this function in Fig. 2.4.

The parameter ε which governs the distribution of maxima of the surface elevation may be calculated from the spectral moments or it may be estimated from the numbers of maxima and zero upcrossings.

According to Rice (1944) the number of maxima N_c and that of zero upcrossings N_z in the record with a duration of T_R are given by: $N_c = \sqrt{m_4/m_2}\, T_R \qquad N_z = \sqrt{m_2/m_0}\, T_R$

Hence,

$$\varepsilon = \sqrt{1 - \left(\frac{N_z}{N_c}\right)^2} \tag{2.36}$$

The proportion of negative maxima r is given by:

$$r = \frac{1}{2}\left[1 - (1 - \varepsilon^2)^{1/2}\right] \qquad (2.37)$$

ε may also be obtained from the statistical moments (defined by Equations 2.14 and 2.15) and is given by:

$$\varepsilon^2 = \frac{\pi - 4\rho}{\pi - 2\rho}$$

where

$$\rho = \frac{(\mu_1')^2}{\mu_0' \mu_2'}$$

The above analysis and results refer to wave amplitude and not to crest-to-trough wave height which is more readily understood by the practicing engineer. The distribution of crest-to-trough height is not readily obtained, but for small values of ε the Rayleigh distribution is a good approximation.

2.4 Presentation of Wave Data

Many of these statistical parameters are considered to be theoretically redundant if the power spectral density function has been calculated. For example, theoretical values of zero crossing period and peak distribution may be derived from a knowledge of the spectral width. In addition, if the spectral width is zero then the theoretical relationships between $H_{1/10}$, H_s , H_{mode} etc. and the variance become valid, thus eliminating much time-consuming computation. However, the above relationships are based upon a normal distribution for the surface elevation which may

not always be the case, but it turns out that in practice, the relationships are good approximations, even in the case of the wave height averages for spectra with ε greater than zero.

From the results obtained previously it appears that by calculating the power spectral density function, many of the required statistical properties may be gleaned from it. Draper (1966 and 1963) and Tucker (1963) make use of the theoretical work of Longuet-Higgins and others to estimate the statistical characteristics of a wave record from a few simple measurements. Although this method was designed primarily with chart records in mind, it is also a useful method for presenting wave data from other sources.

The theoretical basis is largely that developed by Tucker (1963). Previous methods have used crest-to-trough wave heights of individual waves, apparent period of highest waves, or some other average period of an arbitrary group of waves when describing a wave system. Difficulties arise in these methods because of the necessity to decide upon which short period waves to ignore. Differences in wave recorders accentuate these difficulties because of the various degrees at wave attenuation.

The National Institute of Oceanography has approached the wave height definition problem by taking the height of the largest wave as being the sum of the highest crest (A) and the lowest trough (C) from the mean. Goda (1970) defines his individual waves by the zero up-cross method which is consistent with this approach. This maximum wave height is denoted by H_1 and it is assumed that

the record has been corrected for recorder errors. The zero crossing period T_z is then determined as follows. For a given length of record the zero up and down crossings are counted and this figure is halved to give the number of zero upcrossings N_z . The zero crossing period is then given by the record length divided by The mean crest period T_c is then calculated in a similar manner and from Equation 2.36 the spectral width ε may be obtained.

$$\varepsilon^2 = 1 - \left(\frac{T_c}{T_z}\right)^2 \qquad (2.38)$$

Tucker (1963) derived an expression for H_1 in terms of N_z and D_{rms} the root mean square of the surface elevation as:

$$H_1 = D_{rms} 2(2\Theta)^{\frac{1}{2}}(1 + 0.289\Theta^{-1} - 0.247\Theta^{-2}) \qquad (2.39)$$

where $\Theta = \ln N_z$

Thus, by observing the maximum wave height and the number of zero crossings, the variance and, hence $H_{1/10}$, $H_{1/3}$ etc. may be estimated. All that is missing, in fact, is a knowledge of the frequency components present in the wave record. A cross-check may be performed since a similar analysis had been made for the second highest wave and N_z .

The data produced by analysing many records in the above manner may be presented conveniently in the manner used by the National Institute of Oceanography, which is briefly as follows.

Wave height is presented as a percentage excedance per unit wave height interval. This usually shows the significant wave height and the most probable value of the highest wave in a specific interval of time.

The zero crossing period and spectral width parameter are conventionally plotted as histograms. Significant wave height is related to zero crossing period by means of a scatter diagram. Lines of constant steepness are included on these to indicate the severity of the conditions. The cumulative persistence diagram is useful when planning projects and gives the duration of a particular significant wave height. Thus, the wave climate of an area derived from a large number of records may be presented by five diagrams, in a manner readily understood by the practising engineer. However, the error in these diagrams depends upon the range of frequencies in the spectrum. Very little information can be obtained from ϵ and T_z about the spectrum without actually calculating it. However, it is very much easier to assimilate mentally half-a-dozen diagrams than a large number of power spectral density plots. For specific investigation, by means of model studies for example, the spectral representation may reveal vital information concerning the response of a structure to frequencies which would be overlooked by merely considering the aforementioned diagrams.

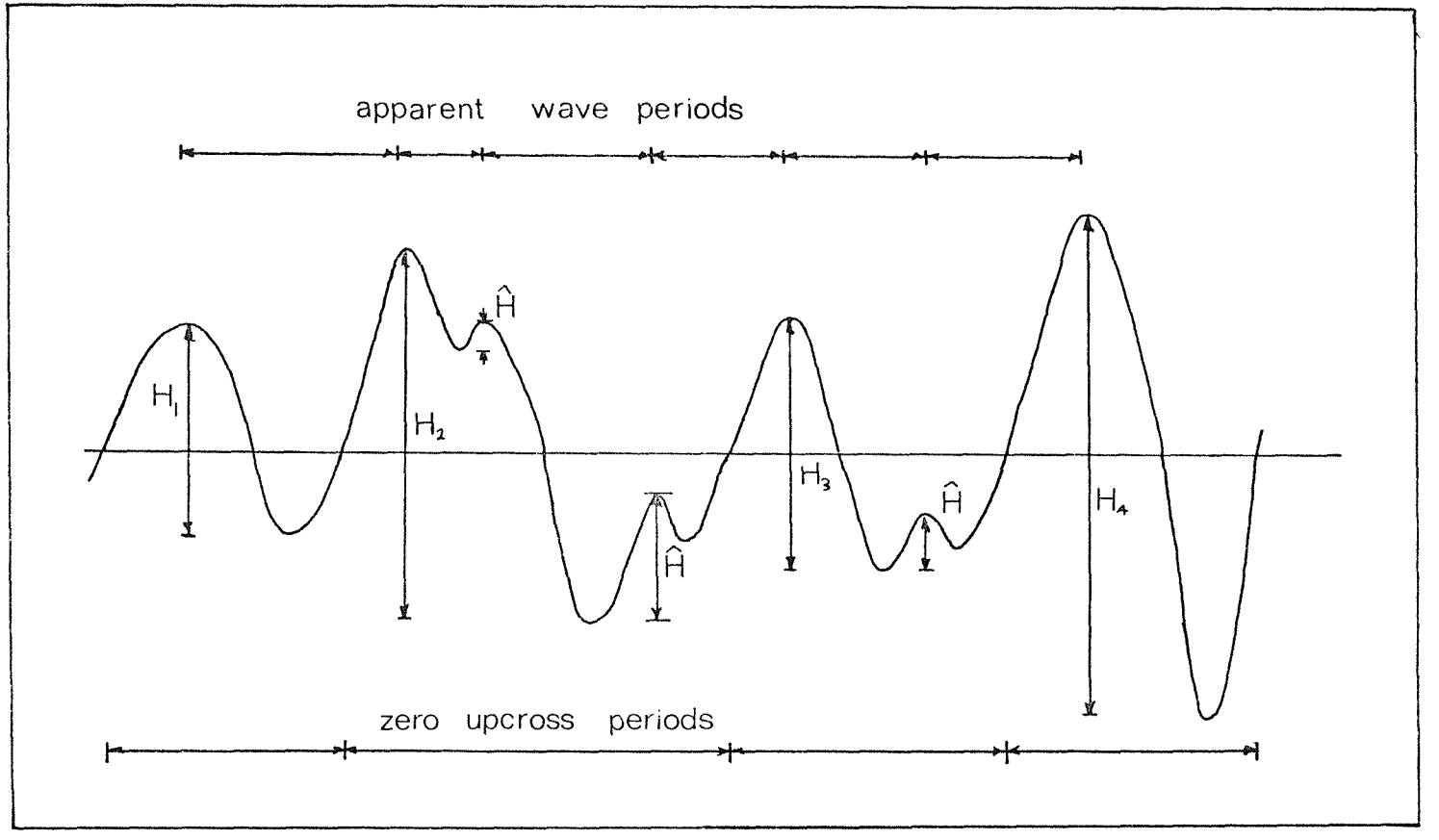

FIG. 2.1 Definition of Wave Heights and Periods

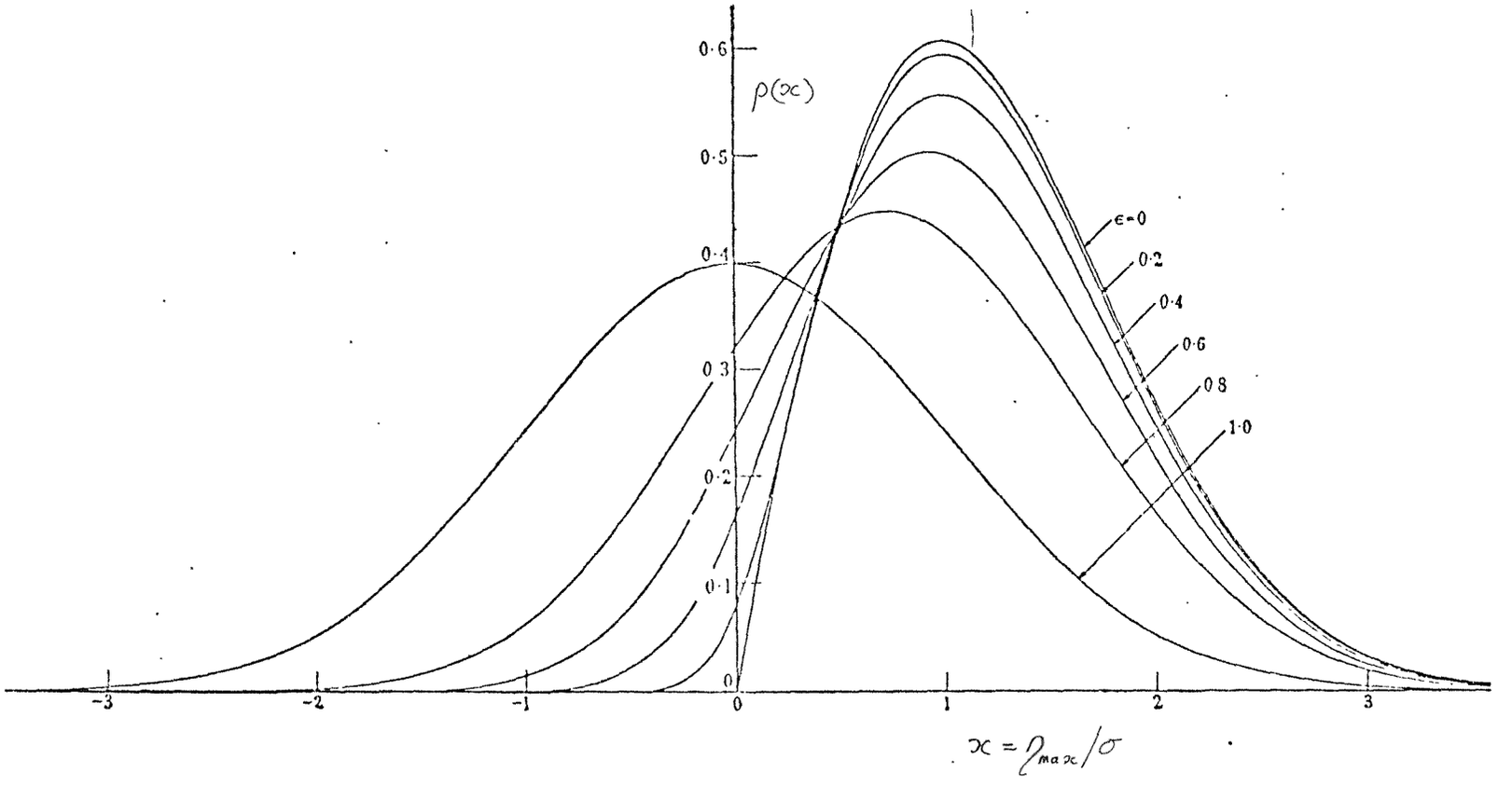

FIG. 2.2 Probability Density Distribution of the Elevation of Maxima for Various Values of Spectral Width (After Cartwright and Longuet-Higgins (1956))

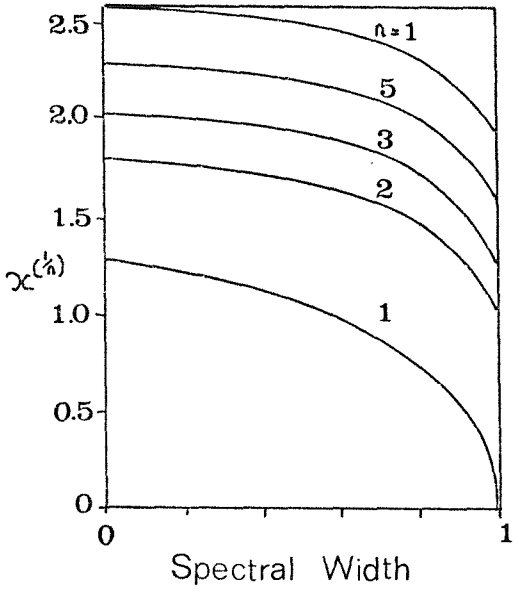

FIG. 2.3

The Mean Height of the $1/n$ Highest Maxima ($\alpha^{1/n}$) as a Function of Spectral Width (After Cartwright and Longuet-Higgins (1956))

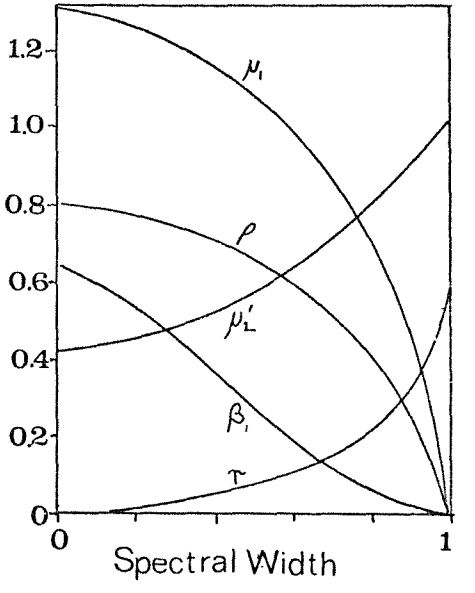

FIG. 2.4

The Variation of Mean μ_1, Variance μ_2', Skewness β_1, Proportion of Negative Maxima ν, and $\rho = (\mu_1'^2/\mu_0'\mu_2')$ as a Function of Spectral Width (After Cartwright and Longuet-Higgins (1956))

3. THE SPECTRAL ANALYSIS OF SOME TYPICAL WAVE RECORDS

3.1 Records Available

The following records were available:-

(i) Chart records from an OSPOS pressure recorder off the coast of Malta in 1967, made available by George Wimpey & Co. Ltd.

(ii) Chart recordings of waves off Eastbourne Pier from both a pressure recorder and a surface recorder from the National Institute of Oceanography. Recordings made 19.1.55.

(iii) Magnetic tape records of waves at Les Minquiers, Jersey, (see Fig. 3.1) taken by a Wave Rider Buoy in conjunction with Hovercraft trials. These were made available by the National Physical Laboratory, Hythe (Hovercraft Division) dated January 1971.

(iv) Punched tape records from a Wave Rider Buoy sited off the NAB tower - October/November 1970 (see Fig. 3.2), made available by Interservices Hovercraft Unit, Lee-on-Solent.

All the records were analysed, except those from Malta. These were in the form of chart records, a typical trace being shown in Fig. 3.3, but the amplitude is so small that digitization using the process outlined later for dealing with the Eastbourne records would not yield sufficiently accurate results for spectral analysis.

3.2 Chart Records from Eastbourne Pier

The operation of the surface recorder is described by Draper (1957). The chart records used were, in fact, photocopies of the originals, the originals having been produced by a photographic process resulting in the paper on one side of the water surface being black (exposed) and the other side white (unexposed). A typical trace of the water surface elevation is shown in Fig. 3.4.

In order to analyse these records, they had to be digitized before being fed into the University Computer. Several methods were examined, including optical and manual curve followers, both of which proved impractical.

Eventually, a manual curve follower/data logger, known as OSCAR, was located in the University. One record was digitized using this instrument, but the process was very tedious and involved moving the paper and re-setting axes each time a new length of record was to be dealt with. The datum position of the axes was found to 'drift' by up to 5 per cent during the digitization.

The digital record obtained was used to explore some basic properties of spectral analysis. A simple program was written in Fortran and implemented using the University's 1907 computer. The program involved statistical routines to find variance and wave heights etc. The results of this part of the analysis were as follows:-

Record No.	-	E6.3
Water Depth	-	6 metres
Wind	-	South West (fresh)
Interval of Digitization	-	0.206 seconds
Variance	-	300.91 cm.
Mean	-	Zero
Skewness	-	0.148
Kurtosis	-	2.883
Significant Wave Height	-	62.1 cm. ($H_s/\sigma = 3.69$)
RMS Wave Height	-	43.7 cm. ($H_{rms}/\sigma = 2.52$)
$H_{1/10}$	-	75.2 cm. ($H_{1/10}/\sigma = 4.34$)
Zero Crossing Period	-	3.408 s
Number of Waves	-	64

The spectral analysis was simply an implementation of Equations 2.38 and 2.39. Initially, no special lag window was used and 40 and 80 lags were used. The power spectra and auto-correlation functions for these two cases are shown in Fig. 3.7 and 3.8.

Fig. 3.7 shows the auto-correlation function for 40 lag intervals. The most striking feature is that it does not tend to zero as rapidly as expected. The power spectrum for this case shows a marked peak at approximately 0.2 Hz and a negative region above 0.4 Hz . The peak is clearly the frequency of the predominant waves and since it is so clearly defined the wave trace should have an important sine wave component. This is also borne out by the reluctance of the auto-correlation function to tend rapidly to zero. For $m = 80$ the periodic component is clearly still visible and

on the corresponding power spectrum has a better resolution (because of choosing a greater number of lags) and the negative excursion is smaller in magnitude.

This negative power in the spectrum may, at first sight, seem to lead to doubt in the use of this analysis, but it has a plausible explanation. The digital computation process does introduce errors simply as a result of rounding etc. These, however, are very small. The real answer lies in the fact that the auto-correlation function does not effectively become zero during the lag time considered. As a result, the negative side-lobes on the spectral window involved play a significant part in the computation. The almost periodic nature of the negative part of the spectrum confirms this. This is an example of the spectral window 'colouring' the spectrum, the effect being much pronounced because of the distinct peak in the spectrum.

Two special lag windows, Triangular and Tukey, were used to produce the spectra shown in Fig. 3.9, again using 80 lag intervals. The results are very similar, only marginal differences being noticeable, the negative portion from the Triangular lag window computation being reduced in magnitude more than in the other.

The above computations with $m = 80$ yield spectra with 27 degrees of freedom, i.e. the bounds of the 80 per cent confidence band are within +38 per cent and -35 per cent of the estimated spectral density.

A further computer program was written to calculate the spectrum via the fast Fourier transform. The result of this is shown in Fig.3.10.

The most striking feature is the lack of negative values which is an important advantage of this method. Spectra using no data window and the cosine taper discussed in Appendix 2. were calculated, the result of the latter producing a smoother shape.

Another computer program calculated the properties of the spectrum giving a spectral width of 0.705 and a peakedness of 3.254.

The values quoted earlier for H_s/σ etc. show a reasonable correlation with the theoretical values considering the high value of spectral width and relatively short record length.

3.3 Magnetic Tape Recordings from Jersey

The magnetic tape recordings were far easier to handle in that most of them could be fed directly into the computer as an analogue signal. However, there were some problems with interference and unlocking of the signal. In this case, the record was digitised and the interference removed before being analysed.

The computer used was that at the Data Analysis Centre of the Institute of Sound and Vibration Research, University of Southampton. Analogue signals were fed into an analogue-to-digital converter and put on to a disc file ready for any computation to be performed digitally.

It was desirable to have as many degrees of freedom as reasonably possible. The length of record was such that 70 degrees of freedom were feasible. This required 18.6 minutes of real time record and care was needed to select a length of recording free from spurious signals. This was equivalent to approximately two thousand values sampled at two samples per second real time.

If the required number of samples could not be obtained free from interference, the disc file was punched on to paper tape and the spurious values removed before analysing the file.

With 70 degrees of freedom the 80 per cent confidence limits are at $0.77\bar{a}$ and $1.23\bar{a}$, where $\bar{a}$ is the computed value.

Programs from the Data Analysis Centre's suite of programs were used to analyse the data, giving a statistical breakdown and power spectral density. The statistical moments (variance, skewness and kurtosis) together with the maximum and minimum values encountered were output to the teletype. The power spectral density was output via a graph plotter and the co-ordinates of the graph onto punch tape. From the punch tape, the spectral moments were obtained using the main computer, hence the spectral width and peakedness were calculated.

Originally, the recordings had been made on a Sangamo 14-track tape recorder, then re-recorded onto a THERMIONIC FM tape recorder and being speeded up by a factor of 16. This greatly decreased data acquisition times of the computer but necessitated some compensation to be made in the computation process.

The statistical moments were output in volts and had to be scaled to produce wave heights etc. in metres. The power spectral density was in normalised form (i.e. the area under the curve is unity). However, the frequency axis has to be divided by 16 to compensate for the speeding up during re-recording. This, in turn meant that the power spectral density values had to be multiplied by 16 since the area under the curve must remain constant.

The full details of the analysis are as follows:-

Sampling Rate	2 samples/sec.
Nos. of Samples	2334
Degrees of Freedom	70
Resolution	0.03 Hz

The method of presentation suggested by Draper (1966) and outlined in Section 2. was not used. This was because only a limited number of records were available and the Draper approach is more suitable for obtaining an overall impression of the wave climate, whilst the spectral approach used here indicates the conditions at a particular time.

The power spectra have been plotted in non-normalised form using real values (i.e. metres, not volts). As a result, the area under the curve is equal to the variance (σ^2). These values were checked by numerical integration and the difference between this and the value obtained by the statistical moments program is less than 10 per cent in most cases (see Table 3.1).

The spectral width varies between 0.56 and 0.86 whilst the peakedness between 0.86 and 1.7. A scatter diagram of these is shown in Fig. 3.11.

The power spectral density plots show two important characteristics of the sea conditions. There are characteristically two frequencies at which the spectral energy may be concentrated. These are a "swell" entering the area with a frequency of 0.08 Hz and locally generated waves with a predominant frequency of between 0.2 and 0.3 Hz. The spectra are shown in Fig. 3.12 - 3.26. It is

very noticeable that waves generated locally are much smaller than the "swell" which was generated outside the area and this is to be expected since the winds causing these conditions have a velocity of 18 knots (typically) and flow over a fetch of about 20 miles. Another interesting feature of the spectral approach to wave analysis is shown by the results from Sorties 2b. and 11. The variances are very similar, 1640 cm.^{2} and 1680 cm.^{2} respectively. However, the shape of the spectra are not the same, the maximum value for 2b. being 14,520 cm.^{2}sec. whilst that for 11 is 25,600 cm.^{2}sec. The values of $H^{\frac{1}{3}}$ from the chart records are 1.09m. and 3.2m. respectively. Furthermore, the spectral widths are 0.64 and 0.81 respectively. The explanation of this is that the sea conditions in Sortie 11 are characterised by a narrow single peaked spectrum representing high energy low frequency swell waves. Physically, this would mean a smooth sea with very long waves. Sortie 2b. consists of a two-peaked spectrum indicating the presence of a "swell" and locally generated waves. Physically, there would be a very confused sea state, perhaps with some waves feathering with smaller wave height than the previous condition and the swell much less discernible.

3.4 Comparison with Theoretical Spectra

Since the wave records analysed are all taken from the same coastal region it was thought that the most suitable spectra for comparison was that of Darbyshire (1961) for coastal conditions.

Upon examining the field spectra, it became evident that most of the records consisted entirely of swell, or partly of swell and locally generated waves.

Consideration was given to comparing only the spectral peak due to the locally generated waves, but since the wind speed was usually only 10 knots and with a fetch of about twenty miles, only an approximate correlation was expected. Indeed, in some cases, a peak corresponding to locally generated waves was missing entirely.

The Darbyshire Spectra for Sorties 2a., 2b., 3b., and 15 were calculated. The results are not well related. The theoretical spectra only correspond to the high frequency peak of course, but the position of this is only approximated and the actual values too are rather approximate. This is really to be expected since only the local wind speed was recorded for the time of the trial and the overall weather situation was not considered and perhaps a better way would be to relate the spectrum to a wave height - Hogben (1969).

Comparison of the theoretical spectra with the two sets of data was not made since wind speeds for the area of recordings were not readily available.

3.5 Punched Tape Records from the NAB Tower

Three punched tapes of storm waves off the NAB Tower in the Solent were available for analysis. However, the tape coding was not compatible with the University tape reader format. The tapes consisted of 3 digit integer numbers separated by a new line

character, but the parity was odd, whereas the IS08 code used by the University computer required even parity. The problem was solved by using a machine built by the Psychology Department for converting odd parity to even parity tape. Each line of tape was read and converted into two lines of even parity. The four least significant characters of each line of input tape being punched onto the least significant characters of the new tape and an identifying character in bit seven, the correct parity being established by character eight. The remaining four bits of a second line with identification given by a character in bit six, with parity being corrected as before. The net result is that each line of odd parity tape is converted into two lines of even parity tape, the characters of which are either the first nine letters of the alphabet or punctuation marks in IS08 code. A special program was written in ALGOL, making use of the character reading facility, to read the tape into the computer. Each character was read in turn and stored as its internal machine code representation, e.g. A was read in as 3873. Knowing the machine code it was a simple job to convert each eight line set into an integer number and a new line character. The resulting set of numbers was then stored on magnetic tape.

The spectral and statistical analyses were the same as those used on the Eastbourne records, the results of which are shown in Table 3.2, together with details of the records. 80 lag intervals were used to calculate the auto-correlation function, thus giving 45 degrees of freedom for records N1 and N2 but 30 for N3, since only

1200 samples had been taken. The sampling interval had already been set when producing the punched tape at 0.5 secs., so limiting the maximum frequency to theoretically 1.0 Hz, but in practice, it is often desirable to have a greater margin where spectral analysis is concerned. This illustrates one of the major disadvantages of punched tape records. The auto-correlation function was smoothed by using Bartlet lag window before being cosine transformed into power spectrum. The three resulting spectra are shown in Figs. 3.27 - 3.29. These spectra show very similar trends considering that they were recorded at times differing by at least two weeks. The shapes are very similar, all consisting of a single peak, the predominant part of which is between 0.1 and 0.15 Hz. The magnitude of the peaks are also very similar. Spectra such as this would suggest a fully arisen sea state for the area consisting of relatively local waves, generated perhaps in the English Channel.

Also of interest in this case is the relationship between the statistically derived parameters and those obtained from the spectrum. For record N3 the zero crossing frequency f_z is 0.155 Hz whilst the peak frequency f_p is 0.11 Hz. The former is, of course, affected by the relative amount of energy contained in each frequency band and so it would be reasonable to expect some correlation between the discrepancy between f_p and f_z and the spectral width and peakedness. For example, a spectrum with low spectral width would have better agreement between f_p and f_z . However, no such correlation was obvious from these spectra. It is interesting to note that the values of spectral width and peakedness lie in a

different range than those for the Jersey records.

3.6 Relationship between the Spectrum and Averaged Properties of Wave Records

The recent trend towards the use of random sea states in model testing has brought an interesting problem concerning the validity of previous tests conducted with regular waves, having a wave height equal to the significant wave height and a period equal to the zero crossing period. The significant wave height, if taken as four times the square root of the zero-th spectral moment (variance) is generally a good approximation to the actual value for spectral widths less than about 0.8. Since it is usual to calculate wave length from the zero crossing period when wave steepness H/L is used as a parameter in regular wave testing (e.g. overtopping of breakwaters) great caution must be exercised when relating these results to a random sea state, as will be obvious from the following discussion.

Ignoring the fundamental differences in effect of a random sea state and a regular wave action, since this is difficult, if not impossible, to express quantitatively, but has been shown to exist by Kraai (1969) for example, the zero crossing period is obtainable from the spectral moments using a relationship derived from Rice (1944):-

$$T_z = 2 \left[\frac{\int_0^\infty f^2 S(f)\, df}{\int_0^\infty S(f)\, df} \right]^{1/2} \qquad (3.1)$$

In relating this to the wave spectrum it is convenient to define a zero crossing frequency f_z which is the inverse of the zero crossing period. For a spectrum with a low spectral width and consequently a well-pronounced peak, the zero crossing frequency should coincide with the frequency of maximum energy. This is to be expected since the wave train in this case is almost a sinusoid. For spectra having double peaks, the zero crossing frequency often lies in the trough between the two peaks. This produces problems when attempting to relate model tests in regular waves to real sea state conditions. If, for example, the zero crossing frequency is used as the frequency of the regular waves, for the narrow spectrum described previously this would be acceptable, but for the double peak spectrum the model tests would be using waves of a frequency which has negligible energy in the actual spectrum. It has been suggested that the use of one or two modal frequencies will overcome this. However, this also provides some problems when dealing with almost flat spectra where the modal frequency is not clearly discernible.

A further alternative is to plot the cumulative spectrum

$$S'(f) = \int_0^f S(\xi)\, d\xi \qquad (3.2)$$

The significant frequency f_s (say) is then defined as the frequency corresponding to the frequency at 70 per cent (say) of the total energy. However, serious problems arise when relating this to regular waves and justifying the choice of 50, 60, 70 or

any other percentage of total energy as the significant frequency.

3.7 The Effect of Noise on the Properties of the Spectrum

Almost all computed spectra contain noise either as a result of unavoidable electronic processes or from digital computation. This noise usually becomes evident as a residual energy at the higher frequencies in the spectra. Occasionally spectra also contain appreciable energy at zero frequency. This is often due to a very low frequency D.C. drift in the mean signal or (particularly with telemetered information) an offset signal due to unlocking. The use of band pass filters can remove this noise when it is outside the frequencies of interest. However, some noise is always likely to be present in the spectrum.

The computation of zero crossing period, spectral width and wave heights from the spectrum are affected by this noise since they are functions of the spectral moments. The zero-th spectral moment is altered least and the highest moments most as one would expect.

A suggested method of approaching this problem is to plot cumulative spectra. The high frequency noise is then removed by ignoring any energy above, say 95 per cent of the total, then computing the spectral moments in the usual way. This is useful because it also avoids the 'noise' produced at high frequencies by the intrinsic errors in the computation. The results from a test of the Fourier transform highlights this effect. A sine wave was input to the program and the spectra consisted of a single peak and white noise with a magnitude of the order of 0.5 per cent of the

main peak. However, the spectral width was computed as 0.538 whereas the same calculation using a 95 per cent cumulative cut-off produced a spectral width of 0.065. This method was used in the analyses described in the previous section. However, it can be argued that since the noise may be said to be 'white noise', then a constant energy should be subtracted from the spectrum at all frequencies (see Fig. 3.31). Whichever method is adopted it is likely to produce a more realistic measure of the true spectral properties.

Noise arising from computation as a result of, for example, side lobes on spectral windows, is unavoidable in any realistic analysis and is usually regarded as constant.

3.8 Summary

It has been shown that a power spectral density function can yield all the common parameters found in regular or simple statistical analysis of wave records to a fixed accuracy. However, the use of these parameters such as significant wave height and zero crossing period can be misleading when comparing regular and random waves, the parameter approach being simpler as many sea states can be presented at once using two or three parameters for each. The spectral representation gives much more information but requires a separate plot of the spectrum for each case.

Spectral results using different computation methods can differ and whilst a uniform method would be preferable, it is not essential and in some cases impossible.

The most important requirement for spectral analysis is that the conventions used and the computational method (such as spectral window) are clearly defined.

Sorrie No.	Date	Wind Speed Knots	Direction Degrees	Fetch Naut. Miles	H_{max} cm	σ^2 cm²	Skewness	Kurtosis	$\int_0^\infty S(f)df$	ε	Q_p	Nos. of Predom. Peaks	Notes
2a	7-1-71	18½	180	19.75	100	1314	0.00	3.00	1213	0.68	1.42	2	
2b		12	185	20.00	109	1640	0.00	3.00	1541	0.64	1.37	2	
3a	12-1-71	8½	160	21.8	100	129	-0.101	2.90	125	0.72	1.01	2	
3b		8½	150	21.8	109	167	-0.010	2.83	149	0.78	1.13	2	
4a	12-1-71	8	140	19.9	122	175	-0.026	2.74	161	0.79	1.06	2	
4b		8	150	21.8	128	186	-0.137	2.80	177	0.80	1.38	1	swell
5a	13-1-71	10	125	18.3	112	109	0.050	2.91	789	0.67	1.62	1	swell
5b		10	110	16.9	105	118	0.060	3.03				1	swell
6a	14-1-71	11	100	15.7	113	151	-0.061	2.942	228	0.65	1.54	1	
6b		12	110	16.9	106	163	-0.000	3.078	158	0.56	1.63	1	
11	20-1-71	14	230	50	320	1618	-0 060	2.86	1534	0.81	0.99	1	swell
12a	28-1-71	20	250	50	228	831	0.070	2.617	614	0.86	0.55	1	swell
12b		18	280	50	237	1045	0.049	2.704	1005	0.77	1.30	1	
14	31-1-71	8½	315	50	100	110	0 140	3.135	110	0.85	1.26	1	swell
15a	2-2-71	6	90	14.1	143	238	0.114	3.194	204	0.65	1.70	2	
15b			90	14.1	149	241	-0.584	8.58	227	0.76	1.40	2	

TABLE 3.1 Statistics of Jersey Wave Records

RECORD NO.	N1	N2	N3
Date	10-09-70	16-11-70	03-11-70
$\sigma^2 (cm^2)$	6842	7274	8596
β_1	-0.023	-1.317	-2.487
β_2	2.783	11.511	18.187
$H_s (cm)$	309.9	308.3	324.7
$H_{rms} (cm)$	225.5	221.1	234.7
$H_{1/10} (cm)$	364.7	421.4	481.4
T_z (sec)	6.0	6.42	6.45
ε	0.549	0.583	0.543
Q_p	2.266	1.741	2.008
$f_c (Hz)$	0.125	0.125	0.11
$f_z (Hz)$	0.166	0.155	0.155

TABLE 3.2 Statistics of NAB Tower Records

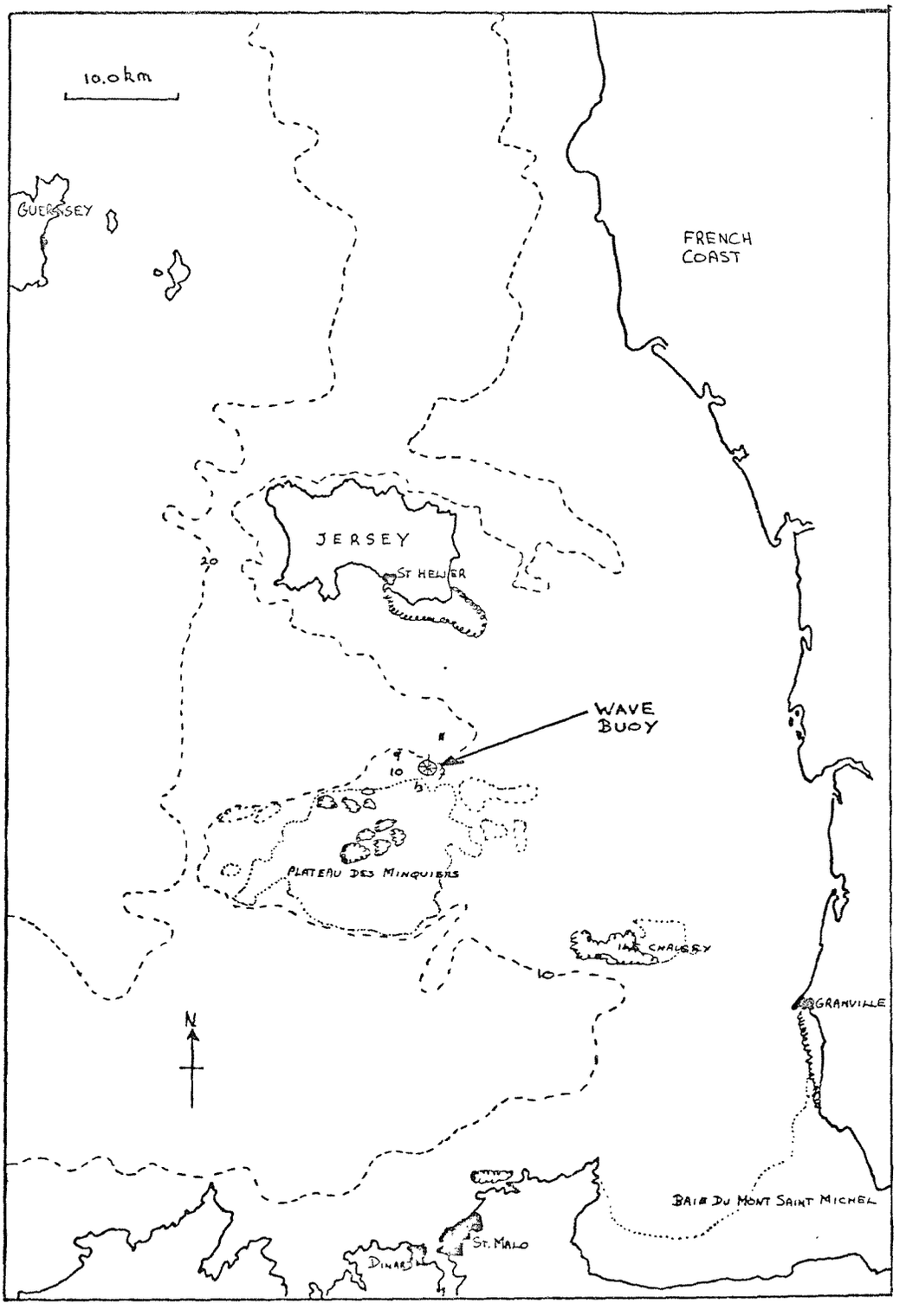

FIG. 3.1 Site of Jersey Wave Buoy

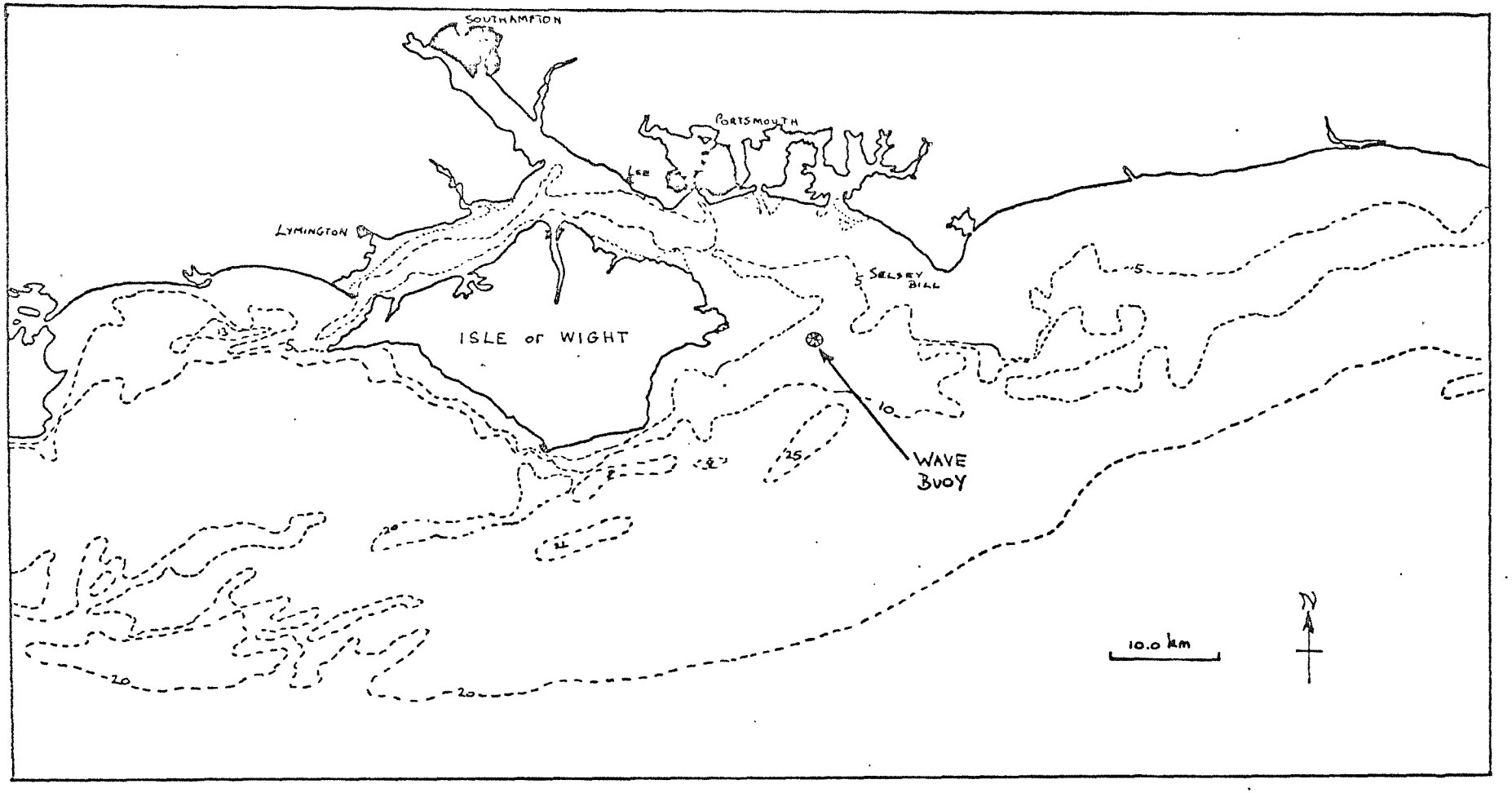

FIG. 3.2. Location of the NAB Tower Wave Buoy

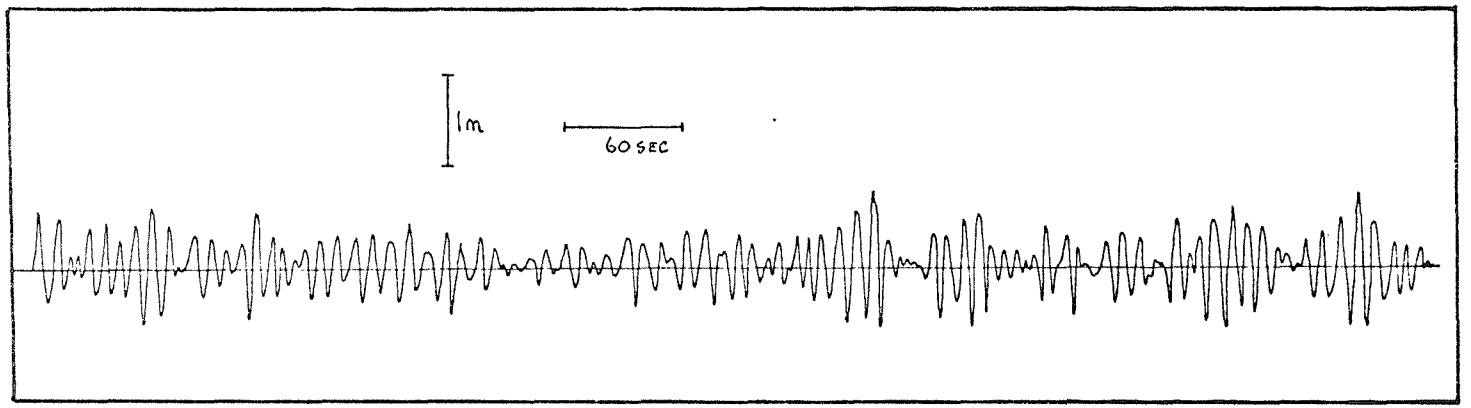

FIG. 3.3 Typical Wave Trace from Malta

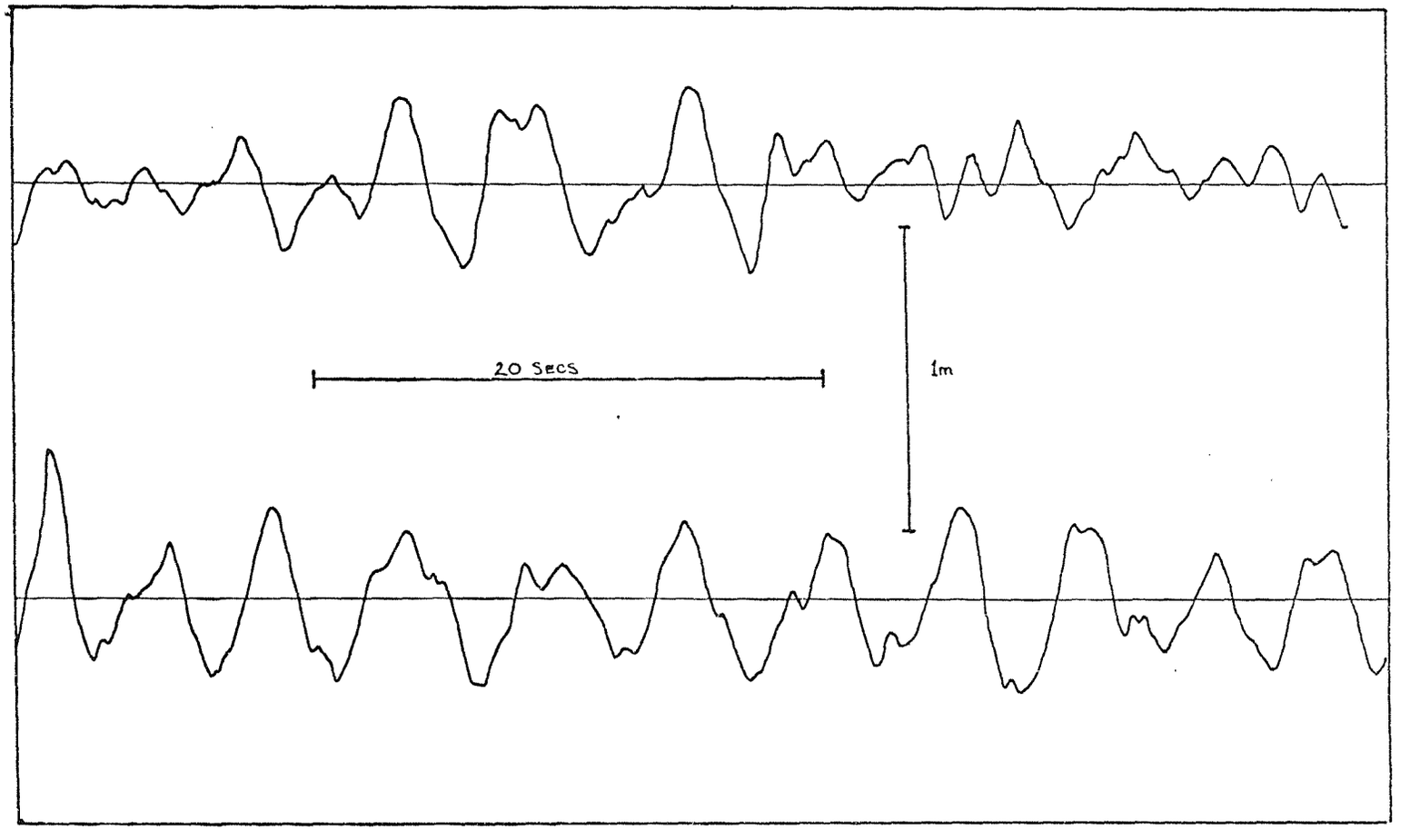

FIG. 3.4 Typical Wave Trace from Eastbourne

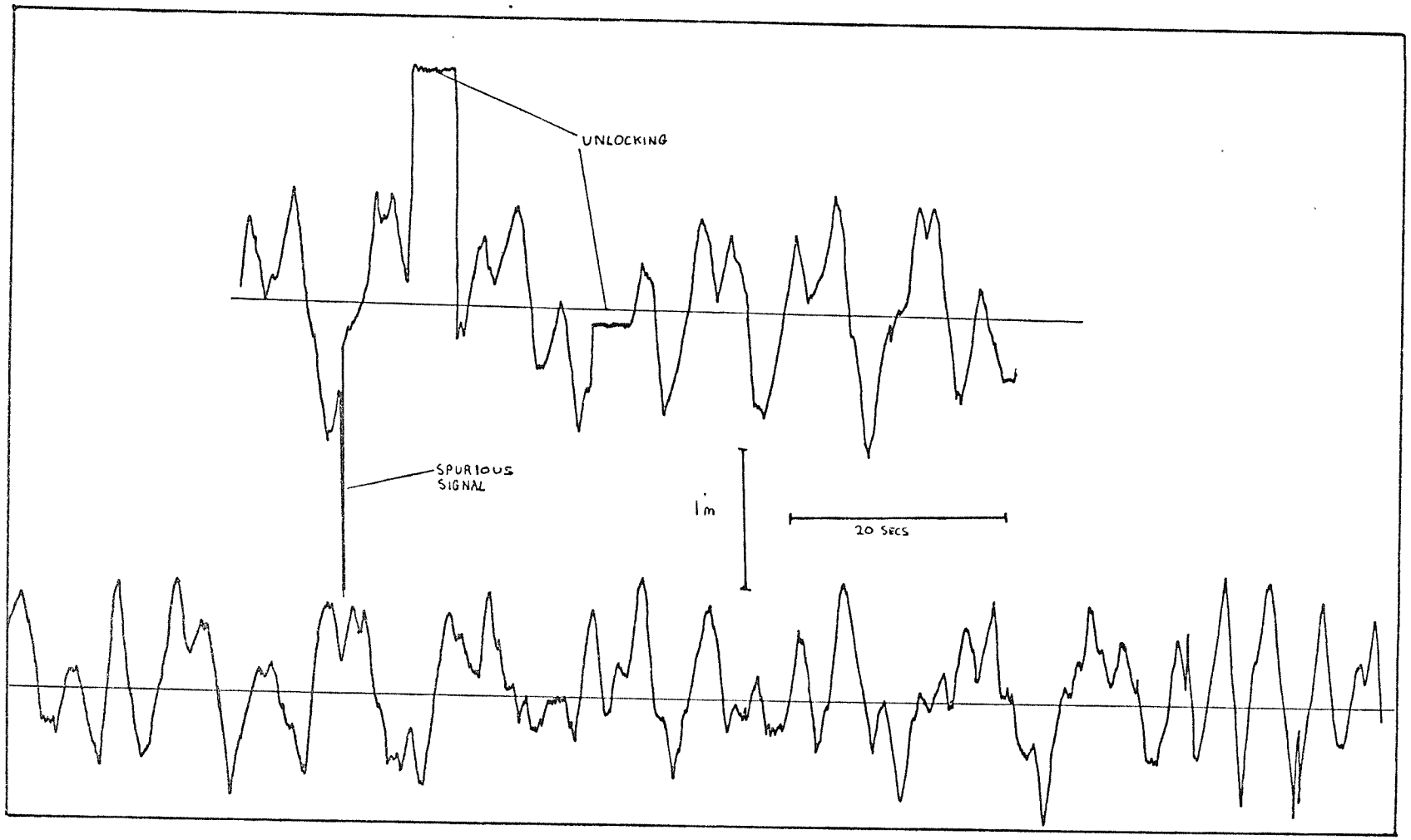

FIG. 3.5 Typical Wave Trace from Jersey (The upper trace contains interference)

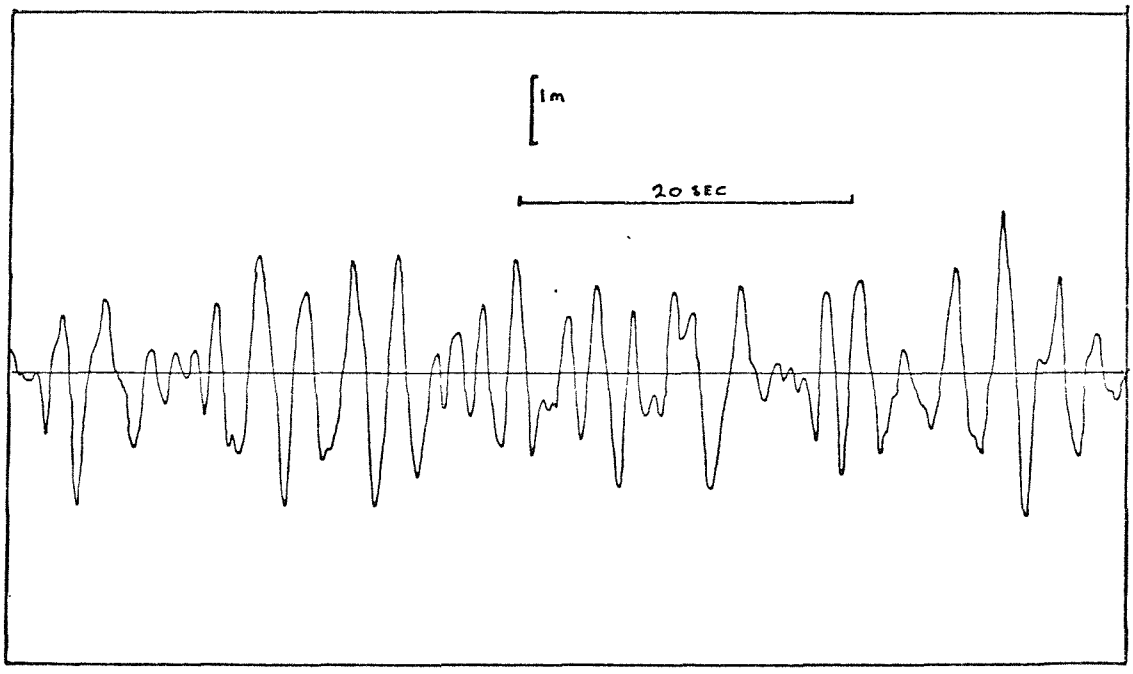

FIG. 3.6 Typical Wave Trace from NAB Tower

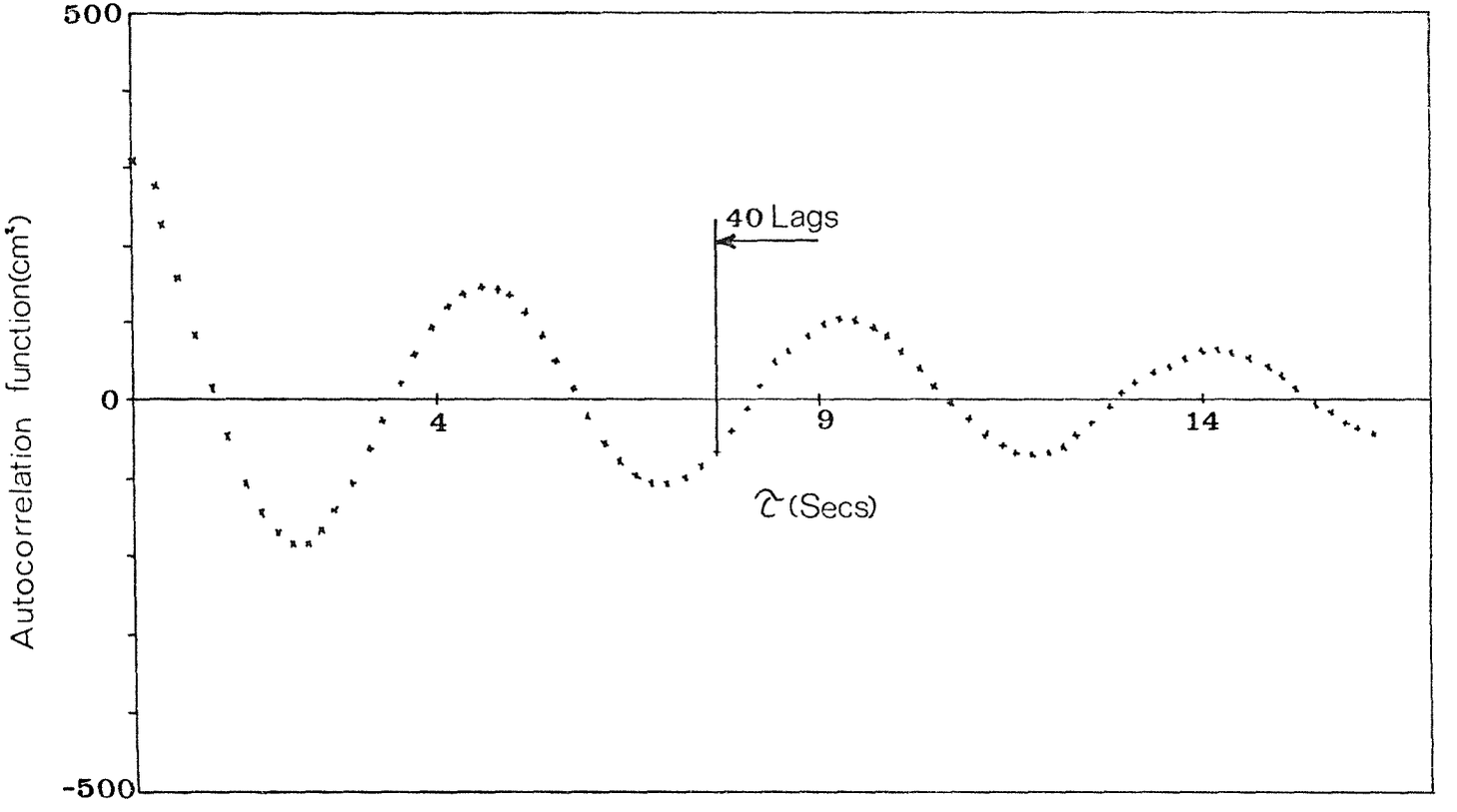

FIG. 3.7 Auto-correlation Function for Record E6.3

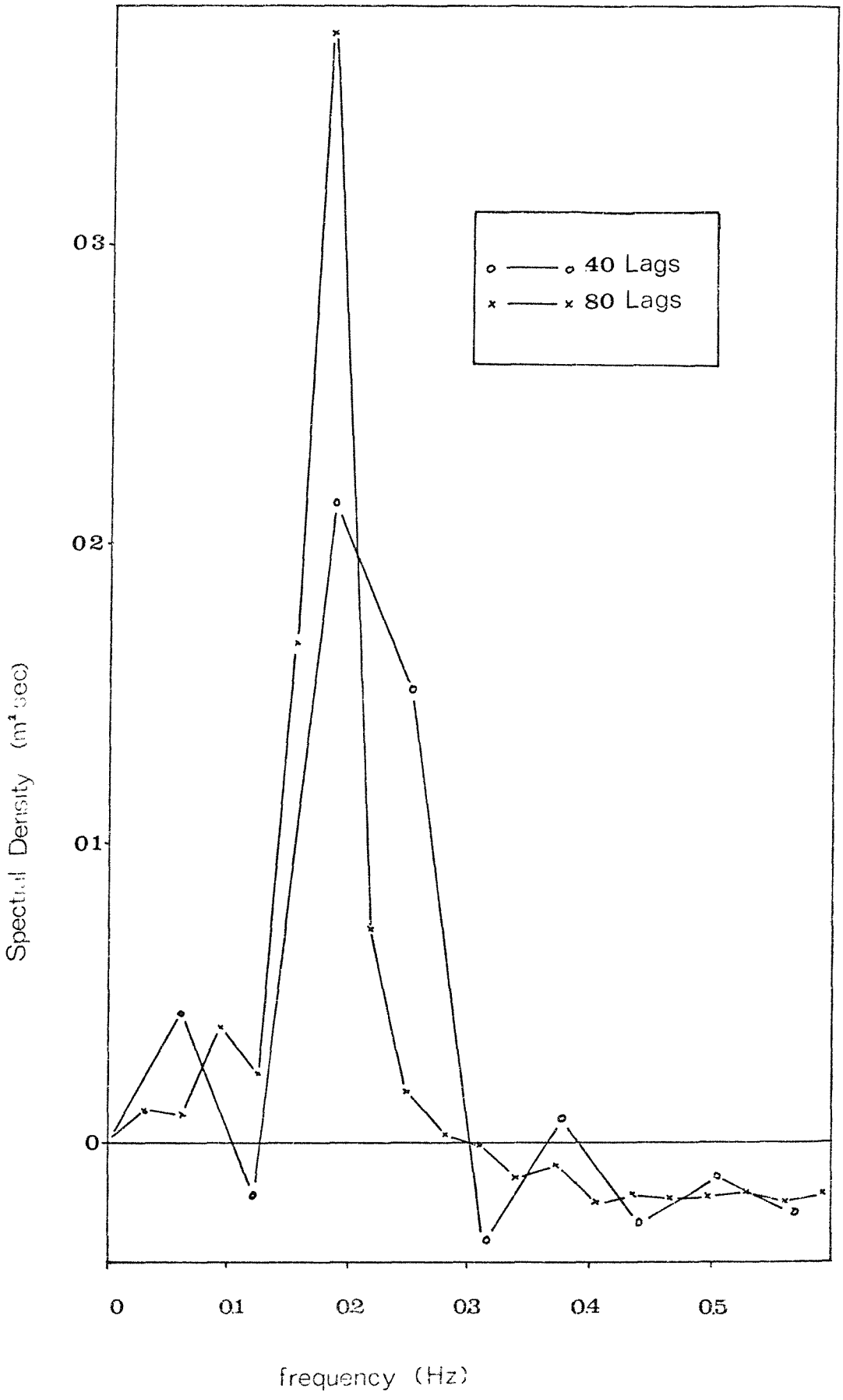

FIG. 3.8 Power Spectra for Record E6.3

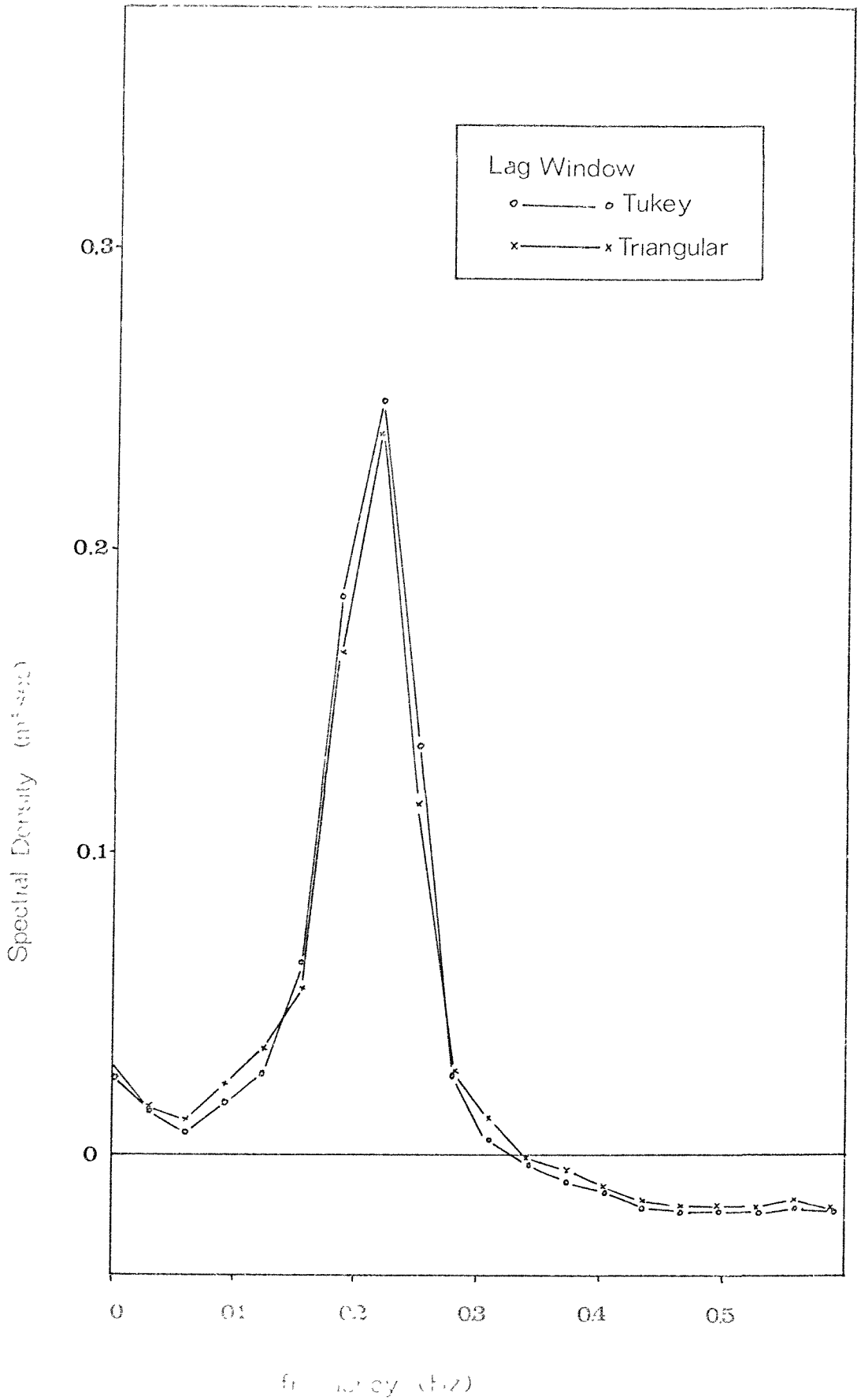

FIG. 3.9 Power Spectra for Record E6.3 using Triangular and Tukey Lag Windows

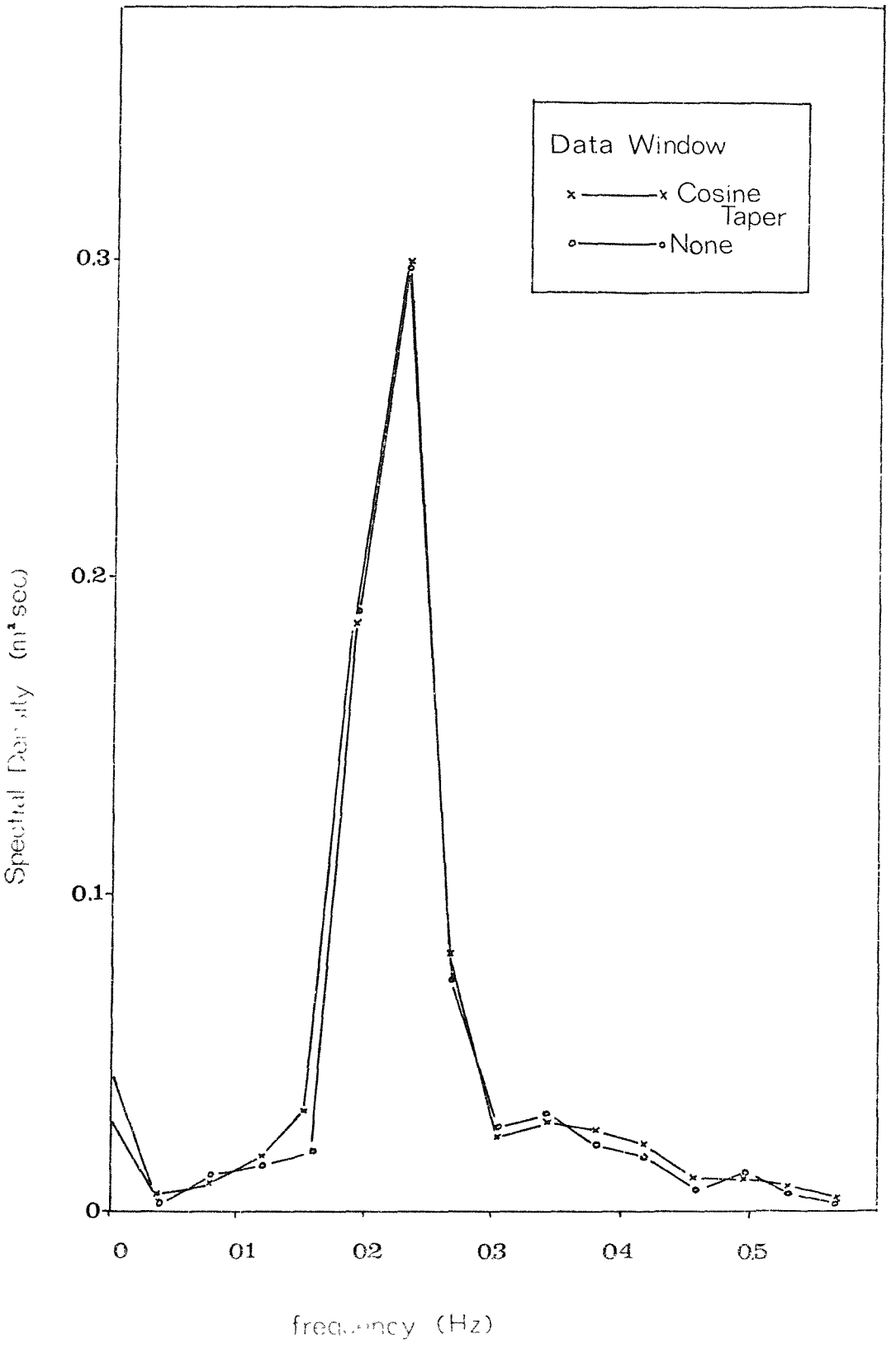

FIG. 3.10 Power Spectra for Record E6.3 via the Fast Fourier Transform

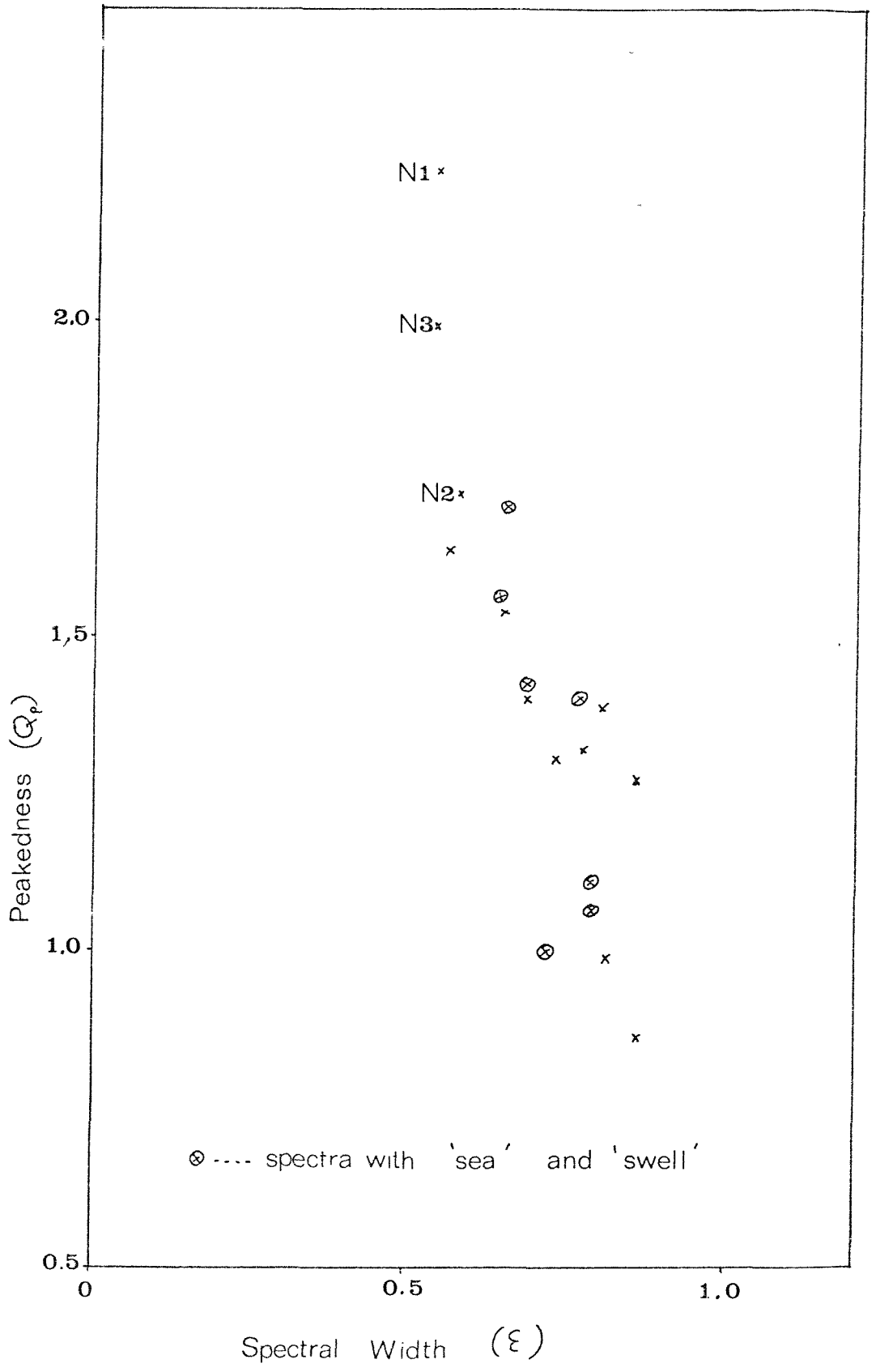

FIG. 3.11 A Scatter Diagram of Spectral Width and Peakedness

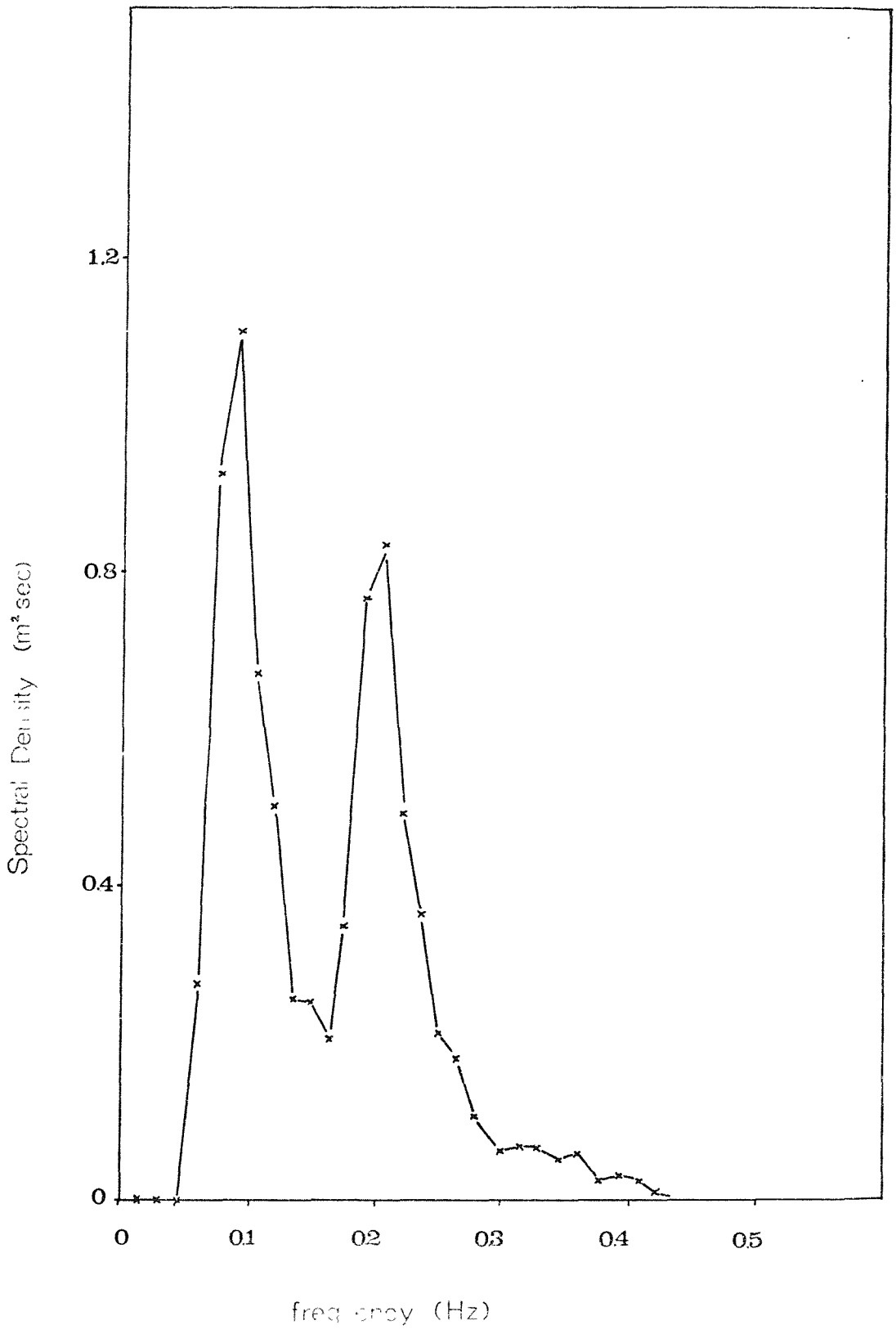

FIG. 3.12 Power Spectrum for Sortie 2A

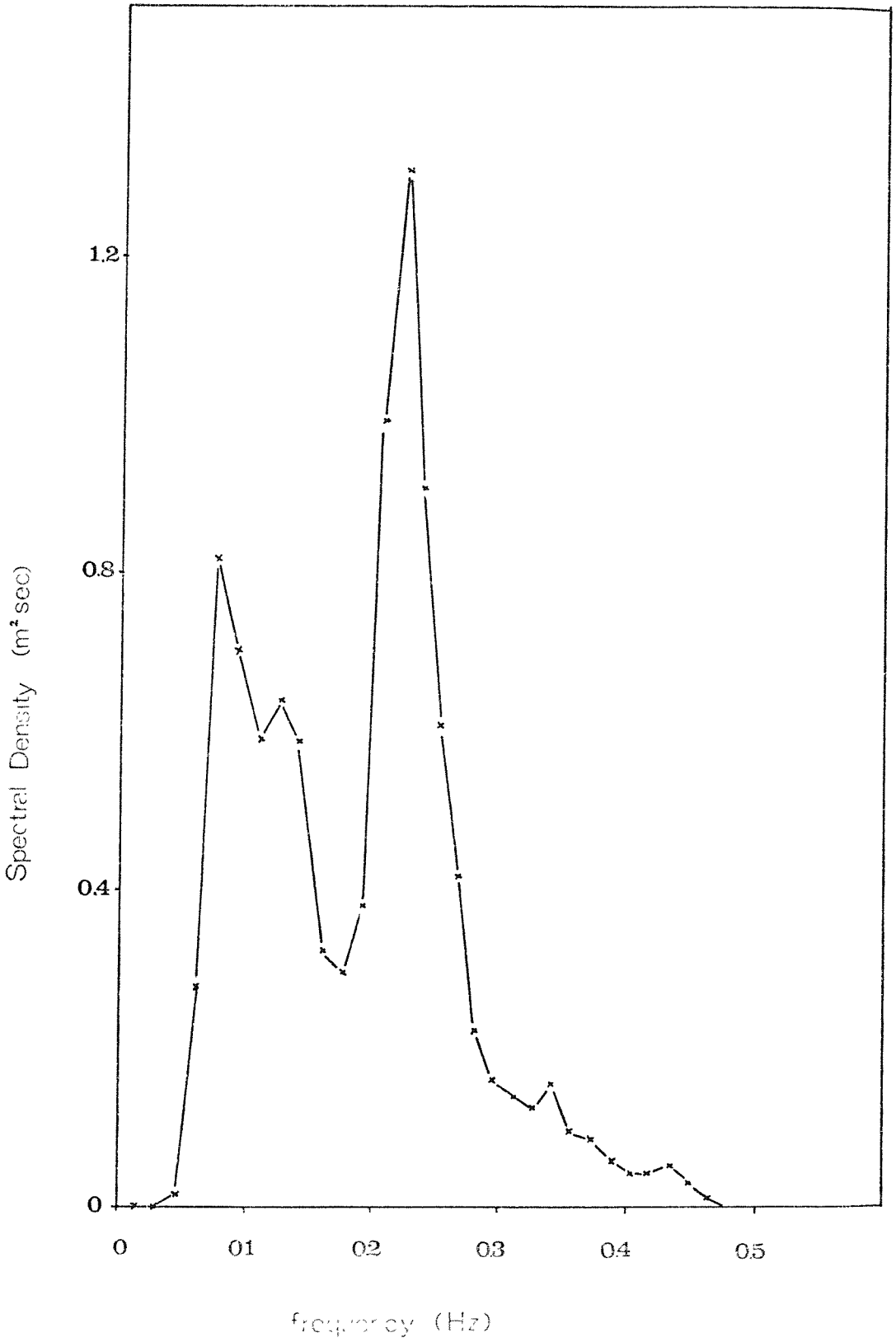

FIG. 3.13 Power Spectrum for Sortie 2B

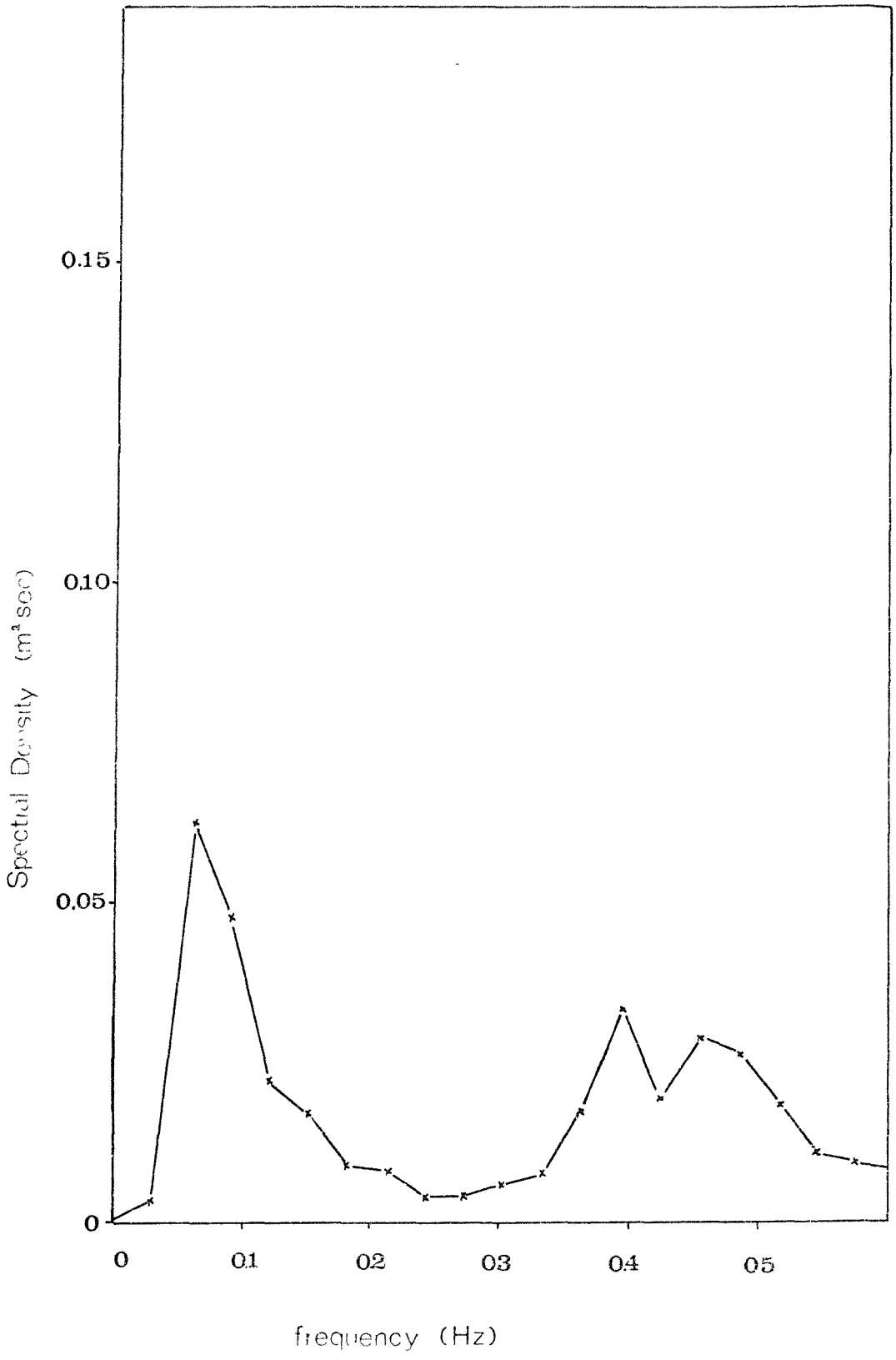

FIG. 3.14 Power Spectrum for Sortie 3A

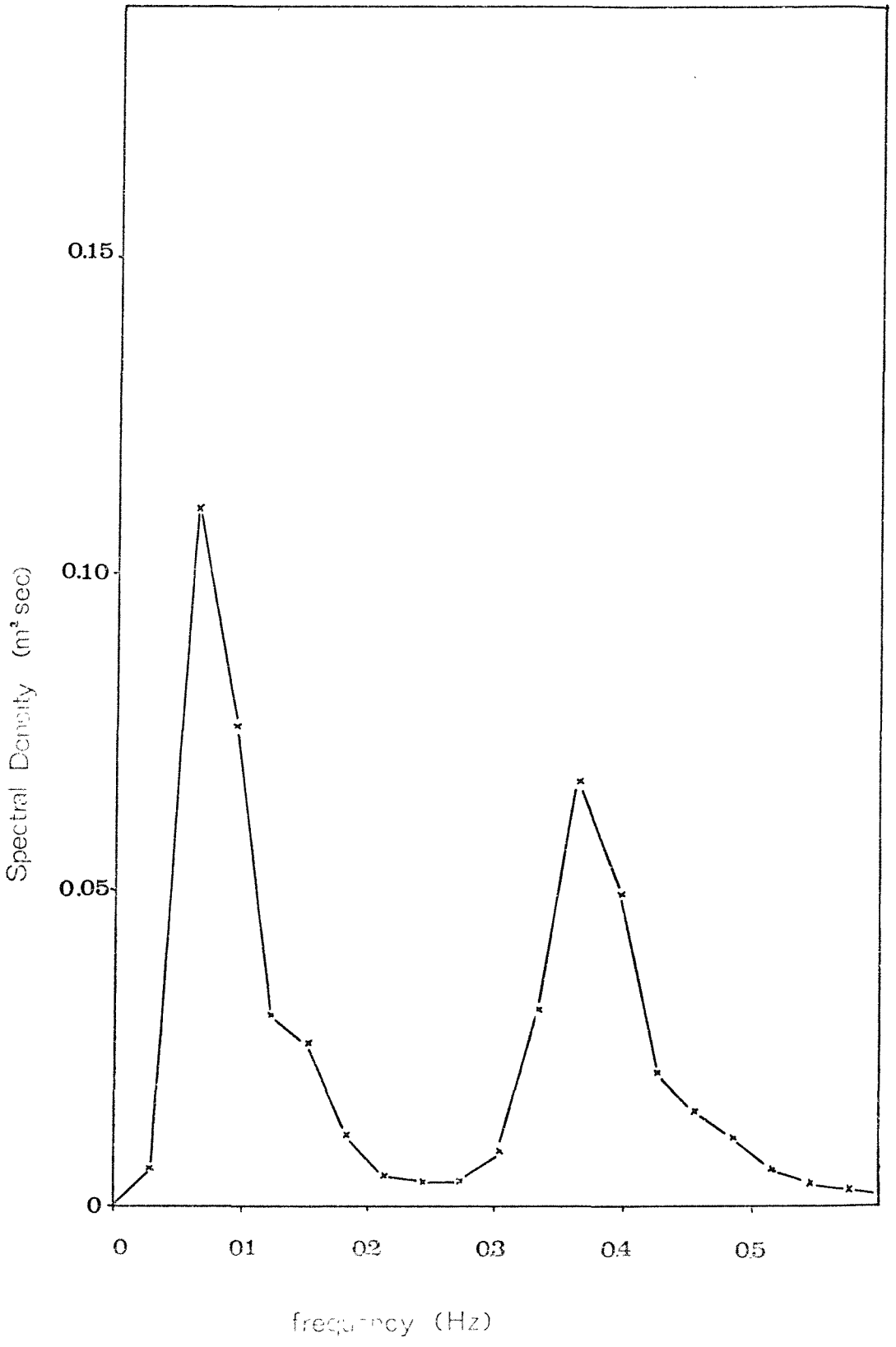

FIG. 3.15 Power Spectrum for Sortie 3B

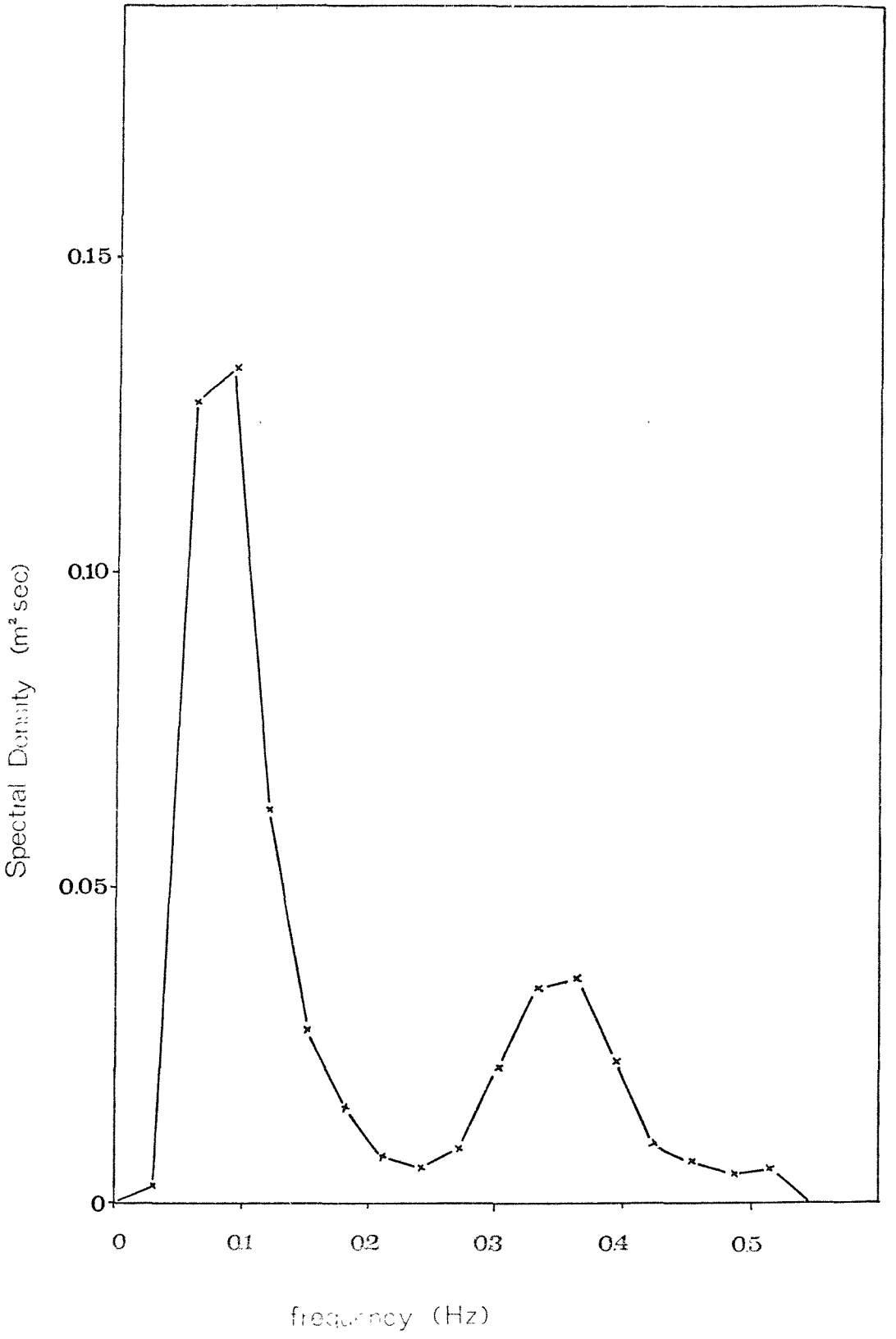

FIG. 3.16 Power Spectrum for Sortie 4A

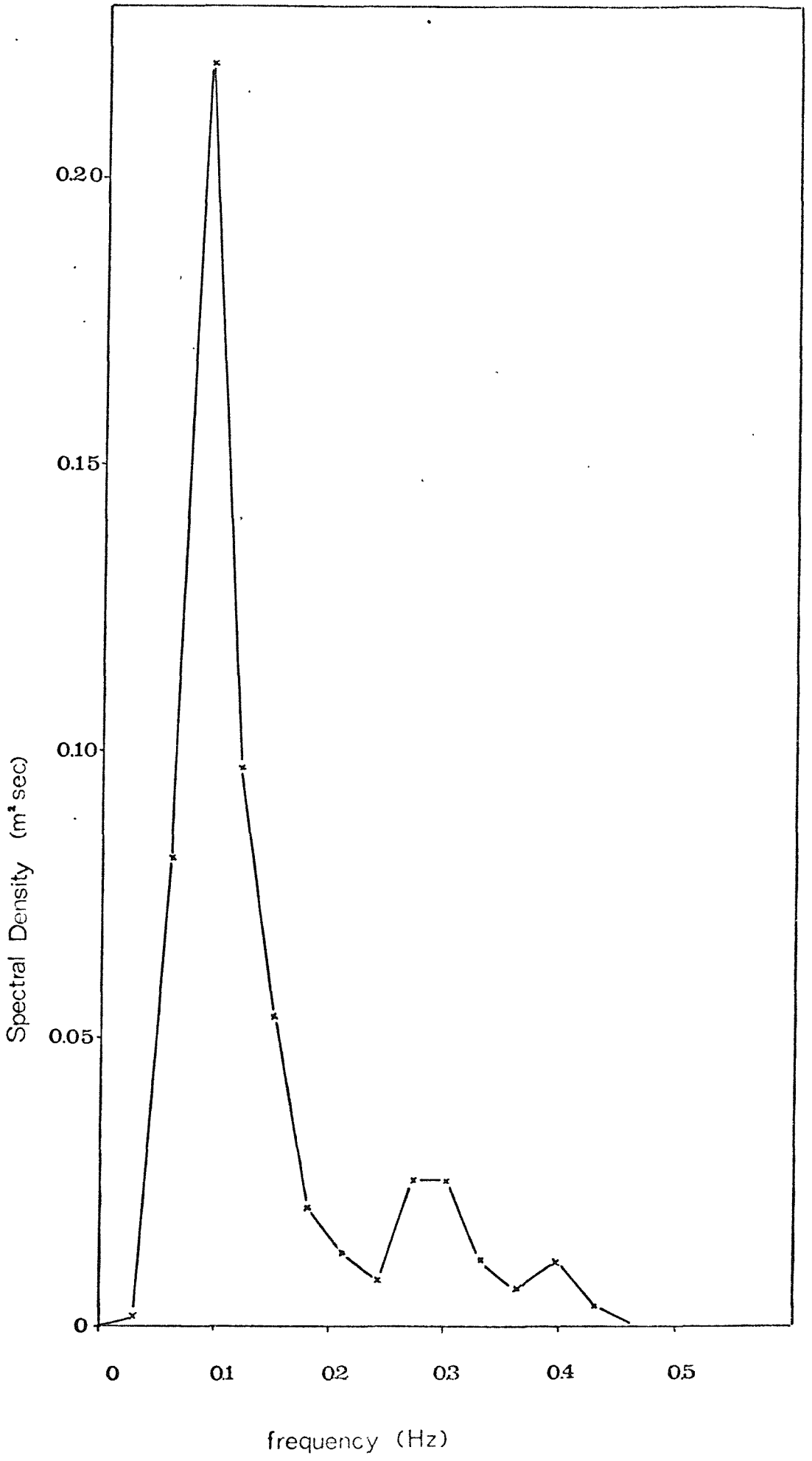

FIG. 3.17 Power Spectrum for Sortie 4B

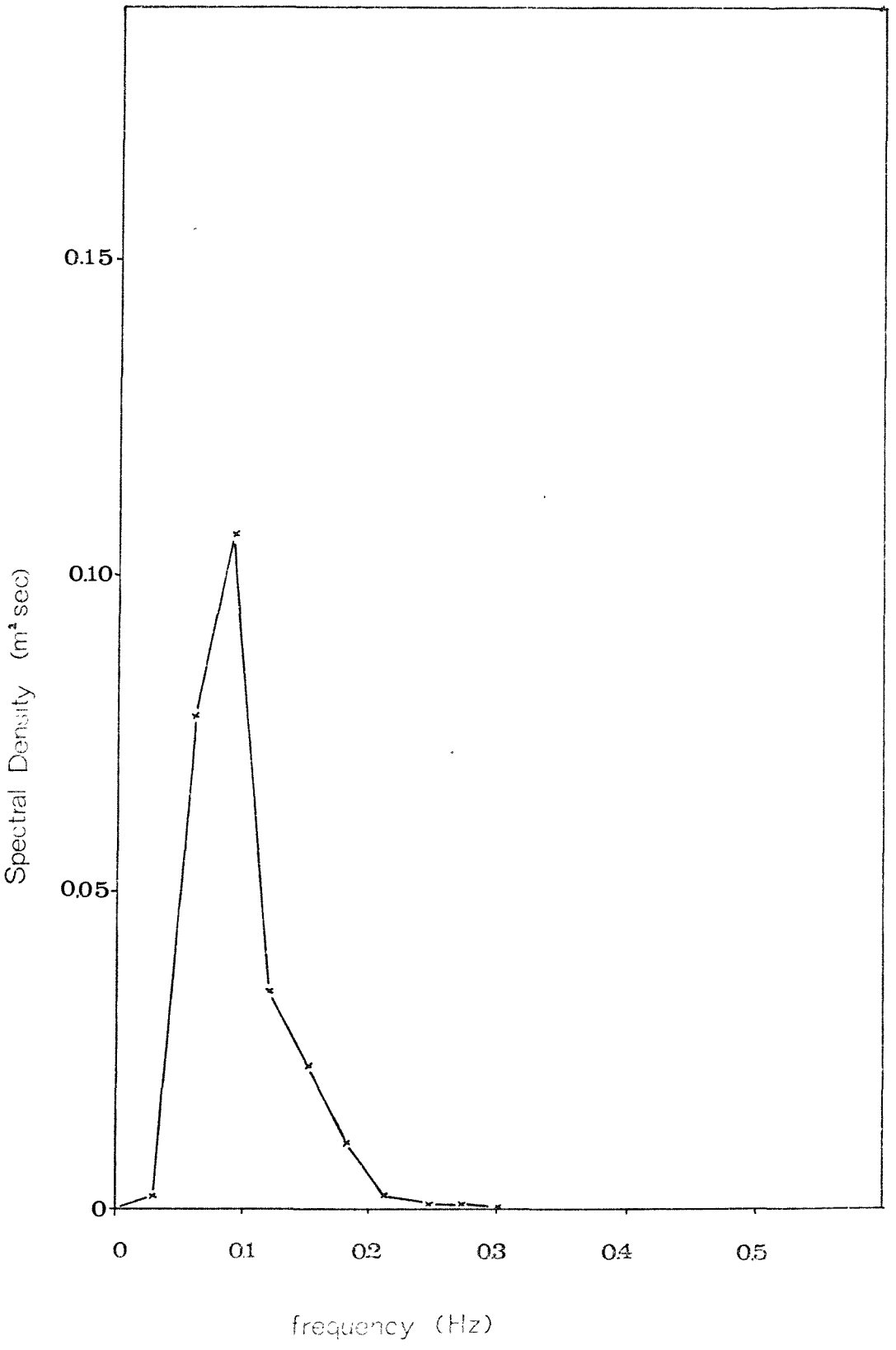

FIG. 3.18 Power Spectrum for Sortie 5A

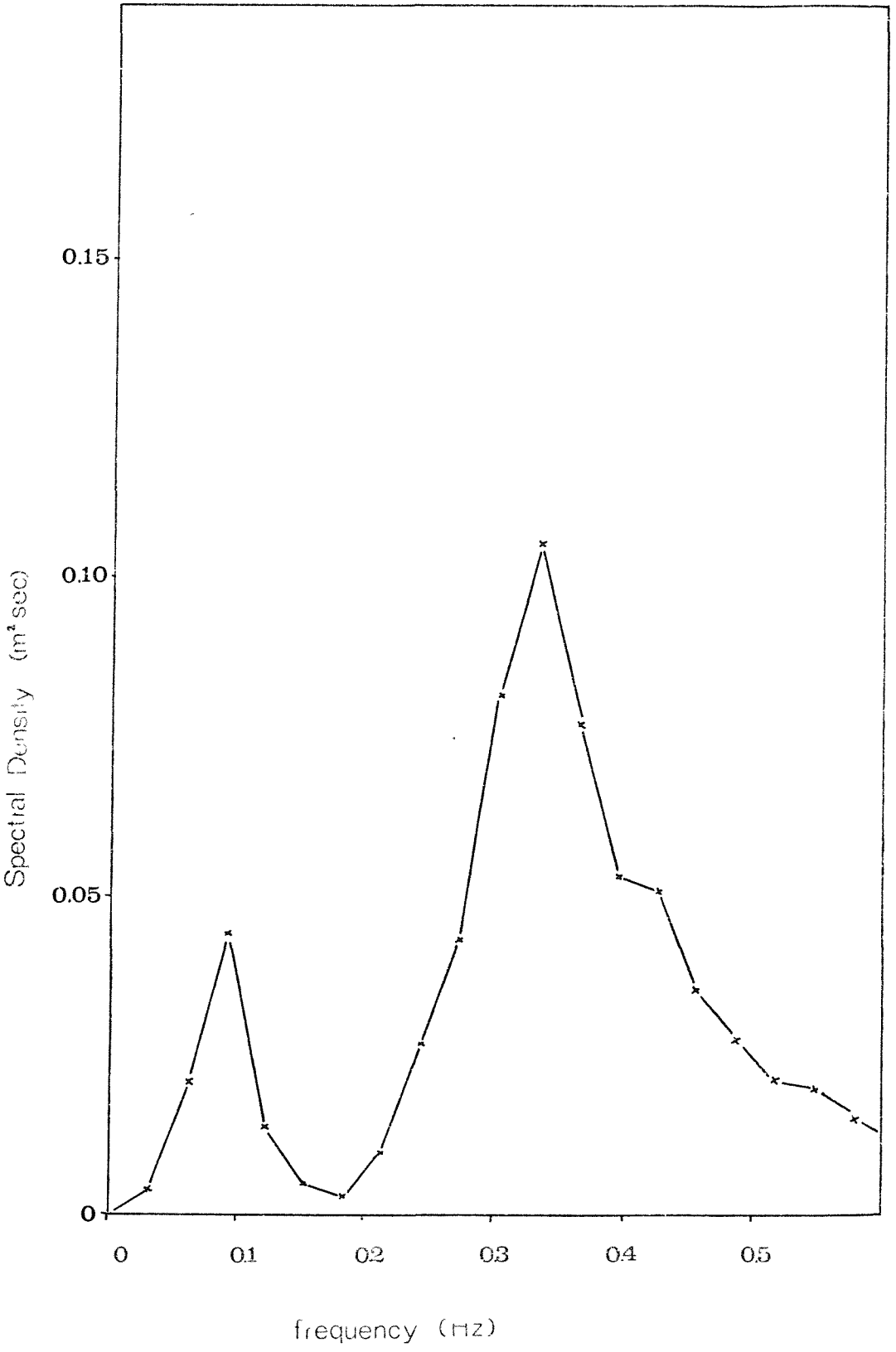

FIG. 3.19 Power Spectrum for Sortie 6A

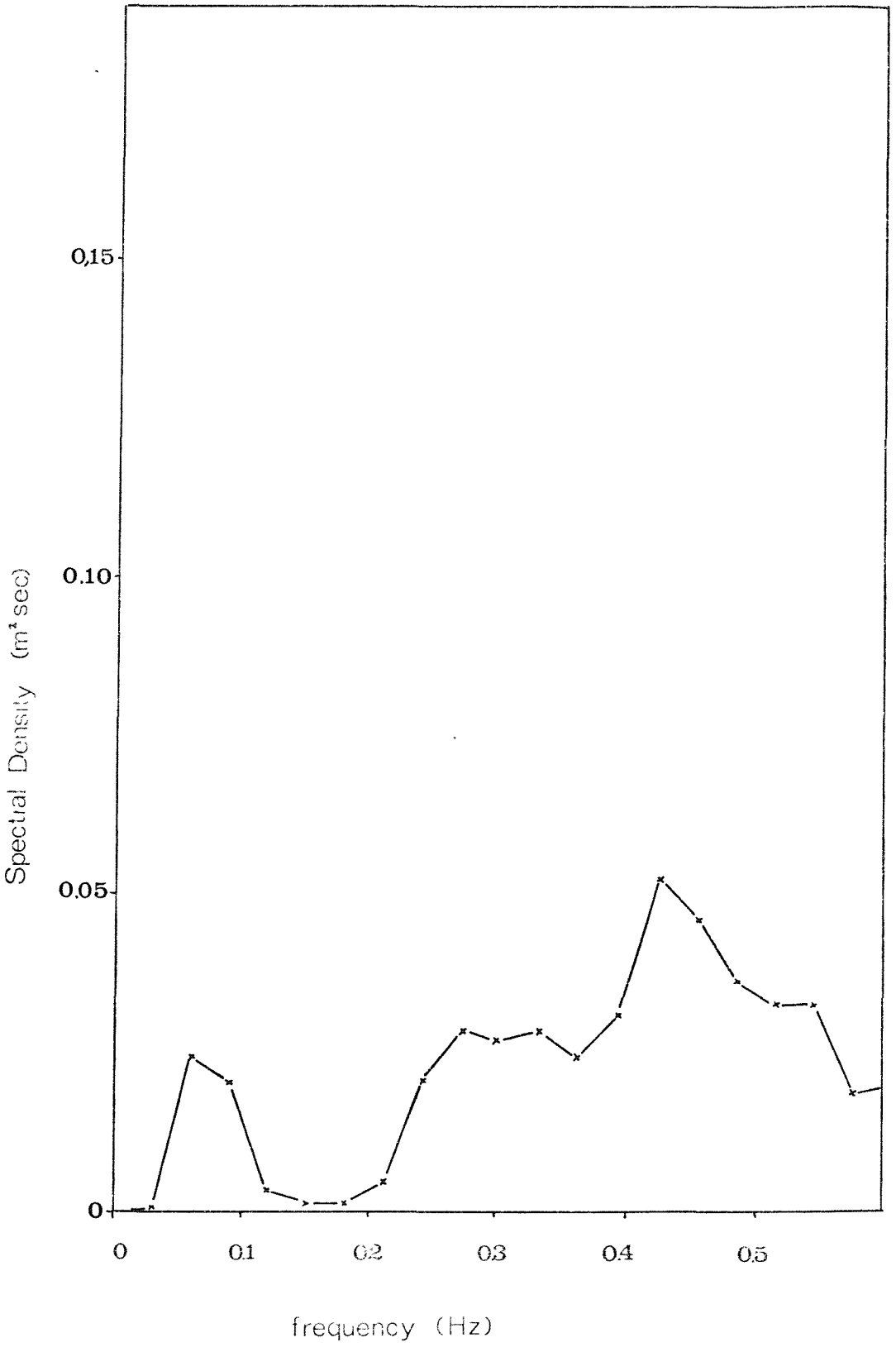

FIG. 3.20 Power Spectrum for Sortie 6B

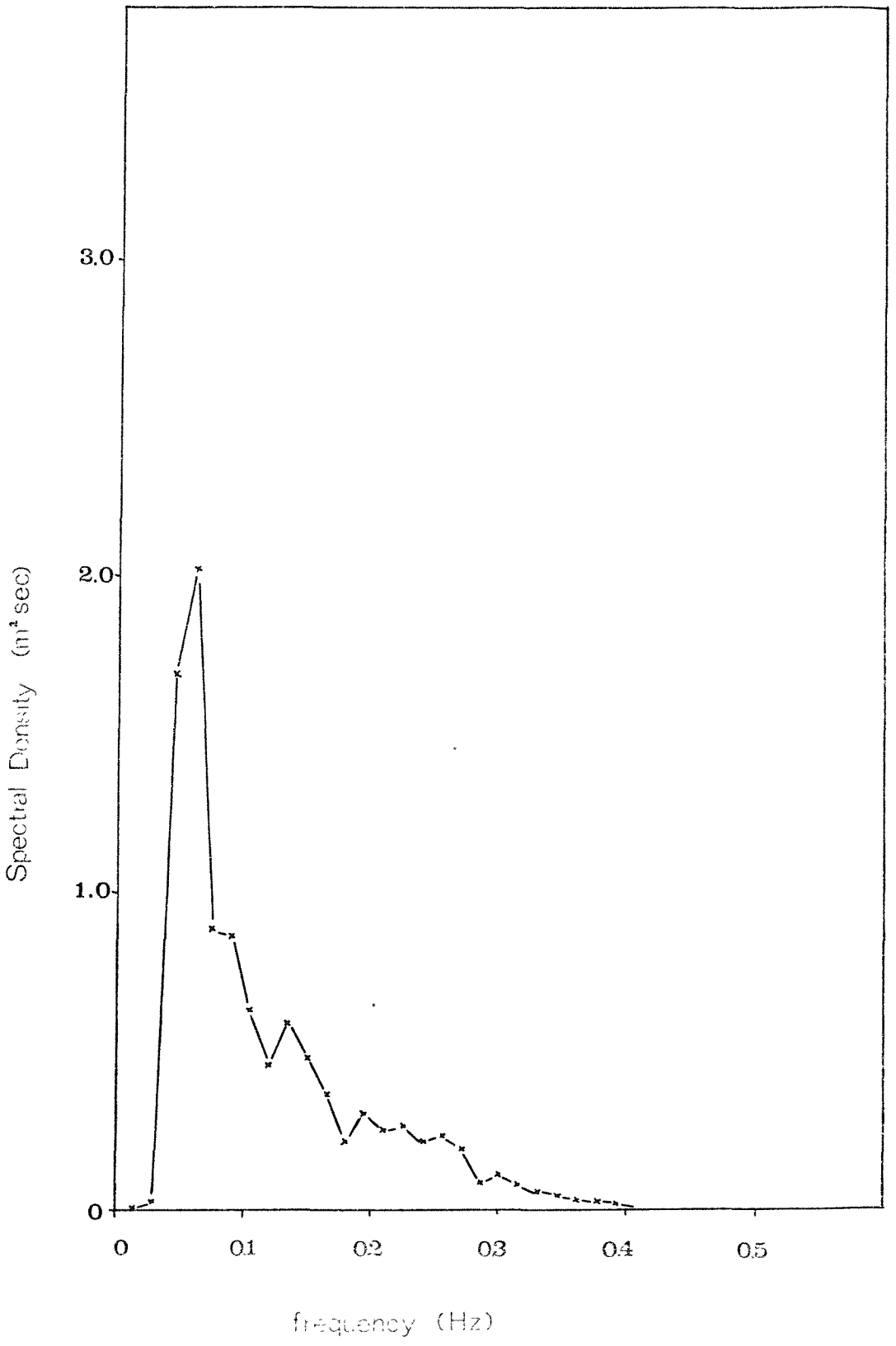

FIG. 3.21 Power Spectrum for Sortie 11

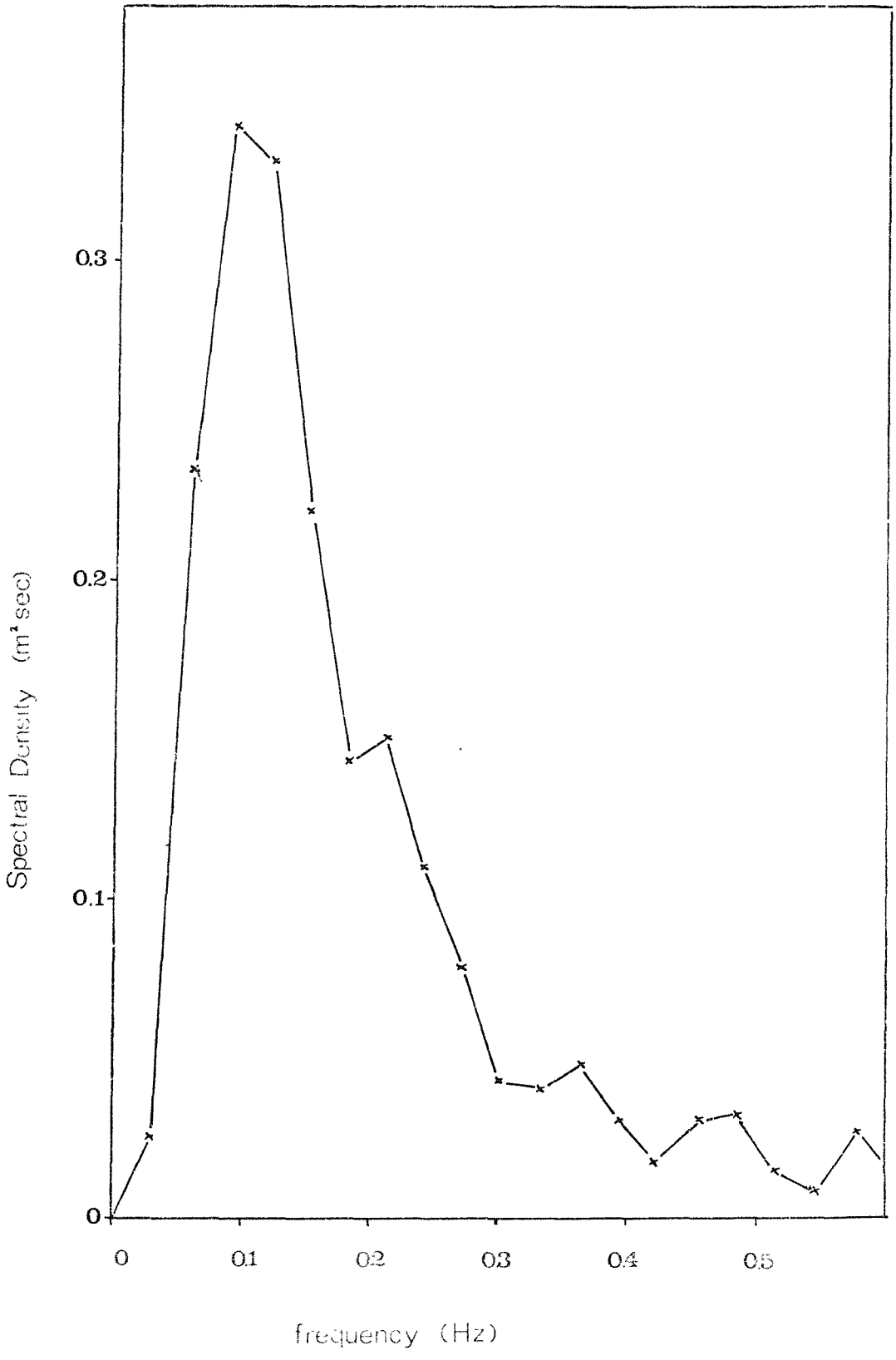

FIG. 3.22 Power Spectrum for Sortie 12A

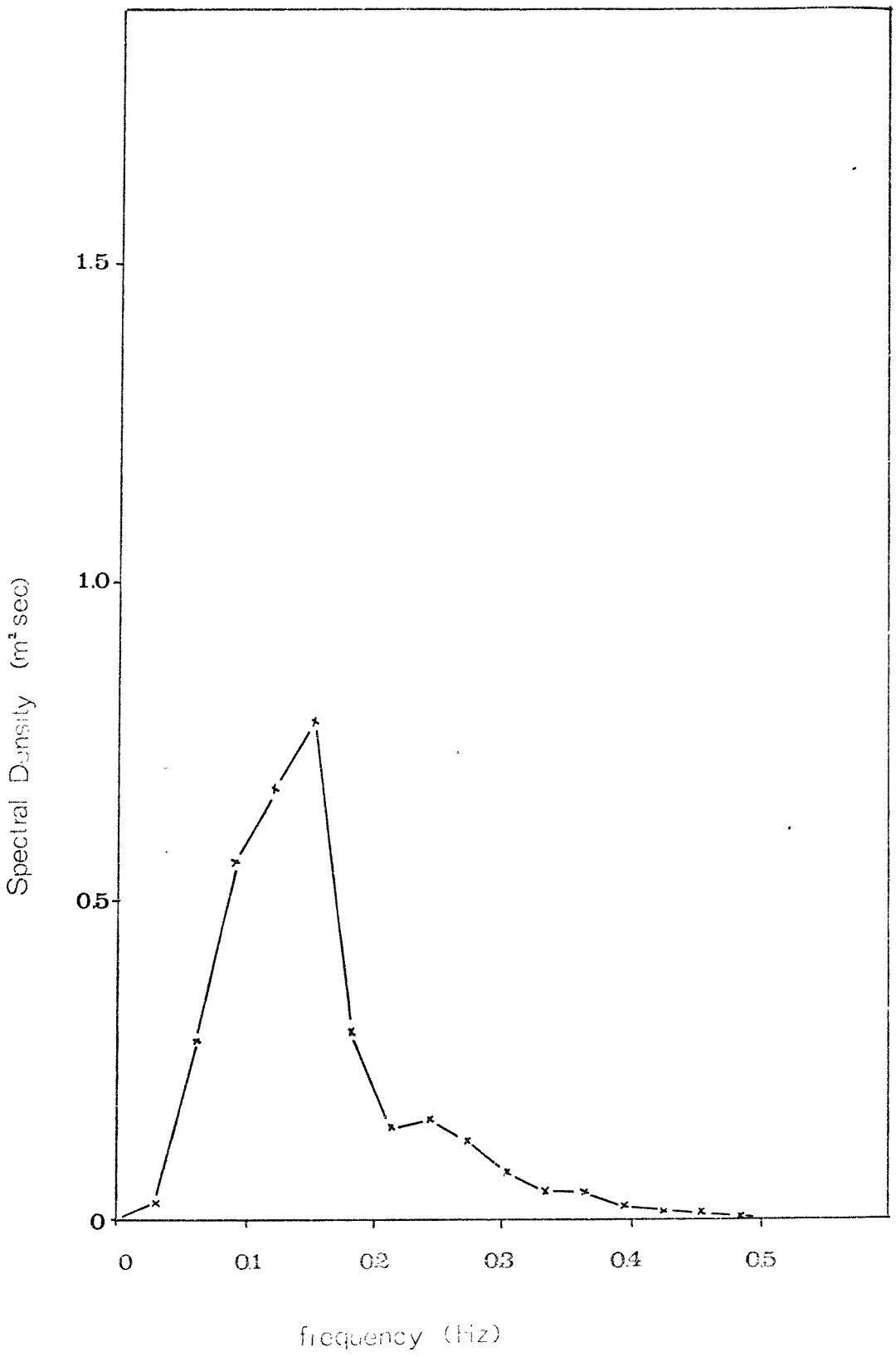

FIG. 3.23 Power Spectrum for Sortie 12B

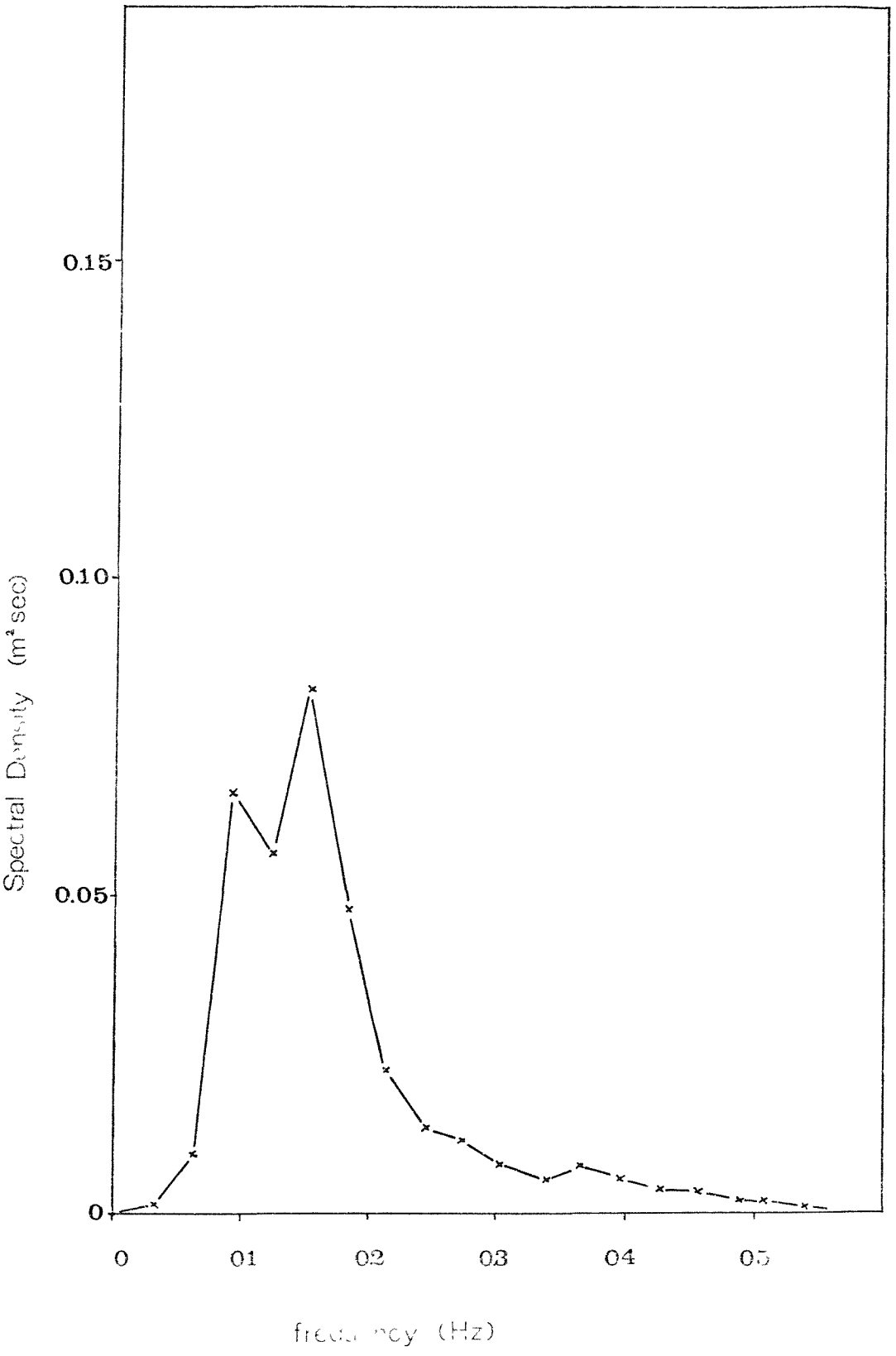

FIG. 3.24 Power Spectrum for Sortie 14

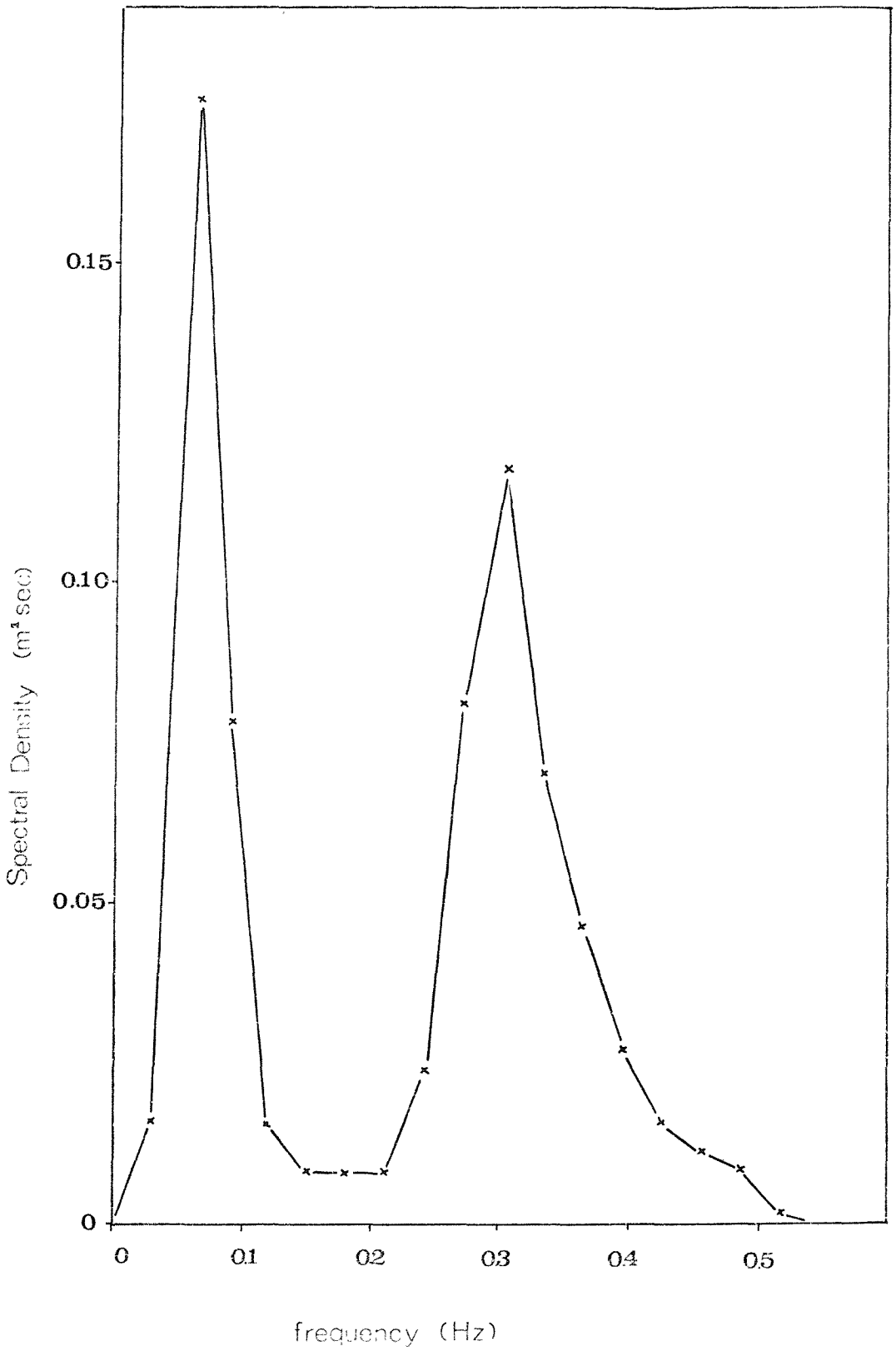

FIG. 3.25 Power Spectrum for Sortie 15A

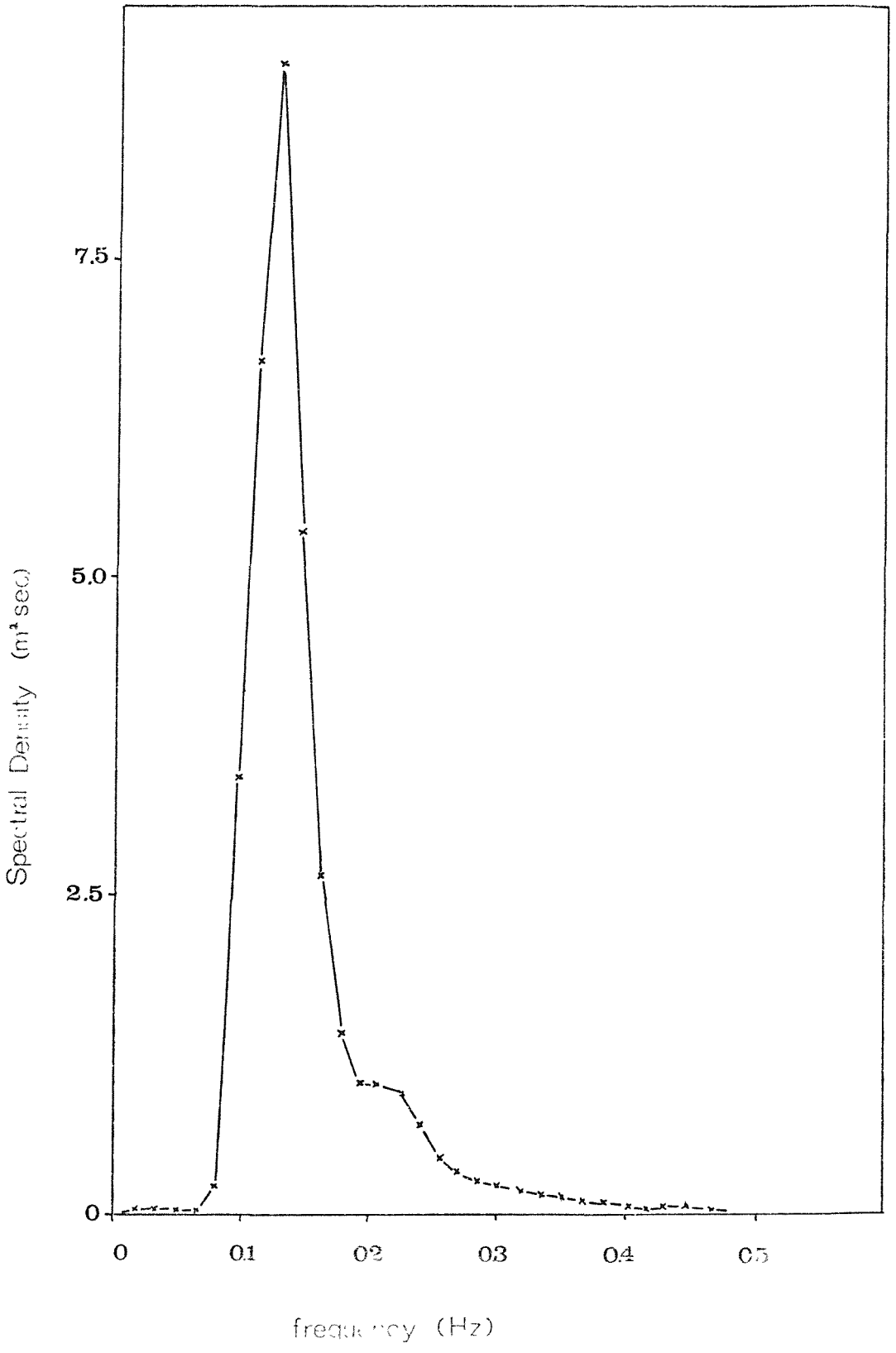

FIG. 3.26 Power Spectrum for Sortie 15B

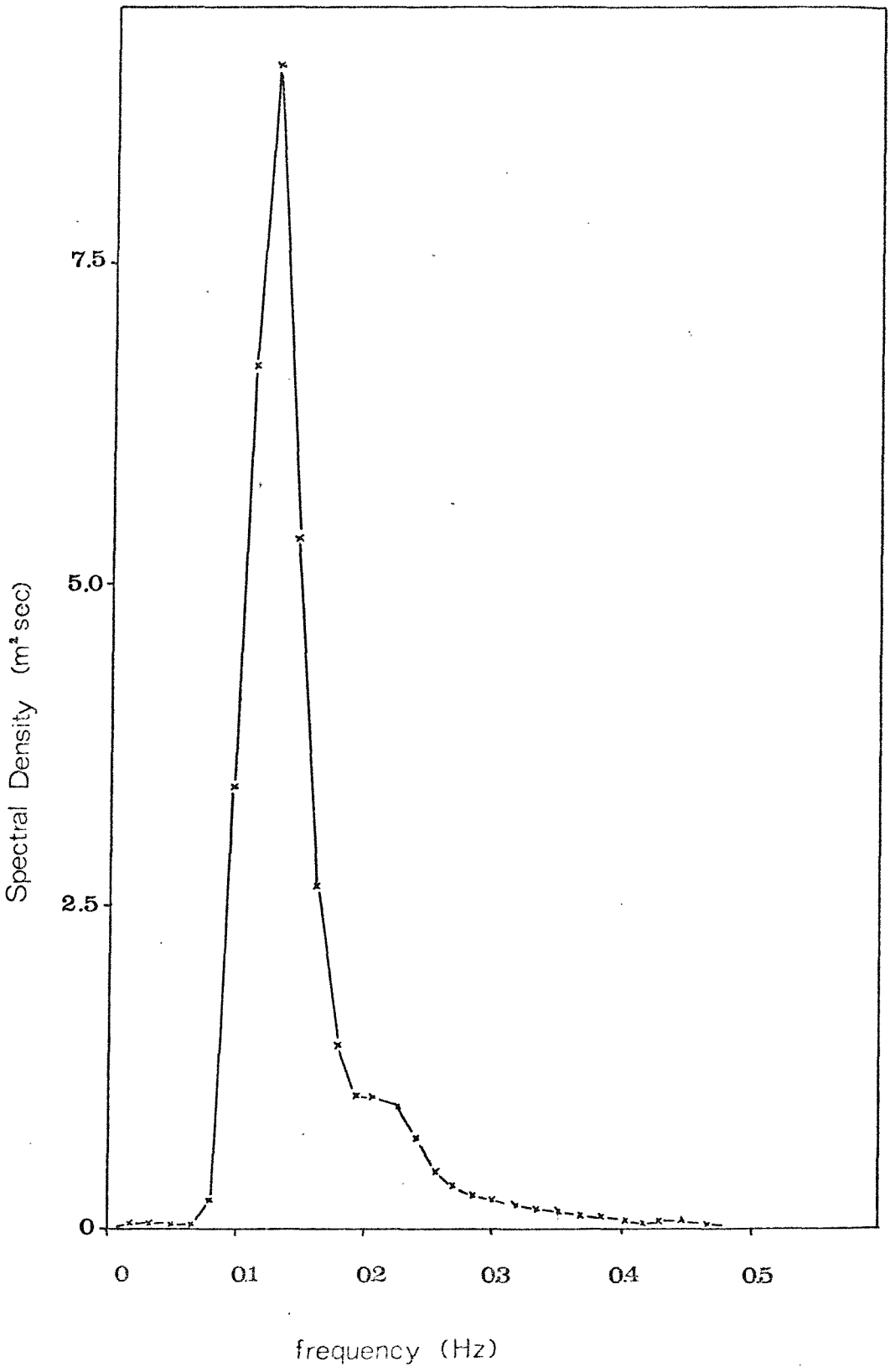

FIG. 3.27 Power Spectrum of Record N1.

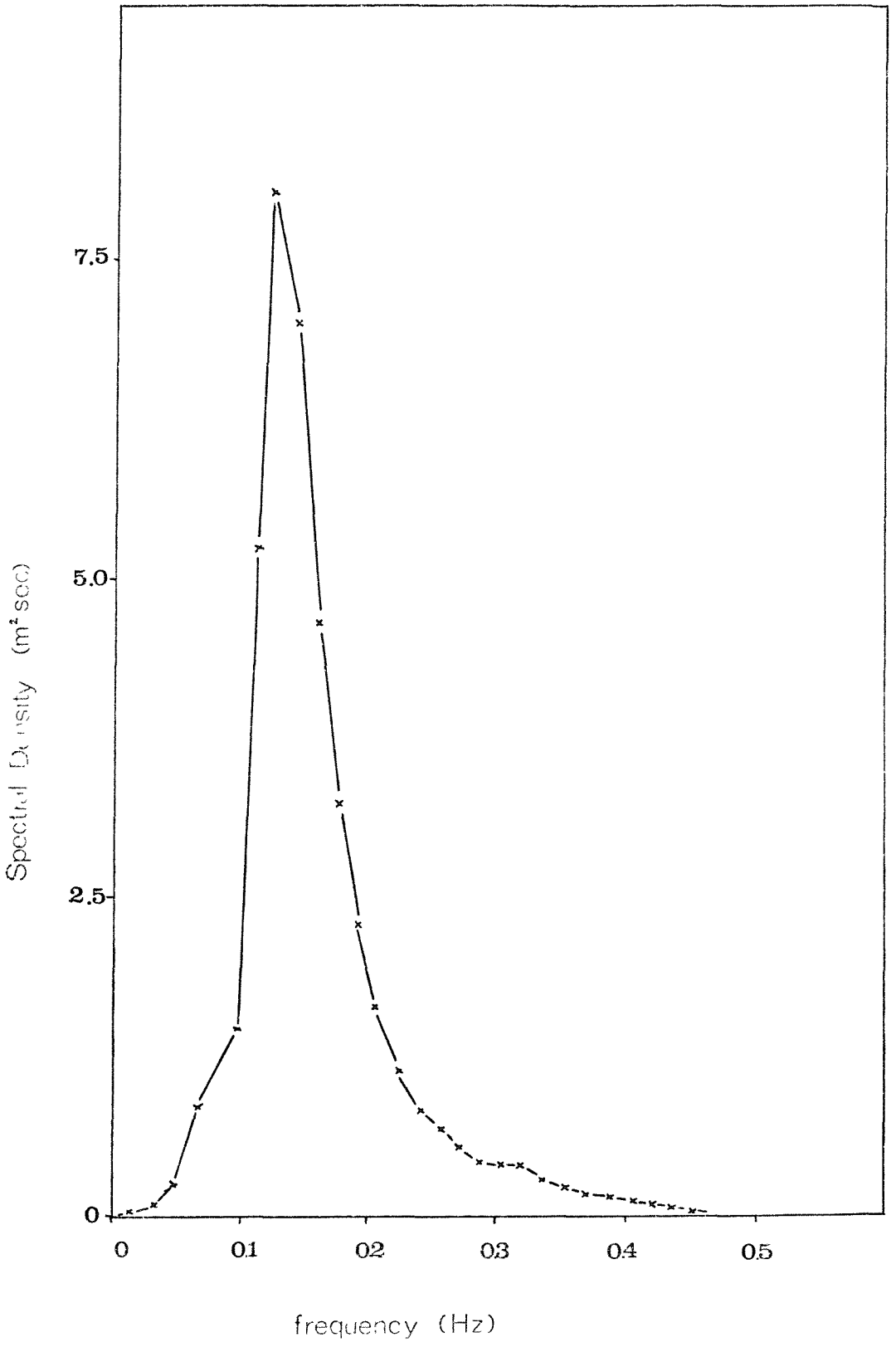

FIG. 3.28 Power Spectrum for Record N2.

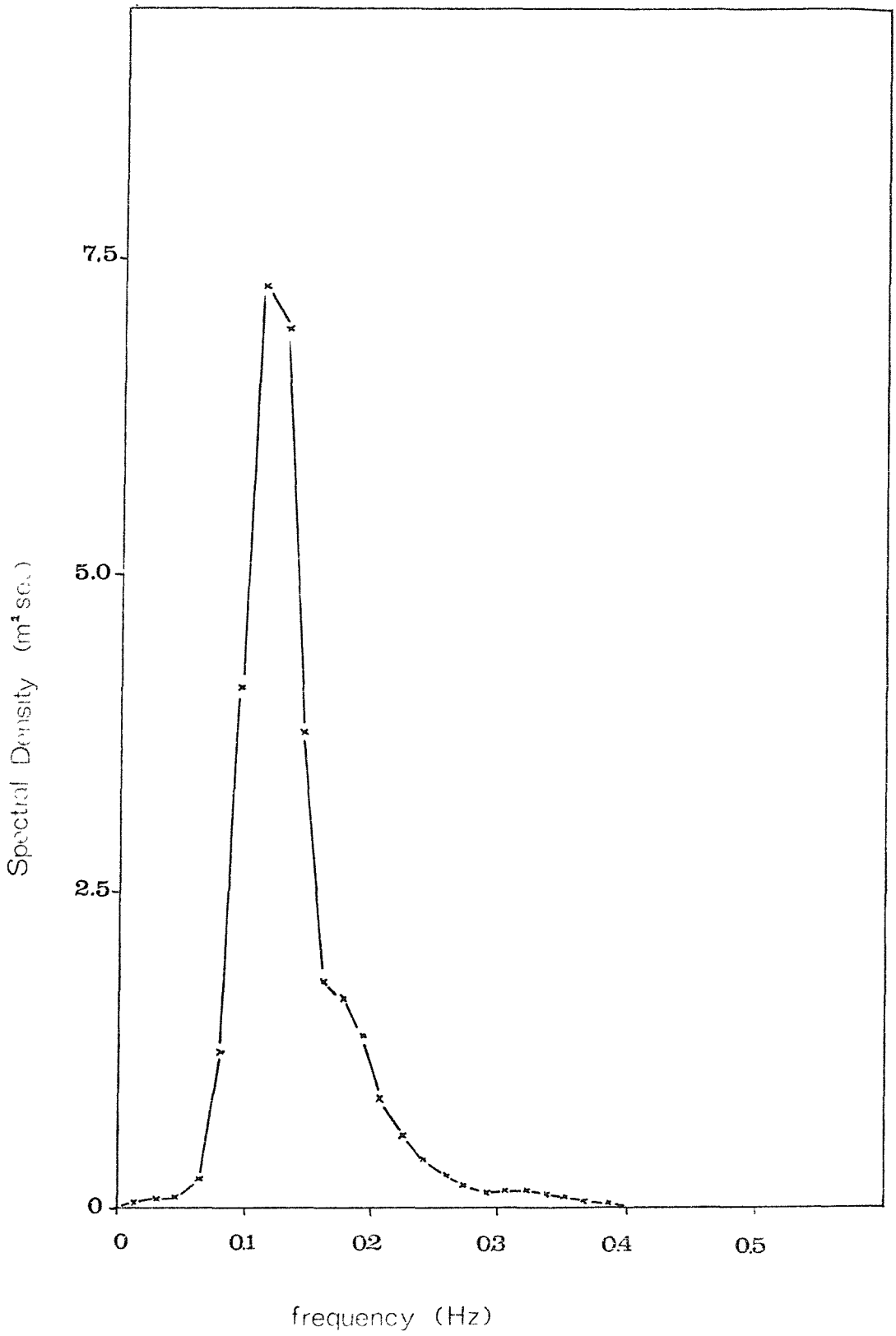

FIG. 3.29 Power Spectrum for Record N3.

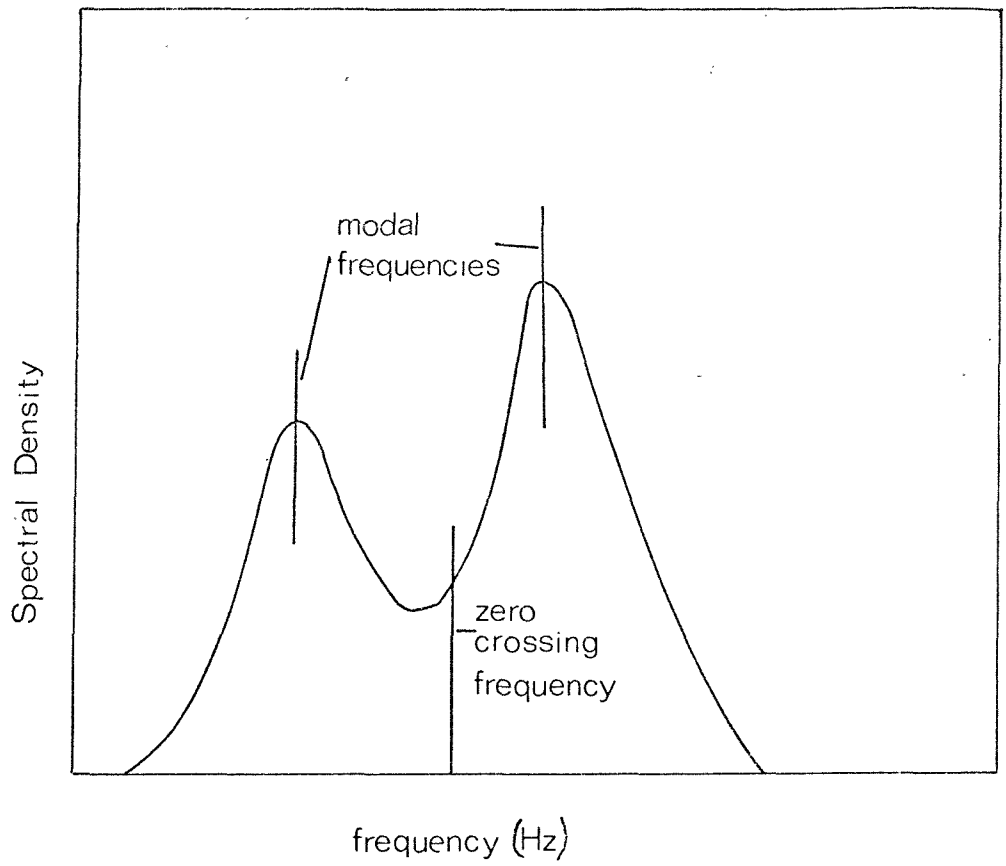

FIG. 3.30 Misrepresentation of the Spectrum by Zero Crossing Frequency

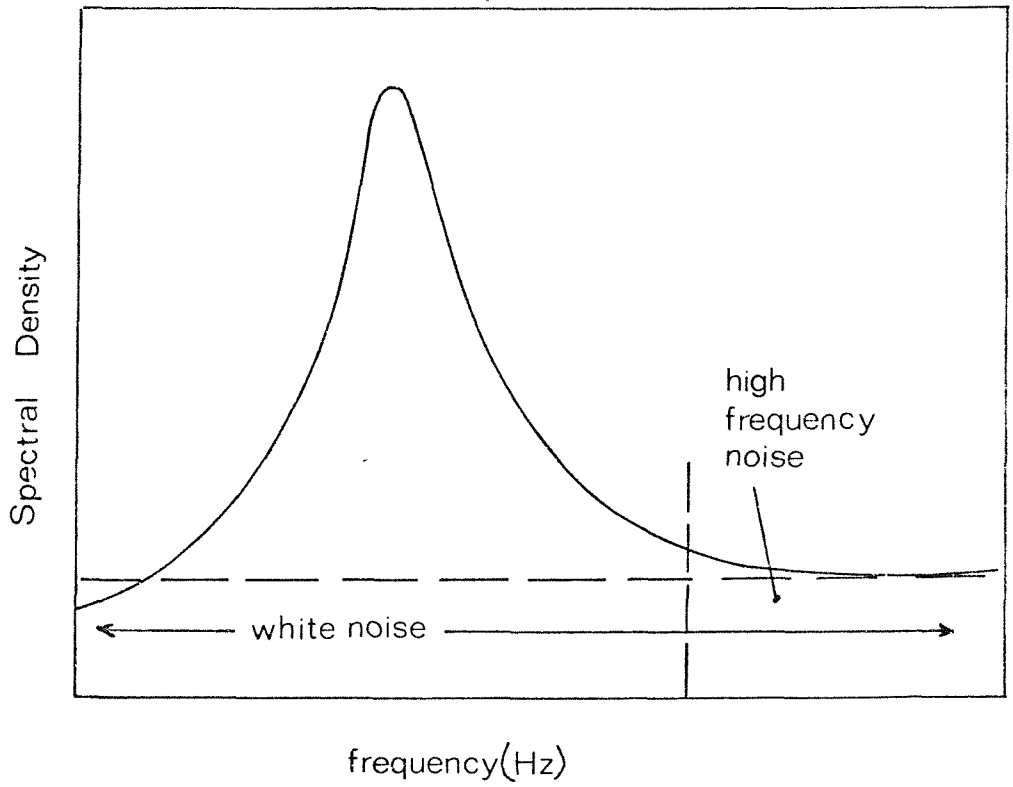

FIG. 3.31 Noise in the Spectrum

4. DESIGN AND CONSTRUCTION OF THE WAVE GENERATOR

4.1 Reproduction of 'sea state' in the Laboratory

The object of the sea state simulation is to be able to model a given spectrum of coastal waves. The spectrum is chosen as the modelling criterion since it may be postulated that only the spectral properties are unique to one sea state. For a given spectrum the statistical properties may be unique, whereas the converse is certainly not true.

The restriction to coastal waves is merely due to the fact that the civil engineer is usually concerned with inshore waters (the notable exception being North Sea Oil rigs). Coastal waves are generally thought of as being those which have a length less than twice the depth. However, the spectra of coastal waves certainly contain deep water waves due to the action of local winds, although their energy compared with the predominant waves in the train may be almost negligible.

This question of the classification of waves to be modelled is an important point for consideration with respect to the type of wavemaker to be used. Common types of wave maker are the piston type, hinged flap, plunger and pneumatic. The piston and hinged flap are the simplest to deal with, the former being suited to production of relatively short waves and the latter for relatively long waves. This arises theoretically from a study of the particle motions of these two extremes of wave length - the shorter the wave

the greater is the attenuation of particle motion with depth. The interest in irregular waves has lead to the need to model both types of wave in the same channel. To meet this requirement a double acting wave generator has been developed, but not reported on extensively, by Delft Hydraulics Laboratory. It consists of a hinged paddle, the hinge of which is on runners. Thus the paddle may act as a piston or hinged paddle, or any mixed condition in-between. In effect, it may be theoretically possible to produce the wave maker motion to suit the exact wave condition that is desired.

An alternative method has been developed by the Hydraulics Research Station, Wallingford, which consists of a wedge sliding along an inclined plane. In this method the depth of forced particle motions is proportional to amplitude. A third novel method reported by Goda and Kikuya (1964) consists of a piston wave generator acting from beneath the channel. Ideally, waves reflected from a structure under test pass over the wave generator and are absorbed by a wave beach. However, a proportion of the wave will be reflected by the sudden change of cross section. If designed to minimise this reflection, the method may prove to be a very desirable approach for short channels as it would avoid secondary reflection from a conventional paddle.

A piston type paddle was chosen for this investigation, because of the need to model predominantly coastal waves and the inherent simplicity of the system. Having decided upon the type of paddle to be used, it remains to select motivation. For irregular waves, oil hydraulics are the obvious choice, the only real

alternatives being an electrical servo-system or perhaps a linear motor. The oil hydraulics has advantages of fast response and ease of control, whilst little is known about linear motors. Further, the use of oil hydraulics to drive a wave maker is not new, and, in fact, they are becoming the most common method of motivation.

Before designing the electro-hydraulic servo-mechanism, it is necessary to set the design criteria of velocity and force to be provided by the mechanism. The velocity and force depend upon the wave to be produced. For sine waves, the velocity is simply the first derivative of the motion and the force required may be estimated from the equations provided by Biesel (1951). It was desired to produce a range of frequencies between 0.2 Hz and 3.0 Hz and an amplitude of, say, from zero to 15 cm. The worst conditions were envisaged as being for maximum water depth (35 cm.) for the estimation of force, since the effective paddle area is larger, and for minimum water depth (say 12 cm.) for the velocity consideration, since a lowering of water depth requires a greater stroke to provide the same wave height at a given frequency. An estimate of the worst conditions likely indicates that a maximum velocity of the order of 30 cm./sec. and forces of less than 450 N may be expected for the regular waves. Provision must be made for the production of irregular waves and to this end, the only real method of estimating the design criteria is by a computer simulation of the typical spectra to be produced and determine the worst conditions of velocity and load produced by the combination of various wave components. Gilbert et Al (1970) provides design curves for

irregular wave generators based on a simulation of the Moskowitz type of spectrum. However, this document was not available at the time of design. As a result, a conservative estimate of the final design criteria of velocity (45 cm./sec. maximum force of 450 N and stroke of 45 cm.) was made.

4.2 Design of the Electro-Hydraulic Servovalve System

The design of the paddle actuating the system was conducted in three stages:

1. Select power supply, servovalve and actuator in order to ensure capability of performing required load dynamics.
2. Select control system and feedback to ensure best possible servo performance in respect of accuracy and response.
3. Check should be made on stability in respect of system gain and cross-over frequency.

4.3 Selection of Servovalve, Actuator and Power Supply

The characteristics required in the final paddle motion were that of moderate response and low loads. This favoured an actuator of small annular area - the actual size being determined by availability of a suitable device, rather than a mathematical derivation. It is usual to select the supply pressure such that it is 1.5 times the load pressure required at maximum load, since this results in a maximum power transmission to the piston. However, with the loads involved in this problem and the area of the actuator, this resulted in a very low supply pressure.

A high supply pressure is desirable from the point of view of achieving a high power output from a lower flow rate, resulting in a smaller power supply and shorter lines, valves and oil supply. In addition faster response is more readily available with a high pressure system. A compromise solution was arrived at (again partly governed by commercial availability) with a power unit capable of producing a pressure of 2000 psi (13.79 N/mm^2) and a flow of 1 gpm (4.546 lpm). The supply to be used in operation would be 1000 - 1500 psi (6.89 - 10.34 N/mm^2). The fluid used is Tellus 23.

Whereas all measurements in this thesis were taken in metric units, it was more convenient to specify the hydraulic requirements in imperial units, since these were used by the manufacturers. In all cases, the metric equivalents are given.

The hydraulic power supply consists of an electric 3-phase motor connected to a fixed displacement oil pump. The pump is immersed in its own oil supply to provide quiet running. A relief valve controls the supply pressure which can be monitored on a pressure gauge. A ten-micron filter is incorporated in the supply line to protect the servovalve. The return line vents directly into the sump, although there is provision for this to be water-cooled. The whole unit was placed outside the laboratory to reduce the noise level and the 3-phase motor is controlled remotely at the wave generator. A system diagram is shown in Fig. 4.1 and a photograph in Plate 4.1.

4.4 The Actuator and Servovalve

The actuator was to be of the balanced, double-ended variety. This meant that a central piston had an equal area on both sides and that the rod passed through both ends of the cylinder. As a result, the control circuitry would be simplified by having equal responses in either direction.

A major problem was that of the length of actuator rod required. This, coupled with the fact that a small annular area meant that an 'off-the-shelf' item was not suitable, since small area actuators had rods which were too small in diameter to be free from deformation due to buckling and bending. Conversely, actuators with adequate rod diameter had too large an area which would require too large a flow rate for reasonably efficient operation. Consequently, Hydromuscle Ltd. were commissioned to produce a special actuator with a suitable rod diameter and annular area.

The rod diameter was 0.875 in. (1.91 cm.) and the cylinder diameter 1 in., resulting in an annular area of 0.184 in.^{2} (1.19 cm.^{2}). The effective length was 18 in. (45.7 cm.).

The specification of the actuator is such that a servovalve delivering 1 gpm (4.54 lpm) at 1000 psi (6.89 N/mm^2) would be adequate for the required response. A Moog servovalve, type 76, was selected to comply with this requirement.

The Moog 76 - 100 is a two-stage electro-hydraulic servovalve incorporating a polarised electrical torque motor operating a flapper pilot stage. The motor armature is supported by a flexure tube

member which also acts as a seal between the electro-magnetic and hydraulic portions of the valve. The flapper of the first stage is rigidly attached to the armature and passes through the flexure member (see Fig. 4.2). Pressure from two nozzles is controlled by the flapper by varying the orifices between the nozzle tip and flapper. The pressure thus controlled is fed to the ends of the second stage spool. A conventional four land spool valve forms the second stage giving an output flow which, at a fixed valve pressure drop, is proportional to spool displacement from the null position. A feedback spring is attached to the flapper and engages the centre slot in the spool. The operation of the valve is briefly as follows. An input current in the coils of the motor induces a magnetic field in the armature and deflects the armature and flapper, the assembly pivoting about the flexure tube. This increases the size of one nozzle orifice and decreases the other, thus causing a differential pressure on the spool. The resulting spool displacement causes a torque in the feedback wire which opposes the original input signal. Spool movement ceases when feedback wire torque equals the input signal torque. The natural frequency of the valve is 140 Hz and has a damping ratio of 0.9. Load flow-pressure characteristics are essentially parabolic, and the flow gain is essentially linear from $\pm$ 5 per cent to $\pm$ 80 per cent of rated current. In the region of $\pm$ 5 per cent rated current from null the flow gain may vary from 50 to 200 per cent of the nominal gain (Fig. 4.2), depending on the tolerances of the particular valve.

4.5 Control System Design

Before considering the detailed design of the control system for the actuator and valve concerned, it is worth discussing the fundamentals of feedback control systems. Essentially, a feedback system is characterised by a system in which the output from a dynamic unit has an effect upon the input quantity, as opposed to an open-loop system, where no such effect is observed. A typical example of an open-loop system is a d.c. shunt motor where a given voltage produces a given motor speed. The command signal in this case is the desired motor speed which is processed by a reference selector (potentiometer) before this reference input is applied to the dynamic unit (armature) to produce the desired output (speed). Conventionally block diagrams are used to represent control systems and the system described above is illustrated in Fig. 4.3(a).

A closed-loop control system on the other hand employs a feedback device, in which the output is represented by a mechanical or electrical quantity. This is compared with the reference input as shown in Fig. 4.3(b). Thus, the comparison between output and reference results in an actuating signal which is the difference in these quantities and acts in a manner to maintain the output at the desired value. The advantage in using a closed-loop system is that the output quantity may be controlled via the feedback in a manner more precise than an open-loop system and, if the system is well designed, almost independently of the load dynamics.

The mathematical analysis of control systems is complicated, involving the dynamics of all the control elements and formulation

of the differential equiations applying to the system. However, a simplified approach provides a useful guide to the system performance. Fig. 4.3(c) shows a block diagram of a control system. The control ratio is defined as the ratio of the controlled variable C to the reference input R. These quantities, together with the transfer function for the dynamic elements are expressed in terms of the Laplace transform variable 's'. The actuating signal E(s) is equal to the reference input R(s) minus the feedback signal B(s). G(s) and H(s) are the transfer functions of the forward and feedback elements respectively. The system may be described by the equations:

$$\begin{aligned} C(s) &= G(s)\ E(s) \\ B(s) &= H(s)\ C(s) \\ E(s) &= R(s) - B(s \end{aligned} \qquad (4.1)$$

combining these produces the control ratio or system function.

$$\frac{C(s)}{R(s)} = \frac{G(s)}{1 + G(s)\,H(s)} \qquad (4.2)$$

The denominator of this equation is the characteristic equation $1 + G(s)H(s) = 0$ and determines the stability and response of the closed-loop system. The open-loop transfer function is defined as the ratio of feedback to actuating signal $B(s)/E(s)$ and the forward transfer function as $G(s)/E(s)$. The simplest case is that of unity feedback where $H(s) = 1$.

The forward transfer function may be made up of simple dynamic elements or complex systems with several internal feedback loops. A generalised expression for the open-loop transfer function is

$$G(s) = \frac{K_n (1 + a_1 s + a_2 s^2 + \ldots\ldots + a_\omega s^\omega)}{s^n (1 + b_1 s + b_2 s^2 + \ldots\ldots b_u s^u)} \qquad (4.3)$$

where a_i, b_i are the constants and K_i is the overall gain of $G(s)$. The system type is designated by the order of the exponent n of s, for example, when $n=0$ the system is designated a Type 0 system. The various types of system exhibit particular properties:

Type 0 - A constant actuating signal results in a constant value for the controlled variable.

Type 1 - A constant actuating signal results in a constant rate of change of the controlled variable.

etc.

The control system for the wave generator was designed to be as simple as possible bearing in mind the required accuracy and frequency response. A system with unity positional feedback was envisaged. The feedback element used was a linear displacement transducer which produced a voltage proportional to position. Manufactured by Sangamo Controls, the transducer was a linear variable differential transducer (LVDT) with a built-in oscillator and detector, and requires only a DC voltage for operation. The output depends upon the load impedance and is linear to an accuracy of 1 per cent. The transducer in effect acts as a reference for the position of the paddle since, by applying a particular voltage to the control system, the paddle will tend to move to the point corresponding to the given voltage. The electronic control element is provided by

means of a Moog servo-controller. Essentially, this consists of two operational amplifiers and a power supply. The first amplifier acts as a comparator between the command signal and the feedback signal, and the second amplifier provides voltage to current conversion to drive the Moog valve via two power transistors. Overall gain may be varied over a 100:1 range. The current output to the valve is proportional to the error signal and, since the load flow of oil is directly proportional to the current, the volume of oil flowing to the actuator is essentially proportional to the error signal. Having selected the components of the control system it remains to check the stability of the system. This involves the explicit description of the components parts and a formulation of the forward transfer functions of the valve actuator combination and the feedback and control circuits. The dynamics of the valve actuator combination is very complicated and a detailed analysis is given by Merrit (1967).

The system block diagram is shown in Fig. 4.1, but it should be noted that this is a simplified version. A complete analysis of the system must take into account:

1. The dynamics of the electronic control system.
2. Servovalve dynamics.
3. Piston and load dynamics, leakage and compressibility effects.

Each of these has its own open-loop gain function characterised by a gain factor, natural frequency and damping ratio. By neglecting lesser effects a simpler expression may be derived which eases component selection. In fact, the lowest natural frequency of the

system controls the stability. This is, in practice, found to be that of the valve-piston-load combination. Thus, a forward transfer function may be derived which should be valid in most cases, and has the form:

$$G(s) = \frac{K}{s\left(\frac{s^2}{\omega_h^2} + 2\frac{\delta_h}{\omega_h}s + 1\right)} \qquad (4.4)$$

where the hydraulic natural frequency $\omega_h = \sqrt{\frac{4\beta_e A_p^2}{V_t M_t}}$

and the damping ratio $\delta_h = \frac{K_{ce}}{A_p}\sqrt{\frac{\beta_e M_t}{V_t}} + \frac{B_p}{4A_p}\sqrt{\frac{V_t}{\beta_e M_t}}$

where K_{ce} - total flow pressure coefficient including leakage,

B_p - viscous damping coefficient of piston and load,

V_t - total volume of flow lines and piston,

β_e - bulk modulus of fluid, K - open-loop gain constant,

A_p - annular area of piston, M_t - mass of piston and load.

The free 's' in the denominator of the above equation indicates integration and that the system is of Type 1. Hence, the positional error will be zero. D'Azzo and Houpis (1966) describe in detail the accuracy and stability of such systems by a variety of methods. Since the parameters of the system may be varied, the Bode diagram was chosen as the most convenient method of stability analysis for this system. By formally substituting $j\omega$ for s in Equation 4.4, the diagram shown in Fig. 4.4 may be obtained. From this, it is possible to establish various stability criteria.

1. The gain for $\omega = \omega_h$ must be less than unity which leads to the criteria $\frac{K}{\omega_h} < 2\delta_h$

2. The crossover frequency is the maximum frequency where closed-loop control is available. Above this frequency the loop gain is less than unity.

3. Since the crossover frequency is approximately equal to K and since the slope of the curve is - 1, K is limited to being somewhat less than ω_h

By substituting numeric values into the expression for the natural frequency, an estimate of 20 Hz was made for this parameter. Although not in the range of operation it was rather low and might limit the gain excessively. The overall gain for the system could be varied over a range 1.42 to 142 sec.$^{-1}$. From criteria 2 and 3 above, the maximum usable gain was of the order of 100 sec.$^{-1}$. From the open-loop gain constant an estimate of the velocity lag may be made. For example, if the gain is 50 sec.$^{-1}$ the error will be 0.6 cm. at a velocity of 30 cm./sec. Naturally, the open-loop gain affects the frequency response functions of the overall system. For ease of operation it is desirable to have a flat frequency response in the range of operation. However, since in all systems there is energy dissipation and there are energy storage elements, this is seldom achieved without compensating elements. The gain required is thus the maximum available consistent with stability. Bearing in mind that the parameters evaluated above were approximations, it was decided to construct the system as designed and evaluate the performance before considering further modifications to improve this. In practice, the system performed satisfactorily and only slight improvements were envisaged.

4.6 Construction and Evaluation

The actuator valve and feedback transducer were mounted on top of the channel on a piece of aluminium 0.25 in. (0.635 cm.) thick with drip trays for the expected seal leakage, as shown in Plate 4.2. The actuator was connected to the paddle via a spherical bearing, a similar arrangement being used for the transducer which was mounted independently above the actuator. A mounting block was provided for the valve remote from the actuator. The hydraulic power pack was located outside the laboratory and 0.25 in. (0.635 cm.) armoured hose used to supply oil to the valve.

Commissioning consisted of firstly flushing the system using a flushing plate in place of the valve in order to remove foreign bodies, without any risk of damaging the fine clearances in the valve. The flushing plate was then replaced by the valve and this was operated by a 1.5 volt battery to provide full port opening whilst the actuator was bled to free trapped air. Finally, the control system was connected to the valve and operated on a low gain.

Performance evaluation was considered in three stages: sinusoidal response, step response and impulse response. Sinusoidal response was investigated using a sine wave generator, frequencies of 0.1 to 3 Hz were considered using a system gain varying between 14 and 60 $sec.^{-1}$. For a gain of 20 $sec.^{-1}$ the motion of the paddle was smooth to the eye over a frequency range of 0.3 to 3 Hz. Below this a slight judder was noticeable near the end of the stroke after changing direction. The effect was more noticeable in one direction and increased with decreasing stroke. A trace from the feedback transducer was produced

on the UV recorder and Fourier analysed for a variety of conditions. A selection of these traces are shown in Fig. 4.5. The judder effect is shown clearly, the magnitude being of the order of 1½ per cent, with a frequency of approximately 10 Hz. This effect should not be given too much importance since from the traces it may be seen that it is very small. The traces were digitized so that the Nyquist frequency was of the order of 10 times the fundamental frequency. This was done by hand, since the length of record required must be one cycle. Computation of the Fourier series components (in terms of amplitude and phase) was performed on the Civil Engineering Department's Wang computer. The higher harmonics were calculated as a percentage of the fundamental and Table 4.1 gives the proportion of 2nd and 3rd harmonic, the remainder being negligible. In all cases, the 2nd and 3rd harmonics are less than 2 per cent and 3.2 per cent respectively. The accuracy of the signal generator being 2 per cent in this respect. The traces also show up a slight flattening at extreme ends of the movement, this being due to the valve changing direction. The response curve of the valve gives some insight into the judder and flattening effects. At valve openings corresponding to less than 5 per cent of rated flow, the gain is non-linear and may lie in the range 50 - 200 per cent of the rated gain. Thus, at or near the null position control will be very imprecise, i.e. the valve may effectively change from shut to slightly open suddenly, so that for low velocities and low valve openings, the valve may open and close alternately, thus producing a juddering motion. An approximate calculation showed that for the flows required (for the velocity) where judder was encountered,

the flow through the valve was in the non-linear region. In effect, there is a region of null valve opening for a finite error signal. The valve is also shown in the step response study to be unsymmetrical in response, hence the judder being more noticeable in one direction. The frequency at which the judder occurs in the simple system used is determined by the higher frequency response specified. For example, by using a piston of twice the annular area reduces the frequency at which judder is noticeable; but also reduces the maximum velocities at useful frequencies. There are two common methods for improving the low frequency response, whilst minimising high frequency velocity reduction. Dither may be applied to the valve so that it oscillates about the null condition or a bleed orifice may be connected across the chambers of the piston effectively increasing the leakage. Dither was applied to the second stage amplifier of the control system at a frequency of 400 Hz with an amplitude of zero to 20 volts, peak to peak. This reduced the judder so that it was undetectable. However, the step response investigation showed that the primary effect of the dither was to reduce the system gain. Since the judder was so small and was not present in the frequencies that were envisaged as being useful, it was decided not to include the dither as a permanent feature.

The step response investigation provided information on the effect of gain and dither upon the speed and accuracy of the system response. The step function was provided by the punched tape interface unit and hence, the paddle motion is a function of the

dynamics of this system. Therefore, the step and impulse responses will be considered later for the complete system.

4.7 The Generation of Command Signal for the Wave Generator

The methods of providing a signal for the wave generator are numerous and several were considered before the existing system was conceived. The most elementary perhaps, is to use an analogue white noise generator and a set of filters to produce the desired output. The output from the white noise generator consists of a mixture of all frequencies. In practice, the bandwidth is limited, because a constant spectral density over all frequencies would lead to an infinite variance. Thus, the principal characteristics of white noise are a constant spectral width and predetermined variance. The filters used may be either single filters corresponding to the desired spectral shape, or a series of filters, each controlling a predetermined bandwidth arranged either in cascade or parallel. There are many disadvantages to this system. The frequency of conventional white noise generators does not usually extend down as far as that required and even if this condition is met, the output suffers from drift and variability.

The synthesis of a suitable single filter to give the required spectrum is difficult and a different filter must be designed for changing spectra. The set of filters is more feasible and has been used quite effectively by Sellars and Loukakis (1966), who used an analogue computer to set up a filter system to produce a Moskowitz spectrum, the real difficulty with these methods being

the construction of filters with a very high cut-off rate. Considerable time, however, was devoted to a feasibility study of constructing a single filter to produce a Moskowitz spectrum. Since this spectrum is available as an analytical expression, the only variable being wind speed, it was postulated that a single filter shape would suffice. However, efforts to produce a realisable form for this filter were fruitless.

With the inherent difficulties involved with the analogue methods of wave synthesis, a digital approach was investigated. Since a medium sized digital computer was available at the University, it was decided to make use of this to generate the command signal for the wave generator. This method has proved convenient, since not only must the desired wave spectrum be provided, but account must be taken of the response of the generator to a command signal and the transfer function between wave motion and paddle motion, both of which may change with system gain and water depth, for example. An analogue signal generator or a dedicated digital system might require hardware alteration to account for these changes, whilst simply changing parameters in a computer program would suffice. Furthermore, a change of desired spectrum may be similarly accommodated. The generation of a suitable digital time series representing a command signal for the wave generator is discussed in the next section. The next problem was to provide an interface between computer and wave generator. Ideally, the command signal would be provided 'on-line'. However, it was obviously out of the question to use the University computer in this way, but it would be by no

means impossible to use one of the new programmable desk top mini computers for this, since the program turns out to be relatively simple.

The most convenient method of recording a large quantity of data from a computer at relatively high speed is either by means of digital magnetic tape or punched paper tape. Punched paper tape was chosen in this case because of the relative cheapness of the hardware required to handle it. Before considering the construction of the punched tape interface in detail, it is of interest to discuss the general design philosophy.

Since the wave generator operates on an analogue principle, the primary job of the interface is to provide digital-to-analogue conversion. Digital data produced from a computer is in a binary code. The binary system of representing data consists of a code of zeros and ones (usually). Each piece of binary information is called a 'bit', thus four bits may be used to represent 2^4 different characters. There are several different binary codes, the most common ones being straight binary and binary coded decimal. These are illustrated in Table 4.2 together with decimal equivalents. Decimal numbers may be represented by straight binary code by simply adding bits to the left (carrying) as the count proceeds. Thus, an n bit binary number may lie in the decimal range zero to 2^n. Binary coded decimal is also worthy of further explanation. In this case, each decimal decade is represented by 4 bits of straight binary code representing 8-4-2-1 respectively. The range of this code is expanded by adding further 4-bit decades. Now digital-to-analogue conversion from one of these binary codes may be achieved

by using an operational amplifier in summing mode, each bit of binary information being applied to an input resistor. Suitable weighting of these resistors produces an output proportional to the binary number. Modern electronics achieves this by means of a monolithic digital-to-analogue converter, with high accuracy and high speed being achieved by integrated circuit techniques. These units commonly accept either binary coded decimal (BCD) or straight binary, typical resolution being either 8-10- or 12 bits, with common maximum output of 10 volts. The straight binary code has a greater resolution than those using BCD for the same number of bits, e.g. 12 bits straight binary represents zero to 4096, whilst 12 bit BCD, zero to 1000. Typical settling times vary between 300 nsec and 20 μsec, so updating rates of 3×10^6 and 5×10^4 times per second are possible. The use of one of these modules simplifies the design a great deal and, in fact, means that the accuracy and updating rate effectively depends on the remainder of the system.

Punched paper tape readers merely provide an electronic output corresponding to the binary coded word on the paper tape, i.e. an output of '1' corresponding to a hole, a zero to no hole. The sensing head of most modern tape readers consists of an optical system, a photo-detector sensing the presence of a hole in the tape. The tape is moved across the head by a toothed wheel which engages the sprocket holes on the tape. This wheel is driven either by a synchronous motor or a stepping motor. The synchronous motor drives the tape at a constant speed, electronic separation of the tape information being derived from a sprocket hole signal. The stepping

motor is used for accurate tape speed and the tape momentarily stops on a single line of tape. The latter method was used for this application. Tape speeds of between zero and 1000 lines per second are realiseable, a typical low-cost reader being capable of 100 lines per second.

The two most important parameters governing the system are that of updating rate and resolution. Naturally, it is desirable to have maximum values for both of these in order to be able to produce a smooth analogue signal. These parameters are predominantly dependent upon tape reader speed, digital-to-analogue converter resolution and paper tape format. The tape code used is ISO8 and the format depends to a certain extent on the programming language used.

ISO8 is an 8-track code employing seven data bits and one parity bit. Of the data bits, three are used for zone identification (0 - 7) and four for numeric identification (0 - 15). Table 4.3 illustrates the use of the two groups of bits. A punch is taken to represent a binary 1 and no punch a binary 0. Thus, the four numeric bits representing the numbers zero to 9 are in binary coded decimal (BCD) code, which simplifies the logic design of the interface.

It is required that the tape contains as little redundant information as possible. Three basic forms are available for transferring integer numbers to paper tape. Each digit or space may be produced individually from the machine code representation using the ALGOL 'write ch' routine, but this method must be treated as a last resort, since it involves considerable computer time.

The ALGOL 'print' routine produces one leading and two trailing spaces accompanying each number and the Fortran 'I' format produces the number and three spaces. The alternative to the latter two is to produce the whole string of numbers as one Fortran record, thus eliminating all extra spaces except at the ends of the record. A further restriction is imposed on the system by the maximum length of tape which may be handled conveniently which, in practice, is 100,000 characters being equivalent to a reel 10 ins. in diameter.

The final design parameters were a result of a compromise between various factors. Hardware choice was between a 2 or 3 digit BCD digital-to-analogue converter and a 100 or 300 maximum character per second tape reader, resolution being governed by the converter and speed by the tape reader, whilst the length of tape is a function of both. Table 4.4 shows the results of various combinations of both, based on a tape format having two spaces between each number. Obviously, the faster reader speed is not feasible because of the large quantities of tape required. It was finally decided to use a tape speed of 100 ch/sec. with the 2-digit converter, the 1 per cent accuracy being compatible with paddle accuracy for a 10 cm stroke, which was thought to be a realistic maximum for most applications. Positional error on full stroke would be 4.5 mm., which was unlikely to be used. Ideally, a $2\frac{1}{2}$ digit converter (or 8-bit binary) would give a 1 mm. error over the maximum stroke.

Finally, the digital-to-analogue converter was so inexpensive that if the 2-digit model proved inadequate, a change could be made to the more accurate model at a later date.

4.8 Circuit Construction

Having selected the tape reader and digital-to-analogue converter, it was necessary to design additional circuitry to provide the following functions:

1. Operation of tape reader at a predetermined rate.
2. Storage of information read by the tape reader.
3. Sequencing of tape reader, storage register, and up-dating of digital-to-analogue converter.
4. Smoothing and scaling of analogue signal.

These operations were performed by digital and analogue circuits, built on a module basis making use of plug-in circuit cards and dual-in-line packaging of the integrated circuits. The circuit cards slide into a card frame and are connected to the inter-module wiring by edge connectors. Dual-in-line sockets provide a convenient method of installing the integrated circuits without soldering, thus easing maintenance. The digital logic circuits are SN 7400, TTL series and require a 5 v. power supply. Logical '1' is represented by 3.5 v. $\pm$ 2 and logical '0' by 0 v. $\pm$ 1.2 v. Typical gating speeds are 18 n sec. for a 2 input NAND gate and power dissipation for the same device is 10 mw. The analogue operational amplifiers are general purpose 741 c. versions utilising a $\pm$ 12 v. power supply.

The punched paper tape reader is a Computer Terminals OR 10 unit. The tape information is detected by an optical tape reader head. A light source is shone through the holes in the tape. The presence of a hole is detected by photo-transistors to which the light is directed by fibre optics to ensure high signal/noise output and eliminate cross-channel pick-up. The photo-transistor operates a transistor switch which in turn is connected to an output buffer in the form of an SN 7475 shift register in which the clock pulse is maintained high to allow the output to change in sympathy with the photo-transistor stage. Data from the buffer is in the form of 8-bit bytes and a sprocket signal for sequencing purposes. The stepping motor of the tape reader has four segments which must be energised in the correct sequence to ensure rotary motion. This is achieved by means of a printed circuit card supplied with the tape reader, and responds to a pulse from the clock circuit.

The characteristics of the motor are such that one pulse advances the tape by one line. The pulse generator which operates at 100 pulses per second originally consisted of two SN 74121 monostable vibrators arranged to be self-triggering. This system, however, proved to be subject to drift of up to 10 per cent due to the variation in supply voltage. A Rastra XR-220 monolithic timing generator replaced this and is accurate to 1.5 per cent. A NAND gate controls the re-triggering of the timing circuit, allowing the ON/OFF switch to determine whether the pulses generated consist of either a continuous pulse train or single pulse. The sequence

is initiated by the single shot switch.

The 8-bit data from the tape reader is fed to a storage shift register which contains two 8-bit words. This shift register consistes of four SN 74175's, integrated circuits 3, 4, 7, 8 on circuit card B. Outputs from these two words, which contain two consecutive lines on the paper tape are fed to 8-input NAND gates (SN 7430) to decode the ISO8 characters representing £, S, F. The four most significant bits from each word are also fed to an 8-input NAND gate to detect the presence of a two digit number being present in the storage register. The £, S, and F characters are used in the control logic and will be discussed later. The least significant bits of each word contained in registers A and B (see Fig. 4.6) are connected to the output register, the four bits in register A consist of the most significant digit of the number (i.e. 'tens') and the B register the least ('units'). As previously stated, ISO8 code is such that the least significant bits are in binary coded decimal (BCD) which is accepted by the digital-to-analogue conversion module so no inter-code conversion is required. When the output from IC 5 on board B (B/5) goes low, (detecting $\overline{\alpha\alpha}$) indicating that a two-digit number is present in the storage register, a clock pulse (CKO) is generated by the control logic and applied to the output register. The output register consists of two SN 74194 4-bit registers, the outputs of which are connected directly to the inputs of the digital-to-analogue converter, thus the pulse CKO updates the converter with the BCD coded information contained in the

storage register. This, then, is the basic data flow through the unit, and it should be noted that a space or null character is needed between each two digits if erroneous outputs are not to result. The logic circuits could easily be altered to avoid this should updating speed of 50 times per second be required. The remaining logic circuits control the sequencing of the shift registers and mean value of the output. Plate 4.3 shows the main storage circuits. Several control functions are provided by the control circuits in addition to the output register clock pulse CKO. The other outputs are the mean value control (MVAL) and output register clear (CLO). The mean value control is necessary for the following reasons. It is convenient if the wave paddle is kept in a central position during the time that no signal is being received from the tape reader. However, the converter output is unipolar so that an input of '50' is applied to the converter as soon as the power is turned on. The '10' and '40' outputs from the shift register are interrupted before they reach the DAC and are fed to a sequence of gates forming a pair of OR gates. The other input to the OR gates is MVAL, this being '1' when a preset of '50' is required. MVAL and CKO are set to '1' and '0' respectively, upon switching on the mains power supply. The operation of the control circuits from this stage depend upon the mode of operation selection.

In the LOOP mode, the first number on the tape inhibits CKO and MVAL and loads the output register. Thus, a continuous tape loop may be used in this mode to generate a periodic motion or a short length

of tape to produce a solitary wave or step function. In the TRIGger mode a herald symbol £S is required at the head of the tape before any numeric information is transferred to the output register. This is necessary to prevent the accidental loading of an unsuitable tape or running a program tape in reverse. A £E is required at the end of the tape to restore MVAL to '1' and CKO to '0'. The choice of mode is set by the TRIG-LOOP switch (see Plate 4.4 for assembled Wave Generator Control Unit and Tape Reader). A flow chart for the operation of the logic unit is shown in Fig. 4.7 and a system block diagram in Fig. 4.8.

The analogue portion of the circuit consisted of two 741C operational amplifiers. The first converts the unipolar output from the DAC into a zero mean signal and inverts the signal. The second amplifier forms a filter with a -3 dB frequency of around 20 Hz and a cut-off rate of 6 dB per octave. Both of these operations may be performed with a single device, but since the filter operation must be performed with the amplifier in inverting mode, and since it was desired to utilise a positive signal to provide positive paddle motion, two inverting amplifiers were used. Three ranges of scale were also provided to suit the paddle motion to be used. Two of these provide full scale movement of 10 cm. and 15 cm., whilst the third can be pre-set by a potentiometer to any desired value.

4.9 The Performance of the Punched-Tape Interface Unit

The first stage in ascertaining the performance of this part of the system was to consider the voltage levels produced by the DAC in

response to a particular number on punched tape. This was achieved by setting the mode selector to 'LOOP' and punching a single number on a length of blank tape, the output being monitored by a digital volt meter. The most significant decade (i.e. tens) was treated separately from the least and the results show that the linearity is excellent and within that quoted by the manufacturers of $\pm$ ½ LSB (0.5 per cent FSD). A similar test was performed on the output from the analogue filter section in order to set the 'zero' paddle position output to earth potential (within $\pm$ 5 mv.) and to check the amplifier linearity. Again, this proved to be within the tolerances set by the DAC module.

The timing and sequencing of the unit was then checked. The clock pulse generator was adjusted to the correct frequency by observing the timing pulses on an oscilloscope which had a built-in oscillator which was accurate to 1½ per cent. Following this, punched tapes were made up consisting of 'ramps', i.e. number sequences, such as 10, 20, 30, 40 etc. and the resulting wave form observed on the oscilloscope. A trace of the ramp inputs to one decade is shown in Fig. 4.14, the results being quite satisfactory. The output register clock pulse was observed simultaneously with the main clock pulse, and timing was as predicted during the logic design.

Whilst considering the response to a ramp input, it is of interest to note that the reconstitution of a wave form using a digital-to-analogue converter intrinsically introduces distortion. The reason for this is shown in Fig. 4.9. The wave form which it is desired to

produce is sampled at equally spaced intervals and these values used to drive the digital-to-analogue conversion. The unfiltered output is a step function, a line through the mean values of which lags the original wave form by half the sampling rate. The output of this signal when filtered is also shown and it is evident that not only is there a phase shift but also some harmonic distortion. The amount of distortion depends upon the synthesis rate. By selecting a suitable up-dating rate, the harmonic content of the wave form generated may be reduced to an acceptable level.

4.10 Appraisal of the Complete System

The investigation of system step and impulse response as mentioned previously was performed by utilising the punched tape reader input, a step being produced by punching 70 on tape (corresponding step is from the mean value of 50 to 70) and an impulse approximated by punching 70 space space 50. The length of the impulse is thus 0.04 seconds. The response of the paddle motion to these inputs is a function of the complete system since the filter in the interface unit output stage will have a finite rise time. Fig. 4.10 shows the positive and negative step responses for a step of 3 cm. and a variety of gain positions, together with the output register clock pulse (positive edge triggering). Original traces were obtained on the UV recorder with a fast paper speed.

For high gains of the order of 60 $sec.^{-1}$, the system was unstable, any error signal causing oscillation of 10 Hz with an amplitude of

3 mm. Decreasing the gain brought stability and a decreasing settling time. For gains of 14 or less, the response was slow and large errors in position of the order of 8 per cent were evident. It is also noticeable that there is some difference (5 per cent approx.) in effective gain in either direction, this being more noticeable in the settling characteristics of the curve than the rising portion and consequently tending to support the null flow non-linearity hypothesis. The impulse response curves are shown in Fig. 4.11 and exhibit similar characteristics to the step response. Fig. 4.12 shows the effect of various amounts of dither, the effect of increasing the peak-to-peak voltage being to decrease the effective gain.

Finally, the frequency response of the system was obtained at varying gains and is shown in Fig. 4.13. During this investigation, it was discovered that the output from the feedback transducer contained noise. The signal level was typically of the order of $\pm$ 1 volt maximum with noise consisting of 1.6 kHz ripple, with magnitude of 0.08 v. peak-to-peak. A simple filter was constructed with a -3 dB cut-off point of 500 Hz , reducing the noise level to 0.002 volts, peak-to-peak. The frequency response was obtained by producing punched tape loops consisting of the ordinates of a sine wave at the appropriate frequency. From the paddle motion observed, the magnitude and phase of the frequency response was calculated. The motion was also assessed quantitatively in respect of smoothness of action. At gains near the limiting value the motion tended to be jerky, whilst for low gains, the amplitude response was too low,

although the motion was very smooth.

Finally, a compromise setting for the gain of approximately 30 sec.$^{-1}$ was used which resulted in positional accuracy of approximately 1 per cent, whilst maintaining a smooth motion and adequate frequency response. In terms of step response, this gain setting produced a single overshoot.

To summarise, the complete system provides a means of producing the motion of the wave-maker as specified by numbers punched on paper tape, with frequency response and accuracy which was considered adequate for the production of programmed waves. Should system requirements demand a better specification, the simple system used provides a basis for achieving this with the minimum of reconstruction. The most desirable modifications which come to mind are:

1. Provision of 3-digit BCD digital-to-analogue converter to provide greater positional resolution.
2. Use of 300 ch./sec. tape reader to produce improved wave form definition.
3. Provision of compensating servo-control circuitry to improve stability.

However, the first two may provide electronic accuracy in excess of the servo-system characteristics.

Frequency	Percentage of Fundamental	
	2nd Harmonic	3rd Harmonic
0.5	0.1	1.4
0.4	1.0	1.4
0.3	0.3	1.8
0.6	0.4	1.4
0.8	0.5	1.2
0.9	1.7	3.2
1.1	1.8	2.6
1.5	1.1	2.9

TABLE 4.1 Harmonic Content of Paddle Motion

Decimal	BCD	Binary
0	0000 0000	0000 0000
12	0001 0010	0000 1100
25	0010 1101	0001 1001
50	1001 0000	0011 0010
75	0111 0101	0100 1101
87	1000 0111	0101 0111
99	1001 1001	0110 0011

TABLE 4.2 Binary Codes

DIAGRAMATIC FORM

		3 Zone Bits			4 Numeric Bits			
ZONE 3,	No. 8 (Represents decimal 8)	0	1	1	1	0	0	0
ZONE 4,	No. 6 (Represents F)	1	0	0	0	1	1	0
ZONE 2,	No. 4 (Represents £)	0	1	0	0	1	0	0

PUNCH TAPE REPRESENTATION

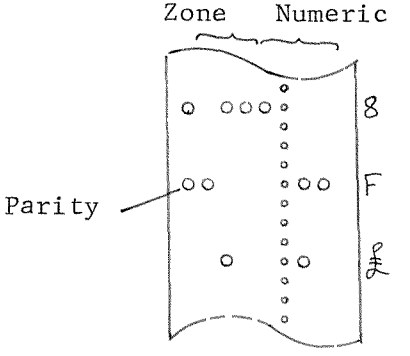

TABLE 4.3 Punch Tape Representation of Characters

Property	Tape Reader Speed	3 Digit BCD Converter	2 Digit BCD Converter
Resolution	100 ch./s.	0.1%	1.0%
	300 ch./s.	0.1%	1.0%
Up-Dating Rate	100 ch./s.	20	25
	300 ch./s.	60	75
Number of Characters for 10 min. Record	100 ch./s.	60,000	60,000
	300 ch./s.	180,000	180,000

TABLE 4.4 Tape Reader Speed and Resolution

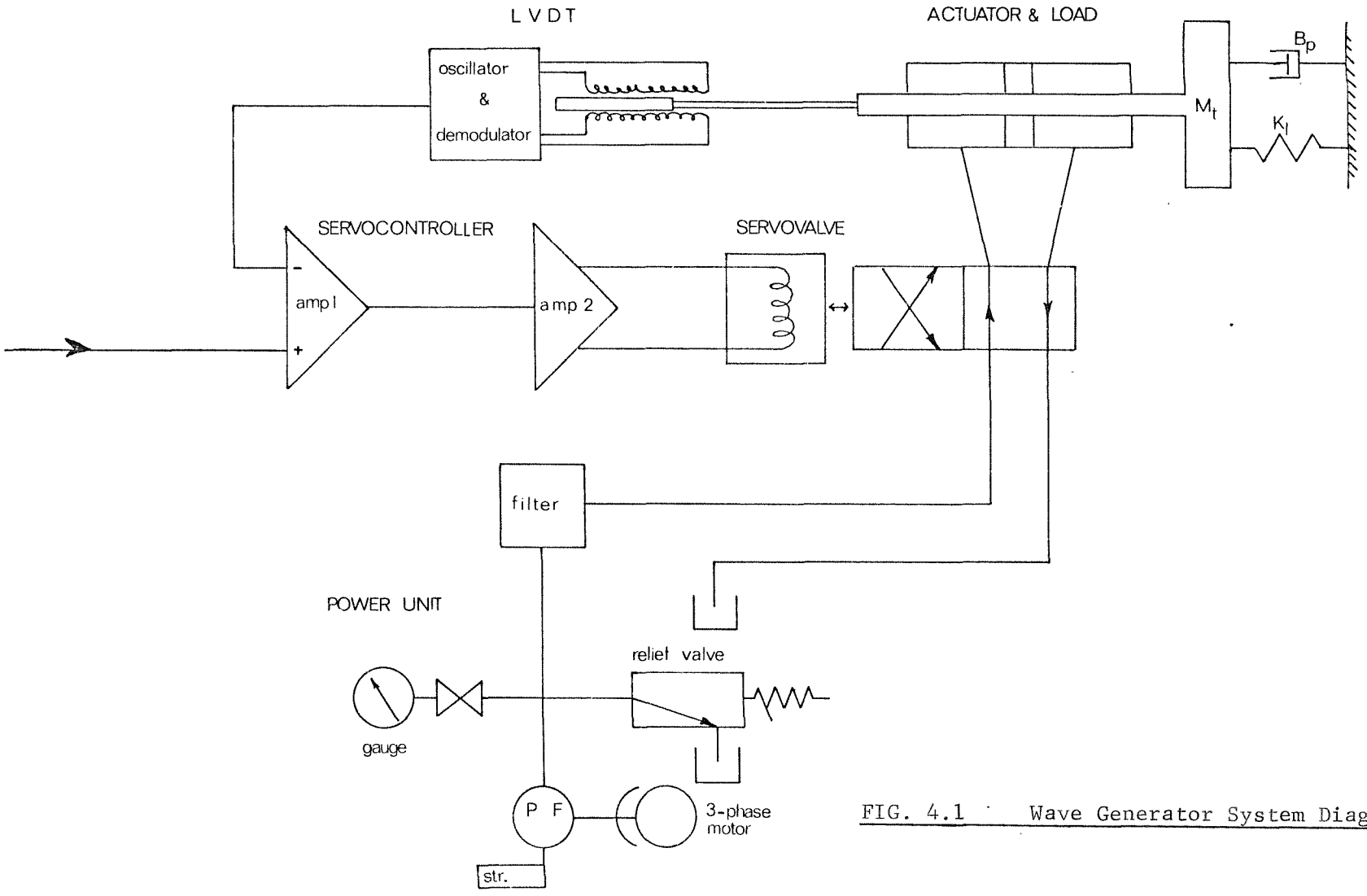

FIG. 4.1 Wave Generator System Diagram

FIG. 4.2

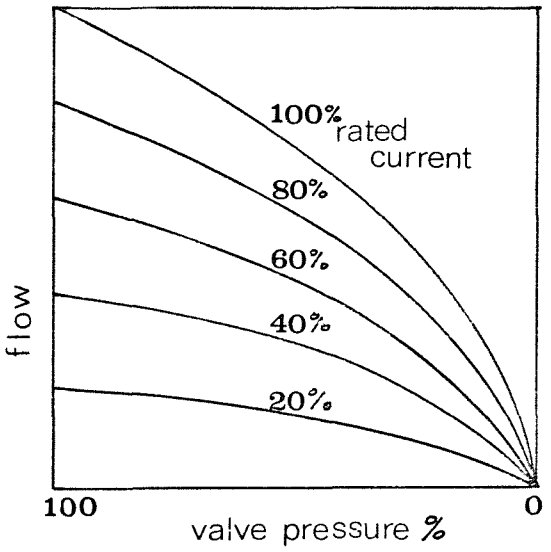

(a) Servovalve Pressure Gain Relationship

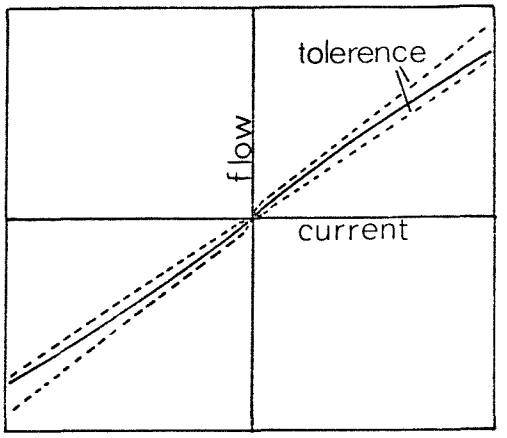

(b) Servovalve Current Gain Relationship

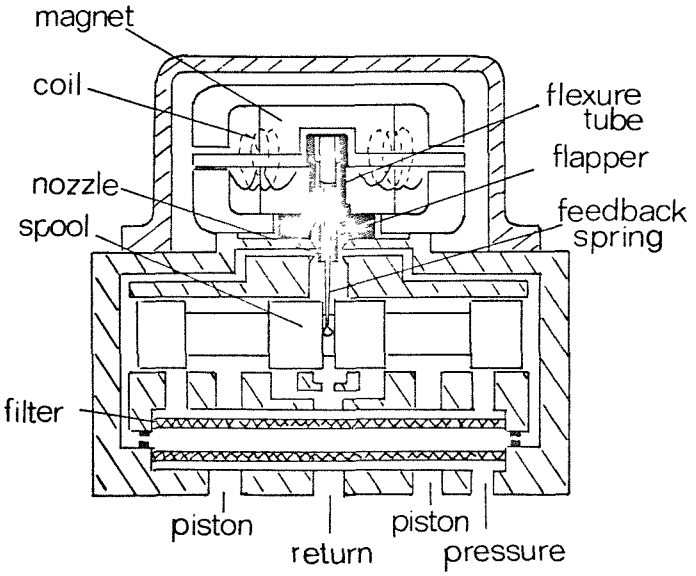

(c) Servovalve Cross-Section

FIG. 4.3

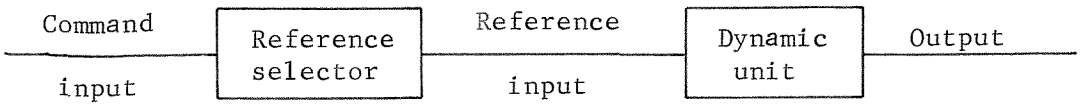

(a) Control System with No Feedback

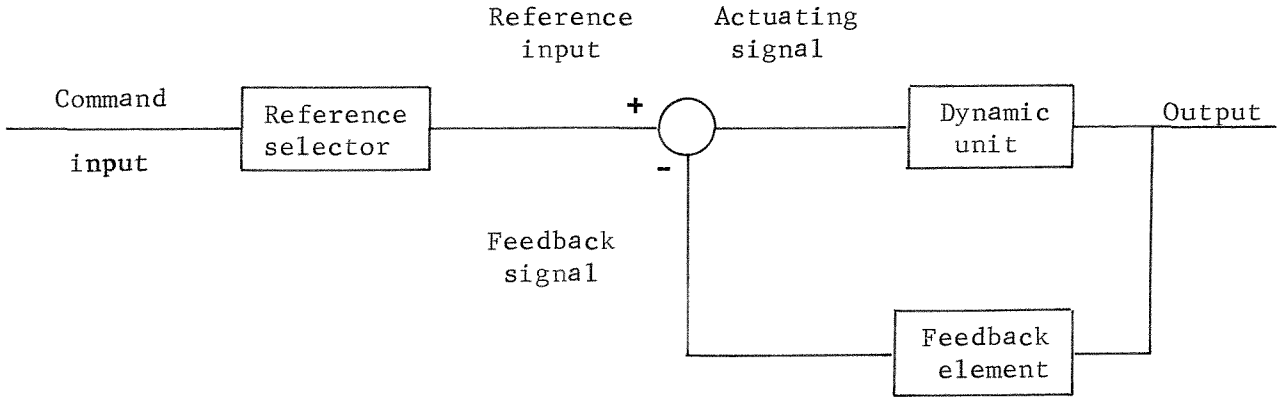

(b) Control System with Feedback

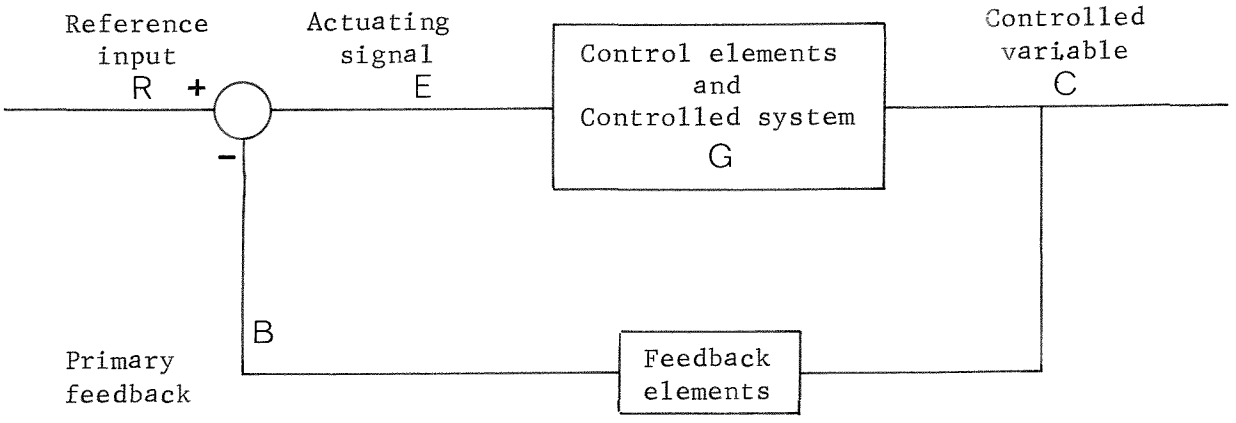

(c) System Definitions

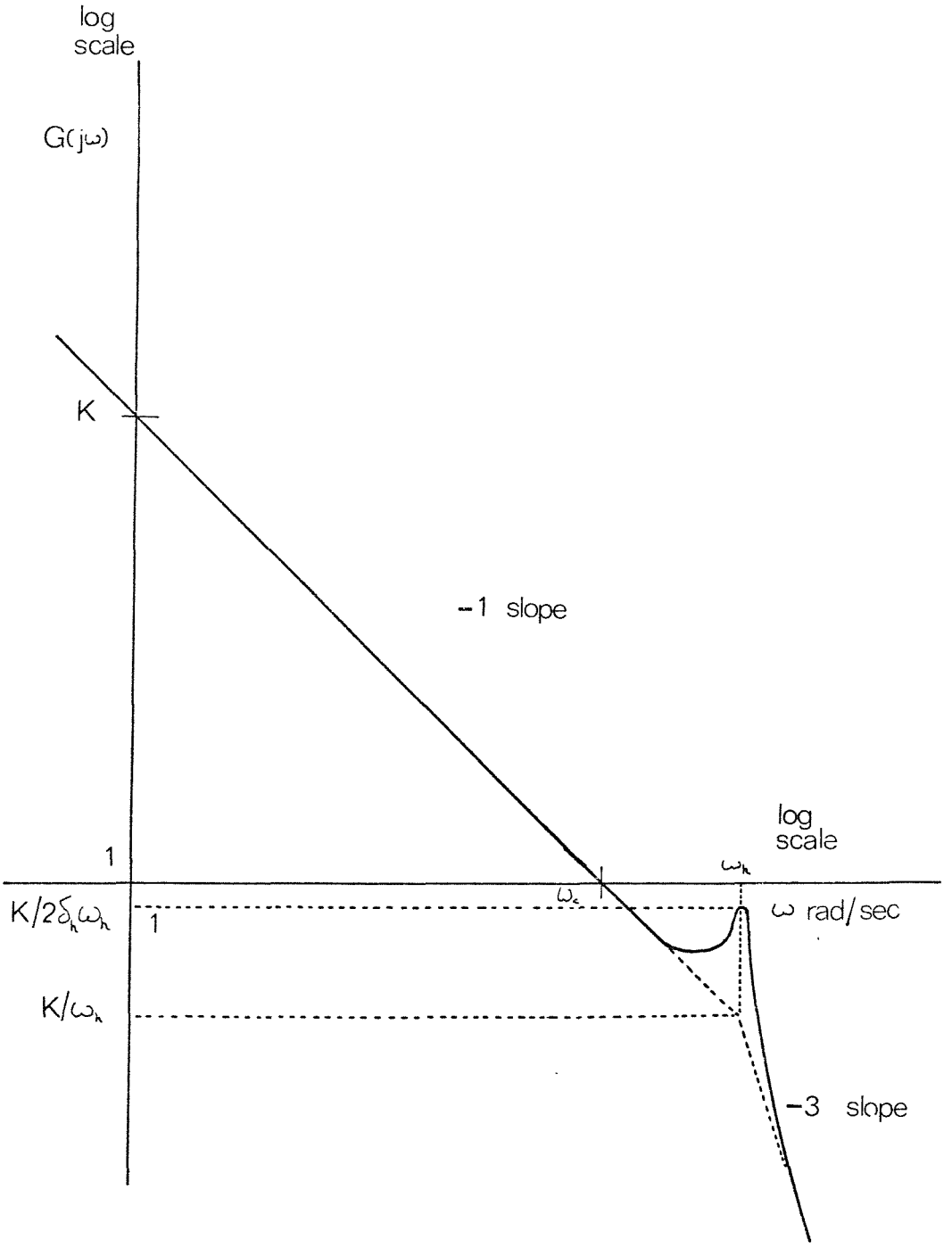

FIG. 4.4 Bode Diagram of Wave Generator Characteristic

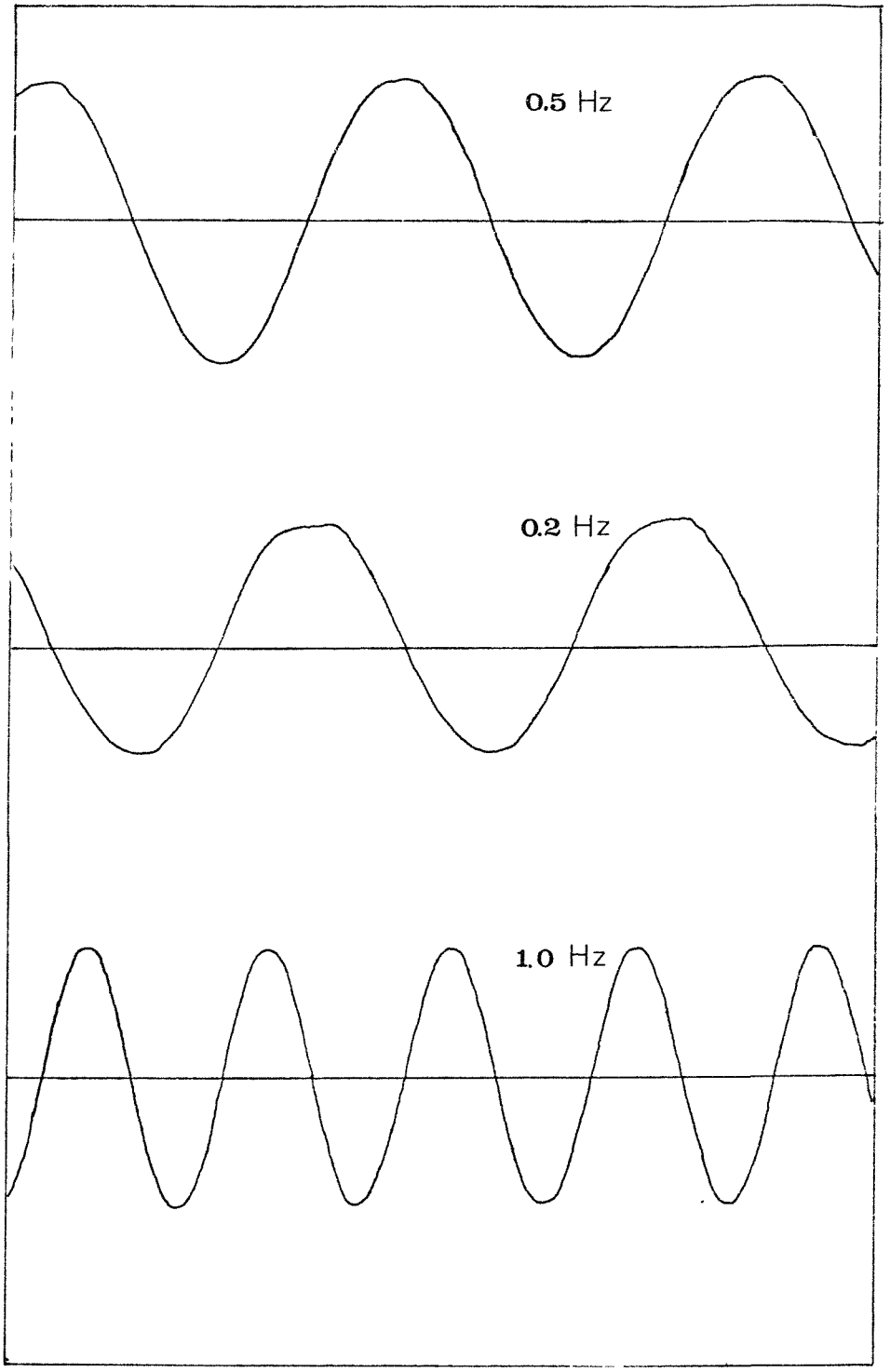

FIG. 4.5 Traces of the Paddle Motion for Sinusoidal Input

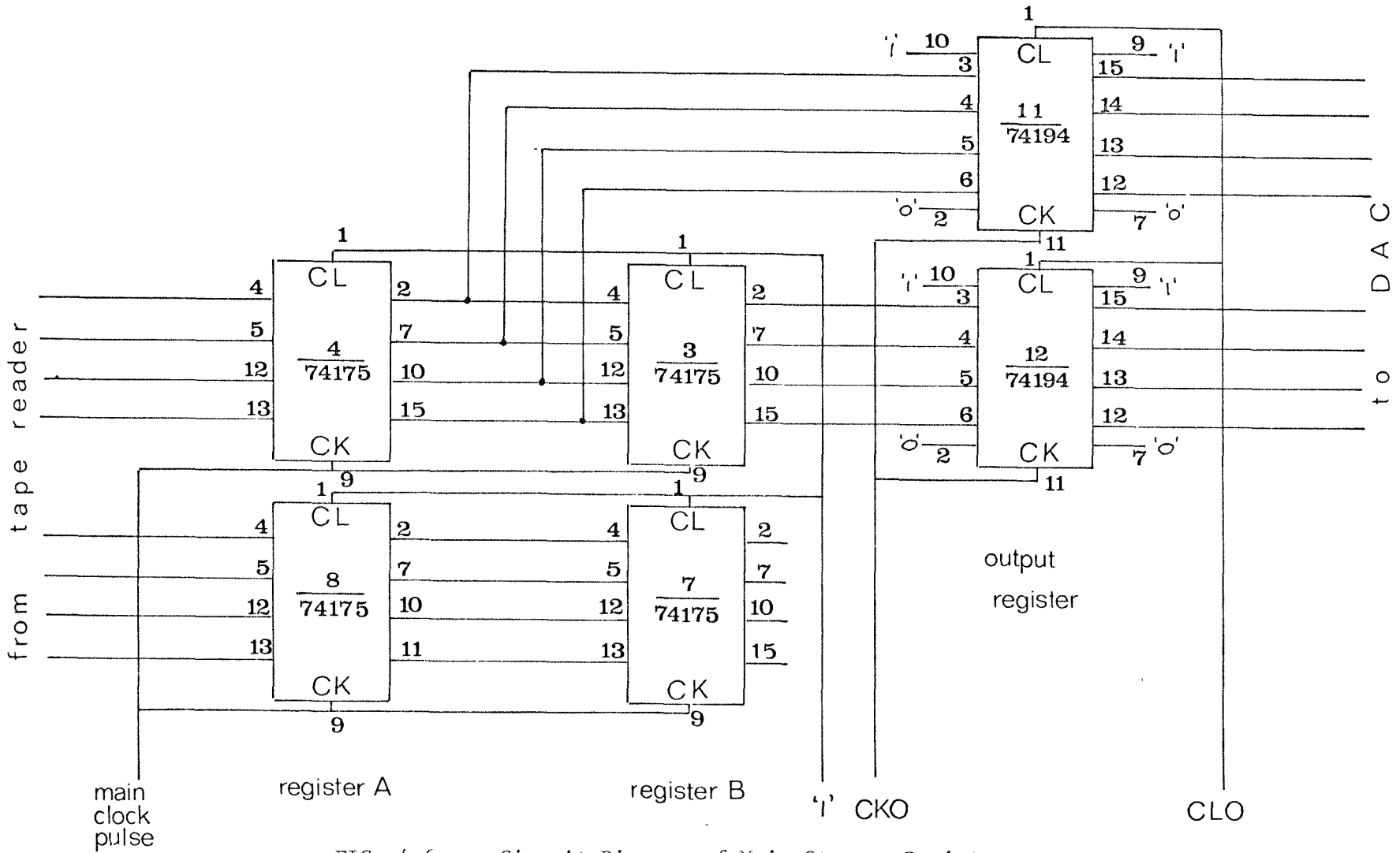

FIG. 4.6 Circuit Diagram of Main Storage Register

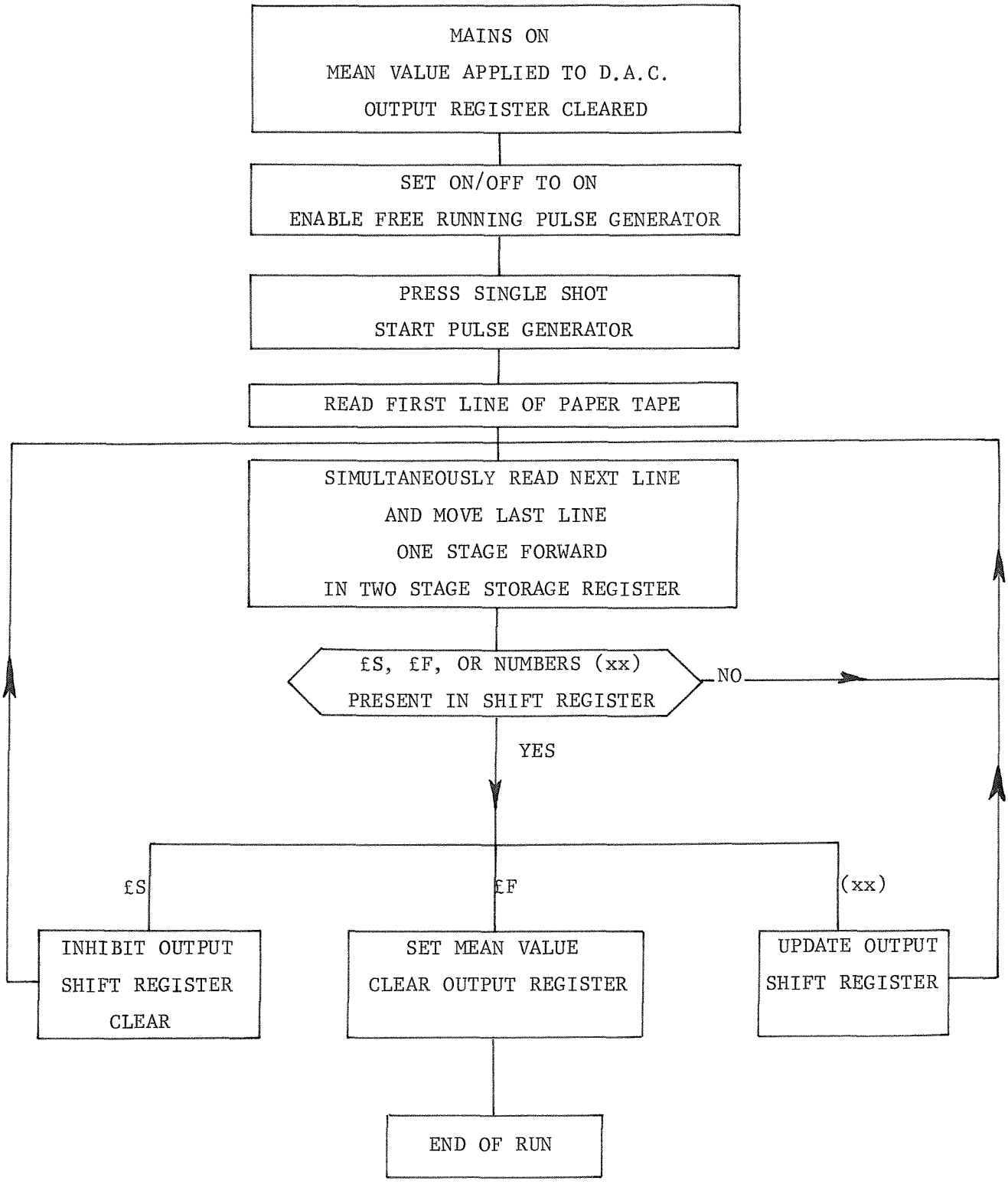

FIG. 4.7 Flow Diagram for

Tape Reader Interface Logic Circuit

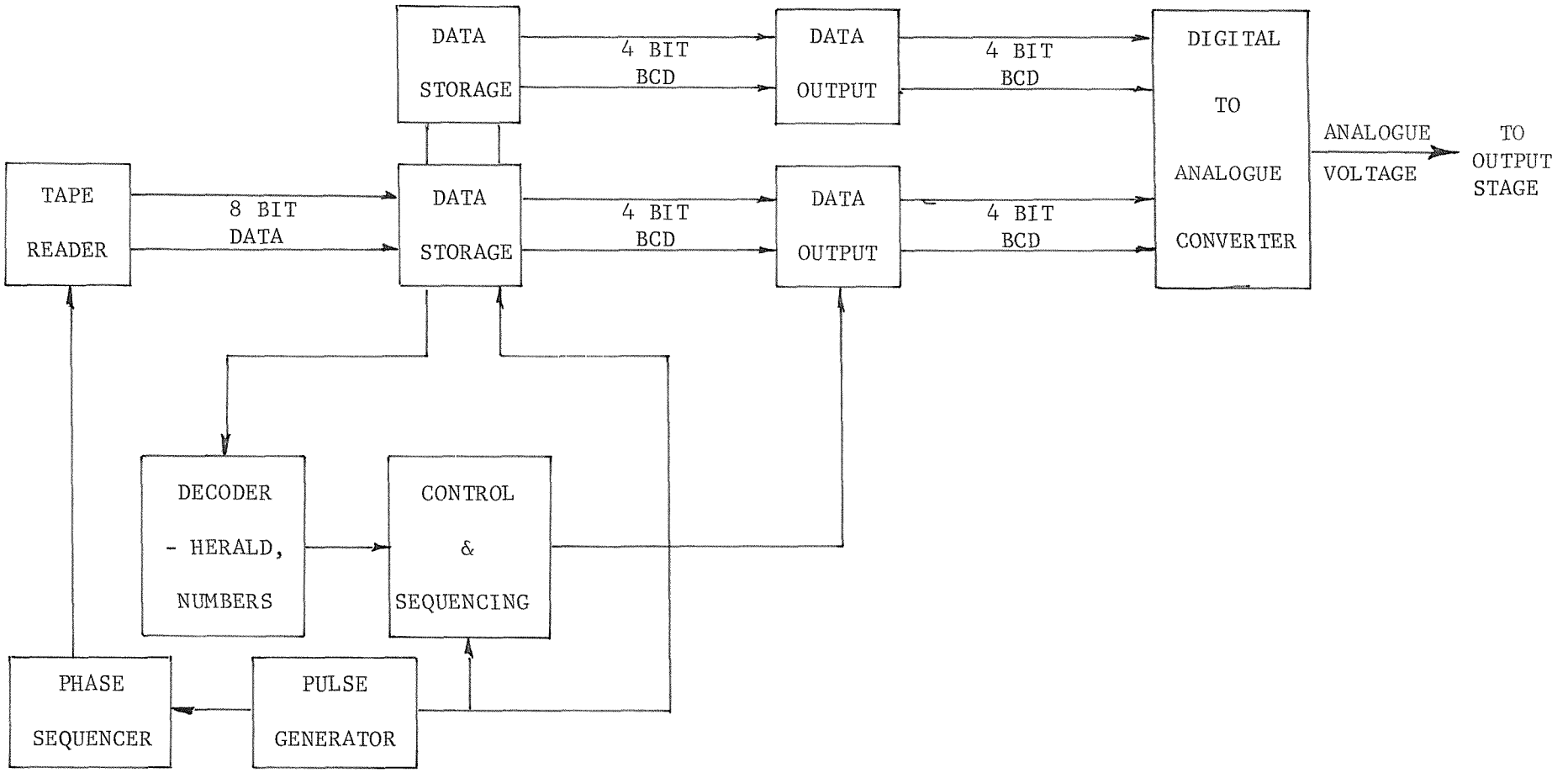

FIG. 4.8 Block Diagram of Punch Tape Interface

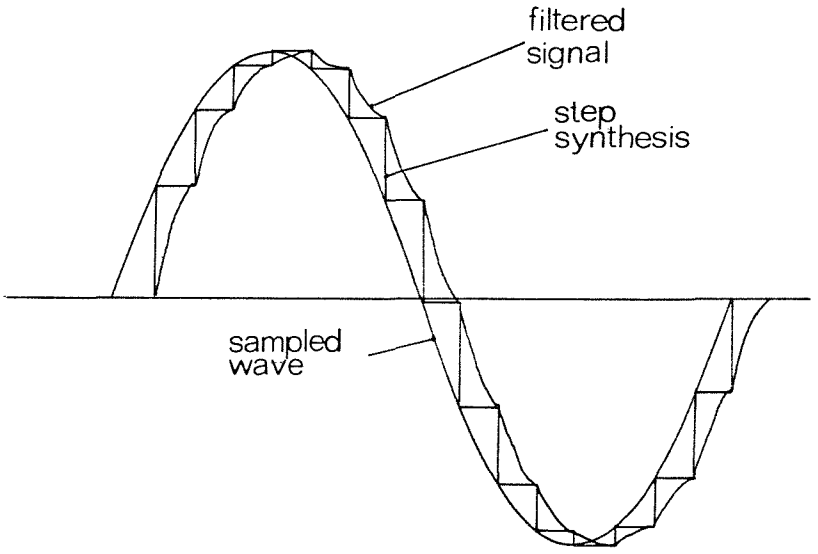

FIG. 4.9 Distortion of Wave Form due to Sampling and Synthesis

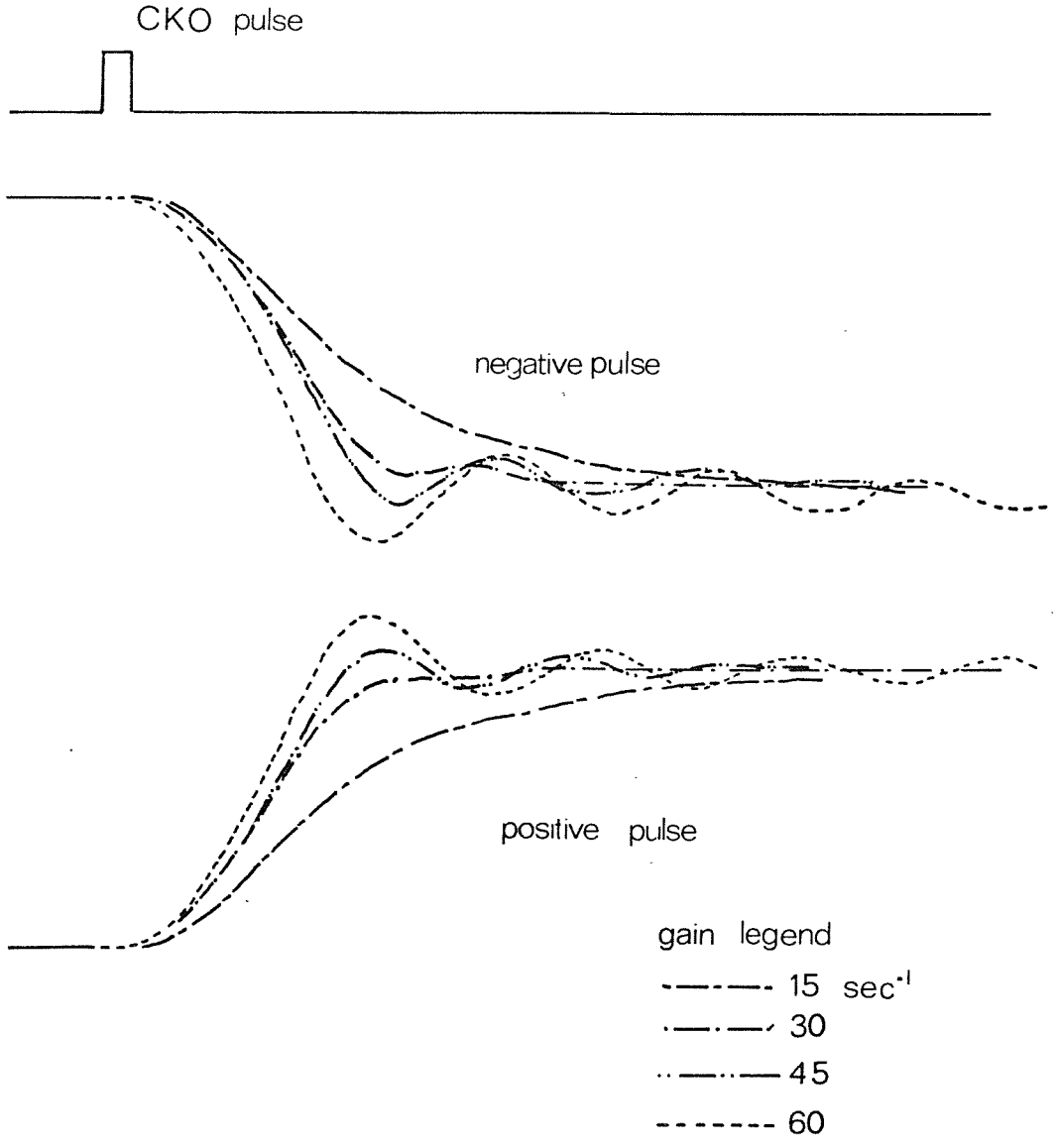

FIG. 4.10 Step Response for Various Gain Settings

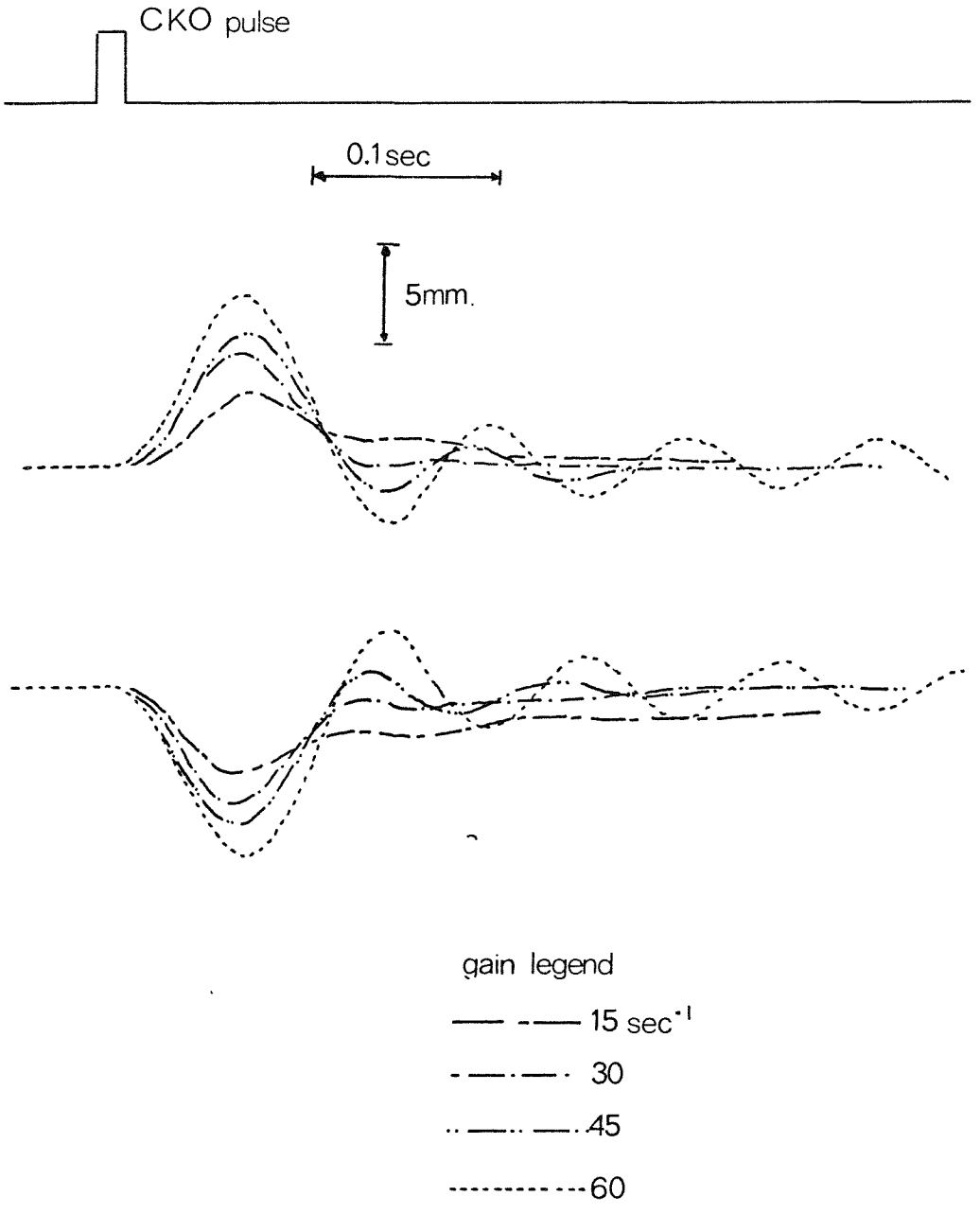

FIG. 4.11 Impulse Response for Various Gain Settings

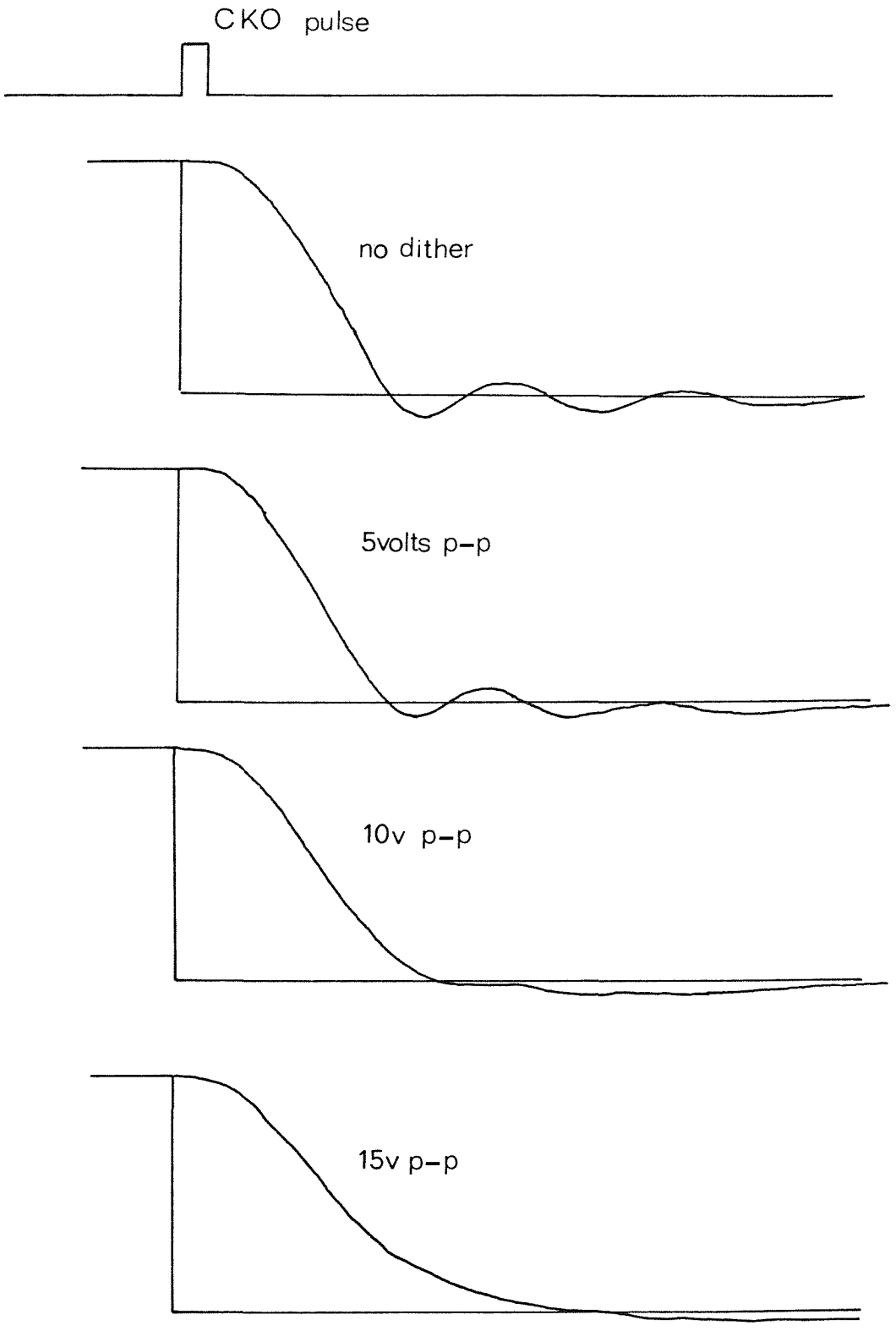

FIG. 4.12 Step Response for Various Dither Settings

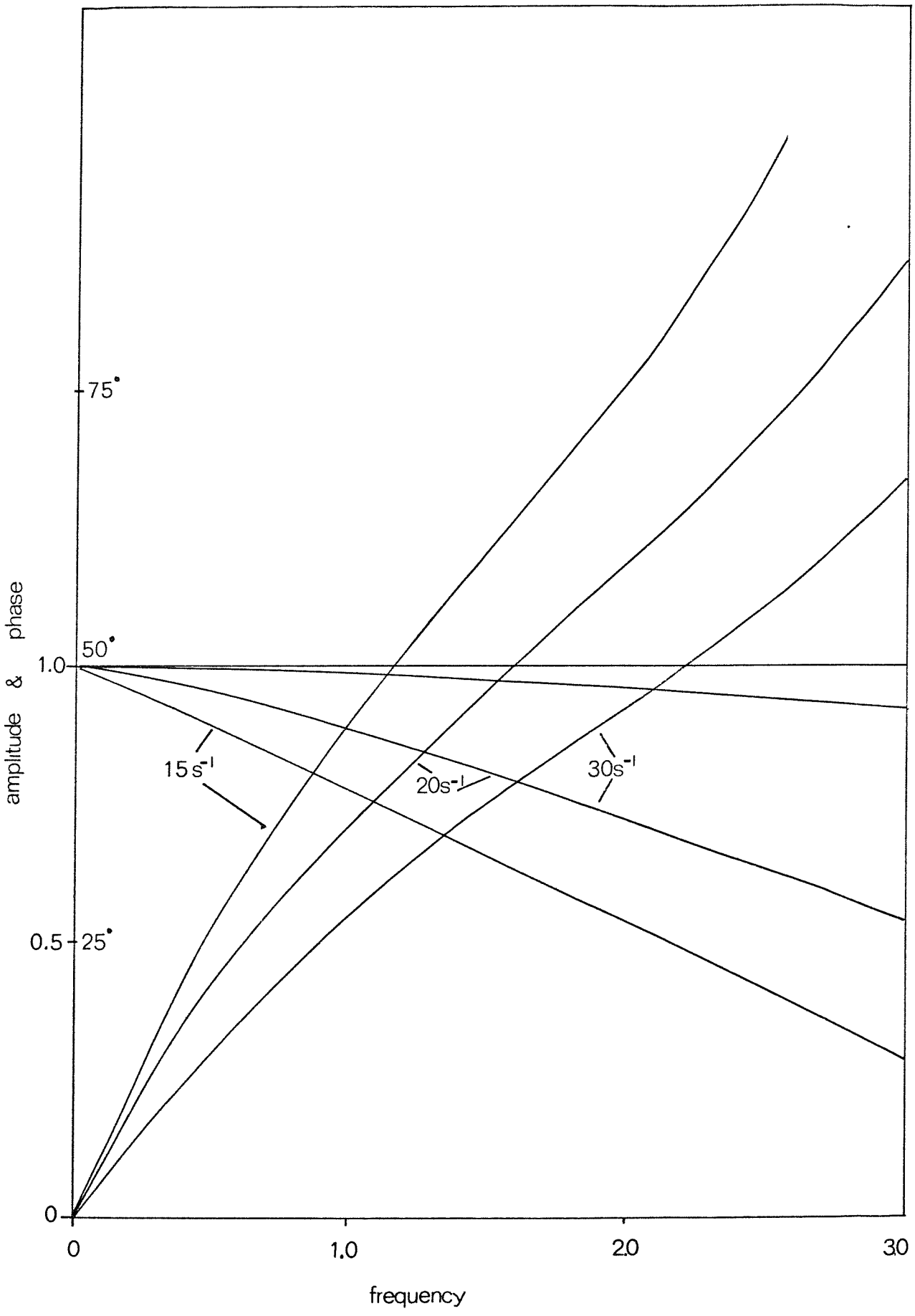

FIG. 4.13 Frequency Response for Various Gain Settings

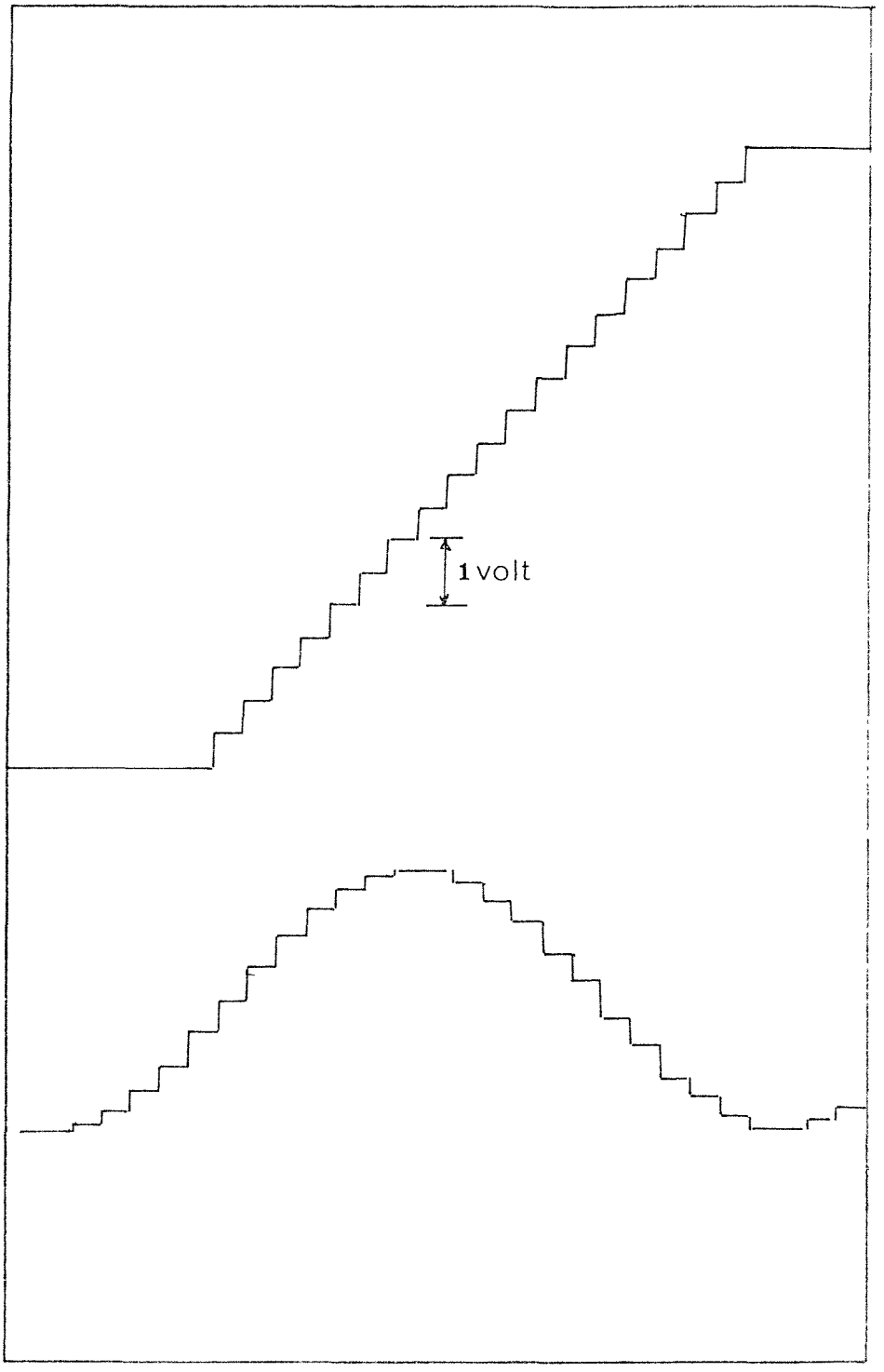

FIG. 4.14 Traces of the Unfiltered Output from the Digital-to-Analogue Converter. The Upper Trace is a Ramp Function, the Lower Trace a Sine Wave.

PLATE 4.1 The Hydraulic Power Unit

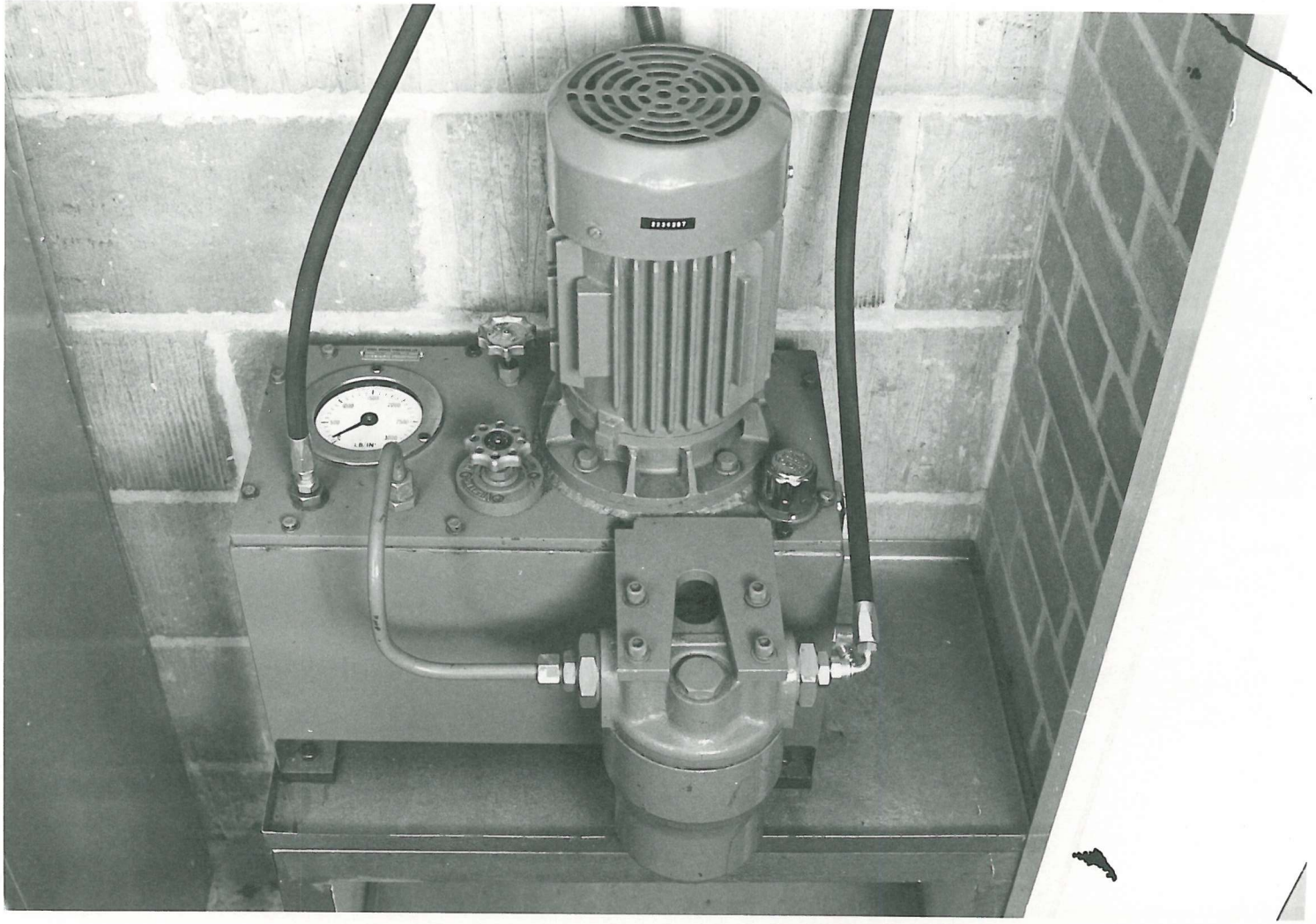

PLATE 4.2 The Wave Generator

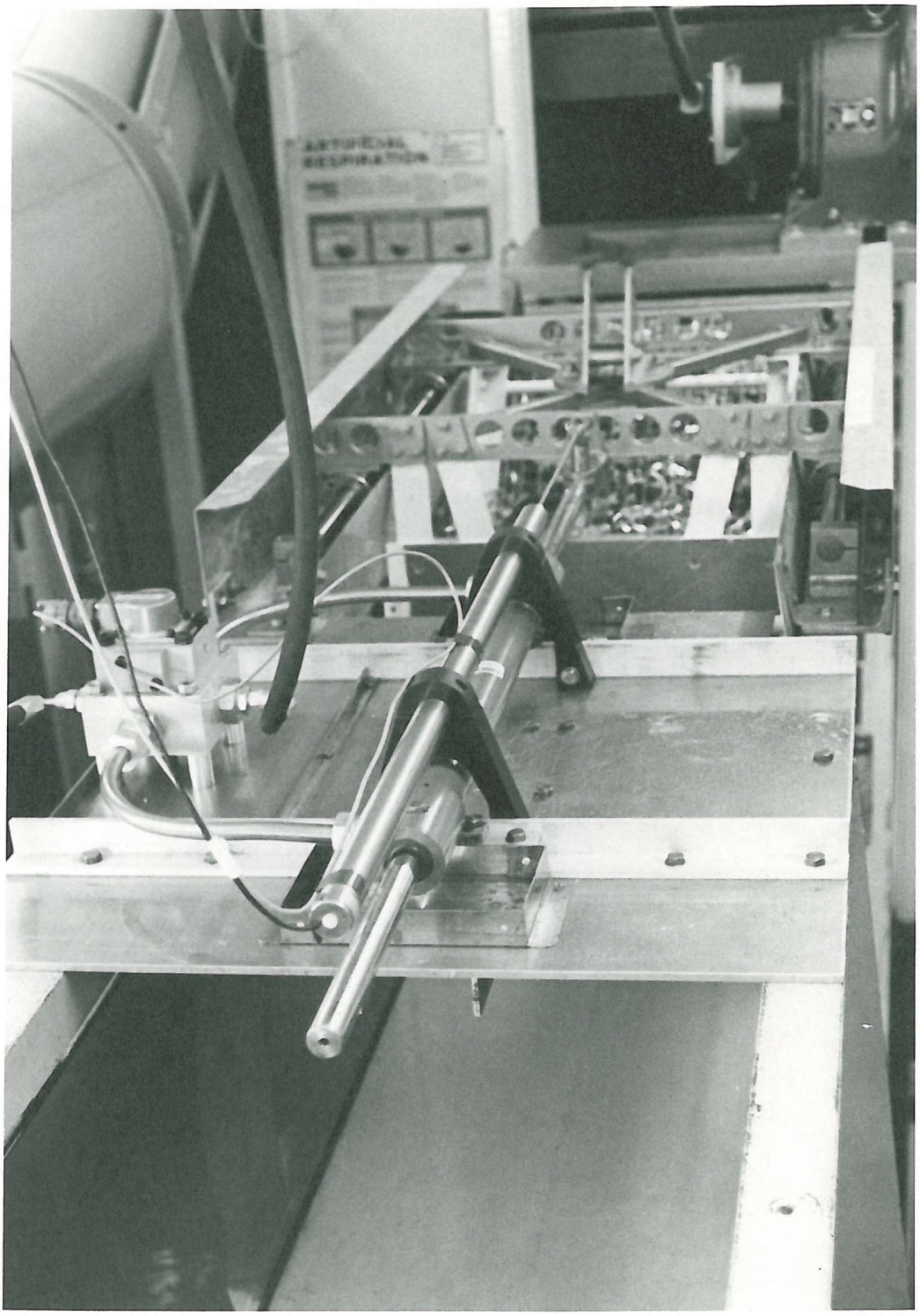
ARTIFICIAL
RESPIRATION

PLATE 4.3 Circuit Card B, containing the Main Storage Registers

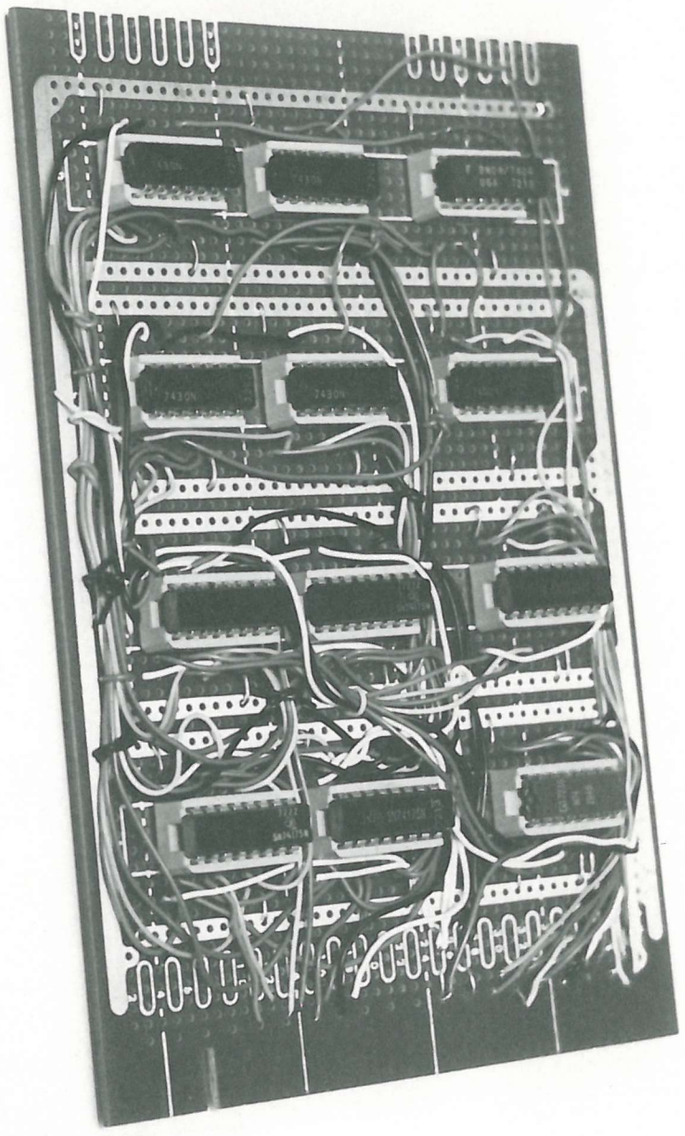
7430N
7430N
7430N

PLATE 4.4 The Wave Generator Control Unit and Punched Tape Reader

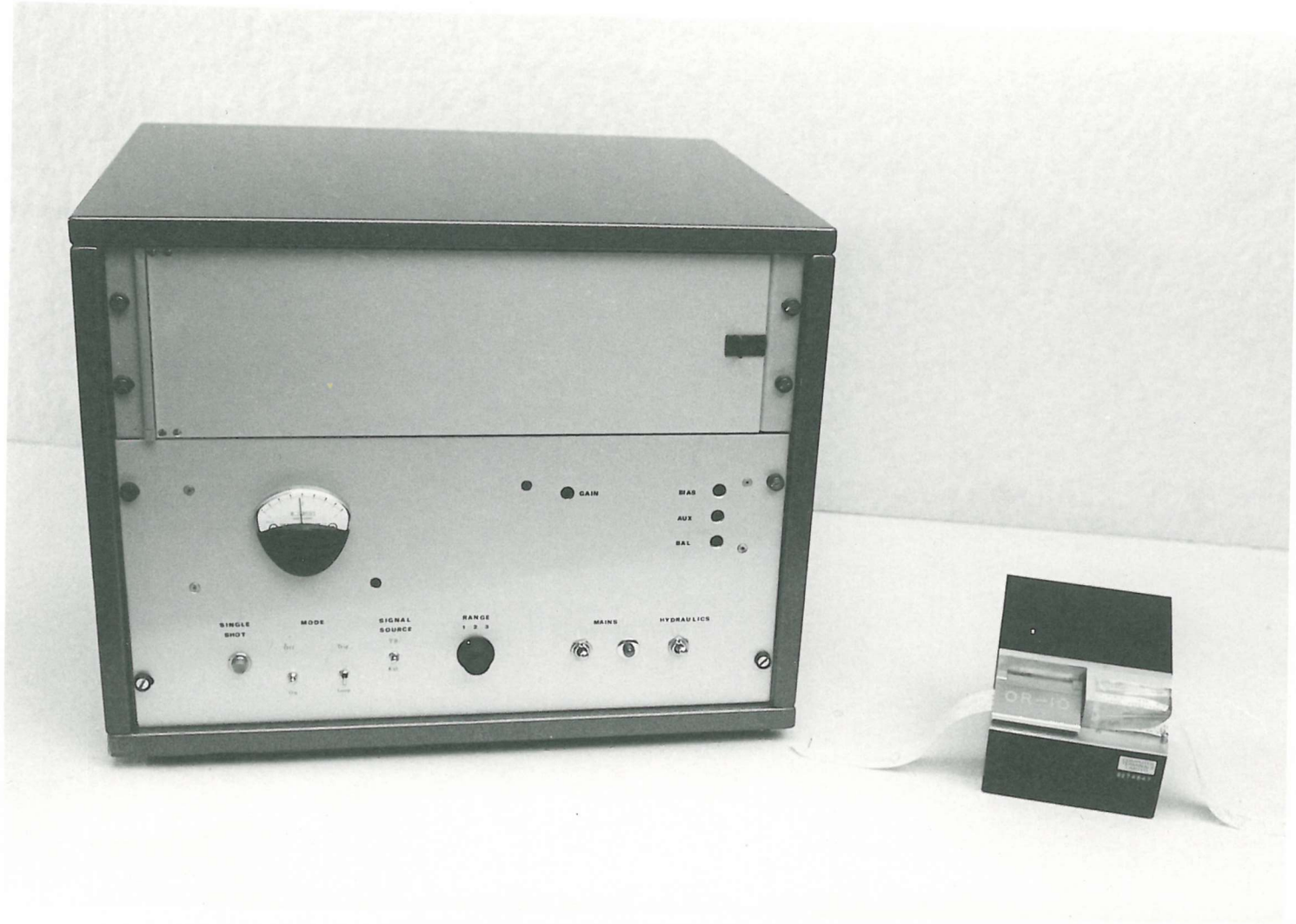
GAIN
BIAS
AUX
BAL
SINGLE SHOT
MODE
SIGNAL SOURCE
RANGE
1 2 3
MAINS
HYDRAULICS

5. SYNTHESIS OF COMMAND TAPES

5.1 Digital Synthesis of Time Series

The purpose of this section is to describe the process by which the command tapes are produced. The command tape is such that the waves produced will have the required spectral density function. Two methods are commonly in use for the digital simulation of sea waves, firstly, by superposition of sine waves and secondly, by the digital filtering of random numbers. The superposition method represents the water surface elevation $\eta(t_k)$ as:

$$\eta(t_k) = \sum_{n=1}^{N} a_n \cos(2\pi f_n t_k + \phi_n) \quad k = 0 \ldots M \qquad (5.1)$$

where a_n is the amplitude of the n^{th} component and ϕ_n the phase. The amplitude is given by:

$$a_n = \sqrt{2 S(f) \Delta f}$$

To avoid the repetition of the time series with period $1/f_1$ it is usual to set Δf_n in a random manner and to assign random values to the phase ϕ_n . The main objection to using this method is that if a spectral analysis is performed on the resulting time series the spectrum tends to become a series of Dirac delta functions at intervals corresponding to the component frequencies if the spectral resolution is fine enough. For larger spectral resolution the impression is one of a continuous spectrum. However, Goda (1970) has used this method with 50 components to investigate the statistical properties of wave records with success, so that there would be little objection

to the modelling of waves in the laboratory by this method, since it is felt that non-linear transformation of energy would more than compensate for the theoretical lack of wave energy at frequencies other than those of the component waves.

The alternative method, digital filtering, is perhaps an aesthetically more acceptable method since it does not recognise the existence of discrete frequency components. Since the real sea state which it is hoped to model consists of a continuous distribution of energy, it is reasonable to expect that this approach may yield a more realistic model. It is usual to filter a sequence of random numbers, generated such that they possess a normal probability distribution and that the magnitude may be predicted.

The filter used may be considered as a constant parameter linear system, the relationship between the input and output of such a system is considered in the next section.

5.2 Characteristics of Constant Parameter Linear Systems

The synthesis of any time series (digitally or analogically) may be considered as the output of a system. To simplify the analysis of such systems, they are usually assumed to be 'constant parameter linear systems'. The system is said to be linear if its response characteristics are homogeneous and additive. This means that the output produced by a constant times the input is equal to the constant times the output produced by the input alone (homogeneous) and that an output to a sum of a number of inputs is equal to the sum of the outputs produced by the inputs acting alone.

If the input is $x(t)$ and the output $y(t)$ then a system is said to be linear if:

$$a_1 x_1(t) + a_1 x_2(t) \longrightarrow a_1 (y_1(t) + y_2(t)) \qquad (5.2)$$

The constant parameter system implies that the characteristics of the system do not change with time.

An important property of a physical passic system is that of casuality - if the input is zero for $t < t_1$ then the output is also zero during the same interval. The dynamic characteristics of a constant parameter linear system may be realised as a weighting function $h(\tau)$ which is the response of the system to a unit impulse $\delta(t)$ applied at a time τ before. It is very useful because the output for any input is given by the convolution integral:

$$y(t) = \int_0^\infty h(\tau)\, x(t-\tau)\, d\tau \qquad (5.3)$$

The lower limit of integration being zero and not ∞ since that for a physically realisable system it is necessary that the system responds only past inputs. Hence, Equation 2. is valid because any input may be resolved into a continuum of unit impulses. The Fourier transform of $h(\tau)$ is known as the frequency response function $H(f)$ given by:

$$H(f) = \int_0^\infty h(\tau) \exp(-j2\pi f\tau)\, d\tau \qquad (5.4)$$

The frequency response function is a special case of the transfer function which is the Laplace transform of $h(\tau)$:

$$H(p) = \int_{-\infty}^{\infty} h(\tau) \exp(-p\tau)\, d\tau \qquad (5.5)$$

where $p = a + ib$

For physically realisable and stable systems, the frequency response function may replace the transfer function with no loss of useful information. Taking Fourier transform of both sides of Equation 5.3 and noting that $X(f)$ and $Y(f)$ are the Fourier transforms of $x(t)$ and $y(t)$ respectively, then:

$$Y(f) = H(f)\, X(f) \qquad (5.6)$$

The frequency response function may be expressed in terms of a system gain factor $|H(f)|$ and phase angle $\phi(f)$ as:

$$H(f) = |H(f)| \exp(-j\phi(f)) \qquad (5.7)$$

Two properties of the frequency response function of a physically realisable system are of interest. The first is that the gain factor is an even function and the phase angle an odd function. This follows from the consideration of the Fourier transform of real time series as in Equation 2.3. Secondly, if one system is followed directly by another and these are described by $H_1(f)$ and $H_2(f)$, the overall system may be described as $H(f)$ where:

$$H(f) = H_1(f)\, H_2(f) \qquad (5.8)$$

so on cascading systems the gain factors multiply and the phase factors add.

The relationship between $x(t)$ and $y(t)$ may also be described by the cross-spectrum and cross-correlation. The cross correlation function $R_{xy}(\tau)$ is defined as:

$$R_{xy}(\tau) = \lim_{T\to\infty} \frac{1}{T}\int_0^T x(t)\, y(t-\tau)\, dt \qquad (5.9)$$

and is a real valued function. It has many important properties which are very useful in system analysis. For example, when $R_{xy}(\tau) = 0$ the $x(t)$ and $y(t)$ are said to be uncorrelated. If $x(t)$ and $y(t)$ are statistically independent, then $R_{xy}(\tau) = 0$ for all time lags. The cross spectral density function is a complex function $S_{xy}(f)$ the real part $C_{xy}(f)$ is the co-spectral density function and the imaginary part $Q_{xy}(f)$ the quadrature spectral density function.

$$S_{xy}(f) = C_{xy}(f) - j\,Q_{xy}(f) \qquad (5.10)$$

Here again, a two-sided cross spectral density $G_{xy}(f)$ is also defined. The importance of these joint properties is illustrated by considering the cross spectrum between input and output of a system, characterised by a frequency response function. $H(f)$ is given by:

$$S_{xy}(f) = H(f)\, S_x(f) \qquad (5.11)$$

Thus, the frequency response function may be estimated from cross-spectra measurement. Another useful quantity when dealing with two records is the coherence function $\gamma_{xy}(f)$ and is given by:

$$\gamma_{xy}(f) = \sqrt{\frac{|G_{xy}(f)|^2}{G_x(f)\, G_y(f)}} \leq 1 \qquad (5.12)$$

When $\gamma_{xy}(f)$ is equal to zero at a particular frequency then $x(t)$ and $y(t)$ are said to be incoherent (which is the same as uncorrelated). The relationship between the probability density function for the output and that for the input is of importance when synthesising a time series. Davenport and Root (1958) show that if $x(t)$ follows a Guassian distribution and the system is linear, then the output $y(t)$ will also follow a Gaussian distribution.

5.3 Implementation of the Digital Filter

A time series with specific power spectral density and probability density function may be produced by exciting a specially designed filter with white noise. White noise has a constant spectral density function and a specific probability distribution. Physically realisable white noise is band-limited because true white noise would have an infinite variance. Borgman (1967) and Shvestsov and Shorin (1969) use the digital version of Equation 5.3, the water surface elevation being given by:

$$\eta(t_k) = \sum_{n=-K}^{n=K} h(\tau_n)\, x(t_k - \tau_n)\, d\tau_n \qquad k = 0 \ldots M \qquad (5.13)$$

where $x(t_k)$ are the series of random numbers constituting the white noise. The coefficients of the impulse response function being computed by a cosine transform of the frequency response function. The frequency response function may be determined by considering the equation:

$$S_2(f) = |H(f)|^2 S_x(f) \qquad (5.14)$$

If the spectrum $S_x(f)$ of the random numbers is equal to unity for the range of frequencies of interest, then it is a simple matter to make $H(f)$ equal to $\sqrt{S(f)}$, the required spectrum. Both Borgman (1967) and Shvetsov and Shorin (1969) assign zero phase angle to the filter and compute the impulse response as a simple cosine transform. In this case, the filter had to take account of the response function of the signal-paddle movement-wave motion system as well as the desired spectrum, the phase response being unlikely to be zero. By making use of the convolution theorum, it is possible to perform the filtering in the frequency domain instead of the time domain and by using fast Fourier transform methods, considerable computing time may be saved. The author has adopted this method and the practical considerations are now discussed.

The synthesis is based upon a fast Fourier transform (FFT) algorith which computes either forward or inverse (IFFT) transforms as described in Appendix 2.

$$X(n) = \Delta t \sum_{k=0}^{N-1} x(k) \exp(-j 2\pi nk/N)$$
$$x(k) = \Delta f \sum_{n=0}^{N-1} X(n) \exp(j 2\pi nk/N) \qquad (5.15)$$

The time series transformed is $x(k)$ where $t_k = k\Delta t$ and the spacing in the frequency domain is $f_n = n\Delta f$

The "white noise" may be regarded as a sampled time series and is generated as a series of pseudo random numbers on a computer by a standard routine, such that the probability density distribution is Gaussian and the series only repeats after 2^{43} numbers. Digital filtering may be performed as:

$$y(k) = \Delta t \sum_{j=-K}^{j=K} h(j)\, x(k-j) \qquad (5.16)$$

$h(j)$ is a weighting function determined by the frequency response of the filter as:

$$h(j) = \Delta f \ \mathrm{IFFT}(H(n)) \qquad (5.17)$$

For a stable system this weighting function must decrease to a negligible value for large t_j . The value of K used must be such that this is achieved. To achieve this filtering in the frequency domain, it is only necessary to note that the convolution theorum states that Equation 5.16 may be replaced by the finite representation of Equation 5.6, viz.:

$$Y(n) = H(n)\, X(n) \qquad (5.18)$$

The time series $y(k)$ is obtained as the inverse transform of Equation 5.18 as:

$$y(k) = \Delta f \times \text{IFFT}\left(H(n) \times X(n) \right) \qquad (5.19)$$

By substituting for $X(n)$ and noting that $\Delta f = 1/N\Delta t$ the filter algorithm is:

$$y(k) = \frac{1}{N} \text{IFFT}\left(H(n) \times \text{FFT}(x(k)) \right) \qquad (5.20)$$

From Equation 5.14 it may be seen that if $H(n)$ is made equal to the square root of the power spectral density function and that if the spectrum of the white noise is unity, then the time series produced will be the sampled time series representing the water surface elevation. In order to produce a real time series the transform of the series must show the property $X(f) = \bar{X}(-f)$ which is represented in the discrete Fourier transform as a mirror image repeat centred about the term $N/2$. So that this real time series can be produced, the product $\text{FFT}(x(k)) \times H(n)$ must exhibit this property. Thus, the frequency response function is represented by $\sqrt{S(f)/2}\,/T(f)$ with a mirror image repeat. $S(f)$ is the desired spectrum and $T(f)$ the frequency response of the wave generating system. This mirror image representation of the transfer function corresponds to the two-sided representation of the frequency response. The usual restriction of limiting the number of transform points to a power of 2 imposes the relationship mentioned previously between the

time interval and frequency spacing. The length of the transforms used to simulate the filter may be the same as the number of data points it is desired to be produced. However, a more efficient method is to filter segments of the record and then to add them.

Some guide to the most efficient length of transform is given by Helms (1967). As an example, suppose that it is desired to produce a time series of 4096 samples at a time interval of 0.04 seconds. The obvious way is to fast convolve with $N = 4096$, using a frequency response with a resolution of 0.0061 Hz. By using a transform of length 256 and performing the convolution several times, the same time series may be produced faster with a resolution of 0.098 Hz. The addition of each segment to produce the complete series does pose a problem. Since the synthesis is an implementation of Equation 5.16, the points computed which lie outside the range $(K-1)\Delta t$ to $(N-K)\Delta t$ are invalid. A method of overlapping the segments eliminates any errors from this source. The last $N-K$ values from the i^{th} segment are used as the first K values of the $i+1$ segment and the first and last K values for the complete series are discarded.

In practice, the accuracy with which the time series produced compared with the desired series in terms of spectral density is limited by the impulse response of the filter. For the above method to produce a realistic simulation the impulse response, computed as the inverse Fourier transform of the desired spectrum modified by the system response, must approach zero within the range $-K\Delta t, K\Delta t$

If the impulse function has a finite value outside this range, then the series produced will differ from the theoretical. This is analogous to computing the raw spectral density from an autocorrelation function which does not become zero in the range considered.

All the spectra considered in Section 6. for modelling were simulated using this filtering technique with a value of 40 for K. The initial results were not encouraging, several peaks and valleys being present in the spectral shape. However, an investigation revealed that the spectrum of the random numbers was not flat. This error was removed by first analysing the random numbers to be filtered and then modifying the filter shape to allow for any deviation from a flat spectrum. A typical double-peaked spectrum is shown in Fig. 5.1, together with the simulated spectra using firstly the raw random numbers and secondly, the modified filter. In this case, no system transfer function was used. The white noise spectrum is also shown. Table 5.1 summarises the results of the command tape generation. The variance of the sea state is represented by σ_p^2. The theoretical variance of the command signal is σ_c^2 and was determined by considering the power transfer through the system for the particular case being considered. In some cases the comparison is excellent, errors being of the order of 2 per cent. Other spectra, notably those of small magnitude, are subject to errors of the order of 20 per cent. There are several anomalies to this table, for example, spectra 2A and 2B appeared to obtain a better

result using the raw white noise. However, this was found to be caused by spikes in the white noise spectrum adding energy to the resulting series. Further tests indicated that by the use of longer Fourier transforms a better approximation to the desired spectrum is achieved by reducing the number of overlaps.

SPECTRUM	σ_p^2 (mm^2)	σ_c^2 THEORETICAL (mm^2)	σ_c^2 RAW RANDOM NUMBERS (mm^2)	σ_c^2 MODIFIED TRANSFER FUNCTION (mm^2)	K
E6.3	287.1	409.6	554.8	395.4	20
N1	235.9	275.3	323.1	282.6	40
N2	257.8	292.3	411.8	287.0	40
N3	203.0	267.5	310.1	262.2	40
2A	93.7	130.9	144.9	113.5	40
2B	119.1	132.8	133.9	111.1	40
11	123.2	196.5	189.2	168.7	40
12B	74.8	98.5	94.5	82.6	40
M25	145.3	92.7	78.9	82.9	40
M30	256.0	201.5	193.3	195.6	40
T1	302.1	250.7	262.9	257.5	40
T2	381.9	292.2	305.1	302.1	40
TN2	15.0	8.0	-	6.7	40

FIG. 5.1 Command Tape Generation Summary

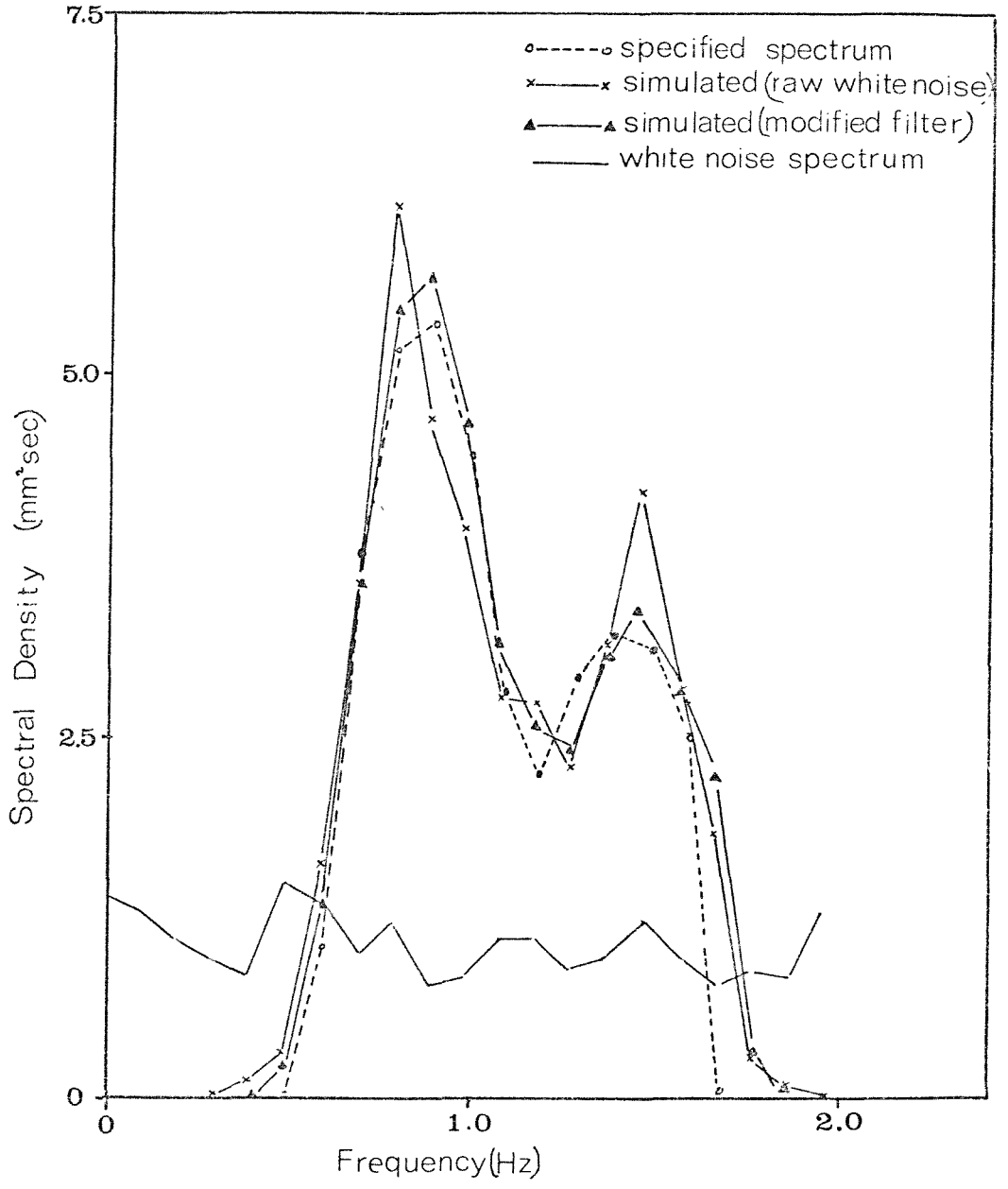

FIG. 5.1 Simulation of Typical Spectrum (T2)

6. EXPERIMENTAL PERFORMANCE

6.1 Experimental Equipment

The experimental work reported on was conducted in a flume at the University of Southampton. The flume is 40 ft. (12.2m) long, 18 in. (0.457m) wide by 18 in. (0.457m) deep. Originally a tilting recirculating flume, considerable work was necessary to convert it into a wave facility. A feature of the flume is the stilling tank at one end which was retained in order to assist the efficiency of any wave absorber installed at that end. The flume is glass-walled for its entire length, support being provided by steel 'U' sections. The tilting capability was also retained from the original installation, this being provided through a hydraulic jack situated 30 ft. (9.15m) from the beach end where a pivot is provided. The flume was levelled carefully before any measurements were taken and the accuracy of construction is such that the maximum deviation of water depth throughout the entire length is 5 mm. Two rails are provided on top of the flume side supports to allow instrument trolleys to be used. These rails are capable of being levelled separately from the flume. Since the base of the wave flume is 53 in. (1.35m) off ground level it was necessary to provide a walkway to provide a convenient working platform. Shelves for instruments were also provided on a nearby wall.

A piston-type paddle was installed at the opposite end from the stilling tank. The paddle consists of an $\frac{1}{8}$ in. (3.175mm) sheet of aluminium cut to fit the channel leaving a minimum gap between the metal and glass. A seal was formed by two flaps of neoprene,

attached to the paddle such that the water pressure effected an efficient seal. The aluminium sheet was attached to a framework of aluminium angle as shown in Plate 6.1. The paddle and supporting framework are supported on linear bearings which run on ground steel shafts supported in three places. The total stroke of the paddle is 45 cm. Initially, a monochromatic generating system was installed, consisting of a Kopp 1¾ hp motor and gear box capable of providing frequencies of 0.3 Hz to 2.3 Hz. A connecting rod of length 120 cms. is provided from the paddle to an eccentric attached to the motor. The eccentric provides a maximum throw of 27.0 cm. which may be set by use of a vernier scale to an accuracy of $1/50^{th}$ mm. The centre line of the axis of rotation of the eccentric is situated 40 mm above the line of action of the connecting rod on the paddle. The power of the motor is grossly over-estimated in order to provide smooth rotational motion over the entire range of amplitude and frequencies, very little power being required to overcome bearing friction in the paddle mechanism.

6.2 Wave Data Acquisition System

The capacitance probe method of measuring water surface elevation used at the University is mainly due to the work of Bullock (1967) and Harris (1973). In essence, the probe forms a capacitor using a length of insulated wire suspended vertically through the water surface. The insulation forms the di-electric whilst the two poles are the conductor and the water. As the water rises and falls, the capacitance varies linearly with depth of immersion. The probe forms

part of the frequency selection circuit of an oscillator, such that the frequency of oscillation varies linearly with capacitance. This frequency modulated signal is fed to a frequency discriminator, which produces a voltage proportional to the water surface elevation. The system of oscillator and discriminator used is a proprietary unit manufactured by Shandon Southern Instruments under serial numbers M.1860 and M.1828. The carrier frequency employed is 2 MHz, a change in capacitance of $\pm$ 10 pF produces a frequency change of $\pm$ 20 kHz which in turn produces an output of 0 to 2 volts from the discriminator.

The probe is constructed from pvc covered miniature stranded (0.7/40) wire 0.89 mm in diameter. It is attached at one end to a hollow perspex box 38 mm by 42 mm, and to a perspex bar 38 mm long and 4.7 mm in diameter at the other end. The two pieces of perspex are separated by two stainless steel strips which also provide electrical connection with the water. The effective length of the probe is 23 cm. with a capacitance of approximately 2 pF/cm. Thus, the maximum wave height which can be measured with this system is 10 cm. However, it was found that the range could be extended to a range of 30 pF without deviating significantly from a linear calibration. A second input has also been provided on the oscillators which responds to a change of 60 pF . The electronics of the system are such that the linearity is better than $\pm$ 1 per cent and the drift better than 0.1 per cent full scale deflection per degrees C. A maximum noise level of 6 mv means that changes of capacitance of 0.006 pF may be detected. This is equivalent to a wave height of

0.03 mm. However, in practice, it is the wave probe meniscus which limits the accuracy to 1 mm. The wire used was found to be free from other vices such as water absorption and wetting effects. It was found that small changes (< 5 per cent) in capacitance due to changes in temperature of the order of $10^{o}C$. affected the calibration, thus the procedure was to calibrate the probe over a limited range daily before use.

The effect of meniscus raises the question as to whether a better system of water surface elevation can be developed. Certainly any system which uses a probe crossing the air water boundary will have a meniscus, however small. Perhaps methods using some form of electromagnetic radiation such as laser inferometry may prove worth development.

Two methods of recording the information produced by the wave probes were used. A six channel UV recorder was used to graphically record the water surface elevation. Electronically, errors in this recorder may be regarded as negligible. Frequency response is also adequate. The resolution of the trace produced is determined by the width of the trace and this was generally equivalent to 1 mm water surface elevation. Interchangeable galvanometers allow a wide range of signals to be recorded on chart paper 17 cm wide. Timing pulses are also provided as spacings of either 0.1 sec. or 1 sec. to an accuracy of better than 1 per cent. Four chart speeds are generally available: 10, 25, 100, 250 mm/sec. A second UV recorder was available if higher speeds were required, the maximum being 1 m/sec. Later, a signal conditioning unit was added to the UV recorder to obviate the

necessity of changing galvanometers and consequent signal matching.

The main method of recording wave data was on magnetic tape using a Thermionic T.3000 Mk. II FM tape recorder. Four channels of data could be recorded as a voltage simultaneously, at any one of four tape speeds 17/8, 3¾, 7½ and 15 in. per second.

Linearity of the recording is typically ± 1 per cent and signal-to-noise ratio of 35 to 39 dB, with adequate bandwidth for the phenomena to be recorded. Any voltage between zero and 15 volts peak-to-peak may be recorded via a built-in attenuator and replayed with a maximum amplitude of ± 1 volt.

Two methods were readily available for the analysis of the tape recordings. A Dynamco Series 6000 data logger was available which digitised the signal and punched paper tape which was compatible with the University computer. A variety of plug-in units make this a very versatile piece of equipment. The digital voltmeter used required an input of maximum amplitude ± 1 volt (compatible with tape recorder), with a resolution of 0.1 mv. The maximum operating rate is 10 samples per second to a timing accuracy of 0.01 per cent. Long term accuracy of the voltmeter is 0.01 per cent of reading in one year. All four channels of the tape recorder may be sampled sequentially, the maximum rate of digitisation will then 2.5 samples per second per channel. By suitable combination of recording speed, replay speed and sampling rate, a maximum 'real time' sampling rate of 40 samples per second for a single channel may be achieved. This process was used only for initial trial runs since the turn-around time on the University computer was too long to allow convenient

analysis of many records.

The Data Analysis Centre, as mentioned in Section 3., was used exclusively in the analysis of the tape recordings. Analysis of the laboratory waves was aided by the addition of routines which enabled wave heights to be determined as well as spectral and statistical properties. This method was also adopted for the analysis of the paddle motion (via the feedback transducer) and command signal.

To summarise, the water surface elevation was recorded via a capacitance probe, either graphically or in computer-compatible form on magnetic tape with a minimum resolution of 1 mm, this accuracy being limited by the meniscus effect on the probe. The linearity of the system was better than 2 per cent. The procedure adopted was to calibrate the wave probe immediately before use by means of the vernier scale attached to the probe carriage. This calibration was then found to be essentially constant over a period of several hours.

6.3 Regular Wave Investigation

An absorbing beach consisting of aluminium swarf and hairlock was installed at the opposite end of the channel to the wave generator. Initially, a mattress 15 cm thick consisting of a wire mesh frame packed with aluminium swarf was installed, with a slope of 1:6. The absorbing effect of this was surprisingly good. With this in mind, two baskets of swarf were constructed and placed in the stilling tank and a further wedge-shaped basket placed in the last section of the flume. Spaces between the baskets of swarf were filled with hairlock.

The complete absorbing beach is illustrated in Fig. 6.2.

Further tests using regular waves produced by the Kopp motor arrangement were performed to determine the coefficient of reflection for this beach. The results are shown graphically in Fig. 6.3. In general, the coefficient is less than 4 per cent, although considerable scatter is evident. This is due to the fact that the magnitude of the phenomena to be measured to determine the reflection approaches the limit in accuracy of the instrument. The envelope method described by James (1969) was used to determine the coefficient of reflection. For a wave height of 10 cm with 1 per cent reflection it was necessary to measure the wave height at two points to an accuracy of 1 mm. Since the reflection of frequencies of interest was so small, it was neglected in all further tests.

In Section 5. the generation of command tapes by a digital linear filter was described. This method assumes that the transfer function from paddle amplitude to wave amplitude may be represented as a linear system. The generation of waves is for certain frequencies non-linear, being more pronounced as wave length increases relative to water depth. The waves produced are characterised by a second harmonic as described by Madsen (1971). In order to be able to make use of the linear theory for predicting wave heights, the harmonic content of waves of various frequencies was examined. The method used for determing the harmonic content of the wave form is similar to that described in Section 4. for dealing with the paddle motion. Fig. 6.4 summarises the test results. Generally, the second harmonic content increases with wave length and amplitude. However, the points for frequencies of

1.0 Hz and 1.4 Hz show a reversal of this trend with respect to wave length. This may be due to instability in the shape resulting from the wave tending to limiting steepness. From these tests it is possible to determine a region where the linear theory may be applied with reasonable confidence.

It was proposed that the transfer function from paddle motion to wave motion be based on small-amplitude theory and is given by:

$$\frac{a}{e} = \frac{2 \sinh^2 \frac{2\pi d}{L}}{\sinh \frac{2\pi d}{L} \cosh \frac{2\pi d}{L} + \frac{2\pi d}{L}} \qquad (6.1)$$

where a = wave amplitude e = paddle amplitude

An investigation into the validity of this equation yielded the graph in Fig. 6.5. In general, the agreement with theory is good for frequencies between 0.5 Hz and 1 Hz whilst at higher frequencies, there is considerable scatter.

The wave length of waves produced in the channel was also measured, two methods being used. Two wave probes were installed a known distance apart for the first method. A trace from each probe was displayed on the UV recorder and from the phase lag between the two signals a simple calculation yielded the wave length. The second method was described by Earattupuzha and Raman (1972) and only one probe was required. Both methods yielded results which agreed within the limits of experimental error. The wave length predicted by Airy theory was compared with the experimental values, the typical difference being of the order of 4 per cent, although differences of up to 10 per cent were noticeable in the shorter waves. All the regular wave studies were conducted with a water depth of 35 cm.

From the previous test, it was possible to define very approximately an amplitude frequency domain in which the linear theory of wave generation may be applied with reasonable confidence. The amplitude is limited in all frequencies by the linear portion of the wave probe characteristics, and at high frequencies by the limiting wave steepness (which was determined experimentally in the regular wave investigation). The low frequency limit is restricted by the generation of secondary harmonics, with a cut-off at approximately 0.3 Hz.

6.4 Programmed Wave Investigation

Punched tapes were prepared using the method described in Section 5. and the resulting performance evaluated in three stages:

1. Accuracy of sea state simulation.
2. Wave-maker motion under programmed conditions.
3. Transfer function between paddle motion and wave motion under programmed wave generation.

It had been hoped that all the prototype spectra described in Section 3. would be simulated in the laboratory. However, in order to produce a reasonable variance for many of the Jersey records a scale factor of the order of 1:10 was required. This produced a model spectrum with very low frequency content which was undesirable because such low frequencies corresponded to a wave length of the same order of magnitude as the length of the flume. In fact, only four records from Jersey were suitable for simulation. The prototype records were thus supplemented by Moskowitz spectra

and two arbitrary shapes chosen to provide a variety of spectral conditions. Details of the spectra used for simulation are given in Table 6.1. A water depth of 350 mm was used for all the tests since this corresponded to the model water depth for the NAB Tower spectra and the model depths for the other spectra were impractical.

The command tapes for the simulation were generated by the method described in Section 5. The frequency response function for the wave generating system consisted of two parts. The relationship between wave amplitude and paddle amplitude was taken as that for small amplitude theory given in Equation 6.1. The second part, that of command signal to paddle motion in terms of amplitude and phase was measured as described in Section 4. for a gain of 25 $sec.^{-1}$ These parts were combined to form $T(f)$ as defined in Section 4. as:

$$T(f) = \frac{a}{e}(f) \times \frac{e}{R}(f)$$

where R represents the command signal. The reciprocal of the frequency response, i.e. the modification to the spectrum to produce the desired filter, is shown in Fig. 6.6. All the command tapes used in the tests consisted of 8000 numbers giving a running time of 5 mins. 20 secs.

The waves produced by the wave generator at a test section 7 m. from the paddle were recorded on the Thermionic tape recorder and analysed in the Data Analysis Centre. The following were computed for each record.

1. Spectral Properties.

(a) power spectral density function, $S(f)$

(b) area under power spectral density function, m_o

(c) spectral width, ε

(d) peakedness, Q_p

The power spectral density function was computed using Hanning smoothing, a resolution of 0.061 Hz and 62 degrees of freedom. The computation was performed via the fast Fourier transform (see Appendix 2.). Parameters 1b, 1c and 1d were calculated on a desk-top computer from a paper tape output of the spectral density function, the latter two being determined from a 95 per cent cut-off point as mentioned in Section 3.

2. Statistical Properties.

(a) probability distribution of water surface elevation $p(\eta)$

(b) variance of water surface elevation σ^2

(c) skewness, β_1

(d) kurtosis β_2

(e) probability distribution of wave heights (normalised with respect to the water surface standard deviation $p(\frac{H}{\sigma})$), waves defined by zero upcrossing method

(f) mean wave height, H_{mean}

(g) root mean square wave height, H_{rms}

(h) the significant wave height, H_s

(i) the mean height of the highest tenth waves, $H_{1/10}$

(j) the distribution of maxima $p(\alpha)$

(k) the number of maxima N_c

Properties 2f, 2g, 2h and 2i were computed subsequent to the main calculation from a punched tape listing of the wave heights.

The power spectral density functions for the simulated sea states are shown in Fig. 6.7 - 6.19, together with the specified spectra. The surface elevation distribution and wave height distributions are also given in these figures and are compared with Gaussian and Rayleigh distributions respectively. A summary of the results is given in Table 6.2.

The values of variance, spectral width and peakedness for the simulated spectra are compared with scaled prototype values in Table 6.3(a). It was hoped to be able to compare significant wave heights for modelled and prototype conditions. However, in a number of cases, prototype values were not available. Table 6.3(b) compares these values for the Eastbourne and NAB Tower spectra.

In order to gain more information concerning the validity of expressions given in Section 2. relating the various wave height parameters to the standard deviation of the record, the following ratios were computed from the simulated sea states:

(a) The ratios of significant wave height, root mean square wave height, and mean height of the tenth highest waves to the standard deviation, H_s/σ , H_{rms}/σ , $H_{1/10}/\sigma$.

(b) The ratio of the standard deviation of the wave heights to the standard deviation of the water surface elevation.

(c) The ratio of mean wave height to standard deviation of water surface elevation.

These ratios are tabulated in Table 6.4 and compared graphically with the theoretical values in Fig. 6.20. The peak distributions

for a number of records are compared graphically with the Rayleigh distribution in Fig. 6.21.

The problem of repeatability was also investigated by repeating the tests on different days. Some difficulty was experienced at first in obtaining reliable results. This was because the gain setting on the Moog Servocontroller is adjusted by means of a screwdriver operated,one turn potentiometer, one complete turn representing a range of 100:1. Consequently, it was necessary to adjust this by trial and error until the correct setting was reached. Modifications are in hand to eliminate this clumsy procedure. Having established the correct gain setting, it was found that the total energy in the spectrum could be repeated with an accuracy of approximately 3 per cent.

The variation of the spectral form was also studied. Initially, the waves were recorded at five stations along the channel. However, differences between the intermediate stations were very small and only two stations are considered in detail. Fig. 6.22 - 6.24 show the variation of the probability distributions of wave height and water surface elevation between the test section 7 m. from the paddle and the first station 1.5 m. from the paddle. The spectral plots are not shown since they were almost identical at both stations. The results are summarised in Table 6.5.

6.5 Wave Maker Motion under Programmed Conditions

Whilst the tests on the generation of programmed waves were being conducted, the command signal and paddle motion were also recorded. The paddle motion was monitored from the feedback transducer signal. By computing the spectral density for each signal and the cross spectral density, it was possible to compute the frequency response function and coherency function by making use of the relationships outlined in Section 5. Typical results are shown in Fig. 6.25.

6.6 The Relationship between Wave Amplitude and Paddle Amplitude Under Programmed Conditions

A method similar to that described in Section 6.4 was used to determine the frequency response function between paddle motion and wave motion and the coherency function for the system. Initially, the frequency response function was computed by complex division of the cross spectrum by the input spectrum. This yielded erroneous results and a large deviation of the coherency function from unity indicated that the system was far from linear. However, calculation of the frequency response by division of the autospectra yielded much more realistic results.

Typical frequency response functions are shown in Fig. 6.26. The erroneous results mentioned are due to the very large phase differences between paddle motion and the wave motion at the probe, which reduces the accuracy of the computations. A comparison between the variance, skewness and kurtosis for paddle motion and water motion is given in Table 6.6.

SERIAL NO. DESIGNATION	SCALE	NOTES
E6.3	1:10	
N1	1:50	
N2	1:50	
N3	1:50	
2A	1:36	
2B	1:36	
11	1:36	
12B	1:36	
T1	-	Arbitrary Spectrum
T2	-	Arbitrary Spectrum
TN2	1:200	N2 scaled to 1:200
M25	1:50	Moskowitz for 25 m./s.
M30	1:50	Moskowitz for 30 m./s.

TABLE 6.1 Details of Simulated Spectra

SPECTRUM	VARIANCE (mm^2)	SKEWNESS	KURTOSIS	NUMBER OF WAVES	SPECTRAL WIDTH	PEAKEDNESS	NUMBER OF PEAKS	H_{rms} mm	H_s mm	$H_{1/10}$ mm	H_{max} mm	m_o mm^2
E6.3	310.0	0.283	1.959	233	0.549	2.644	270	48.7	68.1	84.6	126.0	303.3
N1	238.0	0.129	2.182	244	0.511	2.44	273	42.1	58.8	73.5	81.4	237.2
N2	256.0	0.190	1.74	257	0.517	2.014	321	44.3	60.5	72.3	85.8	256.0
N3	210.0	0.167	1.91	241	0.520	2.134	304	39.3	53.7	67.0	79.9	209.1
M25	139.5	0.155	2.30	324	0.425	2.459	359	30.8	42.6	51.6	66.9	127.4
M30	233.0	0.570	0.61	288	0.449	2.395	315	43.3	58.8	75.2	174.9	219.5
2A	79.0	0.181	4.45	273	0.627	1.480	347	23.6	33.1	40.4	72.3	76.9
2B	94.5	0.206	3.80	303	0.587	1.530	357	26.0	36.0	45.5	98.8	93.3
11	75.9	0.215	4.74	272	0.697	1.253	325	22.4	31.5	41.0	54.7	76.3
12B	65.0	0.125	4.50	273	0.612	1.547	368	21.7	29.9	37.5	53.0	64.2
T1	296.0	0.274	1.44	279	0.462	2.295	308	47.2	64.6	77.1	118.6	290.7
T2	322.0	0.222	1.723	282	0.495	2.28	-	49.75	68.1	83.5	108.1	319.6
TN2	7.45	0.66	-	433	0.429	2.28	353	7.36	10.2	13.1	36.0	7.11

TABLE 6.2 Summary of Statistics of Simulated Spectra

SPECTRUM	VARIANCE (mm^2)		RATIO	SPECTRAL WIDTH		PEAKEDNESS	
	SPECIFIED	SIMULATED		SPECIFIED	SIMULATED	SPECIFIED	SIMULATED
E6.3	287.0	310.0	1.08	0.519	0.549	2.593	2.644
N1	235.9	238.0	1.01	0.549	0.511	2.266	2.44
N2	257.0	256.0	0.99	0.583	0.517	1.741	2.014
N3	203.0	203.0	1.00	0.543	0.520	2.008	2.134
M25	145.3	139.5	0.96	0.513	0.425	1.891	2.459
M30	256.0	233.0	0.91	0.510	0.449	1.958	2.395
2A	94.0	79.0	0.84	0.68	0.627	1.42	1.480
2B	119.1	94.5	0.80	0.64	0.587	1.57	1.530
11	98.3 (123.3)	75.9	0.77	0.801	0.697	0.618	1.253
12B	67.8 (74.8)	65.0	0.96	0.648	0.612	1.484	1.547
T1	302.1	296.0	0.98	0.484	0.462	2.133	2.295
T2	381.9	322.0	0.85	0.489	0.495	2.017	2.126
TN2	15.0	7.45	0.50	0.634	0.429	1.477	2.28

TABLE 6.3a Comparison of Specified Values of Variance, Spectral Width and Peakedness

SPECTRUM	H_{rms} (mm)		H_s (mm)		$H_{1/10}$ (mm)	
	SPECIFIED	SIMULATED	SPECIFIED	SIMULATED	SPECIFIED	SIMULATED
E6.3	43.7	48.7	62.1	68.1	75.2	84.6
N1	45.0	42.1	61.7	58.8	72.7	73.5
N2	44.0	44.3	61.6	60.5	84.0	72.3
N3	46.8	39.3	64.8	53.7	96.0	67.0

TABLE 6.3b Comparison of Wave Heights from Prototype and Simulated Sea States

SPECTRUM	$\frac{H_{mean}}{\sigma}$	$\frac{\sigma(H)}{\sigma}$	$\frac{H_{rms}}{\sigma}$	$\frac{H_s}{\sigma}$	$\frac{H_{1/10}}{\sigma}$
E6.3	2.46	1.25	2.77	3.87	4.81
N1	2.47	1.16	2.72	3.81	4.76
N2	2.52	1.12	2.77	3.78	4.52
N3	2.47	1.12	2.71	3.70	4.62
2A	2.39	1.16	2.67	3.73	4.54
2B	2.37	1.22	2.68	3.72	4.69
11	2.27	1.19	2.57	3.62	4.71
12B	2.42	1.15	2.69	3.71	4.66
T1	2.49	1.15	2.72	3.76	4.48
T2	2.52	1.14	2.77	3.80	4.65
TN2	2.37	1.26	2.70	3.72	4.78
M25	2.44	1.16	2.71	3.74	4.53
M30	2.51	1.17	2.84	3.86	4.93

TABLE 6.4 Wave Height Statistics for Simulated Sea States

SPECTRUM	DISTANCE FROM WAVE GENERATOR (m)	VARIANCE (mm^2)	SKEWNESS	KURTOSIS	T_z (sec)	ε	Q_p	H_{rms} mm	H_s mm	$H_{1/10}$ mm
N2	1.5	261.0	0.33	1.87	1.095	0.567	1.955	43.4	61.3	78.6
	7.0	256.0	0.19	1.74	1.01	0.517	2.014	44.3	60.5	72.3
T1	1.5	319.0	0.34	1.70	1.12	0.472	2.256	48.9	69.3	84.4
	7.0	296.0	0.274	1.44	1.09	0.462	2.295	47.2	64.6	77.1
2A	1.5	80.0	0.184	3.79	1.17	0.644	1.406	23.0	32.6	40.0
	7.0	79.0	0.181	4.45	1.07	0.627	1.480	23.7	33.1	40.3

TABLE 6.5 Comparison of Computed Statistics for Waves Recorded at Distances of 1.5 m. and 7.0 m. from the Wave Generator

SPECTRUM	RATIO OF VARIANCE WAVE/PADDLE MOTION	SKEWNESS		KURTOSIS	
		WAVE	PADDLE	WAVE	PADDLE
E6.3	0.695	0.17	-0.04	2.14	2.92
N2	0.868	0.255	-0.08	2.183	2.80
N3	0.769	0.157	0.05	2.20	3.05
2A	0.71	0.128	0.045	3.88	3.64
11	0.51	0.646	0.04	11.69	3.26
T1	1.19	0.165	-0.03	2.14	3.03

TABLE 6.6 Comparison of Variance, Skewness and Kurtosis of Wave Motion and Paddle Motion for Selected Cases

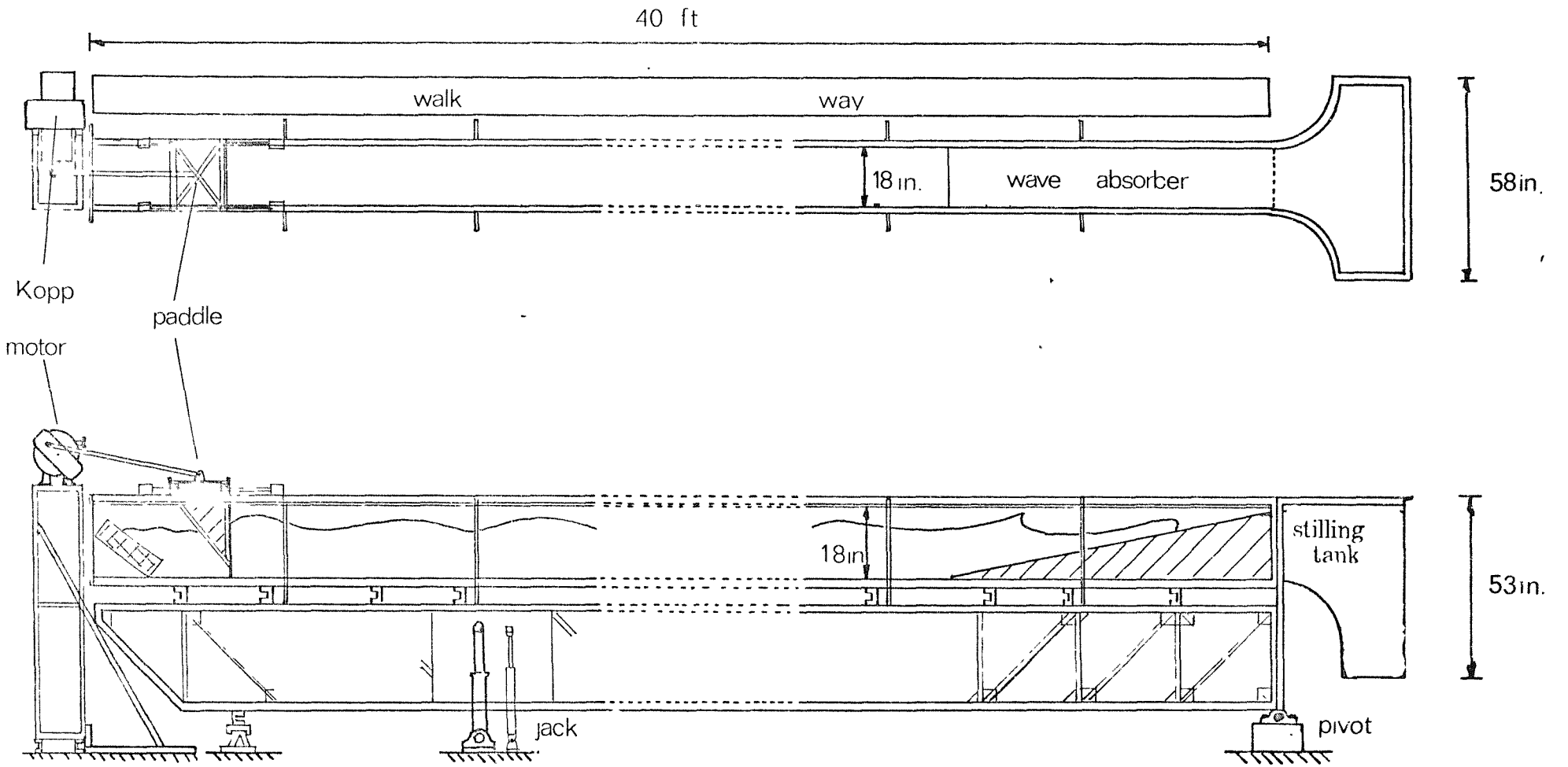

FIG. 6.1 General Arrangement of the Experimental Facility

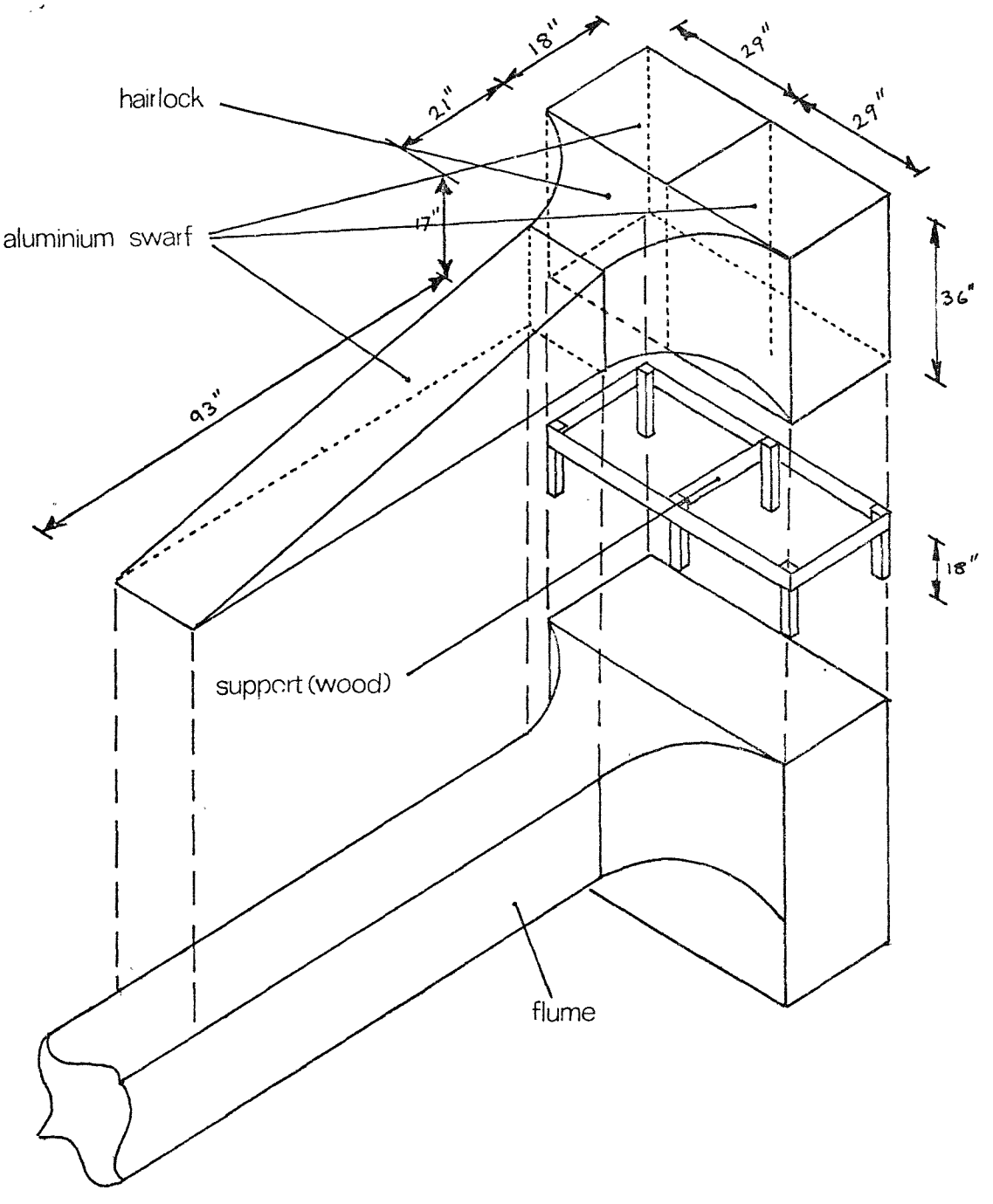

FIG. 6.2 Details of the Absorbing Beach

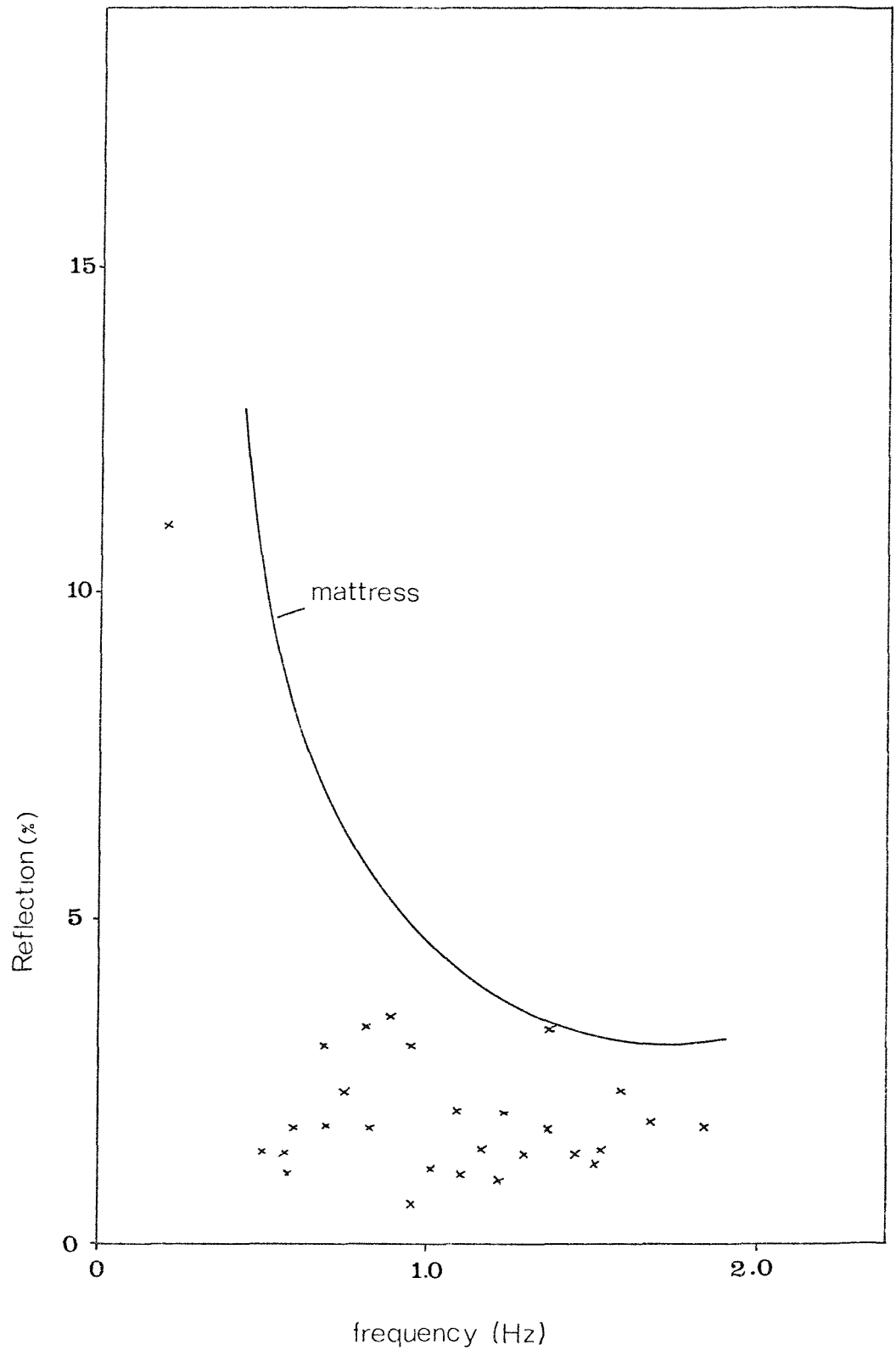

FIG. 6.3 Experimentally-Determined Reflection Coefficient

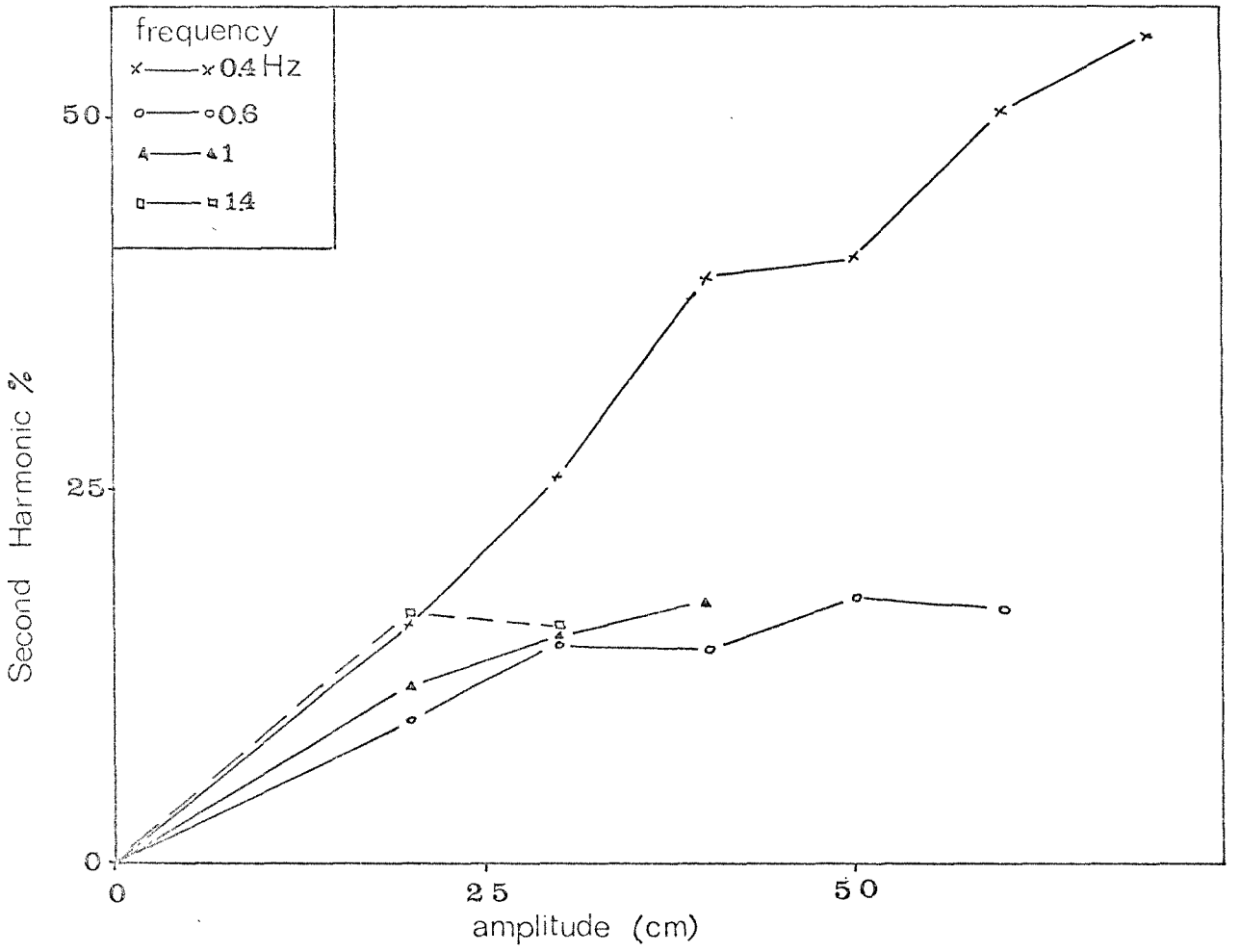

FIG. 6.4 Harmonic Content of the Waves in the Channel (Water Depth = 350 mm.)

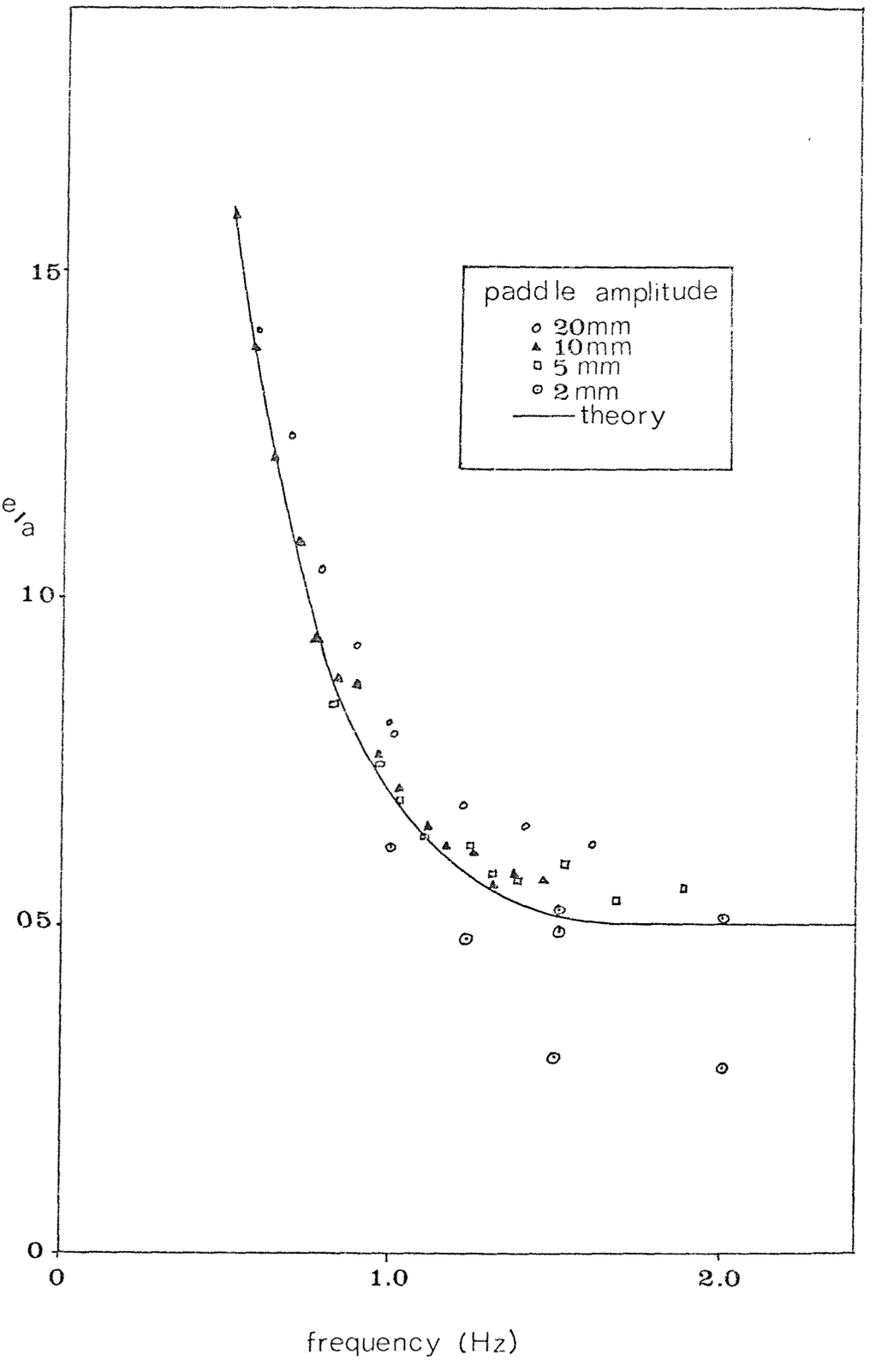

FIG. 6.5 Comparison of Experimental and Theoretical Values of Paddle Amplitude Divided by Wave Amplitude

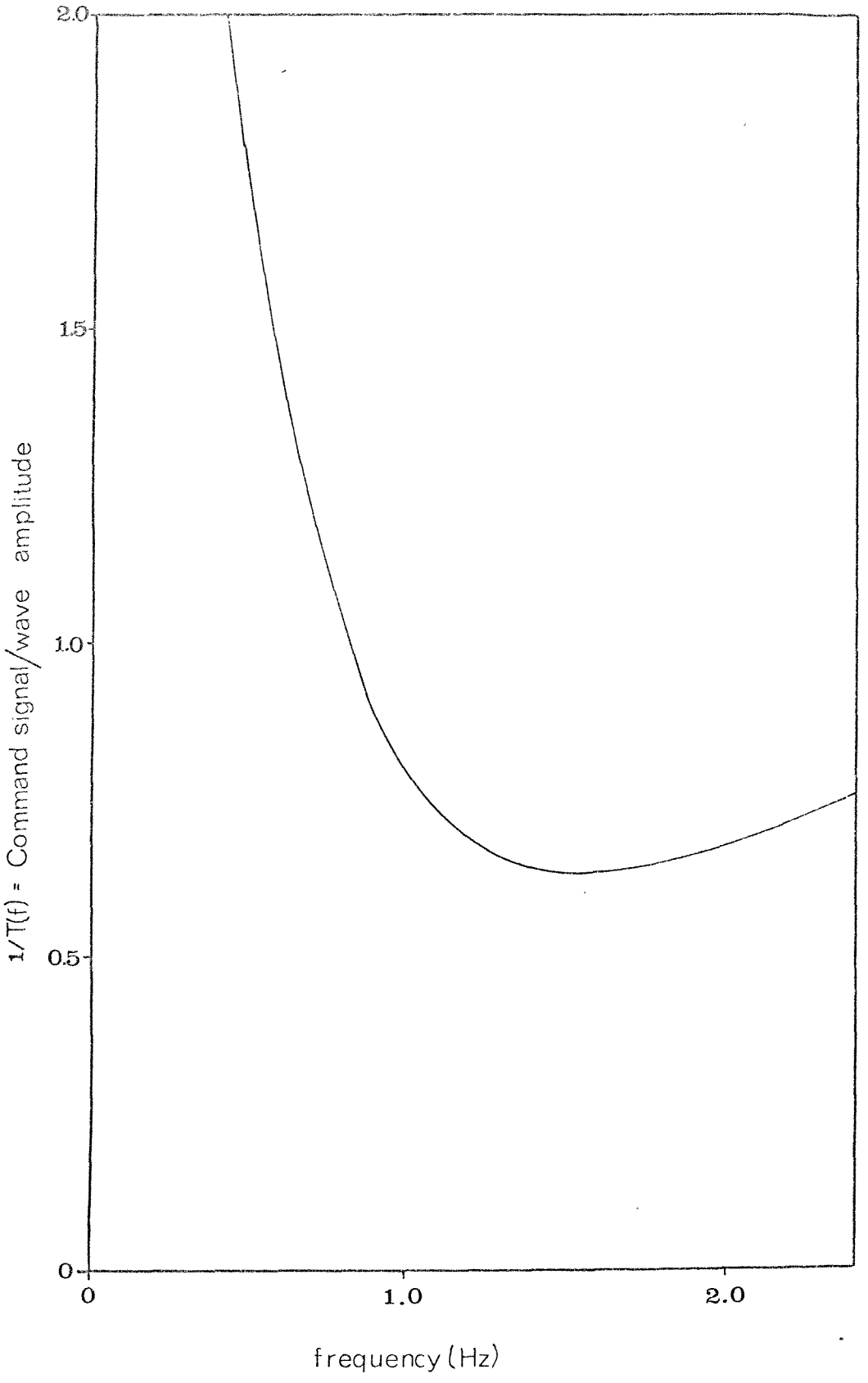

FIG. 6.6 The Reciprocal of the Frequency Response Function used in the Digital Filter

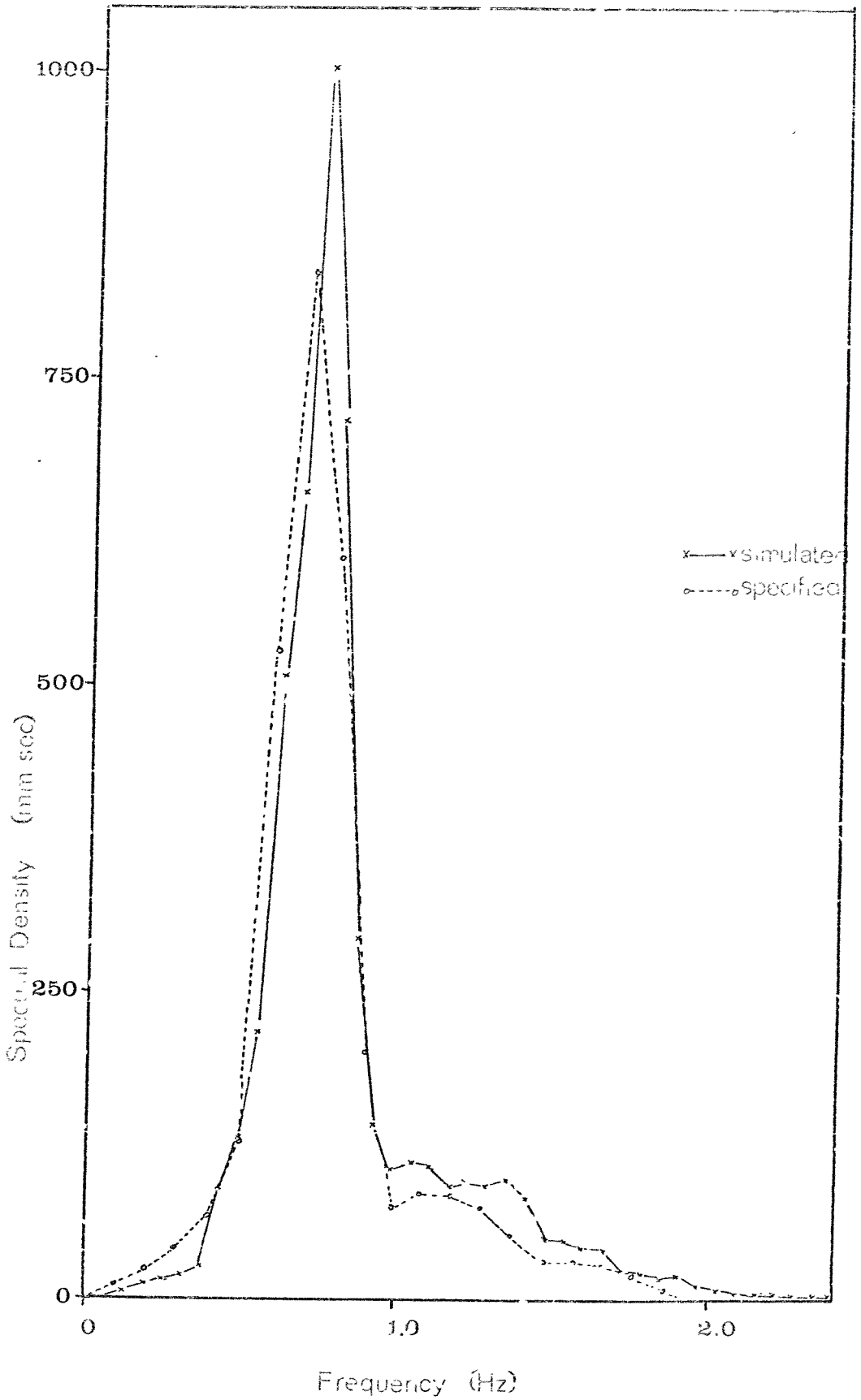

FIG. 6.7a Comparison of Simulated and Specified Values of Spectrum E6.3

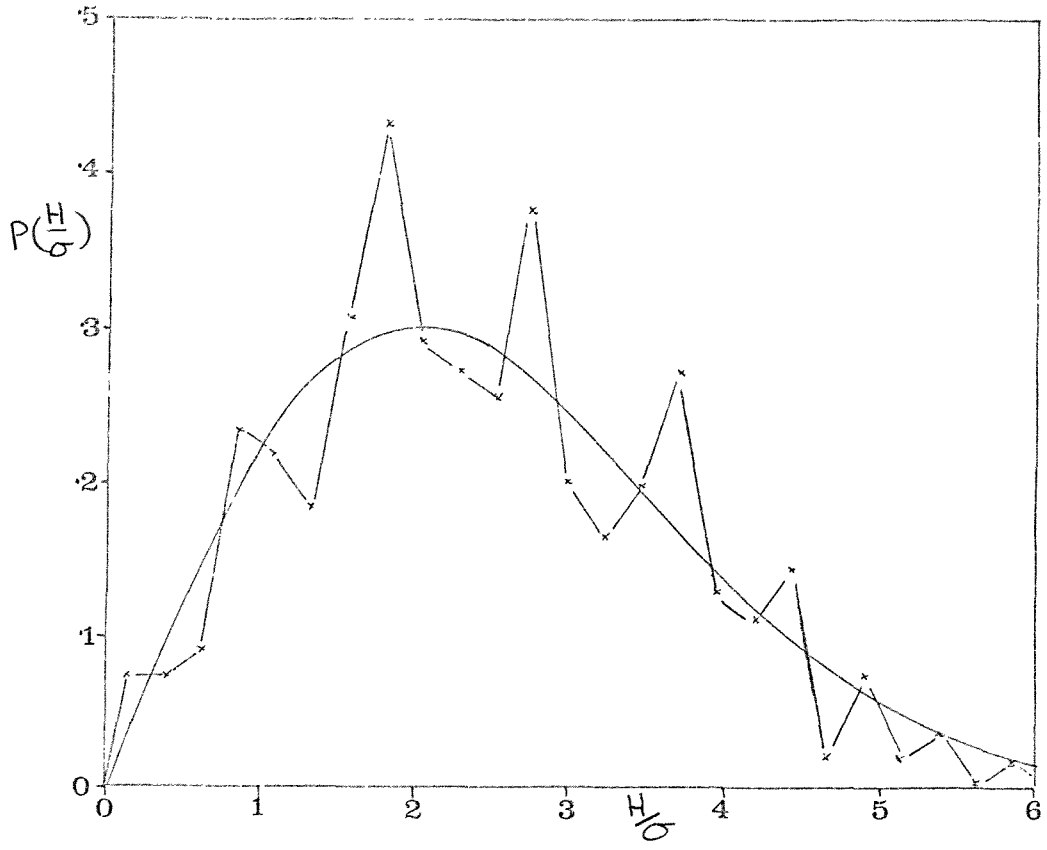

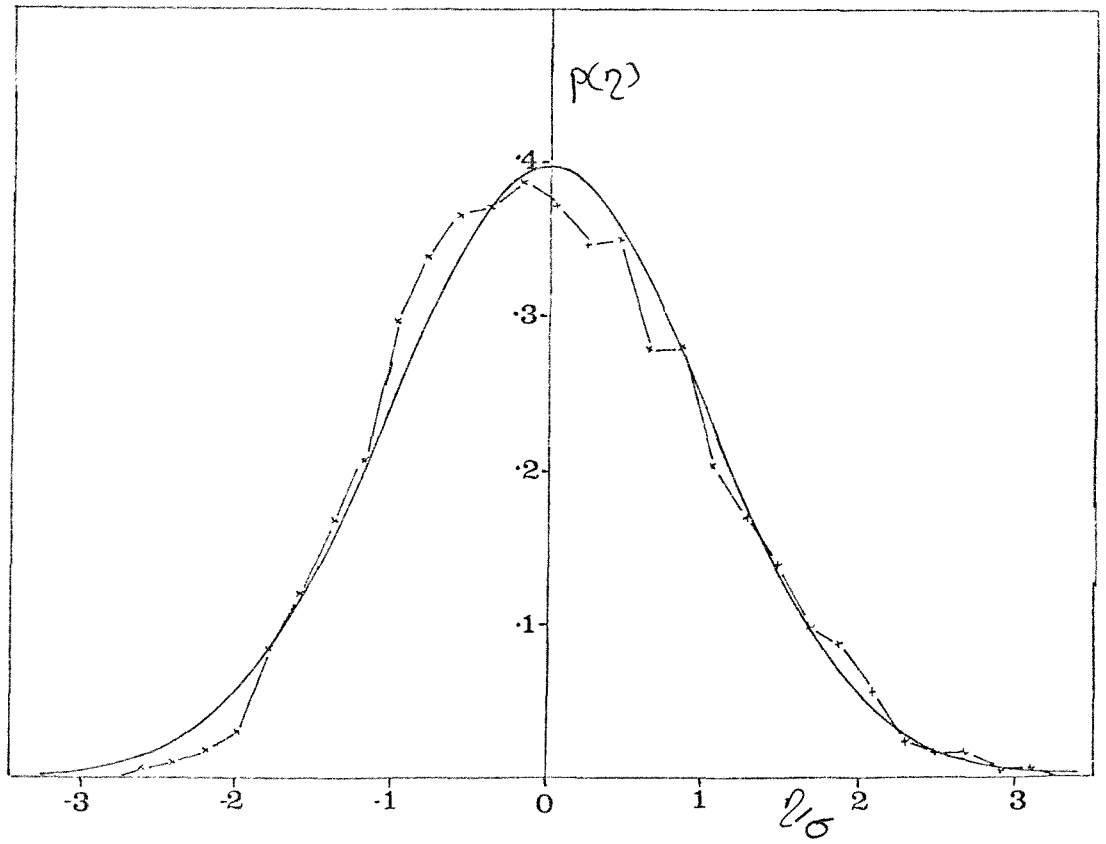

FIG. 6.7b Probability Distribution of Wave Heights and Water Surface Elevation for Spectrum E6.3

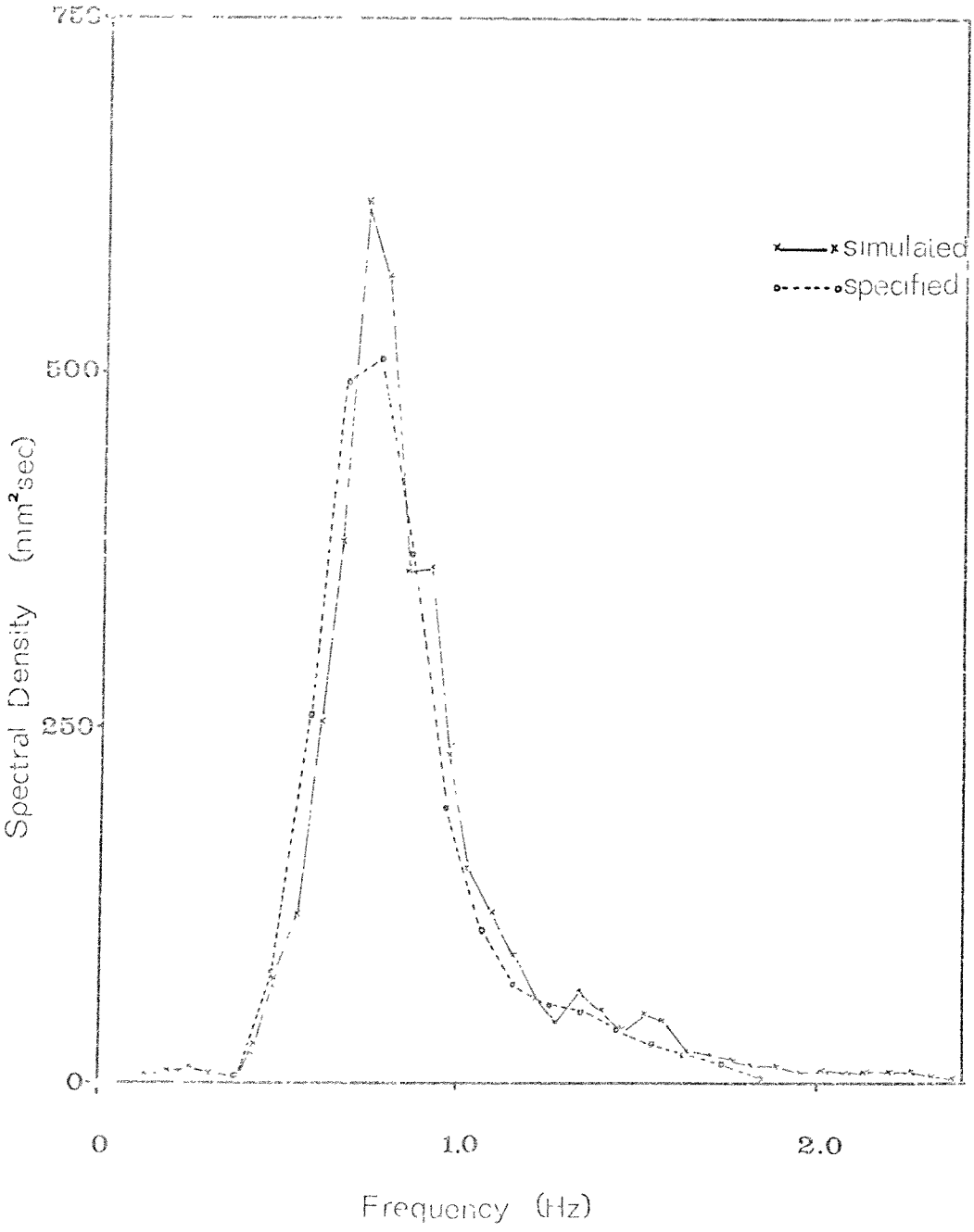

FIG. 6.8a Comparison of Simulated and Specified Values of Spectrum N1

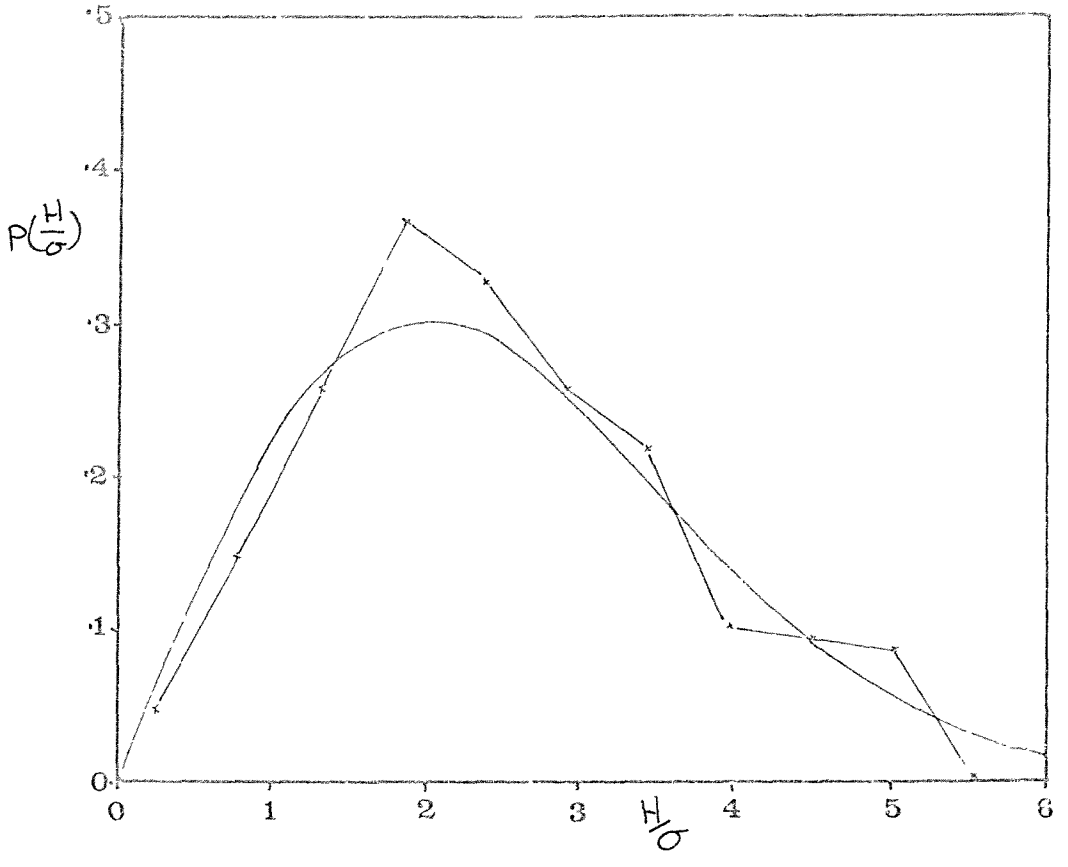

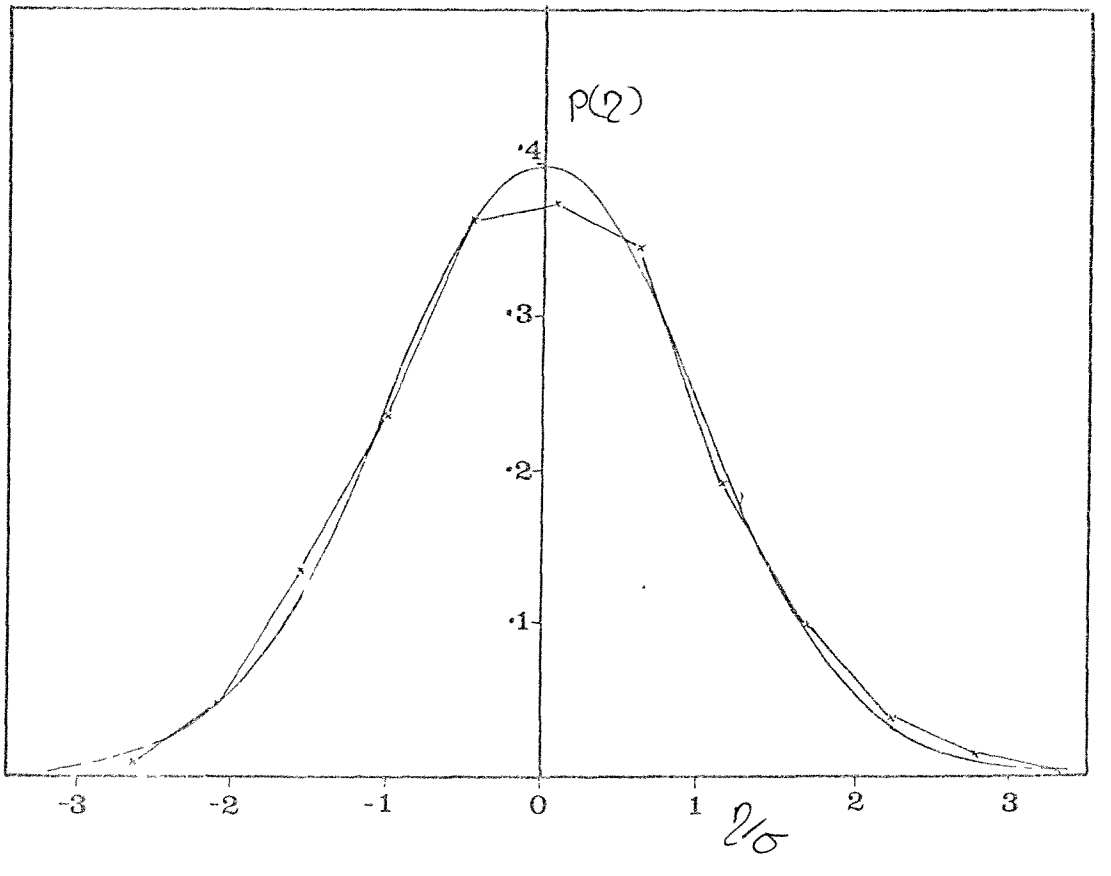

FIG. 6.8b Probability Distribution of Wave Heights and Water Surface Elevation for Spectrum N1

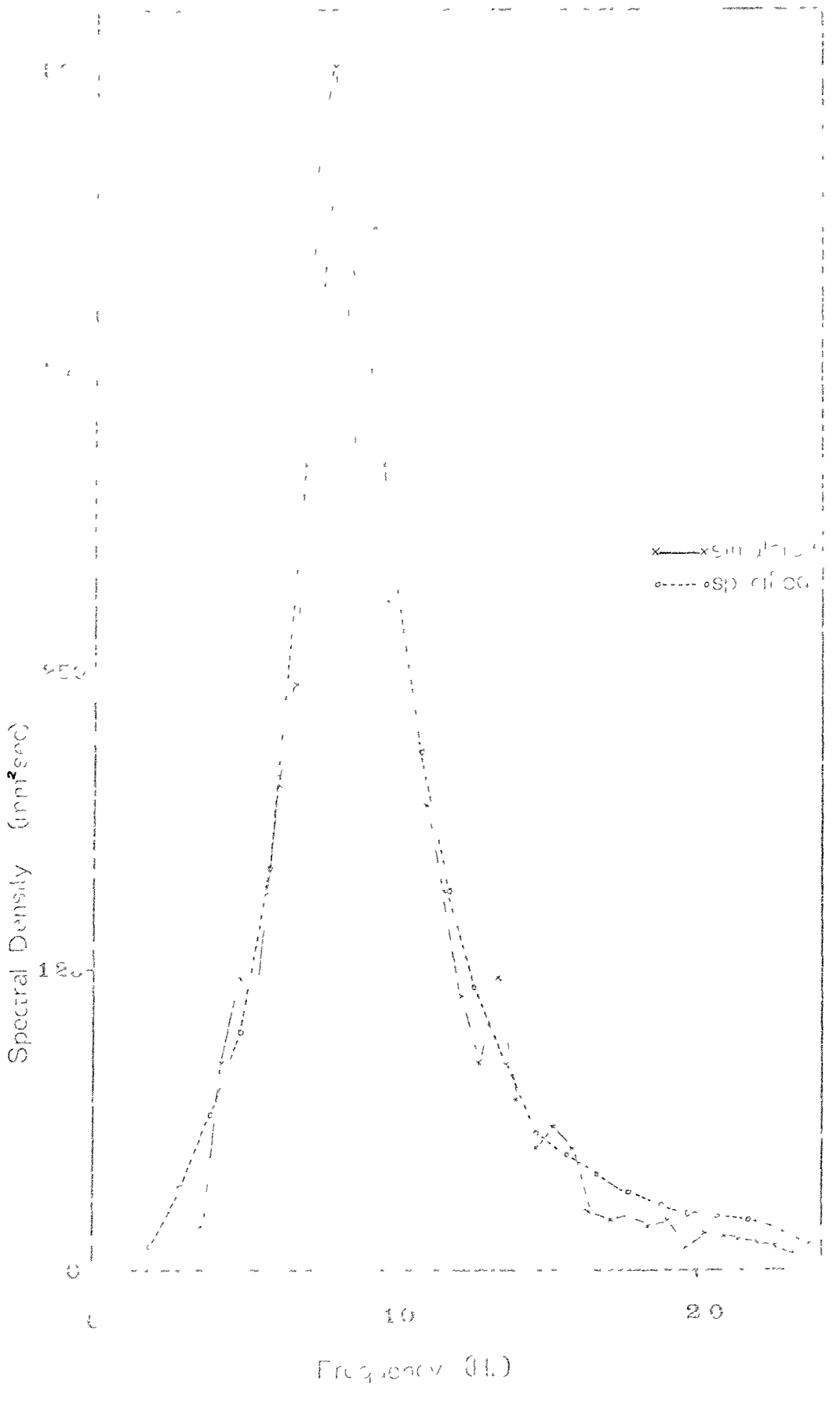

FIG. 6.9a Comparison of Simulated and Specified Values of Spectrum N2

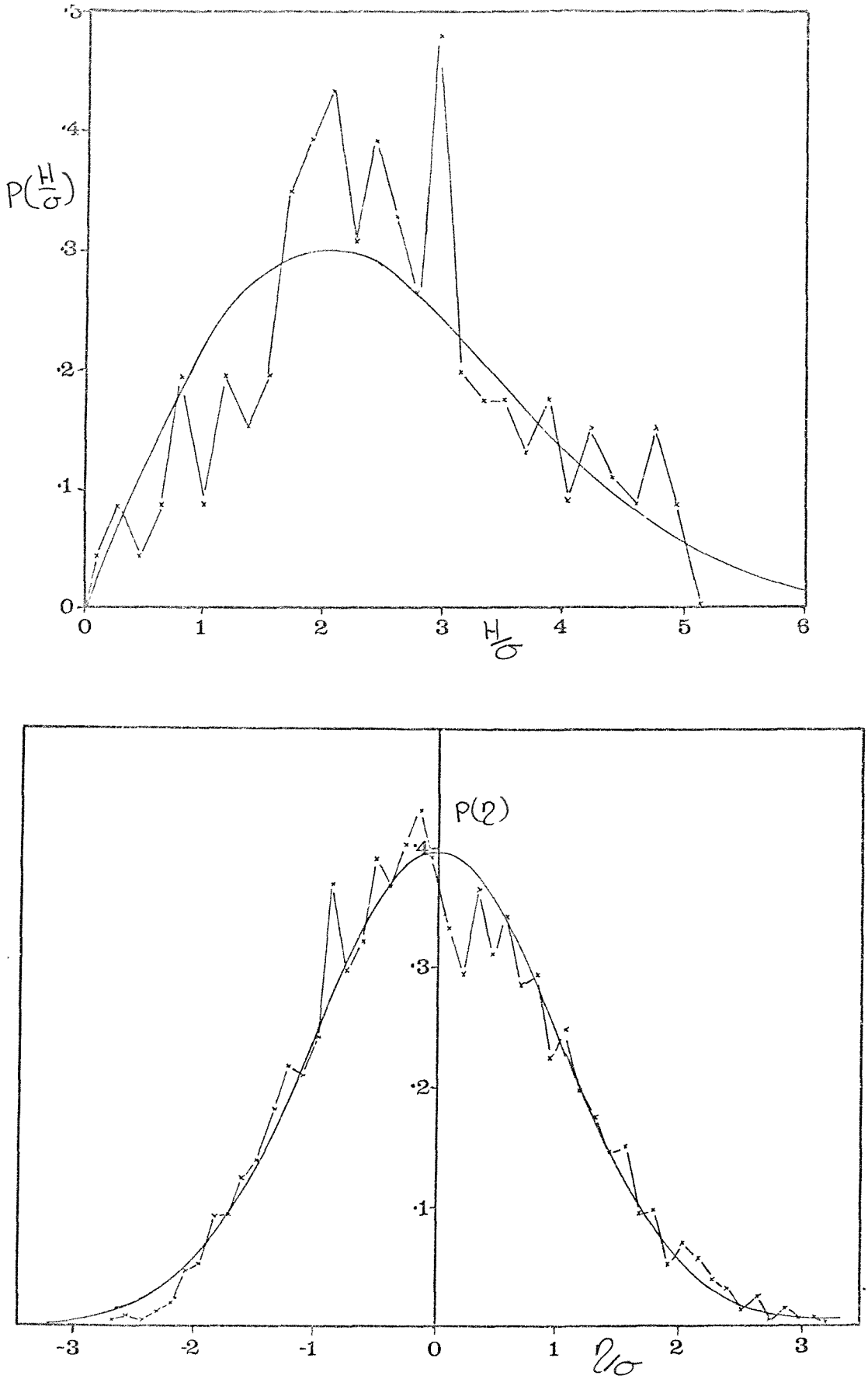

FIG. 6.9b Probability Distribution of Wave Heights and Water Surface Elevation for Spectrum N2

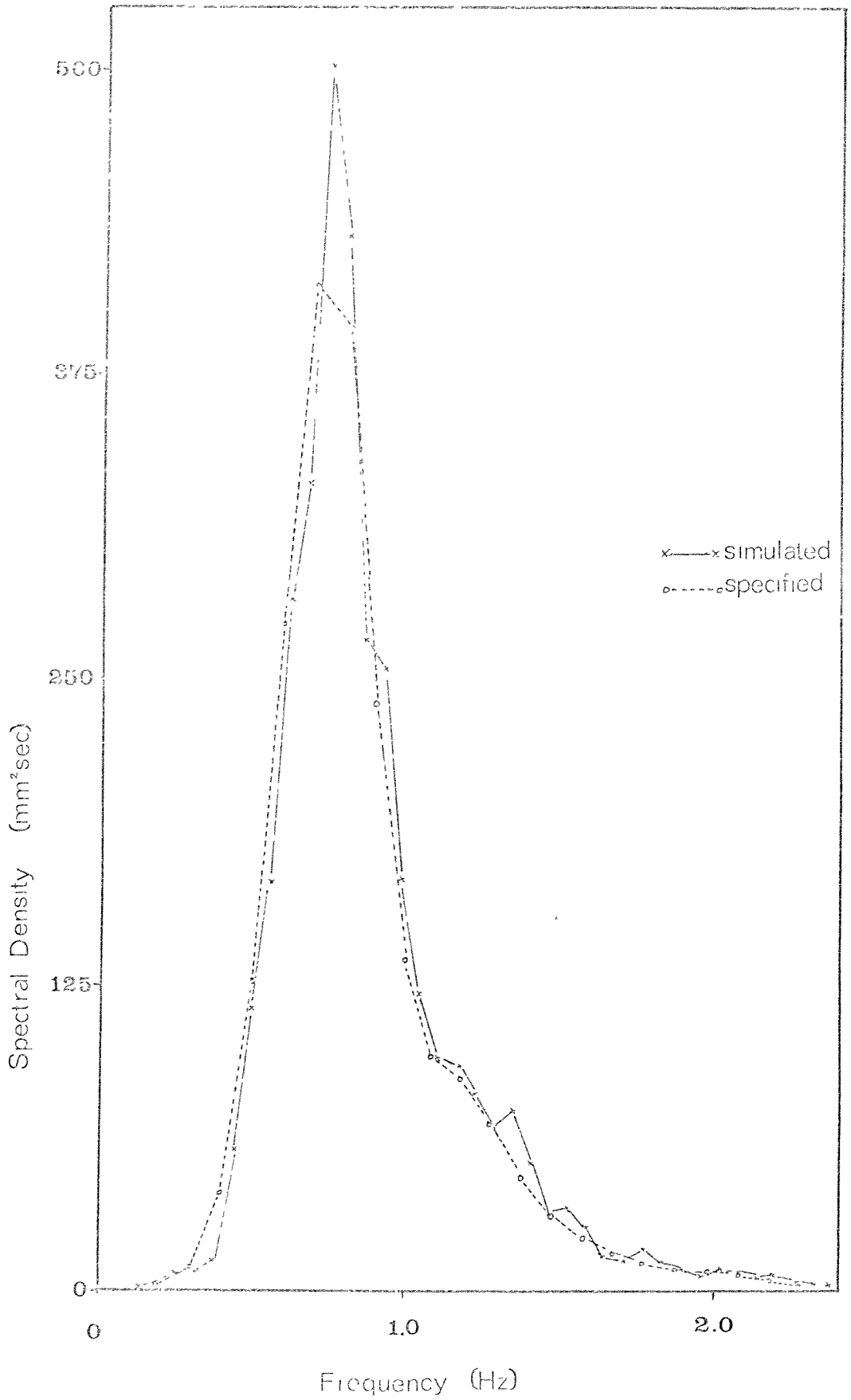

FIG. 6.10a Comparison of Simulated and Specified Values of Spectrum N3

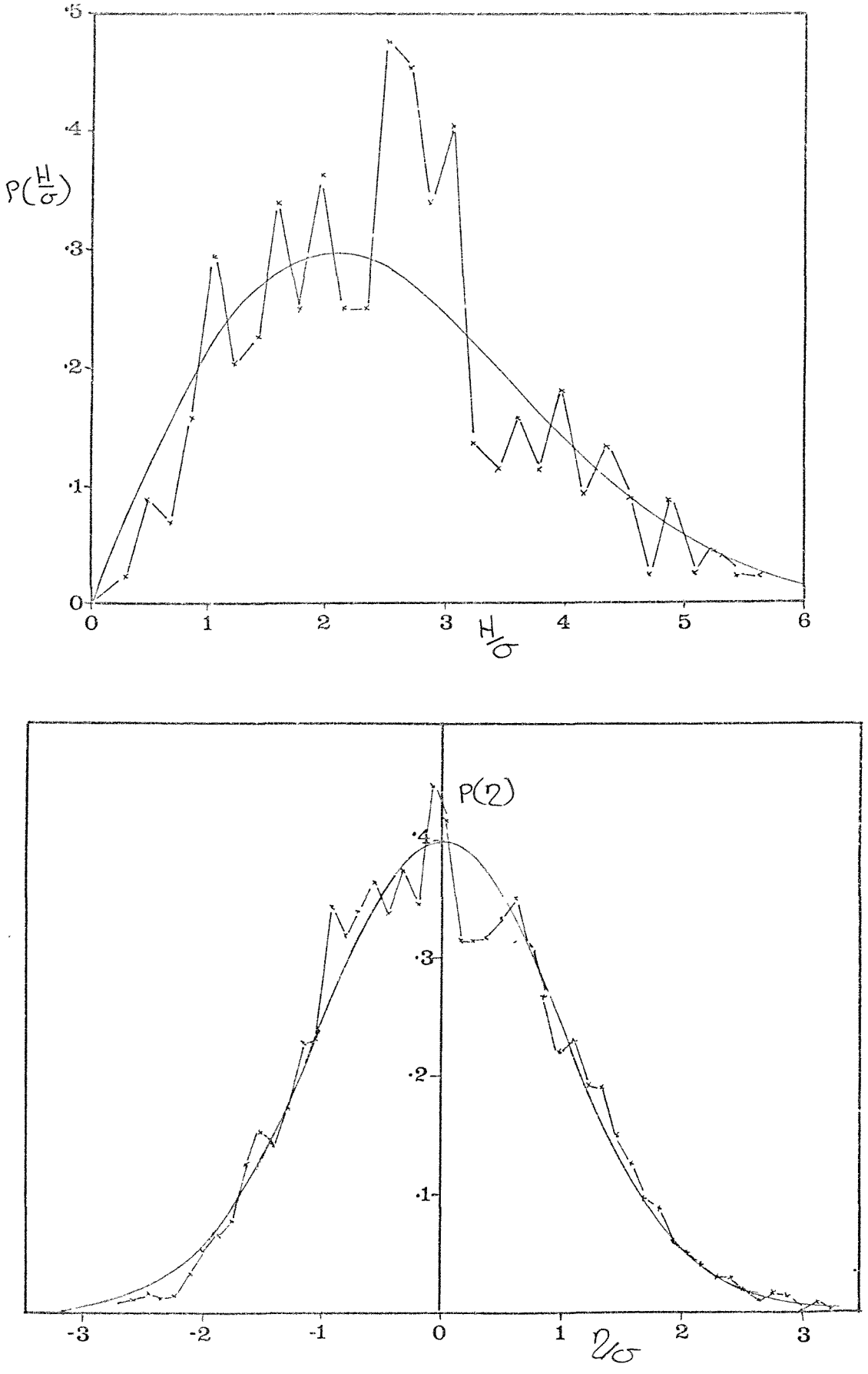

FIG. 6.10b Probability Distribution of Wave Heights and Water Surface Elevation for Spectrum N3

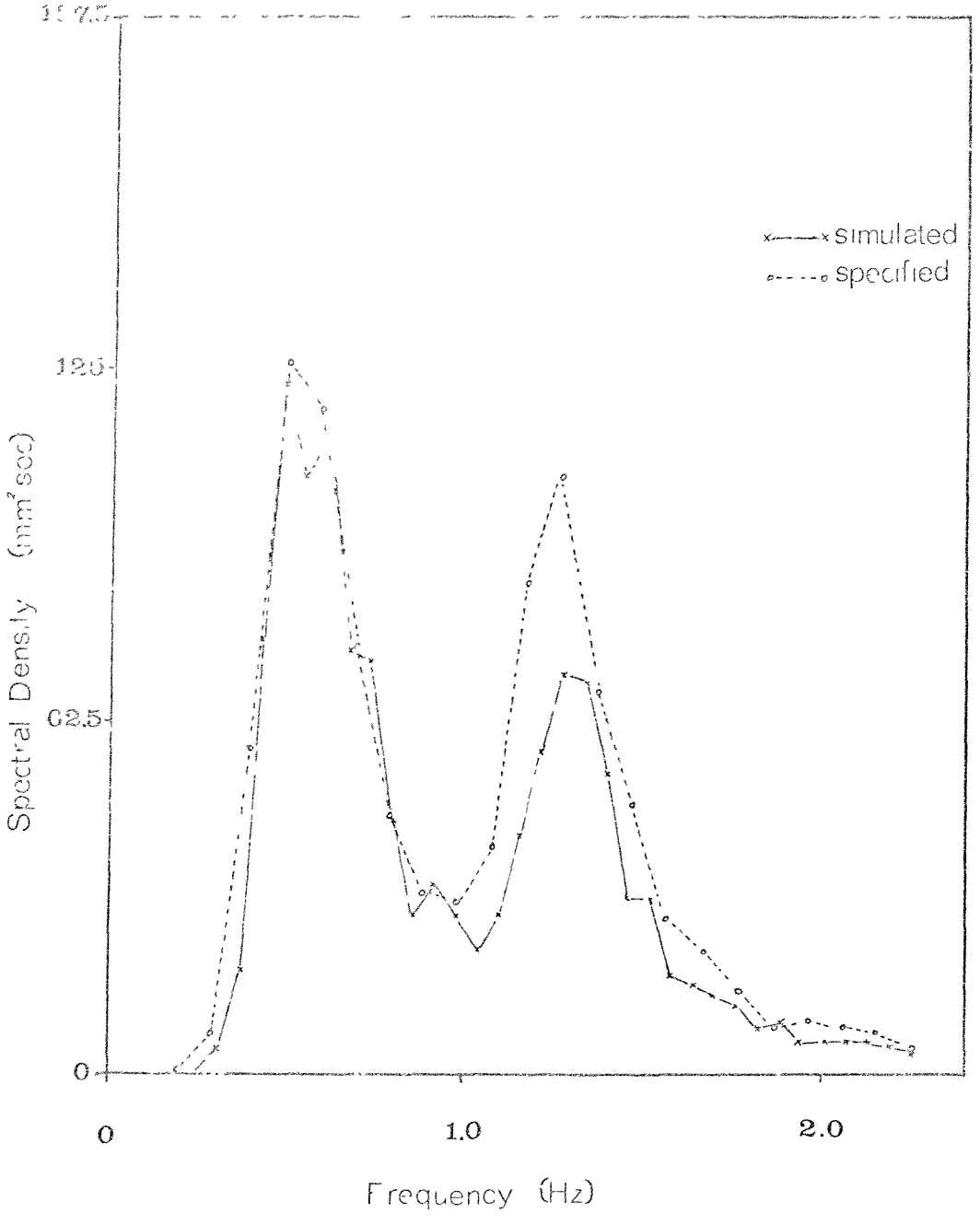

FIG. 6.11a Comparison of Simulated and Specified Values of Spectrum 2A

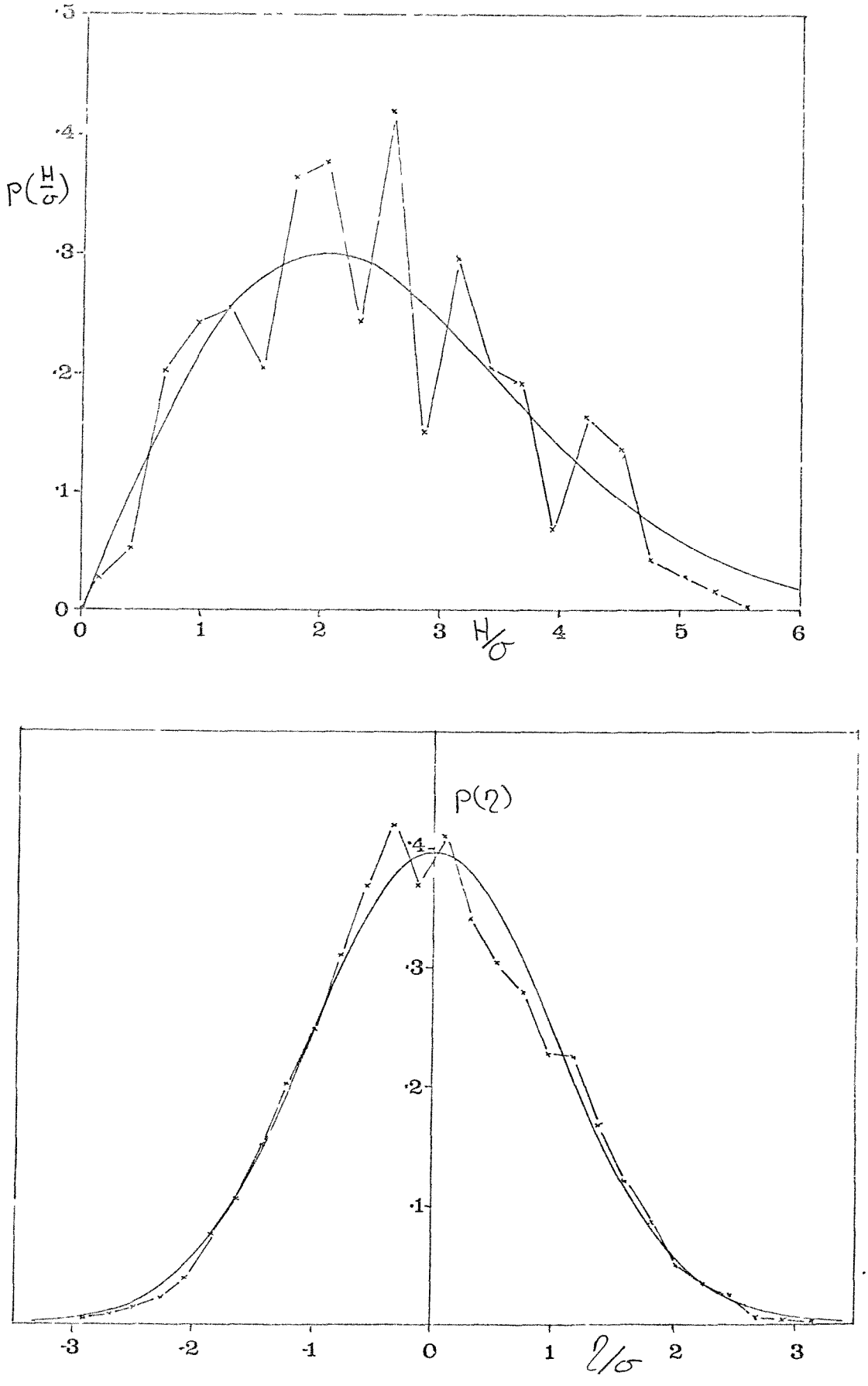

FIG. 6.11b Probability Distribution of Wave Heights and Water Surface Elevation for Spectrum 2A

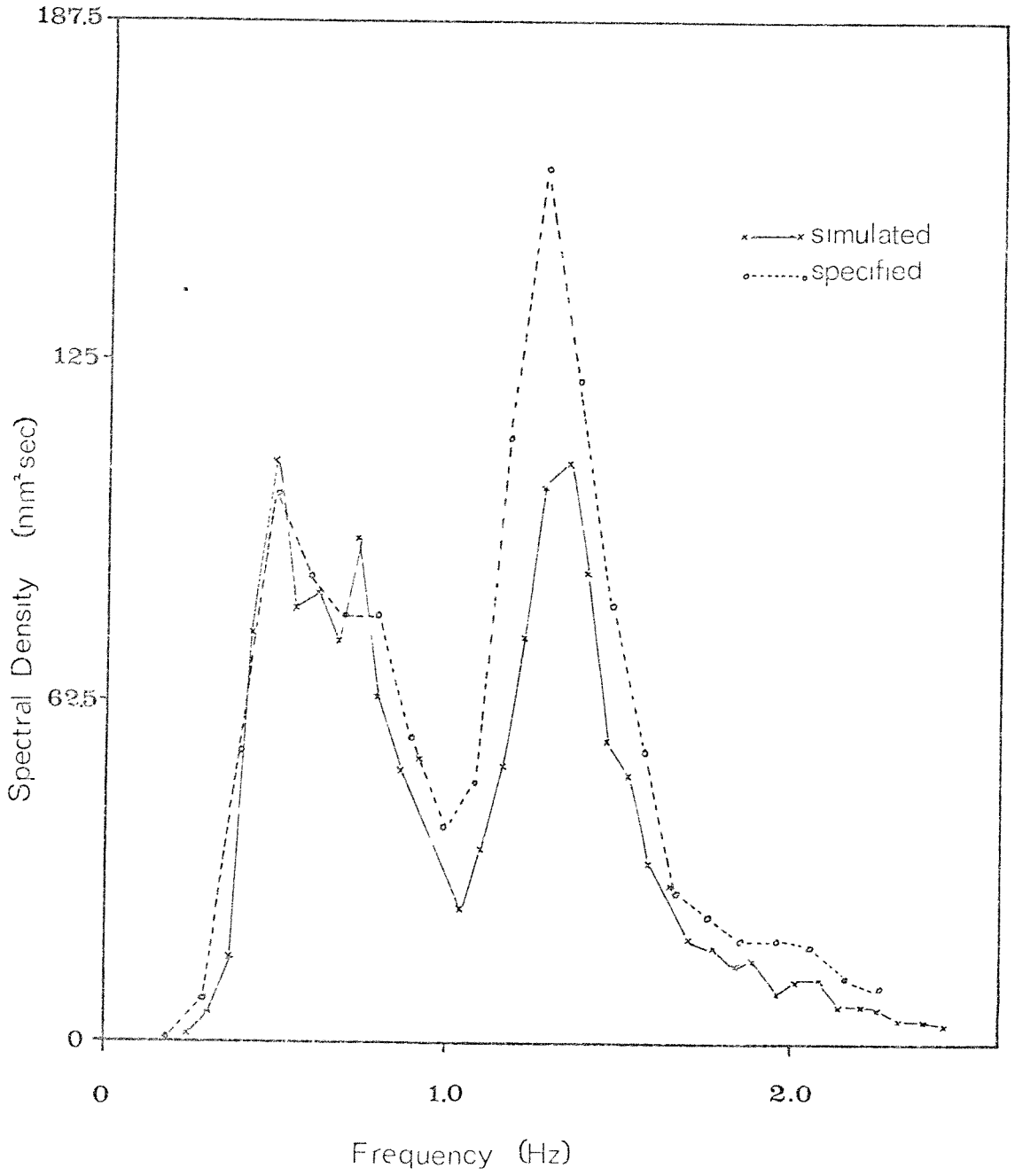

FIG. 6.12a Comparison of Simulated and Specified Values of Spectrum 2B

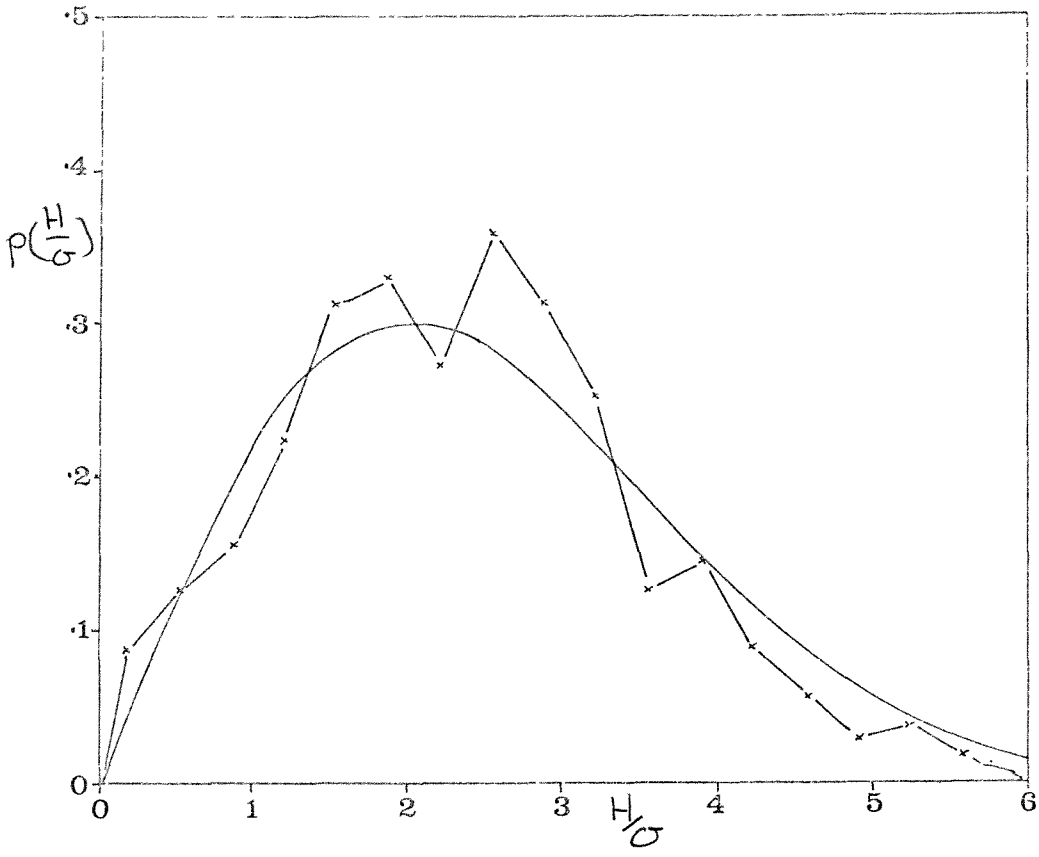

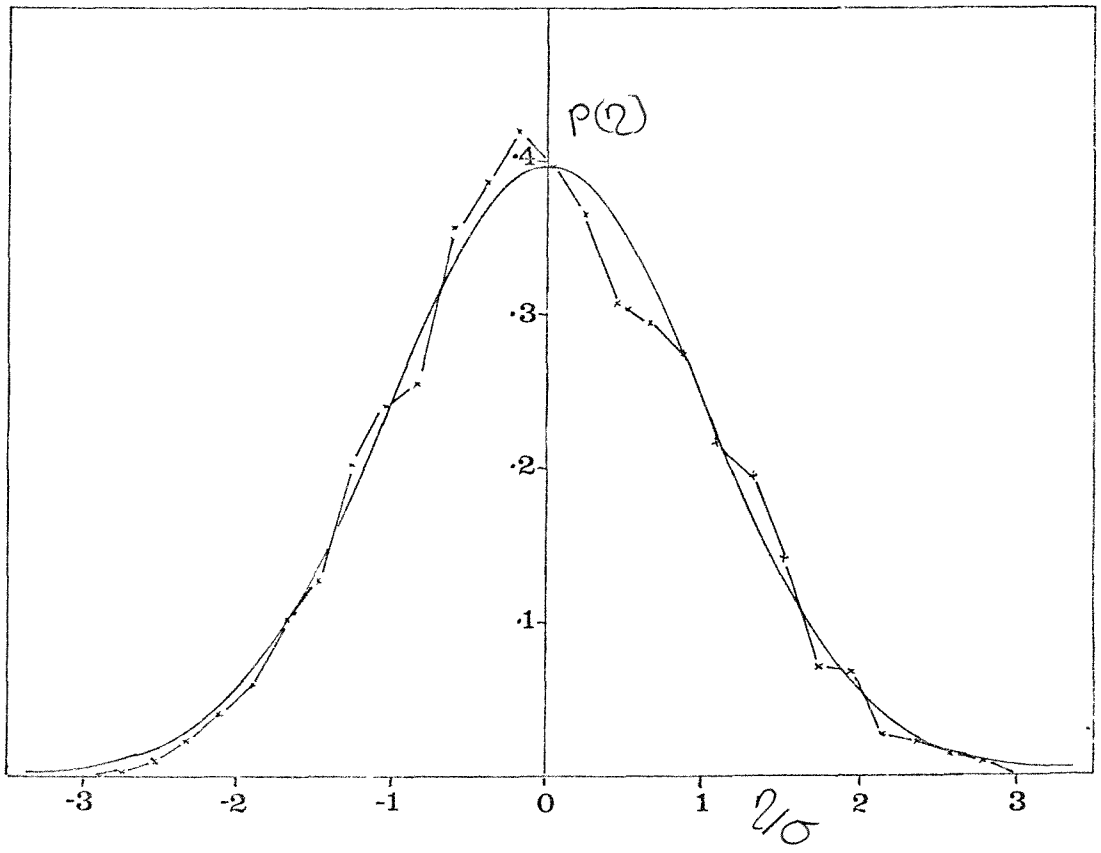

FIG. 6.12b Probability Distribution of Wave Heights and Water Surface Elevation for Spectrum 2B

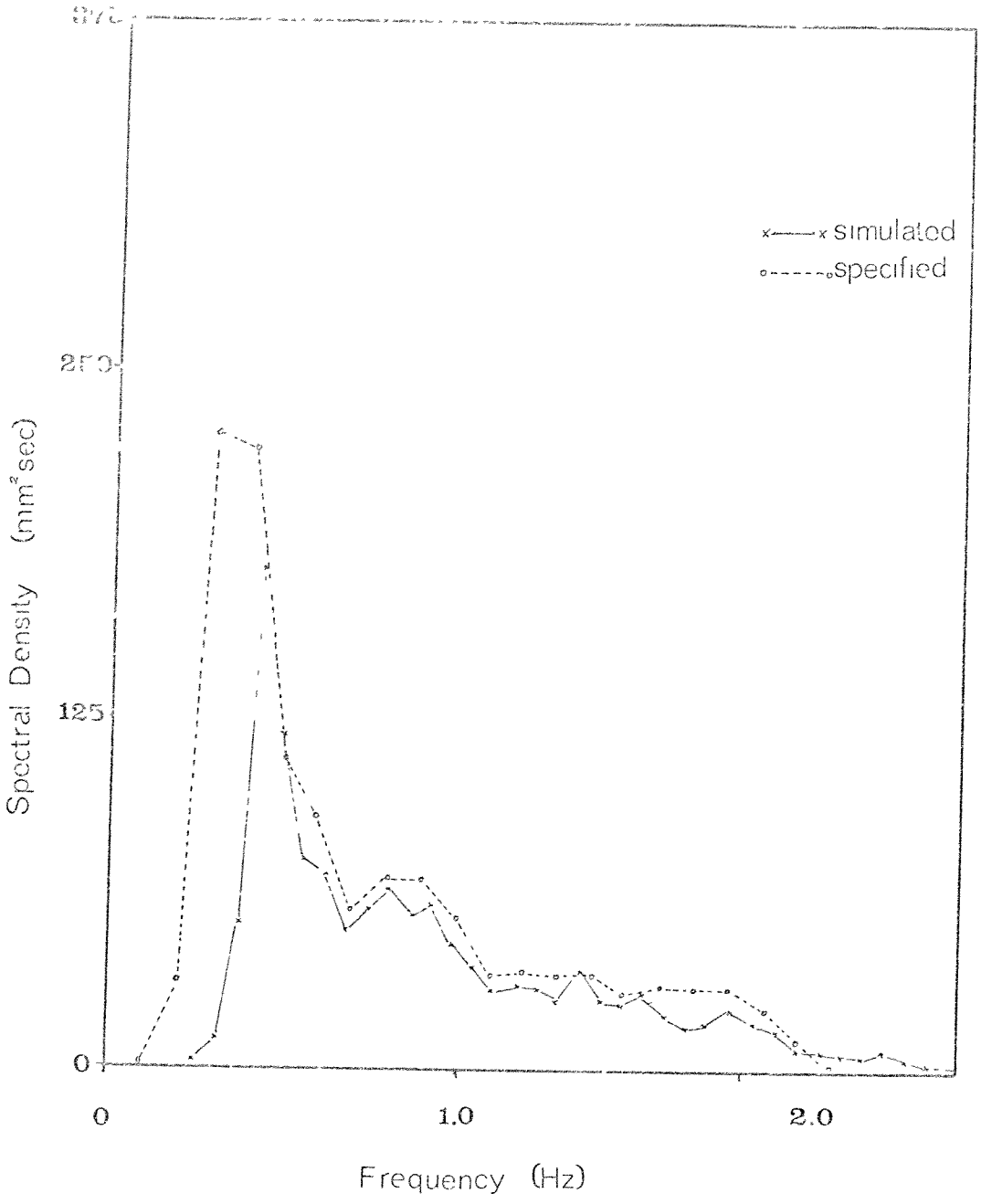

FIG. 6.13a Comparison of Simulated and Specified Values of Spectrum 11

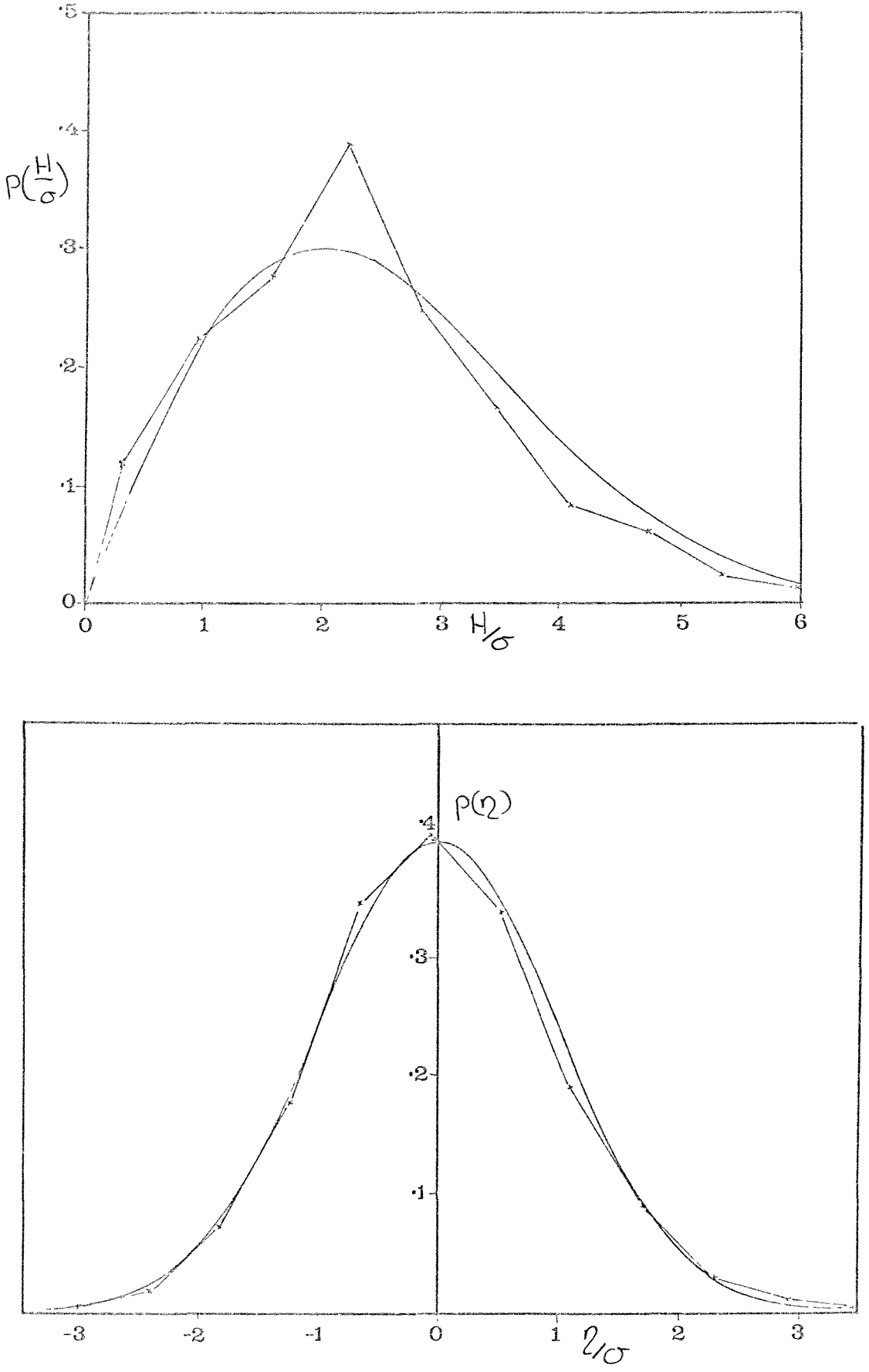

FIG. 6.13b Probability Distribution of Wave Heights and Water Surface Elevation for Spectrum 11

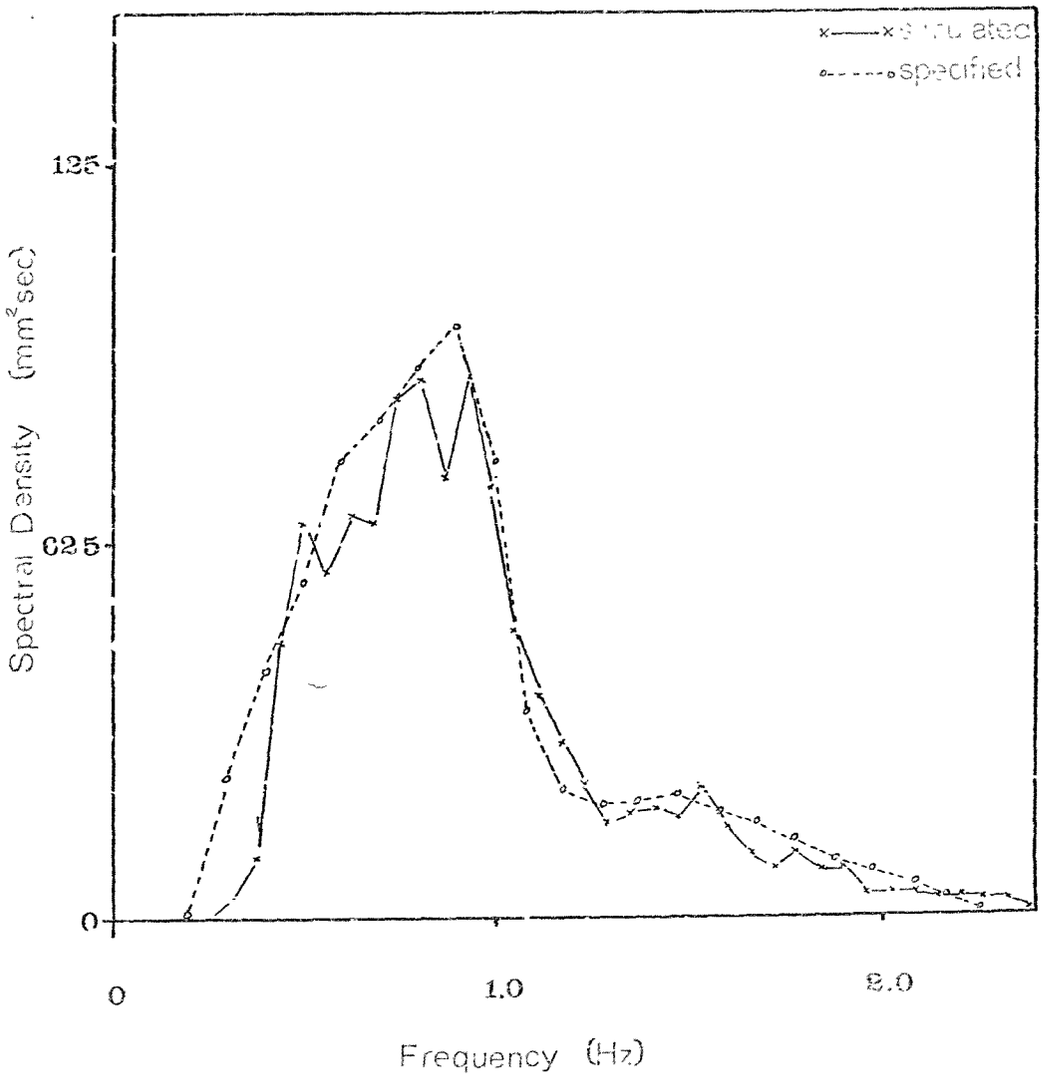

FIG. 6.14a Comparison of Simulated and Specified Values of Spectrum 12B

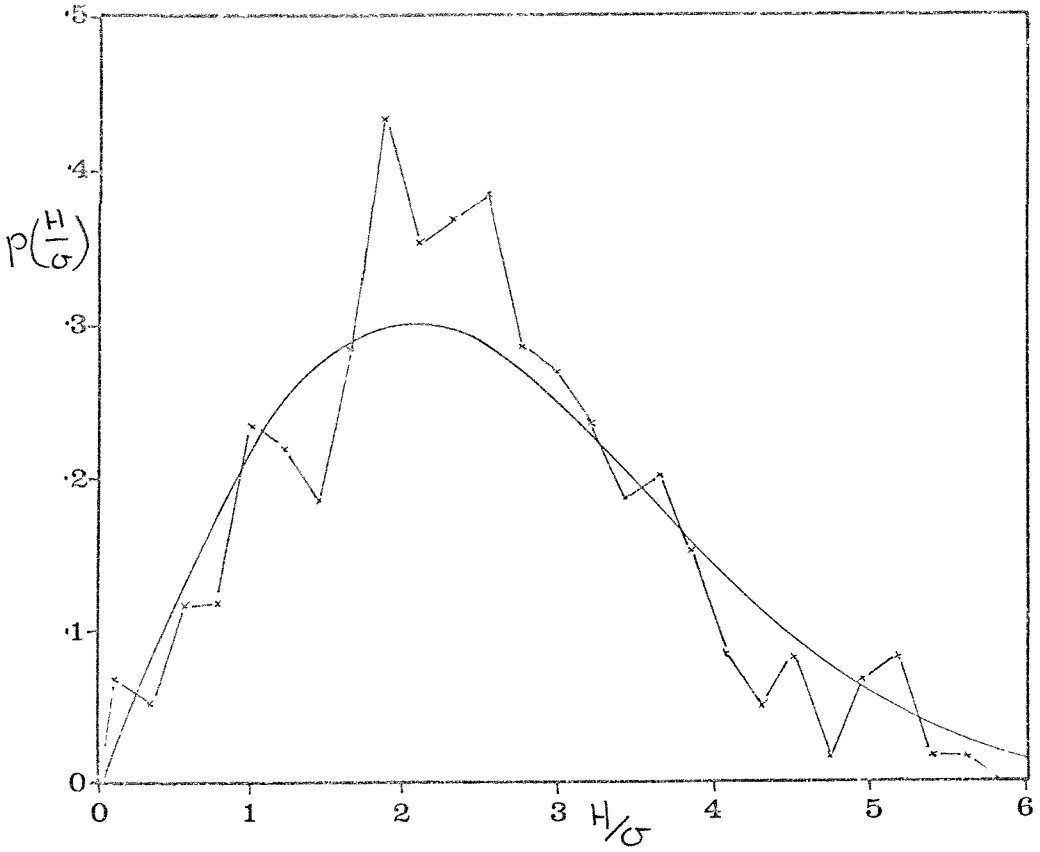

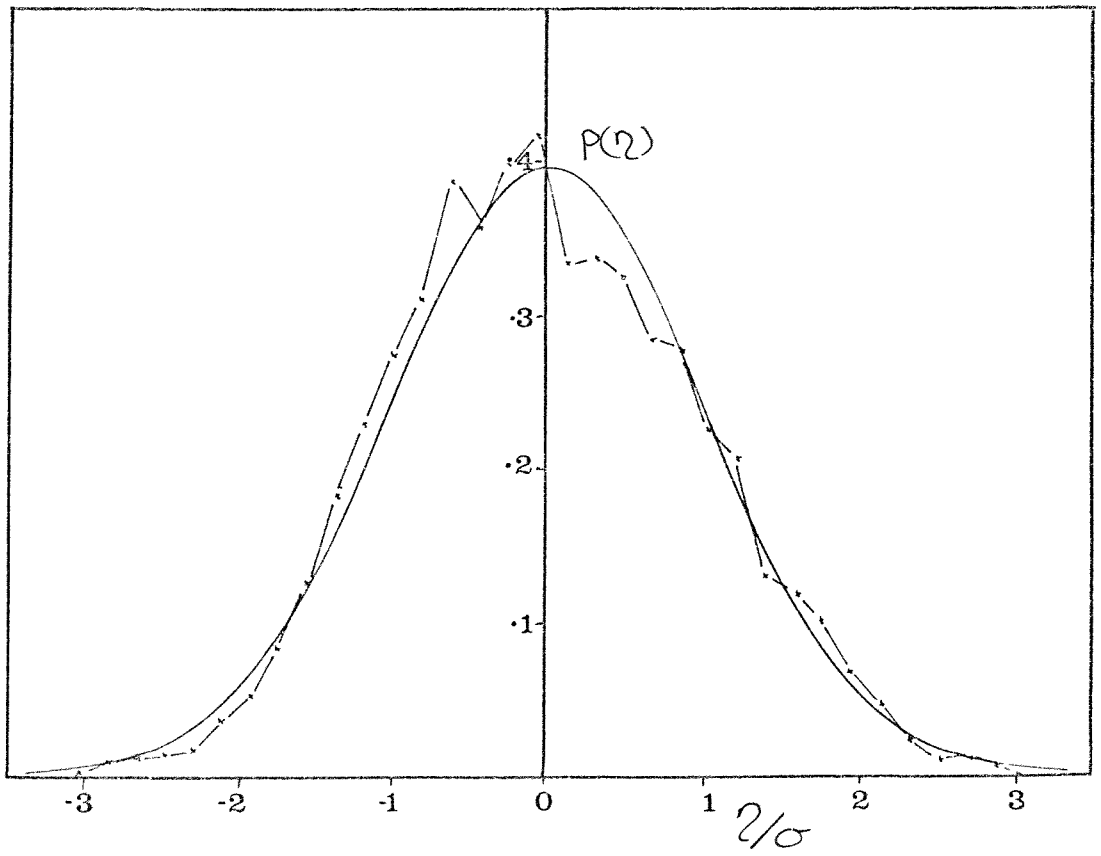

FIG. 6.14b Probability Distribution of Wave Heights and Water Surface Elevation for Spectrum 12B

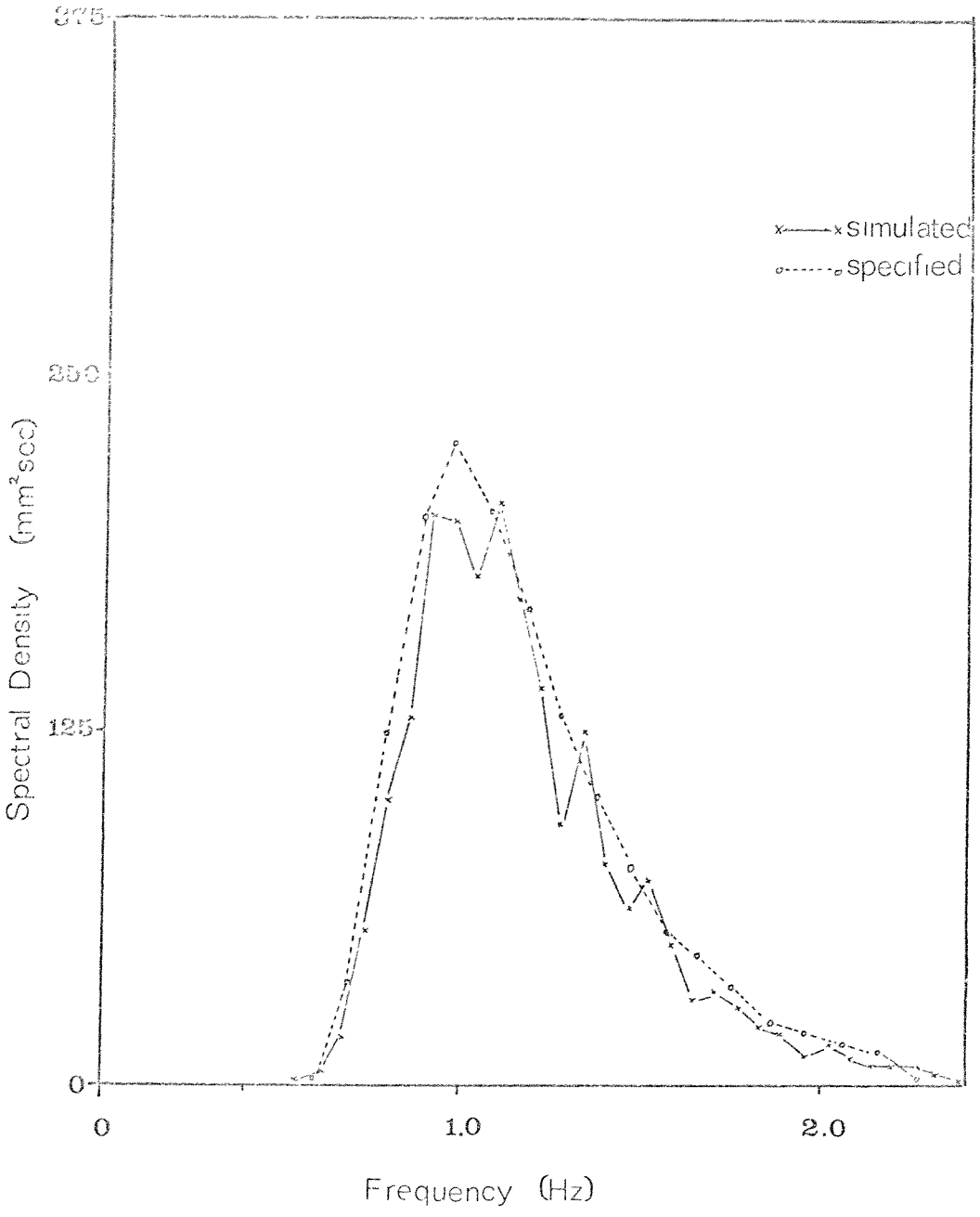

FIG. 6.15a Comparison of Simulated and Specified Values of Spectrum M25

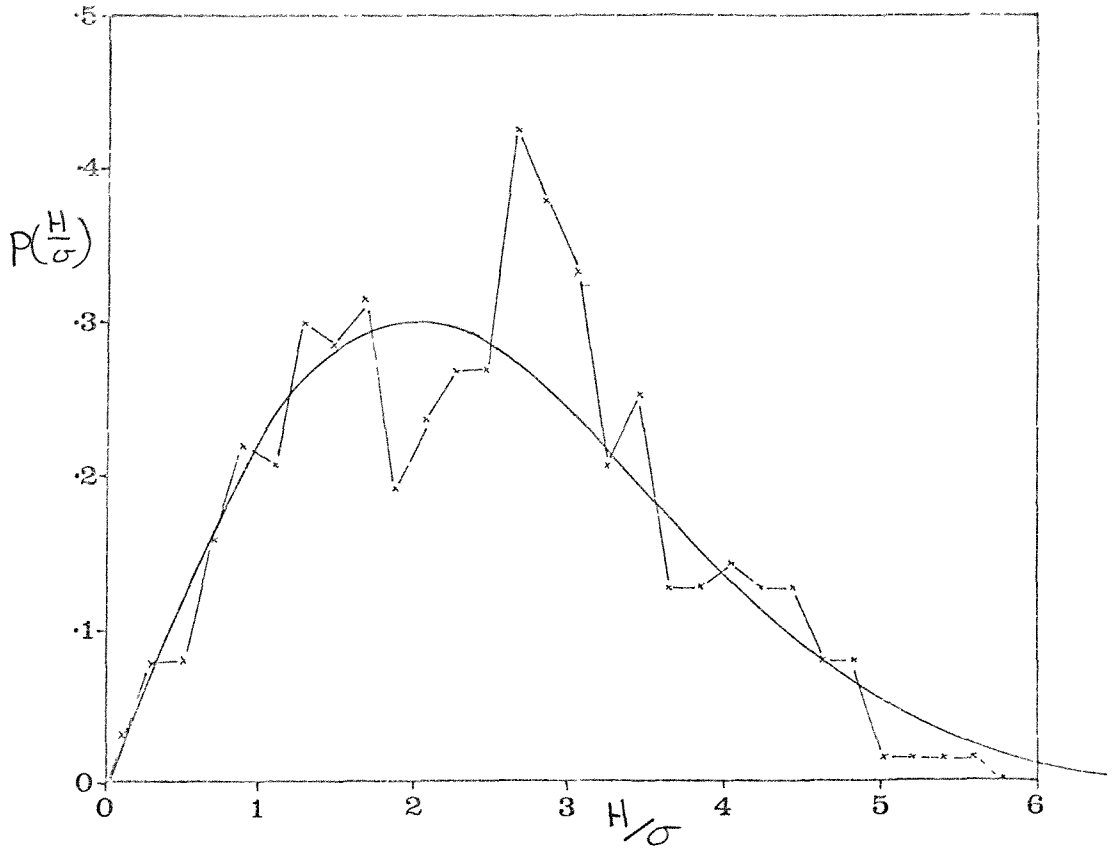

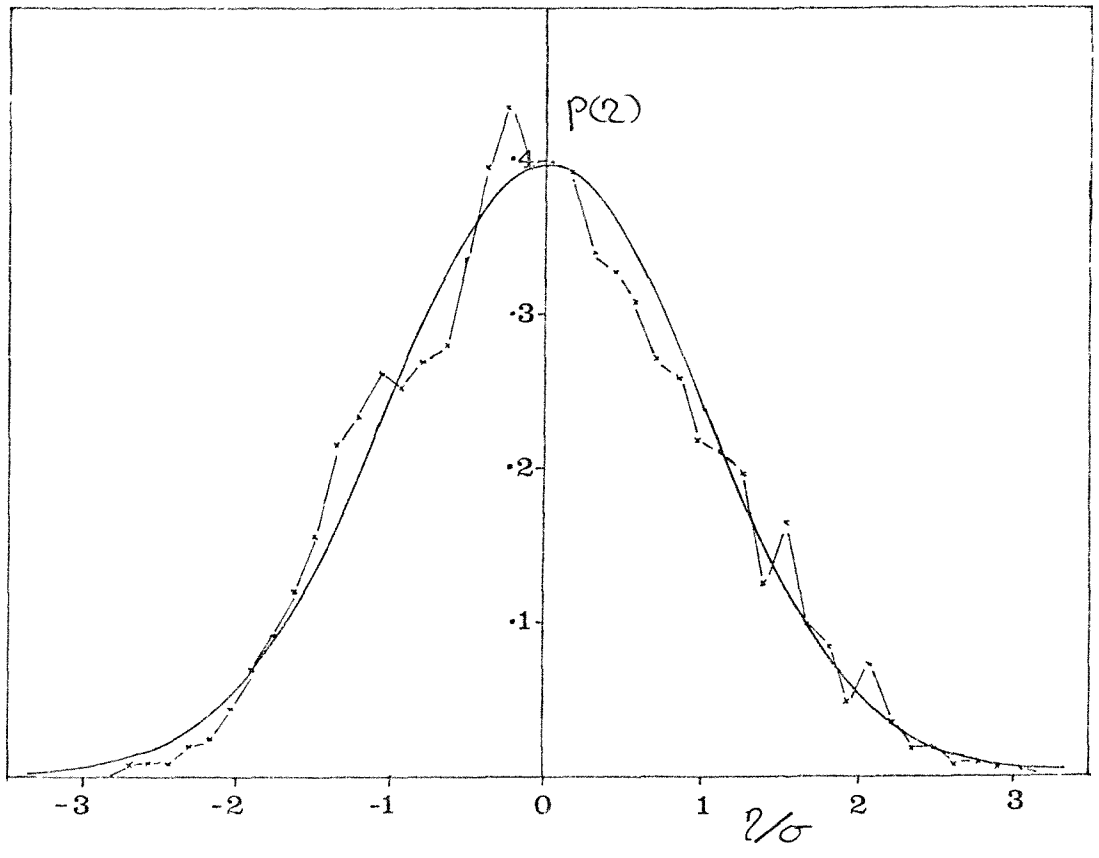

FIG. 6.15b Probability Distribution of Wave Heights and Water Surface Elevation for Spectrum M25

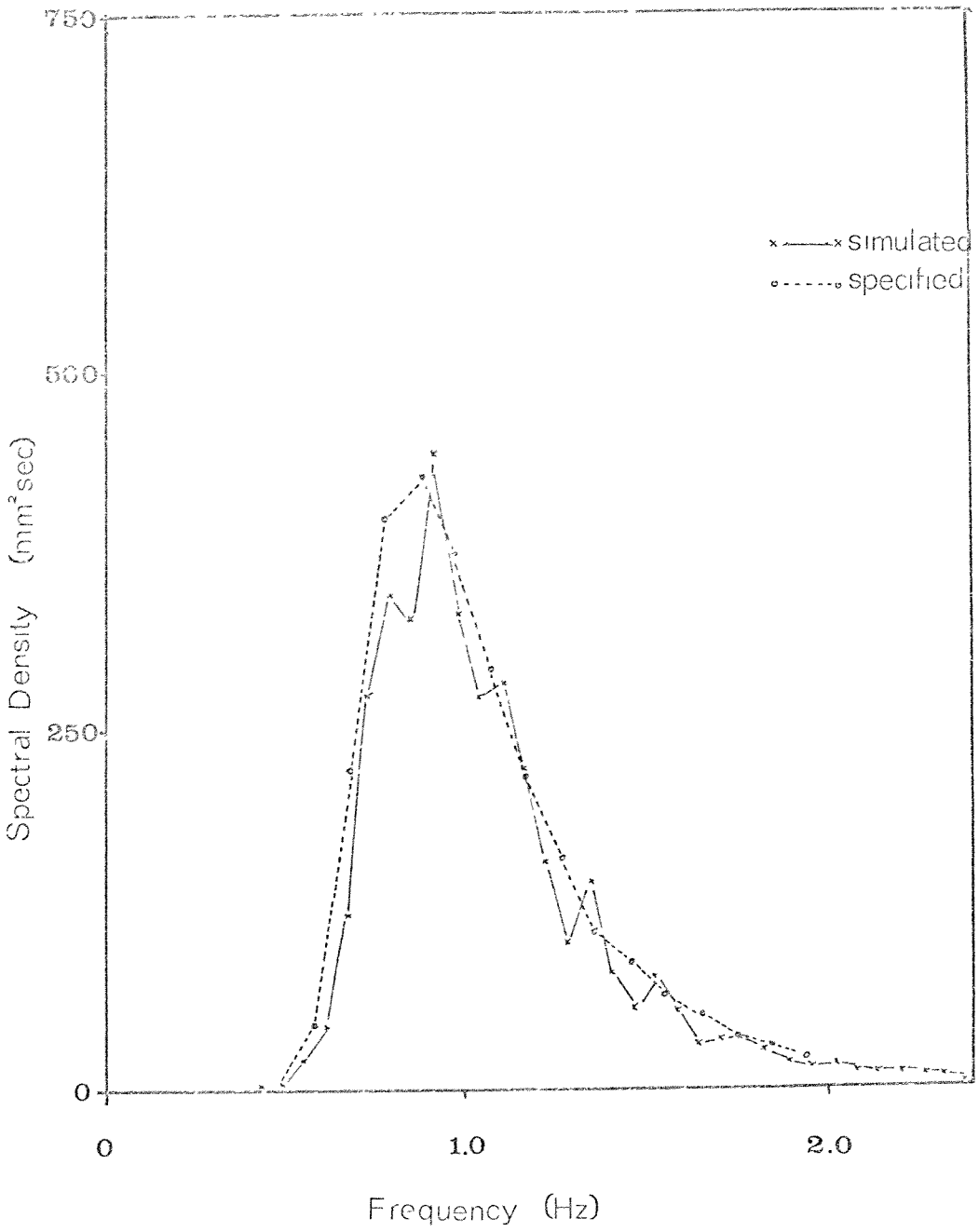

FIG. 6.16a Comparison of Simulated and Specified Values of Spectrum M30

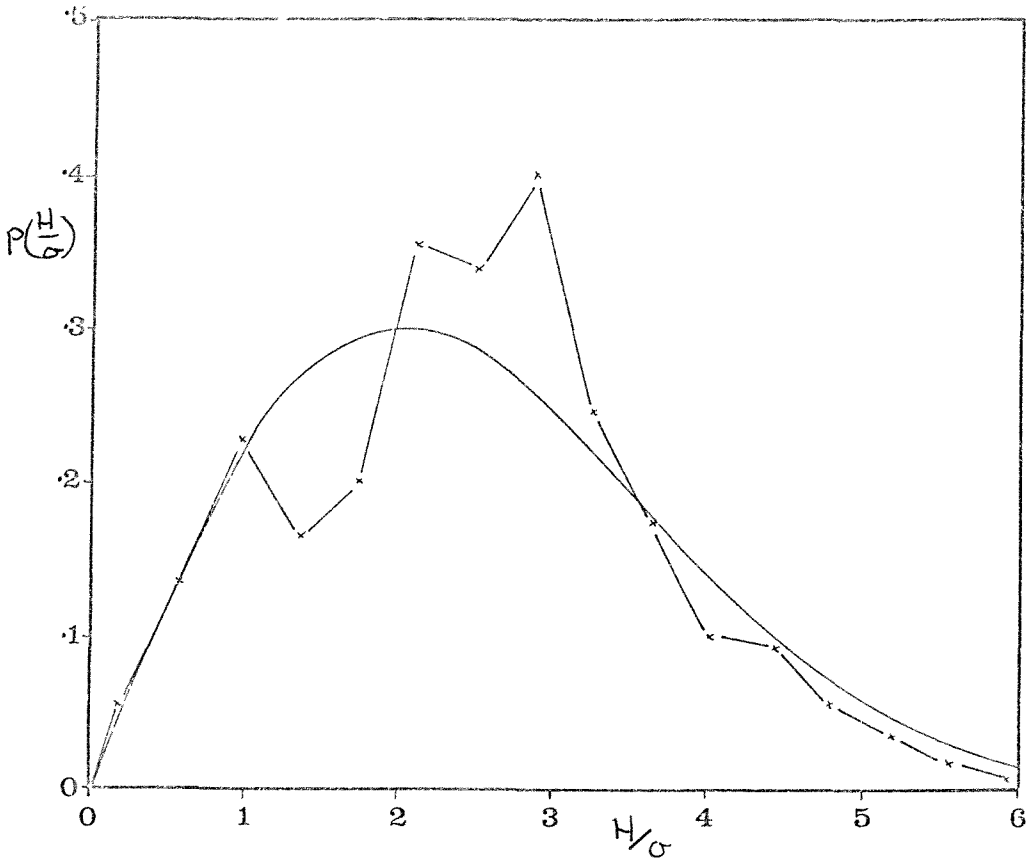

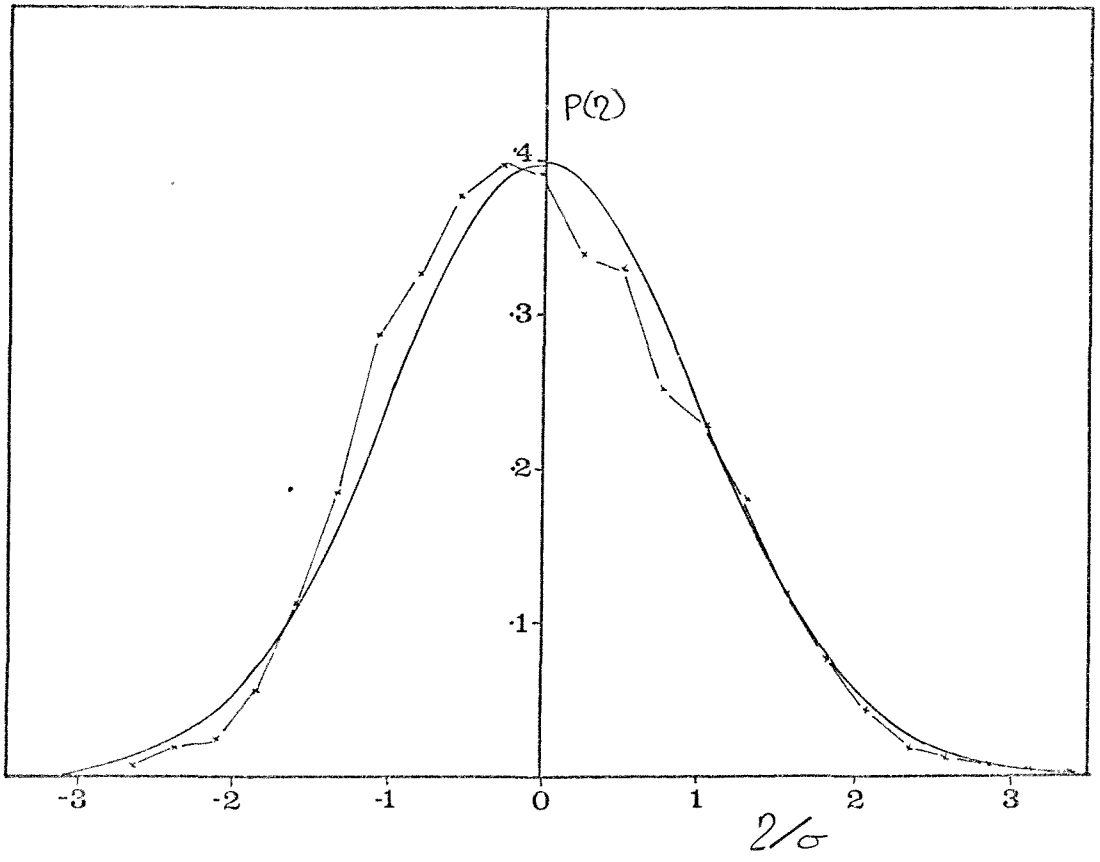

FIG. 6.16b Probability Distribution of Wave Heights and Water Surface Elevation for Spectrum M30

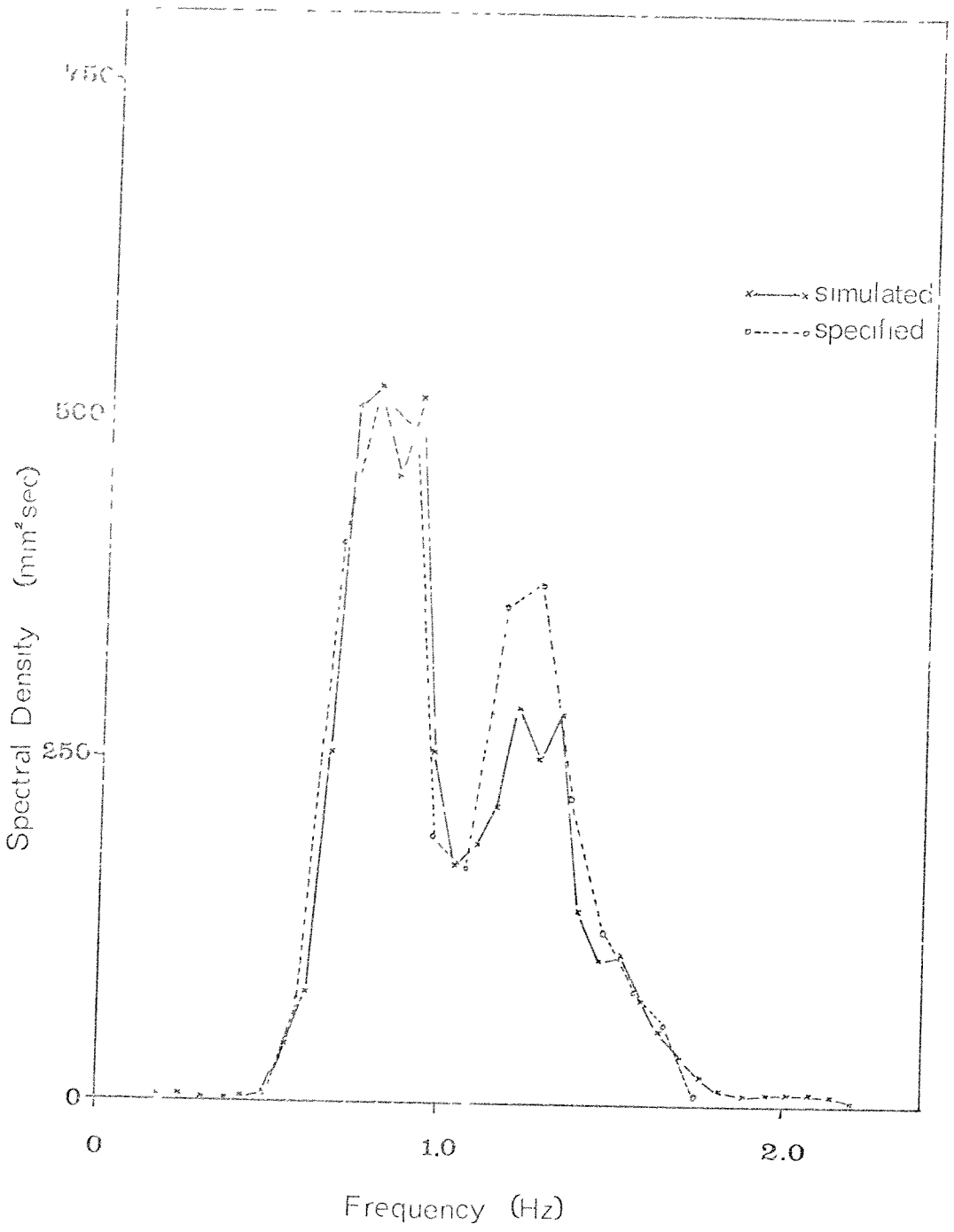

FIG. 6.17a Comparison of Simulated and Specified Values of of Spectrum T1

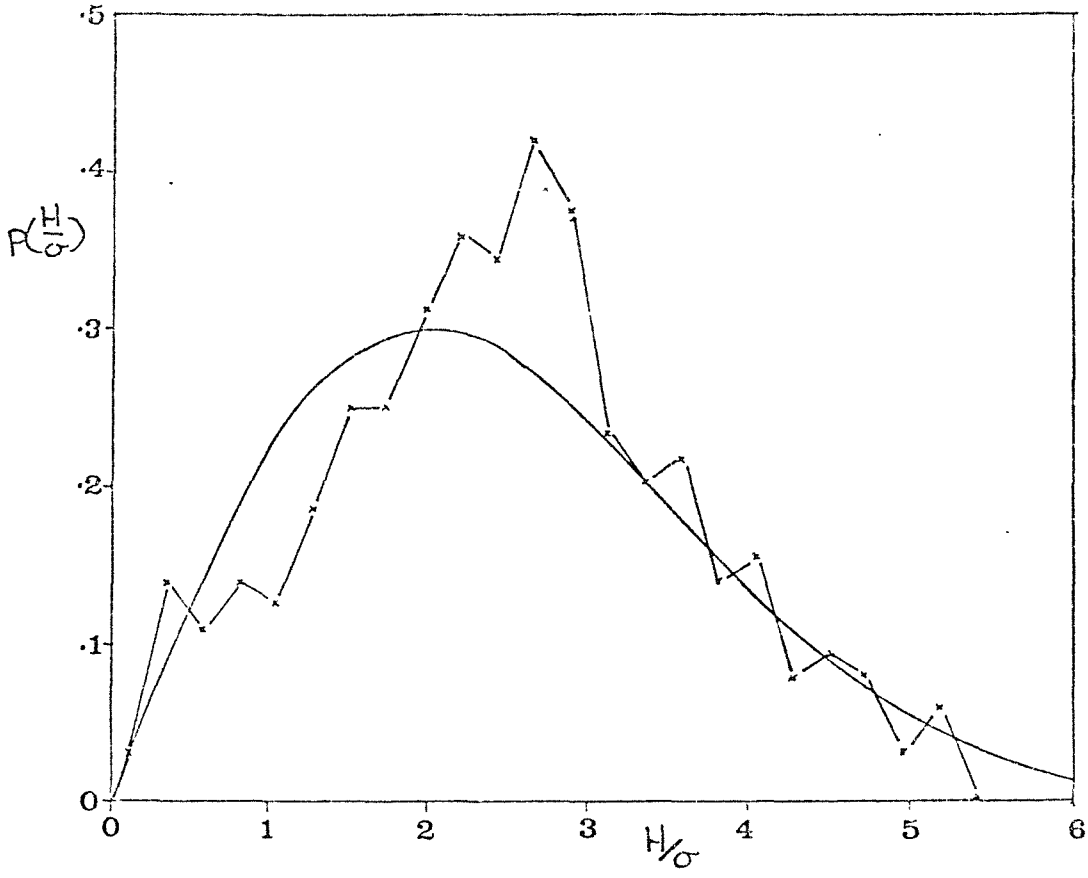

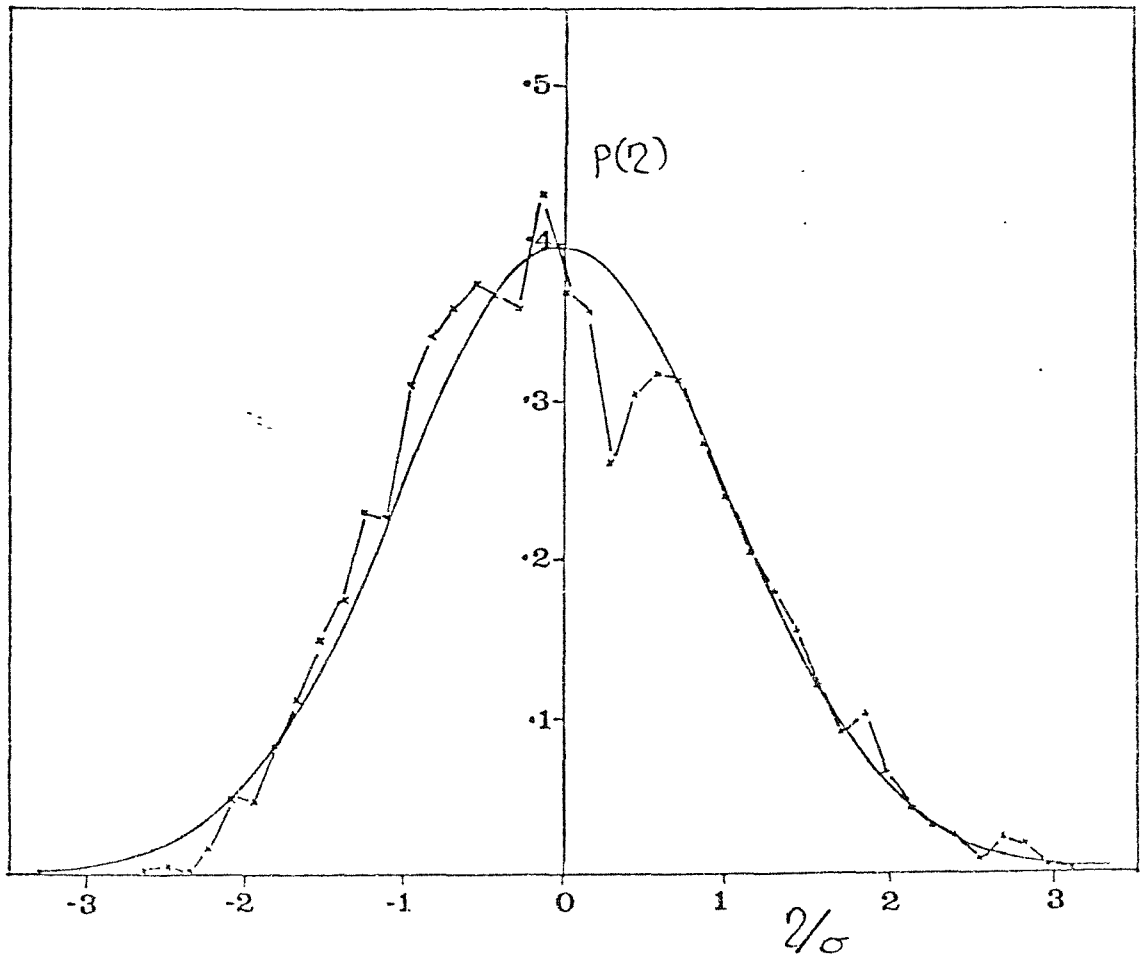

FIG. 6.17b Probability Distribution of Wave Heights and Water Surface Elevation for Spectrum T1

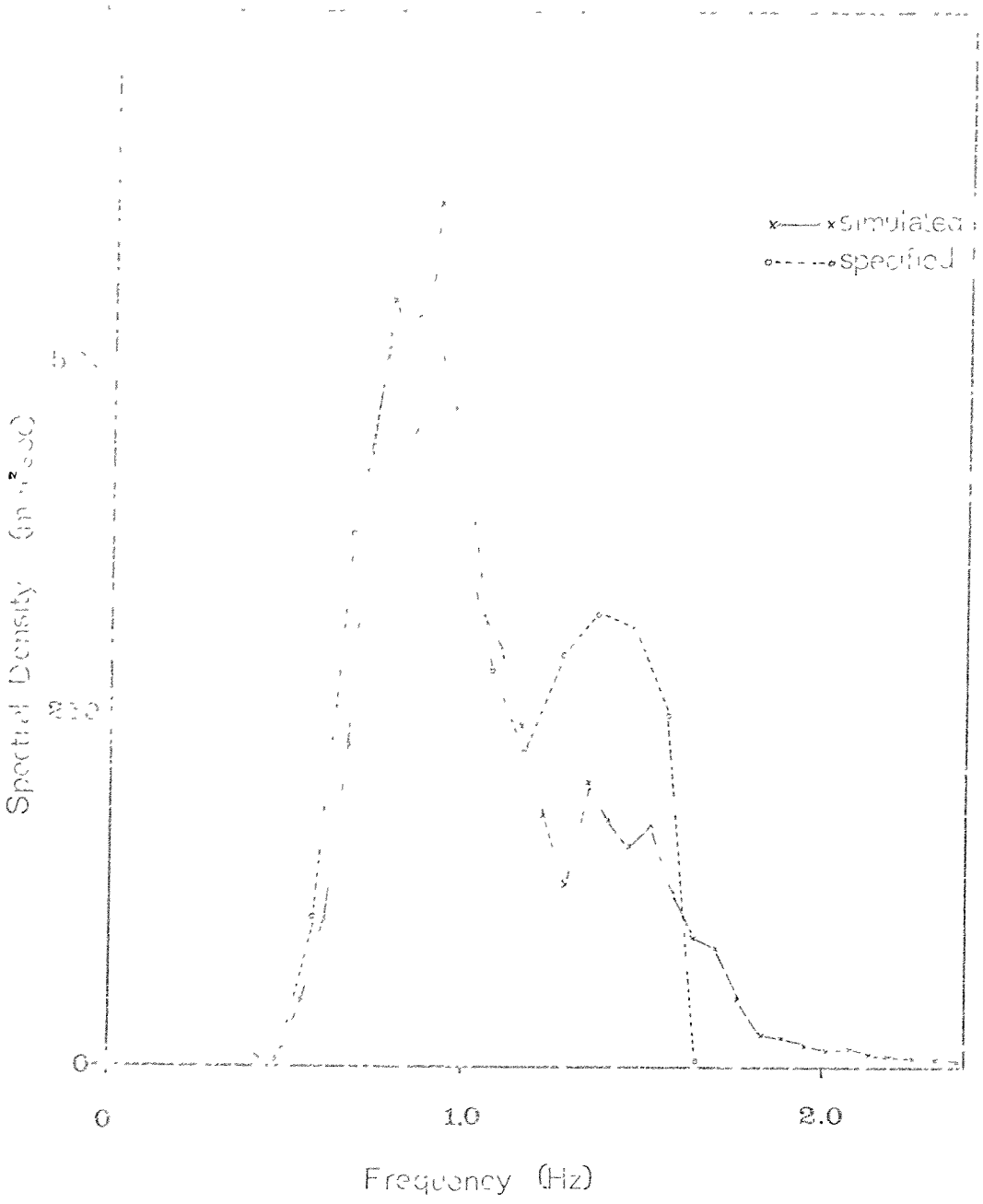

FIG. 6.18a Comparison of Simulated and Specified Values of Spectrum T2

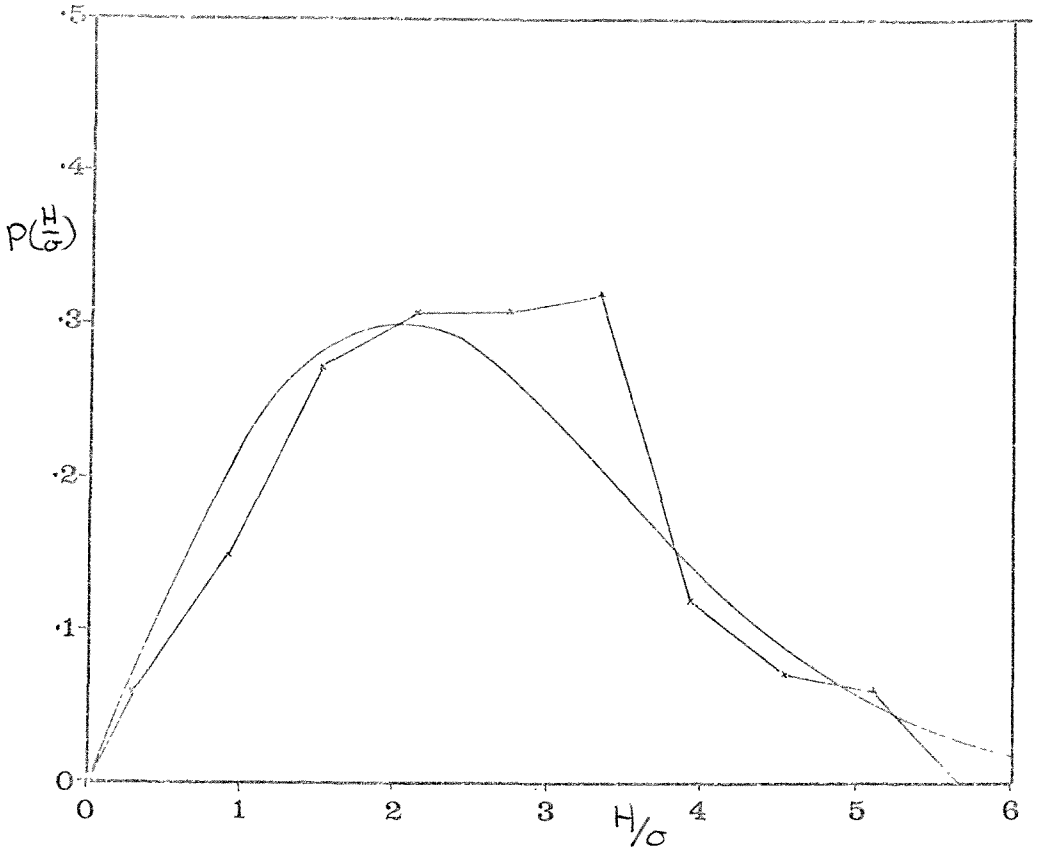

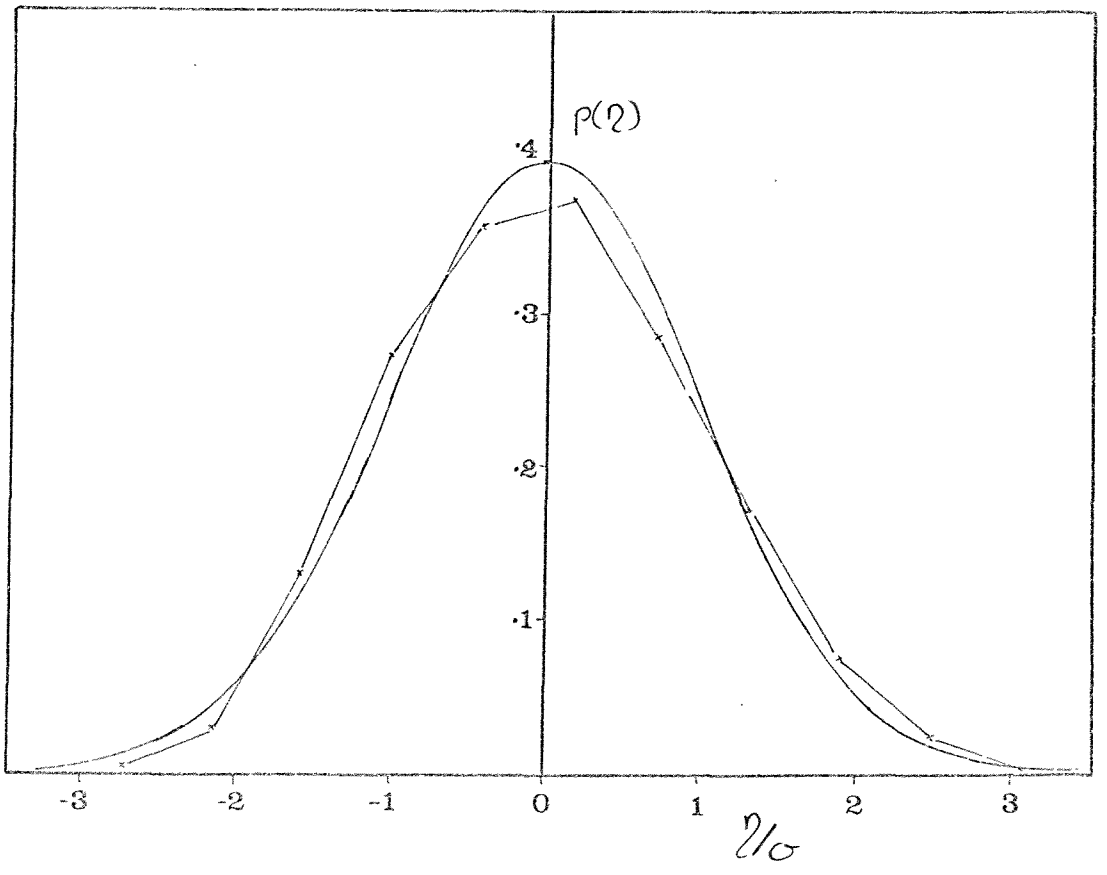

FIG. 6.18b Probability Distribution of Wave Heights and Water Surface Elevation for Spectrum T2

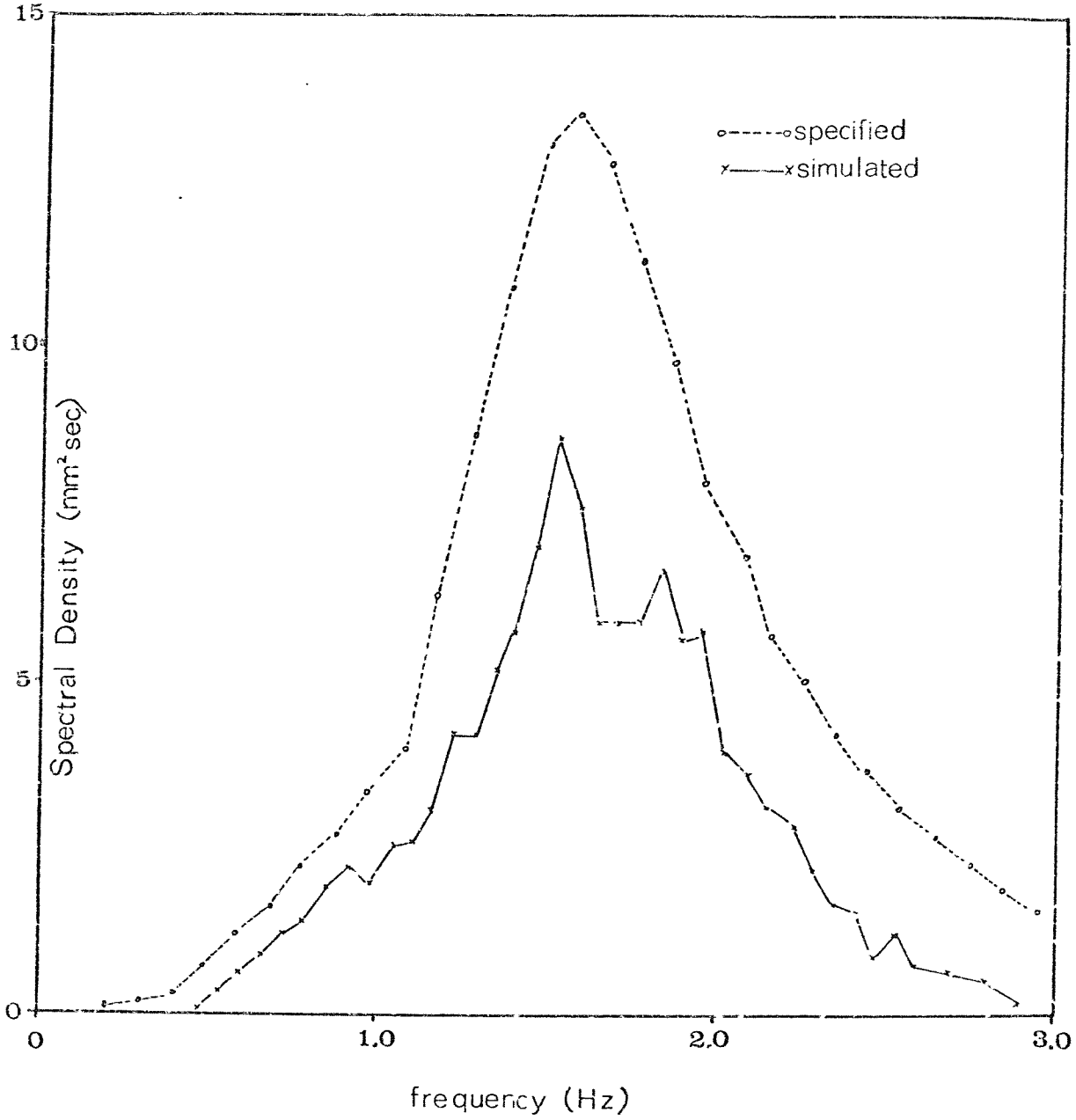

FIG. 6.19a Comparison of Simulated and Specified Values of Spectrum TN2

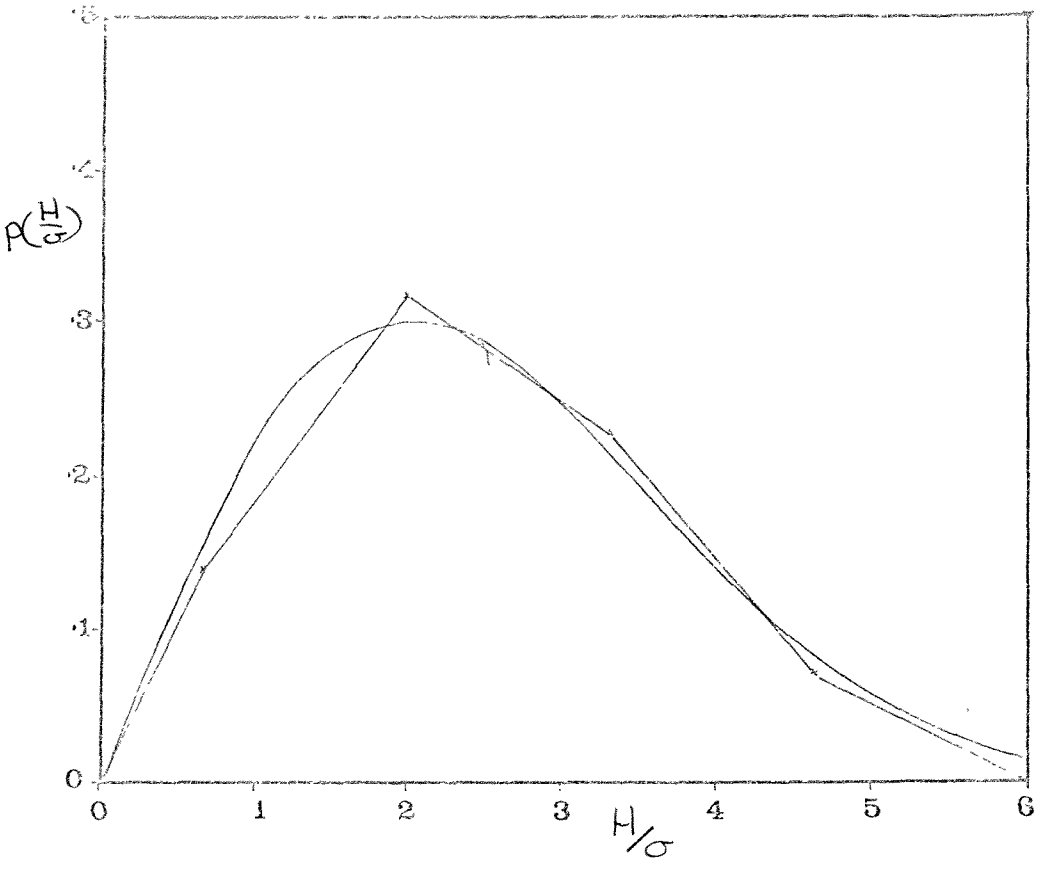

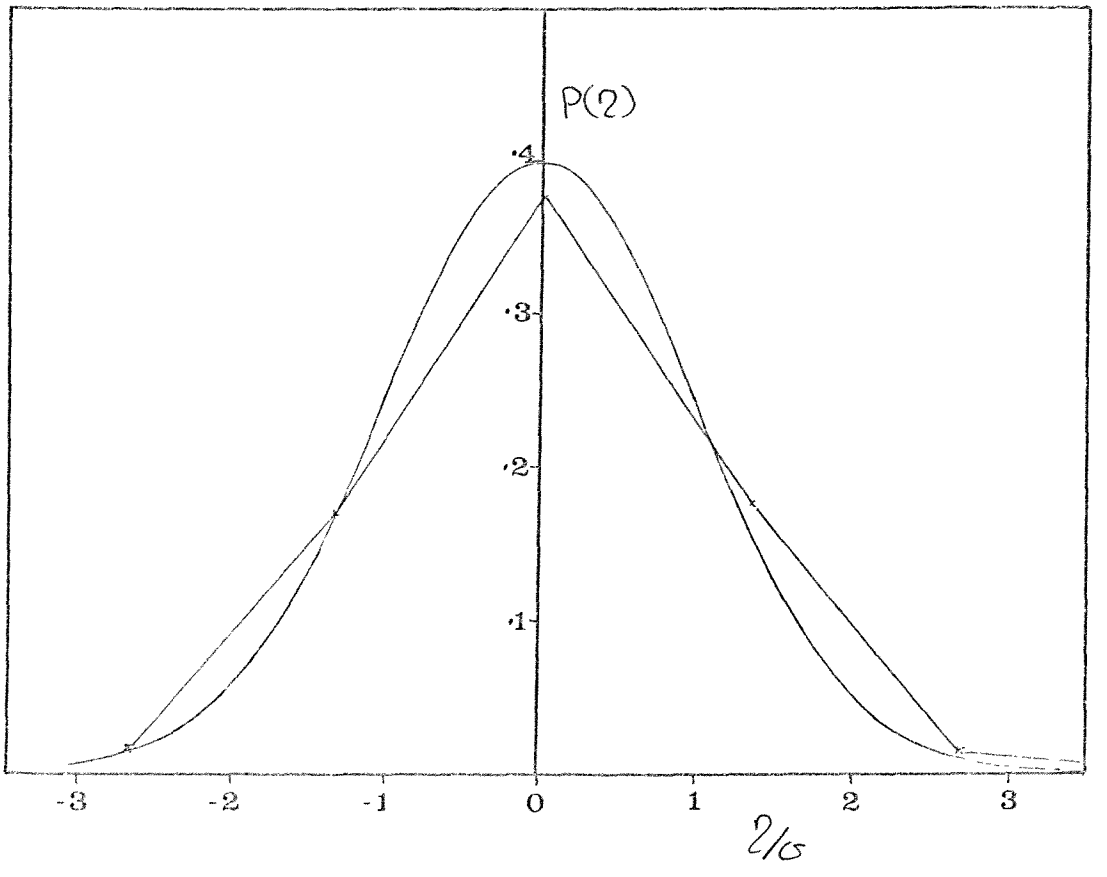

FIG. 6.19b Probability Distribution of Wave Heights and Water Surface Elevation for Spectrum TN2

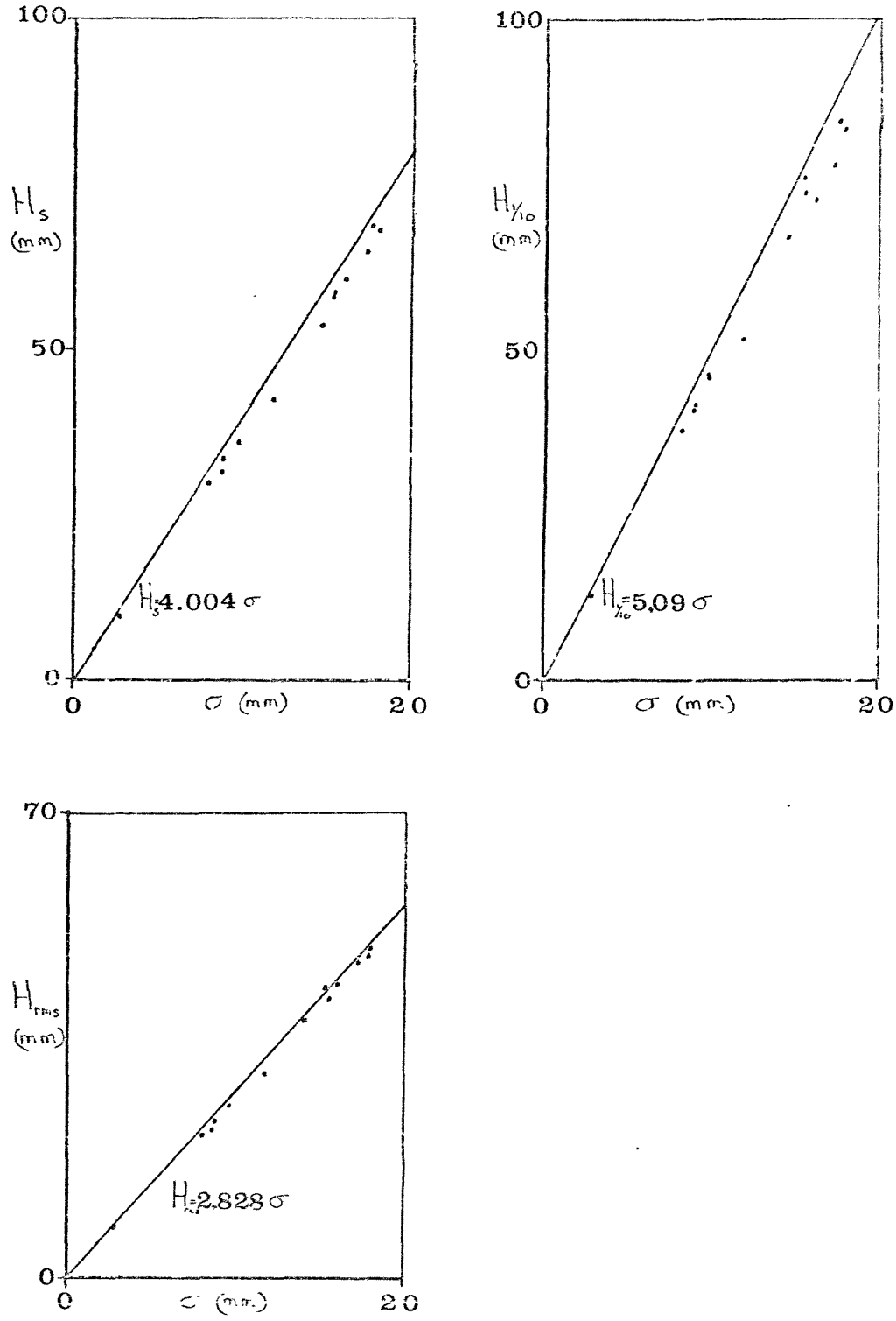

FIG. 6.20 Comparison of $H_{1/10}$, H_s and H_{rms} with Values Predicted by the Rayleigh Distribution

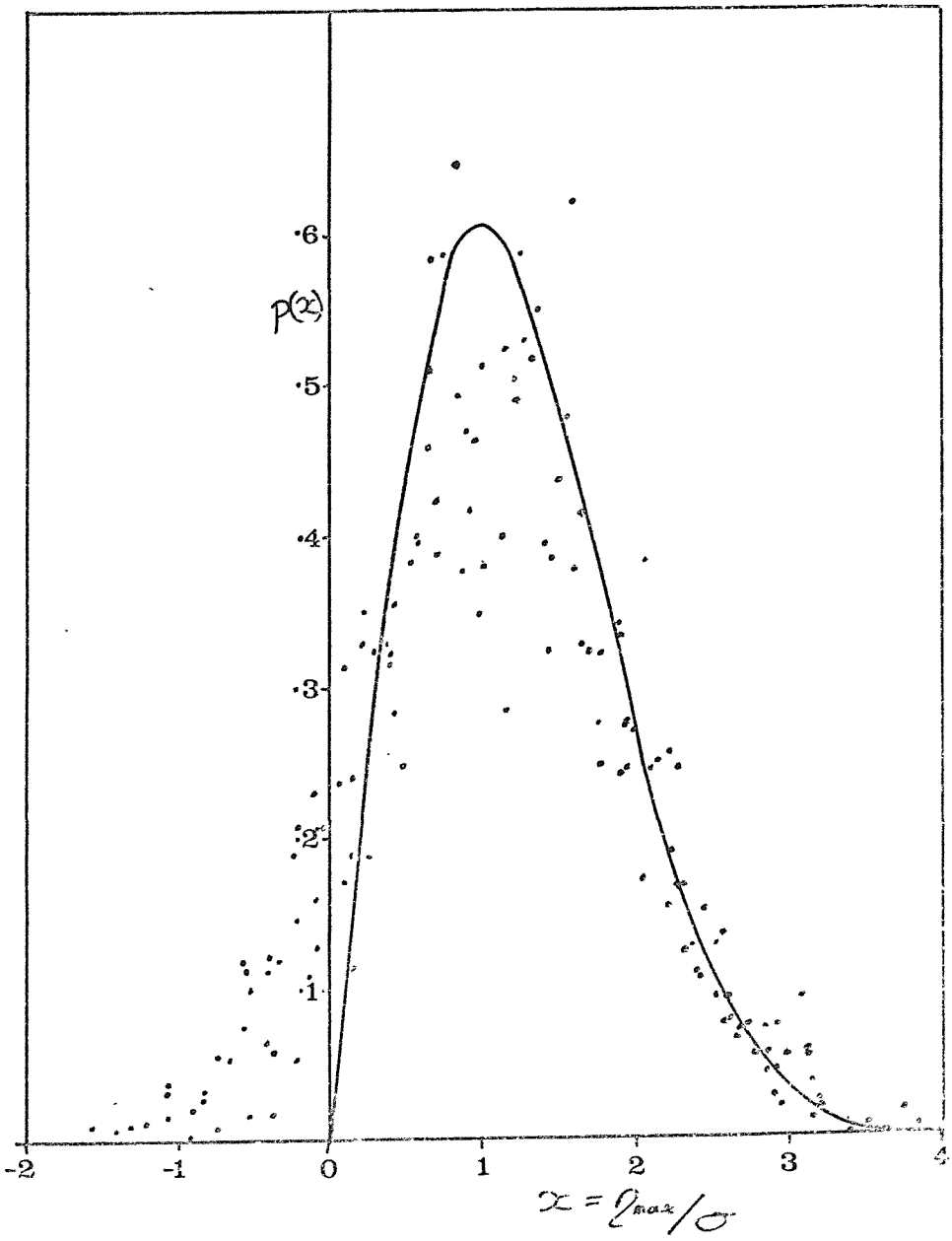

FIG. 6.21 Comparison of Rayleigh Distribution with the Peaks Determined Experimentally

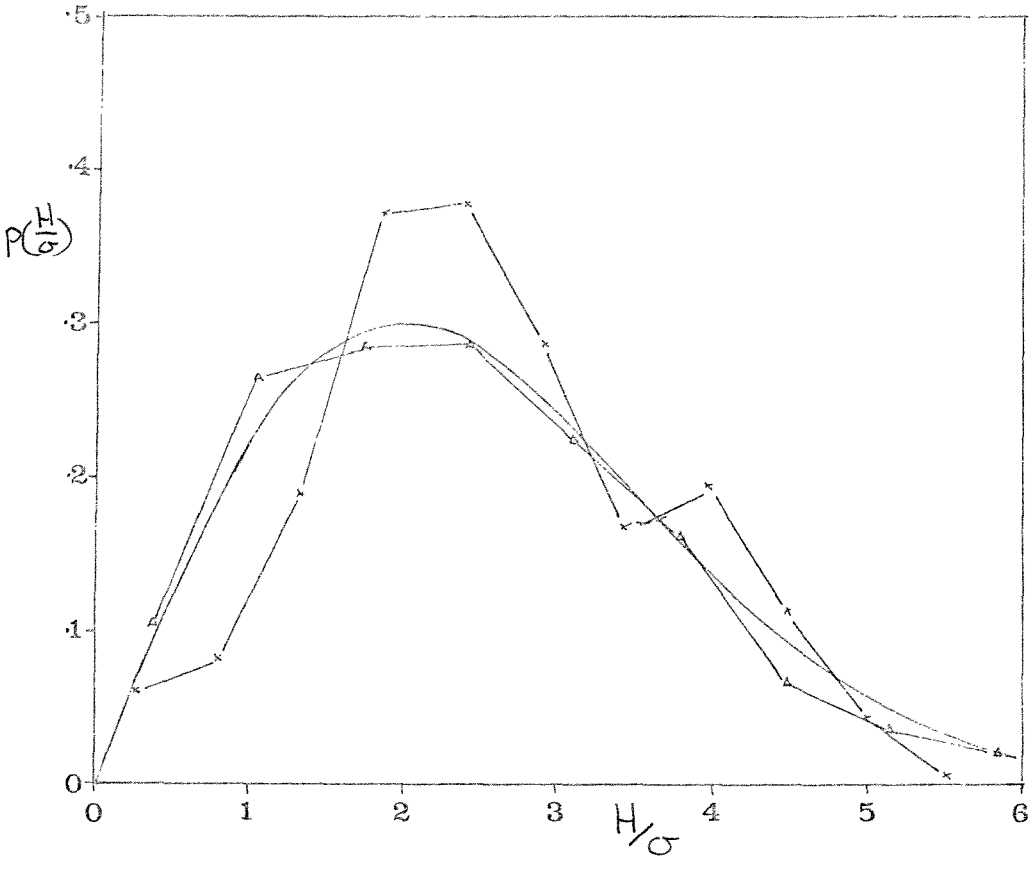

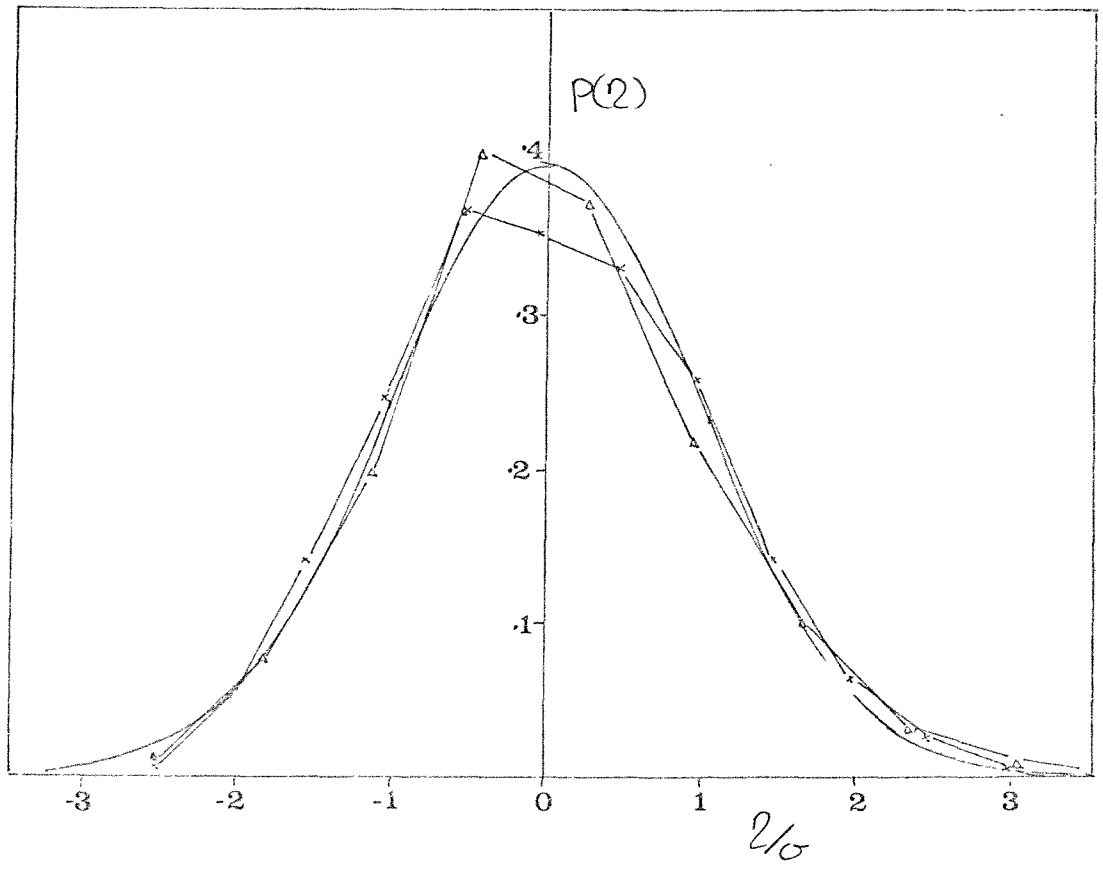

FIG. 6.22 Comparison of the Probability Distribution of Wave Height and Water Surface Elevation at Distances of 1.5 m.(▲) and 7 m.(×) from the Paddle for Spectrum N2

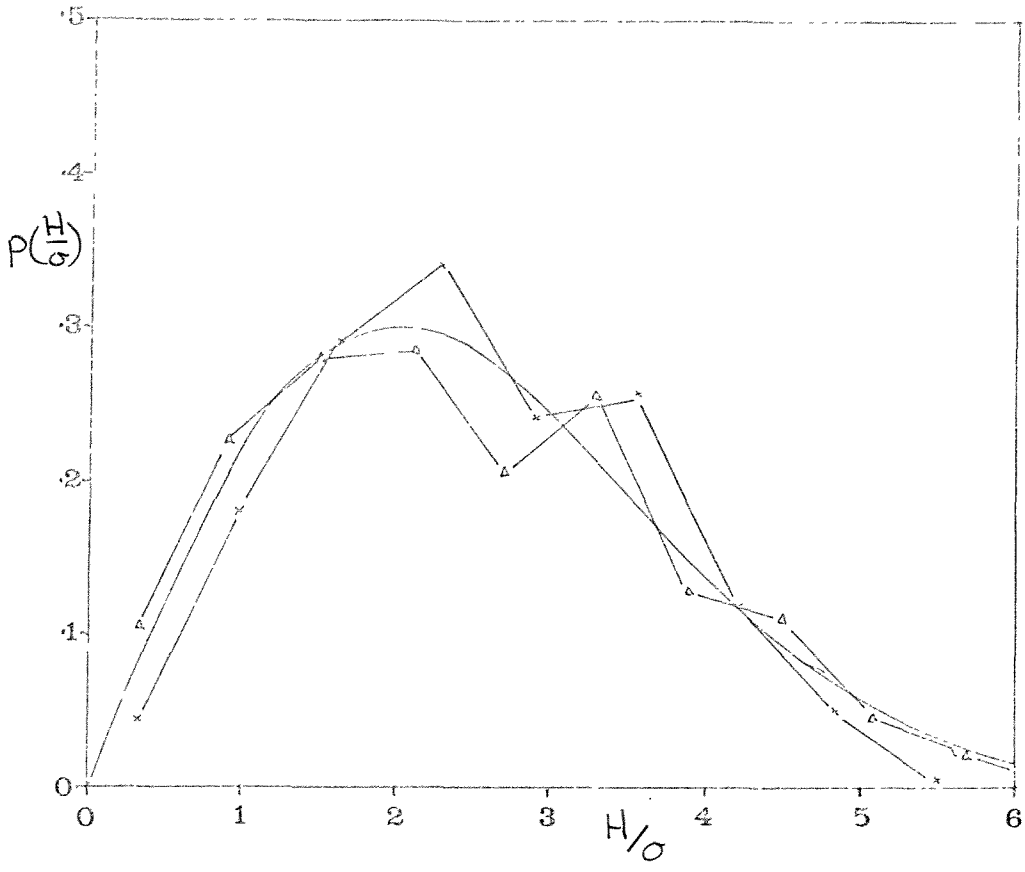

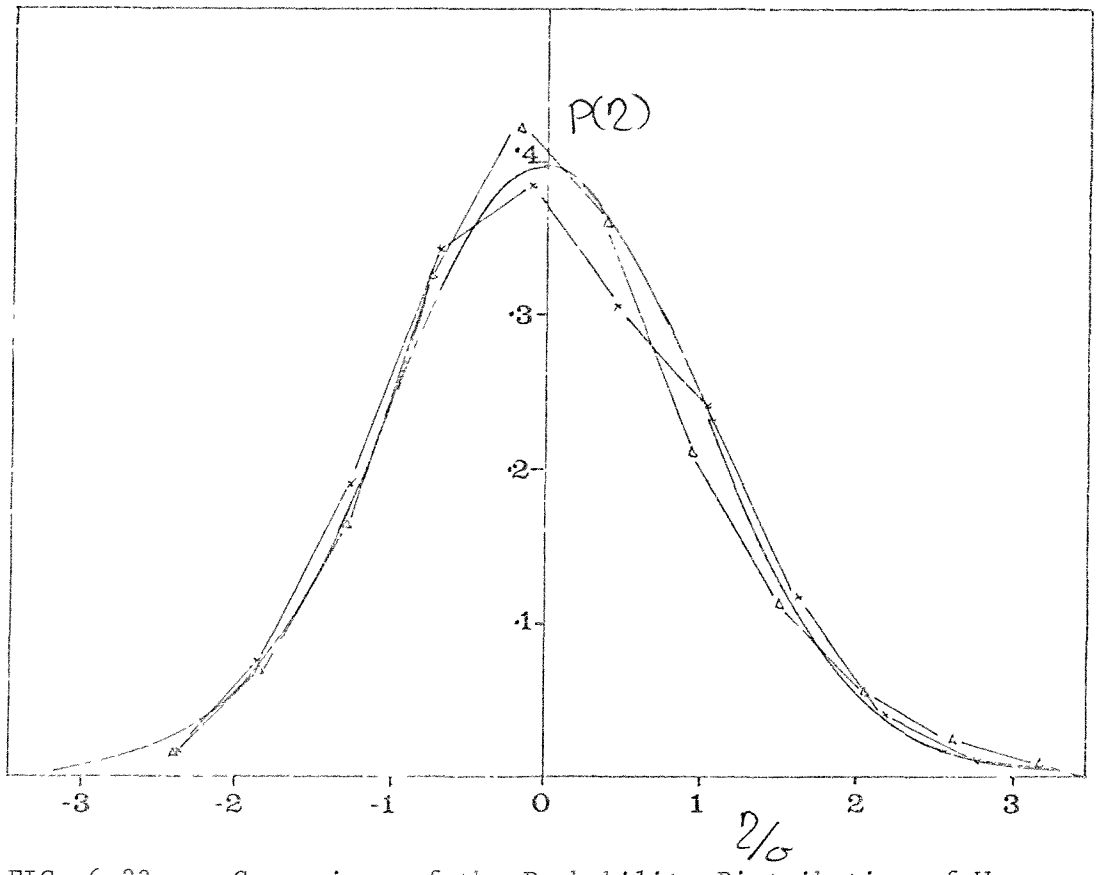

FIG. 6.23 Comparison of the Probability Distribution of Wave Height and Water Surface Elevation at Distances of 1.5 m.(▲) and 7 m.(×) from the Paddle for Spectrum T1

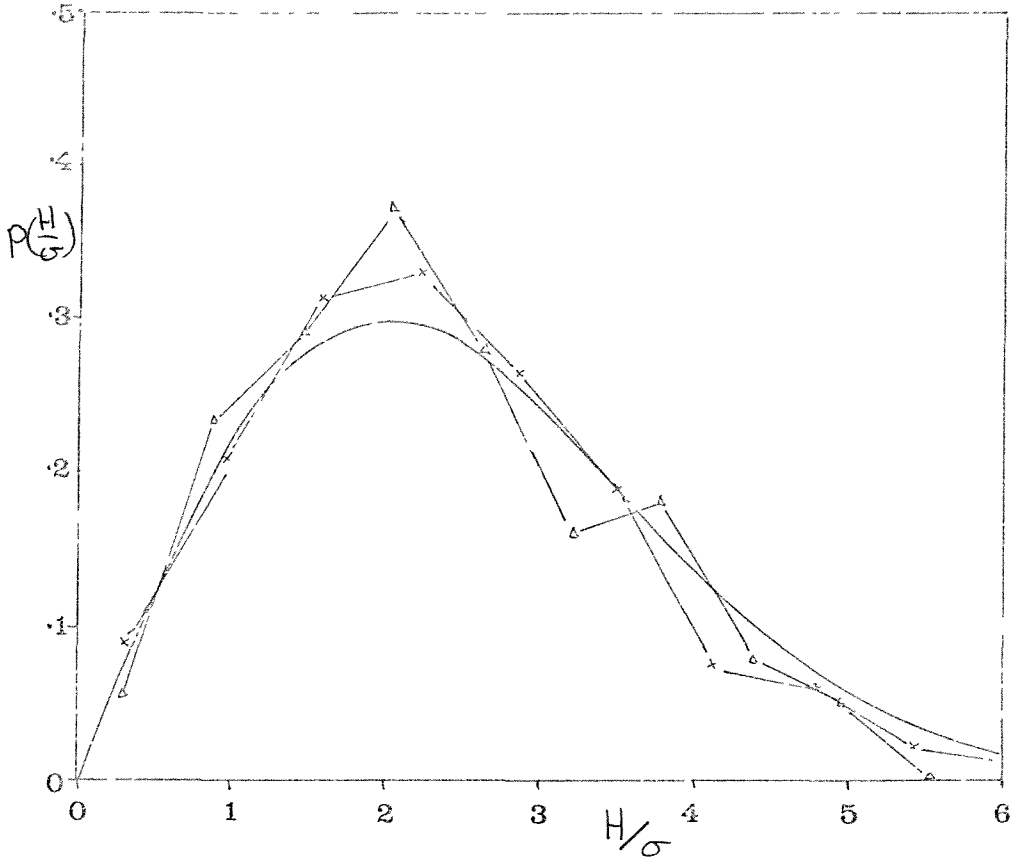

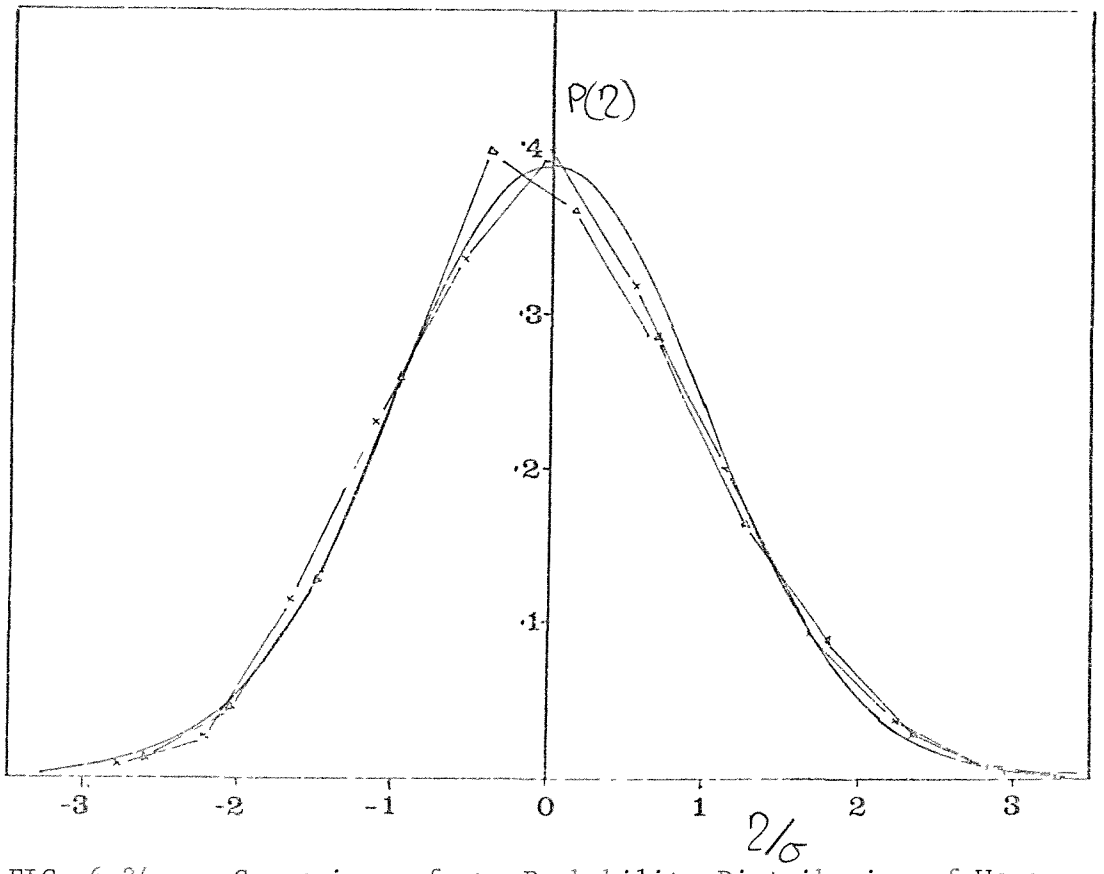

FIG. 6.24 Comparison of the Probability Distribution of Wave Height and Water Surface Elevation at Distances of 1.5 m.(▲) and 7 m.(×) from the Paddle for Spectrum 2A

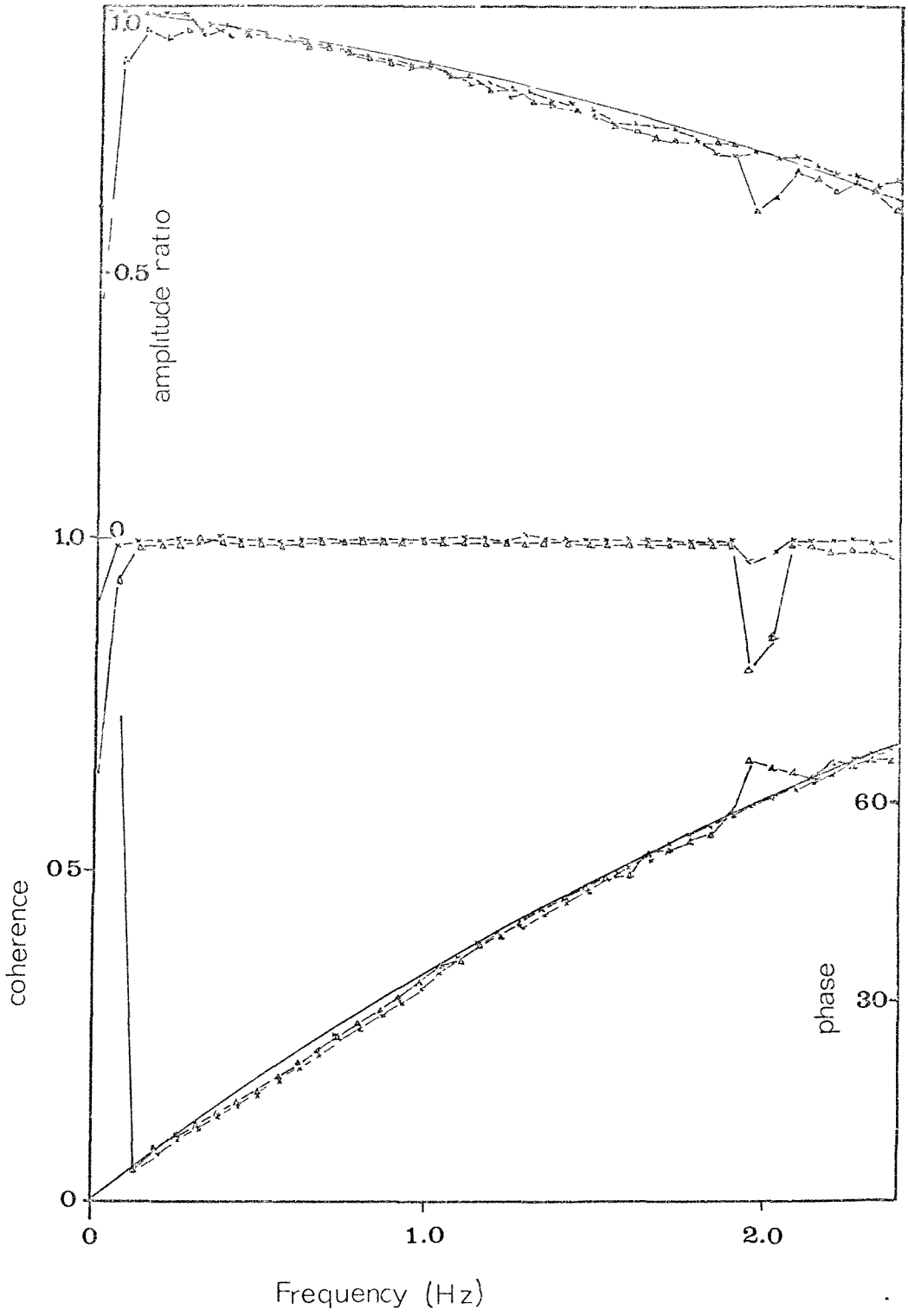

FIG. 6.25 Typical Plots of Coherence Function (centre) and Frequency Response for the Wave Generator

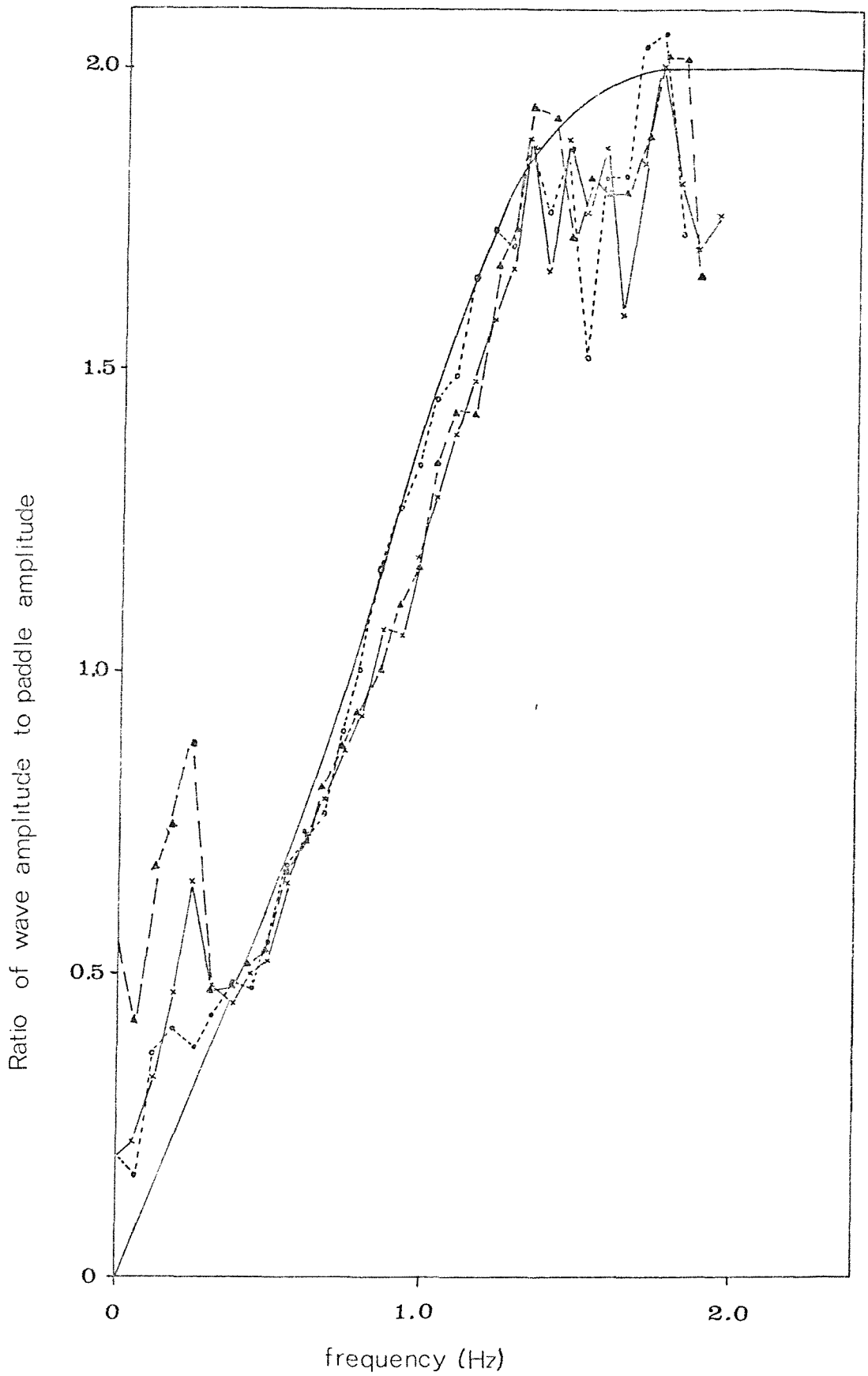

FIG. 6.26 Typical Plots of Transfer Function Estimated from the Programmed Wave Generation

PLATE 6.1 The Paddle of the Wave Generator

PLATE 6.2 A General View of the Channel showing Programmed Waves being produced

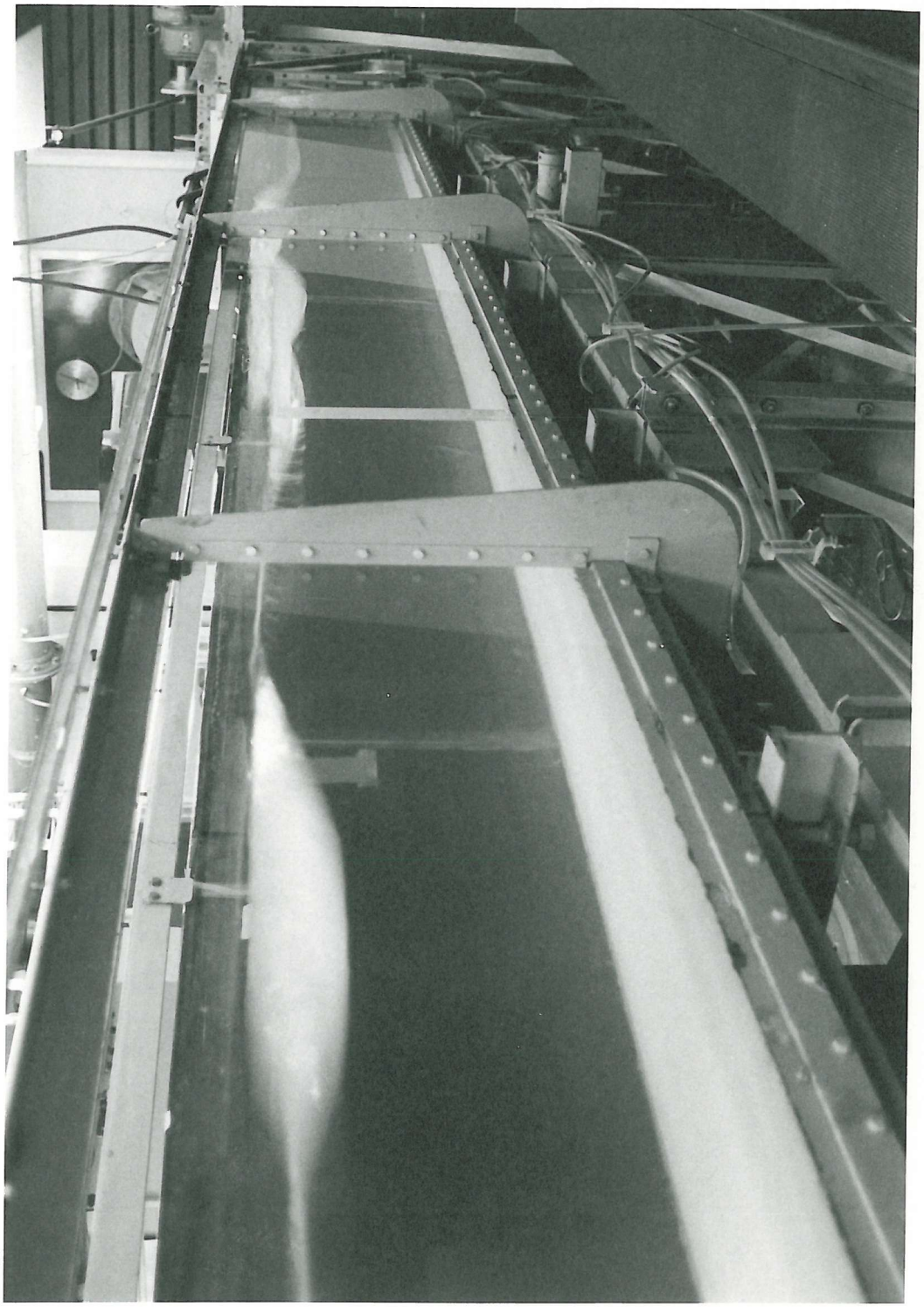

7. DISCUSSION OF RESULTS

7.1 Accuracy of the Simulation

The simulation of the various classes of spectra will be discussed in detail since each illustrates particular points of interest.

The Eastbourne Spectrum is simulated with a variance accurate to 6.6 per cent, the spectral form, however, shows some interesting differences. The peak energy is increased by 8 per cent and shifted to a slightly higher frequency. Difficulty with the production of a suitable command tape for this case tends to suggest that the cause may be found in this process. Spectra from the NAB Tower were simulated with success, errors in variance being less than 3 per cent and the agreement in spectral shape was good. Record N3 is of interest since the prototype exhibited a sharp cut-off at the top of the spectrum, whilst the simulated spectrum was noticeably pointed. This was most probably due to the resolution used to estimate the prototype shape. A greater resolution would probably have revealed a shape similar to the simulated one. It is interesting to note that the simulation process appears to have compensated for the shortcomings of the original analysis.

The spectra from Jersey were not so successfully modelled. Spectra 11 and 12B contained some energy below the cut-off frequency of 0.3 Hz imposed by the digital filter. This was clearly evident in the spectral plots. In calculating the variance, spectral width and peakedness for these, the energy below the cut-off frequency was ignored. Table 6.3a shows the actual variance in brackets. Even

allowing for this, Spectrum 11 still lacked energy at the low frequencies. This may be due to the inability of the command tape generation program to reproduce the very spiked nature of the spectrum. Spectra 2A and 2B show a marked lack of energy in the high frequency peaks. There is evidence that this is largely due to the shortcomings of the digital filter program, since the variance of the command signal for these records showed the worst agreement with the predicted values.

The two Moskowitz spectra simulated are very interesting. The accuracy of the simulated variances for M25 and M30 were too low by 4 per cent and 9 per cent respectively, whilst the variance of the command tapes were too low by 11 per cent and 1.25 per cent respectively. This supports the hypothesis proposed in the next section concerning the disproportionate effect of energy at different frequencies. The spectral shape for both these cases were in good agreement with that specified.

The arbitrary spectra T1 and T2 were the most spectacular. T2 especially, clearly showed the various wave components travelling at different speeds and in some cases, breaking as waves overtook each other. This breaking at various sections of the flume explains the loss of energy in the high frequency peak. The final spectrum TN2 was designed to contain amplitudes andfrequencies which would normally be produced by a wind-generated system. The simulated spectrum was much smaller than that specified and the shape much more irregular. This implies that waves of this frequency may not be simulated readily with this type of generator.

Values of spectral width and peakedness for both simulated and specified spectra were compared in Table 6.3a. Since these parameters depend upon the relative energy at different frequencies and the position of the spectrum on the frequency axis, they should theoretically provide a good indication of the accuracy of the simulation. However, difficulties can occur because of the errors in computing the higher spectral moments, but this may be improved by computing the moments from a truncated spectrum. Bearing this in mind, the spectral width and peakedness were generally in agreement within 10 per cent.

For the simulated spectra from Eastbourne and the NAB Tower, it was possible to make a comparison with the prototype in terms of wave height. Table 6.3b shows that the simulation in this respect was less successful. The number of waves considered for the computation of the three parameters H_{rms}, H_s, $H_{1/10}$ were very different in prototype and model which may have a significant effect upon the calculation. In addition, the prototype records N2 and N3 were found to contain several spurious values which may have affected the process for determining individual waves.

The ratio of the various wave height parameters to the standard deviation of the water surface elevation show a remarkable similarity considering the wide range of spectral shapes considered. This may be due to some extent on the zero up-crossing method of wave height definition since it tends to disregard the small high-frequency waves. The values computed differ from those predicted by assuming a Rayleigh distribution and the probability distribution of wave heights

did not support this assumption. It is worth noting, however, that all values of wave height were less than those predicted theoretically so that the assumption of a Rayleigh distribution for design calculation would yield conservative estimates.

The graphical representation of the probability distribution of water surface elevevation show a positive skewness which was also shown by computed values of skewness. These generally lay in the range 0.13 to 0.50 and were noticeably greater than the prototype values.

7.2 Evaluation of the Complete System

The deviation of the simulated spectra from the specified shape and energy may be considered in four stages:

(i) punch tape generation

(ii) paddle motion

(iii) transfer function approximated by small amplitude theory

(iv) errors in recording and analysis process.

The punch tape generation process as described in Section 5. depends for its success upon the nature of the impulse function corresponding to the desired spectrum of the command signal. The accuracy with which this is represented in terms of the overlap of the filtered signal determines to a large extent the success of the simulation. Errors of up to 10 per cent in Spectra 2A and 2B are noticed for this reason. These errors do not necessarily produce a corresponding error in the wave motion because of the effects of the transfer function. Low frequency waves require a much greater paddle motion than higher frequencies and so a large error due to the error

in not producing the correct variance in the low frequency of command tape may not produce a corresponding error in the waves because the low frequencies make up a small percentage of the total energy. This effect is noticeable in Spectrum T2 for example, where the variance of the command tape is too large by 2.8 per cent, but the waves produced are too low by 2 per cent, with lack of energy in the waves at high frequency being made up for in the command tape by excess energy at low frequency.

From the graph of the frequency response and coherence function in Fig. 6.26, it is evident that the system shows very little non-linear characteristics since the coherence function generally shows only a 1 or 2 per cent deviation from unity. The frequency response shows good agreement with that predicted by the sinusoidal tests.

The problem of gain adjustment in relation to repeatability mentioned earlier is of vital importance if the wave energy is to be predicted reliably. There are two alternatives to improve the situation. The gain used was selected for two reasons. Firstly, to achieve a smooth motion of the paddle and secondly, to compensate for the paddle-to-wave transfer function. The latter being achieved by an increase in the ratio of command signal to wave height at high frequencies, compared with that for a flat frequency response for the wave generator. This was desirable to reduce any high frequency errors due to the truncation of the command signal to integer form in the punch tape generation process. Thus, the gain may remain at this value using a precision drive to adjust the potentiometer to achieve easier repetition of the setting.

The second alternative is to increase the gain until the frequency response is almost flat at the frequencies of interest. In this case, the frequency response is less sensitive to the gain setting but the motion of the paddle becomes less smooth. In fact, the method recommended is the second alternative, but with the precision potentiometer installed such that a lower gain may be used where a perfectly smooth motion is required.

The small amplitude expression for the wave height in terms of paddle motion used for the frequency response of the system appears to be a good approximation to the true situation. There was little evidence of significant changes in wave amplitude down the channel. A slight trend of the zero crossing period to lengthen gave some indication of a tendency for the high frequency waves to lose energy. The spectra at 1.5 m. and 7.0 m. from the paddle also tend to support this, although the effect is too small to account for the energy losses noted in the high frequency peaks of the simulated spectra. The frequency response function varies between 0.25 and 2.0 over the range of frequencies considered, which has some effect upon the quantisation of the time series to provide integer numbers for the command tape. This effect is most noticeable at the higher frequencies and tends to reduce the resolution of the paddle motion. Since the wave amplitudes at these frequencies are always much smaller than those at lower frequencies, the effect is made much worse and results in a loss of precision over this range. The failure to simulate Spectrum TN2 accurately may be due to this. In order to improve the situation, it would be more desirable to either alter the mechanical action of the paddle to produce a flatter frequency response or make

use of wind to reinforce these frequencies. The amplitude of Spectrum TN2 is so small that it is not likely to be used for serious model tests, but merely serves to illustrate the limitations of the system.

The errors imposed upon the experimental results by the water surface recording system have already been discussed. However, during the programmed wave tests it became evident that the system was being used to its limit of accuracy, especially for the spectra with low energy content. Since the accuracy is limited by the meniscus on the probe, an improvement to the system may be to substitute a thinner wire for the wave probe. This was considered for the present condition but because it necessitated an alteration to the oscillator units, it was rejected.

Any errors due to reflection were ignored when computing the spectra, but it should be noted that even though the reflection coefficient was only of the order of 2 per cent, the spectra estimated may vary by a similar amount depending on the position of the wave probe. Following the confirmation that the spectrum could be simulated in certain conditions to this accuracy, consideration was given to the determination of the directional spectrum using two waves probes, and using the method described by Thornton and Calhoun (1972). Unfortunately, lack of time concluded these experiments prematurely.

7.3 The Effect of Secondary Reflection

A major problem associated with short wave channels is the presence of secondary reflection. The wave reflected from a structure under test is reflected almost completely by the wave generator in most cases. In a prototype condition, the reflected wave would travel out to sea and be dissipated. Thus, in these conditions, the wave impinging on the structure may not readily be predicted since it is a property of not only the generator and channel but of the test piece as well. Under irregular wave conditions, the confusion becomes even greater because energy at specific frequencies will be either reinforced or reduced, depending upon the phase of the secondary reflection. A development of the control circuit of the programmable wave generator indicates that it may be possible to avoid these secondary reflections. In conventional form, the controlled variable is the paddle position, the control circuit being represented by Fig. 4.3c. The system involving the paddle motion and water surface is similar to that shown in Fig. 4.3a. If the paddle position is replaced by the water surface as the controlled variable, it may be possible to achieve a better generating system. The method adopted to achieve this was a s follows. A wave probe was attached to the face of the wave generator and the signal from the M.1828 unit fed to a differential amplifier. The command signal was input to the second channel of the operational amplifier and input resistances adjusted to the appropriate value. The output from this summing point was phase-shifted by 90^{o} and used as a command signal for the generator. This phase shift was necessary because the wave amplitude is proportional

to the paddle velocity. The system attempts to move in such a way that the water surface at the paddle follows the command signal.

Lack of time curtailed an exhaustive test of the system, but initial tests indicate that it may prove practical. By replacing the absorbing beach with a flat board it was possible to produce a reflected wave of approximately half the amplitude of the incident wave. A series of five waves were produced and could be observed to reflect from the board and return along the channel. The wave generator (still switched on, but with a constant command signal) almost completely absorbed the series of waves. A further test was run with sinusoidal waves with and without the feedback from the wave probe. During both tests the reflection was measured by traversing a second wave probe and observing the trace on a UV recorder. The tests with feedback produced a perfect envelope shape as predicted by the simple theory often used to determine the reflection coefficient. Without feedback, the envelope was considerably distorted due to the secondary wave reflection. This system was very simple and further development is required before the system may be used on a routine basis.

8. CONCLUSIONS

The system developed for the simulation of coastal sea state consisted of a piston type wave generator actuated by an electro-hydraulic control system. The command signal for the generation of programmed waves was provided, via a purpose-built interface, from computer generated punched tape.

A variety of spectra, including prototype and theoretical, were used to determine the feasibility of simulating sea state in this way. Generally the performance was good. However, the accuracy of the modelling was found to depend upon the magnitude and shape of the spectrum to be produced.

Spectra consisting of a single peak in the range 0.5 Hz to 1.0 Hz were most successfully simulated, the predicted variance generally being accurate to 3 per cent or, in the worst case, 6.6 per cent. Double-peaked spectra with high frequency peaks in the range 1.2 Hz to 1.8 Hz were less accurately reproduced, the low frequency peak showing good agreement with that specified but the high frequency peak being reduced in magnitude. This discrepancy was due to the lack of high frequency energy in the command tape, the natural anihilation of waves by breaking and the attenuation of the small amplitude high frequency waves as they passed along the channel.

A spectrum with very low energy concentrated in a single peak at approximately 1.6 Hz was used to illustrate the limit of accuracy of this type of generator. It must be concluded that if it is desired to produce very small amplitude waves in this range of frequencies, some wind assistance may be necessary. This is due to the fact that

very much smaller paddle amplitudes are required in this region than those for the lower frequencies. These amplitudes tend to approach the limit of accuracy of the command signal.

The command tape used in the programmed wave investigation was produced by digitally filtering random numbers. The fast Fourier transform method used was very efficient but the errors in the resulting time series could not be predicted with confidence. In certain cases, the variance of the command signal was accurate to within 2 per cent but in others, notably in small amplitude double-peaked spectra, errors of 20 per cent were observed. Further research into the filtering system may yield a better knowledge of this process.

When the command tapes were being produced a linear transfer function was assumed for the wave generating mechanism. The validity of this assumption was checked under programmed conditions and found to be valid for both the command signal to paddle motion and paddle motion to wave motion sections of the process. In the latter case, there was some suggestion that the wave heights produced by using the small amplitude theory were slightly less than expected at higher frequencies.

Whilst the simulated wave spectra were being computed, a variety of statistical data for the wave heights and water surface elevation was gathered and used to assess the validity of the theoretical expressions for these. In general, the values of wave height height predicted by assuming a Rayleigh distribution were conservative by up to 10 per cent. The distribution of water surface elevations showed

a marked positive skewness, the values of which were larger than those noted for prototype records. Both of these effects have been noted by other authors.

A method avoiding the secondary reflection from the wave generator was briefly investigated. By attaching a wave probe to the face of the paddle the water surface became the controlled variable. The initial results were encouraging but further research is necessary before the system is feasible for model tests.

9. REFERENCES

Bendat, J. S. and A. G. Piersol

1966 Measurement and Analysis of Random Data. New York. John Wiley & Sons Inc. 4th Printing.

Berge, H. and A. Traetteberg

1969 Stability Tests on the Europort Breakwater. Proc. Symposium on Wave Action, Paper 10. Delft. Hydraulics Laboratory Delft.

Biesel, F.

1951 Etude theoretique d'un certain type d'appareil a houle. La Houille Blanche 6 No. 2 pp. 152-165. English Translation in St. Anthony Falls Hydraulics Laboratory Report No. 39.

Birkhoff, G. and J. Kotik

1952 Fourier Analysis of Wave Trains. Gravity Waves pp. 243-253. Natl. Bur. Standards (US) circ. 521.

Blackman, R. B. and J. W. Tukey

1958 The Measurement of Power Spectra. New York. Dover Publications.

Borgman, L. E.

1967 Ocean Wave Simulation for Engineering Design.
Berkeley. University of California. Report No. HEL 9-13.

Bretschneider, C. L.

1959 Wave Variability and Wave Spectra for Wind-Generated Waves.
Washington. Beach Erosion Board TM 118.

Brigham, E. O. and R. E. Morrow

1967 The fast Fourier transform.
I.E.E.E. Spectrum. Dec. 1967. pp. 63-70.

Bullock, G. N.

1967 A study of the Run-up of Irregular Waves on Uniform Slopes.
Ph.D. Thesis. Southampton University.

Carstens, T.

1966 The Stability of Rubble Mound Breakwaters against
Irregular Waves.
Proc. 10th Conf. Coastal Eng. New York. A.S.C.E.

Cartwright, D. E.

1958 On Estimating the Mean Energy of Sea Waves from the
highest waves in the record.
Proc. Roy. Soc. A.247. pp. 22-48.

Cartwright, D. E. and M. S. Longuet-Higgins

1956 The statistical distribution of the maxima of a random
function.
Proc. Roy. Soc. A.237. pp. 212-232.

D'Angremond, K. and J. H. Van Oorshot

1969 The Generation of Irregular Waves on Model Scales. Proc. Symposium on Wave Action, Paper 3. Delft. Hydraulics Laboratory Delft.

Darbyshire, J.

1961 The one-dimensional wave spectrum in the Atlantic Ocean and in coastal waters. Proc. N.A.S. Conf. on Ocean Wave Spectra. Englewood Cliffs. Prentice-Hall Inc. pp. 27-39.

Davenport, W. B. and W. L. Root

1958 An introduction to the Theory of Random Signals and Noise. New York. McGraw-Hill Book Co. Inc.

D'Azzo, J. and C. H. Houpis

1966 Feedback Control System Analysis and Synthesis. Second Edition. New York. McGraw-Hill Book Co. Inc.

Deacon, G. E. R.

1949 Recent studies of waves and swell. Ocean Surface Waves. Ann. N.Y. Acad. Sci. 51. pp. 475-482

Draper, L.

1957 Attenuation of sea waves with depth. La Houille Blanche 12. pp. 926-931.

1963 Derivation of a 'design wave' from instrumental records of sea waves. Proc. I.C.E. 1963. 26. pp. 291-303.

1966 The analysis and presentation of wave data - a plea for uniformity.
Proc. 10th Conf. on Coastal Eng. New York. A.S.C.E. pp. 1-11.

Earattupuzha, J. and H. Raman

1972 Determination of wave length in flume studies.
Proc. A.S.C.E. 98. No. WW1. pp. 147-149.

Eimbinder, J. (Editor)

1970 Application Considerations for Linear Integrated Circuits.
New York. Wiley Interscience.

Ewing, J.

1962 The generation of discrete wave spectra in a ship tank.
London. National Physical Laboratory Ship Report 35.

Galvin, C. J.

1964 Wave Height prediction for wave generators in shallow water.
US Army Coastal Engineering Research Centre TM4.

Gilbert, G., D. M. Thompson and A. J. Brewer

1970 Design curves for regular and random wave generators.
Wallingford. Hydraulics Research Station Report INT 81.

Goda, Y. and T. Kikuya

1964 The generation of water waves with a vertically oscillating flow at a channel bottom.
Yokosuka, Japan. Report of Port and Harbour Research Institute No. 9.

Goda, Y.

1970 Wave Statistics with Spectral Simulation.
Yokosuka, Japan. Report of Port and Harbour Research
Trust 9, No. 3. pp. 7-57.

Graeme, J. G., G. E. Tobey and L. P. Huelsman

1971 Operational Amplifiers, Design and Application.
New York. McGraw-Hill Book Co. Inc.

Harris, R. J. S.

1973 Ph.D. Thesis on Floating Breakwaters.
To be published. University of Southampton.

Helms, H. D.

1967 Fast Fourier Transform Method of Computing Difference
Equations and Simulating Filters.
I.E.E.E. Trans. Audio and Electro-Acoustics.
AU-15 No.2. pp. 85-90.

Hoeschele, D. F.

1968 Analogue to Digital/Digital to Analogue Conversion Techniques.
New York. John Wiley & Sons Inc.

Hogben, N. (Chairman - N.P.L. Hovercraft Sea State Committee)

1969 The definition of Sea State for Hovercraft purposes.
London. National Physical Laboratory Hovercraft Unit.
Report 8.

Ippen, A. T.

1966 Estuary and Coastline Hydrodynamics.
New York. McGraw-Hill Book Co. Inc.

Ippen, A. T. and P. S. Eagleson

1964 A study of sediment sorting by waves shoaling on a plane beach.
Massachusetts. M.I.T. Hydrodynamics Lab. TR 18.

James, W.

1969 Accurate Wave Measurements in the Presence of Reflections.
Journal Inst. W.E. 23 pp. 497-501.

Kinsman, B.

1964 Wind Waves.
Englewood Cliffs, N.J. Prentice Hall Inc.

Klebba, A. A.

1946 Progress Report on Shore-based Wave Recorder and Ocean Wave Analyser.
Woods Hole Oceanographic Institution.

Kraai, P. T.

1969 Comparison of wind wave and uniform wave effects on a beach.
Shore and Beach 37, No. 2. pp. 60-71.

Longuet-Higgins, M. S.

1952 On the statistical distribution of the heights of sea waves.
J. Mar. Res. 11, pp. 245-266.

Madsen, O. S.

1970 Waves generated by a piston-type generator.
Proc. 12th Conf. Coastal Eng. New York. A.S.C.E. pp. 589-609.

Merritt, H. E.

1967 Hydraulic Control Systems.

New York. John Wiley & Sons Inc.

Moskowitz, L.

1964 Estimates of the power spectrum for fully developed seas for wind speeds of 20 to 40 knots.

J. of Geophys. Res. 69, No. 24. pp. 5161-5179.

Muir Wood, A. M.

1969 Coastal Hydraulics.

Bath, UK. Macmillan.

Papoulis, A.

1962 The Fourier Integral and its Applications.

New York. McGraw-Hill Book Co. Inc.

Pierson, W. J.

1955 Wind generated gravity waves in Advances in Geophysics, 2.

pp. 93-178. New York, Academic Press Inc.

Pierson, W. J. and W. Marks

1952 The power spectrum analysis of ocean wave records.

Trans.-Am. Geophys. Un. 33, No. 6. pp. 834-844.

Putz, R. R.

1953 Statistical analysis of wave records.

Proc. 4th Conf. on Coastal Eng. Berkeley,

The Council on Wave Research.

Rademakers, P. J.

1969 Reflok-Write and Programming Unit Manual for Waverider Buoy System.
Haarlem. Datawel.

Raven, F. H.

1961 Automatic Control Engineering.
New York. McGraw-Hill Book Co. Inc.

Rice, S. O.

1944 Mathematical Analysis of Random Noise.
Bell System Tech. Journal 23. pp. 283-332.

Shvetsov, K. Ya. and A. N. Shorin

1969 The modelling of sea waves by digital computer.
Oceanology 9. pp. 578-584.

Sverdrum, H. U. and W. H. Munk

1947 Wind Sea and Swell: Theory of relations for forecasting.
Washington. U.S. Navy Hydrographic Office Pub. No. 601.

Thompson, D. M.

1970 Tests on a discrete frequency irregular wave generator.
Wallingford. Hydraulics Research Station Report INT 82.

Thompson, D. M. and R. M. Shuttler

1972 Signal Generation for Random Wave Simulation.
Wallingford. Hydraulics Research Station Report INT 103.

Thornton, E. B. and R. J. Calhoun

1972 Spectral Resolution of Breakwater Reflected Waves.

Proc. A.S.C.E. 98 WW4. pp. 443-460.

Tucker, M. S.

1963 Analysis of records of sea waves.

Proc. I.C.E. 26. pp. 305-316

Wiegel, R. L.

1965 Oceanographical Engineering.

Englewood Cliffs, N.J. Prentice-Hall Inc.

APPENDIX 1.

LISTING OF THE DIGITAL FILTER PROGRAM

```
0006                MASTER DIGFILT
0009                COMPLEX CX(2,1024),CTF(1024)
0010                DIMENSION TF(1024),PF(1024),SF(256)
0011                DIMENSION F(256)
0012                DIMENSION WNS(40)
0013                DIMENSION X(9999),NX(256)
0014                DATA START,FINISH/4H ES ,4H EF /
0015          C      READ IN TRANSFER FUNCTION ,SPECTRAL DATA
0016                READ(1,102)SERIAL,DATE,DEPTH,DELT,FMAX,SCALE1
0017                  SCALE=(1/SCALE1)**2.5
0018                  NSTAGE=10
0019                  NL=1024
0020                  NSAMPLE=8000
0021                  DELF=0.098
0022                  DELF1=1.0/(NL*DELT)
0023                  NFMAX=FMAX/DELF
0024                  DEPTH =DEPTH/SCALE1
0025                DO 2 I=1,NL
0026                  F(I)=0.0
0027                  PF(I)=0.0
0028                  SF(I)=0.0
0029             2     TF(I)=0.0
0030                  PI=3.14159
0031          C         READ IN PROTOTYPE SPECTRUM AND ACTUAL FREQUENCY INTERVAL
0032                READ(1,103)DUM1,DUM2,DUM3
0033                READ(1,104)(X(I),I=1,40)
0034                READ(1,105) DELFA
0035                  DELFA=DELFA*SQ RT(SCALE1)
0036          C         INTERPOLATE SPECTRUM AT REQUIRED FREQUENCIES
0037                  FP=0.0
0038                DO 16 I=1,NFMAX
0039                  F(I)=NX(I)*32.0
0040             16 CONTINUE
0041                DO 14 I=1,NFMAX
0042                  FP=(I-1)*DELF
0043                  NI=FP/DELFA
0044                  STEP=FP-DELFA*NI
0045                  SF(I)=F(NI+1)+(F(NI+2)-F(NI+1))*STEP/DELFA
0046             14 CONTINUE
0047                DO 12 I=1,NFMAX
0048                  F(I)=(I-1)*DELF
0049             12 CONTINUE
0050                READ(1,103)DUM1,DUM2,DUM3
0051                READ(1,101)(TF(I),I=1,32)
0052                READ(1,103)DUM1,DUM2,DUM3
0053                READ(1,101)(PF(I),I=1,32)
```

```
0054                  XVAR1=0.0
0055                  XVAR=0.0
0056                DO 11 I=1,NFMAX
0057                  SF(I)=SF(I)*SCALE
0058                  XVAR=XVAR+SF(I)*DELF
0059             11 CONTINUE
0060                  NFMAX=FMAX/DELF
0061                WRITE(3,310)
0062                WRITE(3,315)
0063                WRITE(3,311)NL,NSAMPLE,SCALE1,DELT
0064                WRITE(3,315)
0065                WRITE(3,312)SERIAL,DATE,DEPTH,XVAR
0066                WRITE(3,314)(SF(I),F(I),I=1,NFMAX)
0067                WRITE(3,315)
0068                WRITE(3,313)
0069                WRITE(3,314)(TF(I),F(I),I=1,NFMAX)
0070                DO 13 I=1,NFMAX
0071                  XVAR1=XVAR1+(TF(I)**2.0*SF(I))*DELF
0072             13 CONTINUE
0073          C               FOR SPECTRUM BY WHITE NOISE  SPECTRUM
0074                READ(1,103)DUM1,DUM2,DUM3
0075                READ(1,101)(WNS(I),I=1,40)
0076                DO 50 I=1,34
0077                  SF(I)=SF(I)/WNS(I)
0078             50 CONTINUE
0079                DO 51 I=1,NFMAX
0080                  TF(I)=SQ RT(SF(I)/2.0)*TF(I)
0081             51 CONTINUE
0082                  NFMAX=FMAX/DELF1
0083                DO 60 I=1,256
0084                  SF(I)=0.0
0085                  F(I)=0.0
0086             60 CONTINUE
0087                DO 61 I=1,NFMAX
0088                  FP=(I-1)*DELF1
0089                  NI=FP/DELF
0090                  STEP=FP-DELF*NI
0091                  SF(I)=SF(I)+(TF(NI+2)-TF(NI+1))*STEP/DELF
0092                  F(I)=PF(NI+1)+(PF(NI+2)-PF(NI+1))*STEP/DELF
0093             61 CONTINUE
0094                DO 62 I=1,NFMAX
0095                  TF(I)=SF(I)
0096                  PF(I)=F(I)
0097                  F(I)=(I-1)*DELF1
0098             62 CONTINUE
0099                WRITE(3,315)
```

```
0100                WRITE(3,317)
0101                WRITE(3,314)(TF(I),F(I),I=1,NFMAX)
0102                  XTRA=SQRT(XVAR/XVAR)
0103                WRITE(3,316)XTRANS
0104               DO 10 I=2,NFMAX
0105                  TF(NL+2-I)=-PF(I)
0106                  TF(NL+2-I)=TF(I)
0107            10 CONTINUE
0108               DO 6 I=1,NL
0109                  DUMR=TF(I)*COS(2.0*PI*PF(I)/360.0)
0110                  DUMI=TF(I)*SIN(2.0*PI*PF(I)/360.0)
0111                  CTF(I)=CMPLX(DUMR,DUMI)
0112            6 CONTINUE
0113                  NSUM=0
0114                  NK=0
0115                  B=SQRT(DELF1*NL)
0116                  NTRANS=NSAMPLE/NL
0117            4 CONTINUE
0118              DO 3 I=NK+1,NL
0119                 CX(1,I)=CMPLX(GOSAEF(0.0,B),0.0)
0120            3 CONTINUE
0121              CALL FASTFT1(CX,NSTAGE,-1,0)
0122              DO 5 I=1,NL
0123                 CX(1,I)=CTF(I)*CX(2,I)
0124            5 CONTINUE
0125              CALL FASTFT1(CX,NSTAGE,1,0)
0126                 NK=100
0127              DO 7 I=1,NL-NK
0128                 X(NSUM+I)=REAL(CX(1,I))
0129            7 CONTINUE
0130                 NSUM=NSUM+NL-NK
0131              DO 23 I=NL-NK+1,NL
0132                 CX(1,I-NL+NK)=CX(1,I)
0133           23 CONTINUE
0134              IF(NSUM.LT.NSAMPLE)GO TO 4
0135                 NSAMPLE=NSUM
0136               WRITE(3,503)START
0137                 NI=NSAMPLE/50
0138              DO 9 I=1,NI
0139              DO 20 J=1,50
0140                 NJ=(I-1)*50+J
0141                 NX(J)=X(NJ)*0.67*50
0142           20 CONTINUE
0143               WRITE(3,502)(NX(K),K=1,50)
0144            9 CONTINUE
0145               WRITE(3,503) FINISH



0146       C        STATISTICAL ANALYSIS
0147              CALL STATS(X,NSAMPLE,VAR,XMEAN,XSKEW,XKURT)
0148               WRITE(3,320)VAR,XSKEW,XKURT
0149               WRITE(3,301)XMEAN
0150           99 CONTINUE
0151              STOP
0152          101    FORMAT(10F5.2)
0153          102    FORMAT(2A6,4F6.3)
0154          103    FORMAT(3A8)
0155          104    FORMAT(10I5)
0156          105    FORMAT(F10.5)
0157          301    FORMAT(1H ,F6.3)
0158          302    FORMAT(1H ,F6.3,3X,F6.3)
0159          320     FORMAT(1H1,30X,20HSTATISTICAL ANALYSIS//
0160             1   1H ,30X,20H--------------------////
0161             3   1H ,20X,11HVARIANCE = ,3X,F8.3/
0162             4   1H ,20X,11HSKEWNESS = ,3X,F8.3/
0163             5   1H ,20X,11HKURTOSIS = ,3X,F8.3)
0164          310    FORMAT(1H1,20X,24HIRREGULAR WAVE GENERATOR/
0165             1            1H ,20X,30HSYSTEM COMMAND TAPE GENERATION/
0166             2            1H ,20X,29HBY DIGITAL FILTERING USING A/
0167             3            1H ,20X,29HFAST FOURIER TRANSFORM METHOD)
0168          311    FORMAT(1H ,20X,17HFILTERING DETAILS/
0169             1            1H ,20X,15HFFT LENGTH  =  ,3X,I4/
0170             2            1H ,20X,22HNUMBER OF SAMPLES  =  ,3X,I5/
0171             3            1H ,20X,4 HSPECTRUM MODELED ACCORDING TO FROUDE LAW/
0172             4            1H ,20X,27HWITH A LENGTH SCALE OF 1 : ,F8.3/
0173             5            1H ,20X,38HINTERVAL OF DIGITIZATION IN MODEL  =  ,F8.3)
0174          312    FORMAT(1H ,20X,3 HORIGINAL SPECTRUM (AFTER SCALING)//
0175             1            1H ,20 X,10HRECORD NUMBER  =  ,3X,A8,3X,4HDATE  =  ,A6/
0176             2            1H ,20X,14HWATER DEPTH  =  ,F8.3,3X,11HVARIANCE = ,F8.3/
0177             3            1H ,20X,3 HSPECTRAL,4X,9HFREQUENCY/
0178             4            1H ,20X,7HDENSITY)
0179          313    FORMAT(1H ,20X,4 HSPECTRUM ADJUSTED BY TRANSFER FUNCTION  =  /
0180             1            1H ,20X,14HTRANSFER,4X,9HFREQUENCY/
0181             2            1H ,20 X,11HDISTRIBUTION)
0182          316    FORMAT(1H ,20X,11HPOWER TRANSFER  =  ,F8.3)
0183          314    FORMAT(1H ,20 X,F8.5, 2X,F8.5)
0184          315    FORMAT(1H ,20 X,'----------')
0185          317    FORMAT(1H ,20 X,20H SPECTRUM TRANSFER FUN,TIO
0186             1            1H ,20X,14HFREQUENCIES)
0187          318    FORMAT(1H ,17 HNO. OF OBSERVATS  ,F6.3,3X,5HSEC)
0188          501    FORMAT(5X,20I4)
0189          502    FORMAT(1I2,50I4)
0190          503    FORMAT(A6)
0191                 END
```

```
0192                SUBROUTINE STATS(X,N,VAR,XMEAN,XSKEW,XKURT)
0193          C         THIS COMPUTES THE  MEAN,MEAN SQUARE,SKEWNESS AND KURTISIS
0194          C              OF THE  N VALUES IN THE ARRAY X
0195                DIMENSION X(N)
0196          COMPUTE MEAN VALUE
0197                   XMEAN=0.0
0198                DO 1 I=1,N
0199                   XMEAN=XMEAN+X(I)
0200              1 CONTINUE
0201                   XMEAN=XMEAN/N
0202          COMPUTE VARIANCE,SKEWNESS AND KURTOSIS
0203                   VAR=0.0
0204                   XSKEW=0.0
0205                   XKURT=0.0
0206                DO 2 J=1,N
0207                   VAR=VAR+((X(J)-XMEAN)**2/N)
0208                   XSKEW=XSKEW+((X(J)-XMEAN)**3/N)
0209                   XKURT=XKURT+((X(J)-XMEAN)**4/N)
0210              2 CONTINUE
0211                   XSKEW=XSKEW/(VAR**1.5)
0212                   XKURT=XKURT/(VAR**2)
0213                RETURN
0214                END

END OF SEGMENT, LENGTH   126, NAME  STATS
```

```
0215                SUBROUTINE FASTFT1(X,NSTAGE,SIGN)
0216          C              THIS IS THE FAST FOURIER TRANSFORM WITHOUT SORTING
0217          C              DEVELOPED BY UNRICH(1969)
0218          C              X IS THE COMPLEX ARRAY CONTAINING THE DATA POINTS
0219          C              X(2,1024) INPUT IN COLUMN 1, OUTPUT FOR INVERSE
0220          C              XTRANSFORM IN COLUMN 1, NORMALIZED OUTPUT FOR
0221          C              FORWARD TRANSFORM IN COLUMN 2, UNNORMALIZED FORWARD
0222          C              TRANSFORM OUTPUT IN COLUMN 1
0223          C              NSTAGE:NUMBEROF STAGES AND POWER OF TWO WHICH N IS
0224          C              N=2**NSTAGE
0225          C              SIGN=-1:FORWARD TRANSFORM
0226          C              SIGN=+1: INVERSE TRANSFORM
0227                COMPLEX X(2,1024),W
0228                INTEGER R
0229                   N=2**NSTAGE
0230                   N2=N/2
0231                   FLTN=N
0232                   PHI2N=6.2831853/FLTN
0233                DO 5 J=1,NSTAGE
0234                   N2J=N/(2**J)
0235                   NR=N2J
0236                   NI=(2**J)/2
0237                DO 4 I=1,NI
0238                   IN2J=(I-1)*N2J
0239                   FLIN2J=IN2J
0240                   TEMP=FLIN2J*PHI2N*SIGN
0241                   W=CMPLX(COS(TEMP),SIN(TEMP))
0242                DO 4 R=1,NR
0243                   ISUB=R+IN2J
0244                   ISUB1=R+IN2J*2
0245                   ISUB2=ISUB1+N2J
0246                   ISUB3=ISUB+N2
0247                   X(2,ISUB)=X(1,ISUB1)+W*X(1,ISUB2)
0248                   X(2,ISUB3)=X(1,ISUB1)-W*X(1,ISUB2)
0249              2 CONTINUE
0250                DO 3 R=1,N
0251              3    X(1,R)=X(2,R)
0252          C
0253                IF SIGN.GT.(,C) RETUR
0254                DO 6 K=1,N
0255              6    X(2,R)=X(1,R)/FLTN
0256                RETURN
0257                END

END OF SEGMENT, LENGTH   2[1, NAME  FASTFT1
```

APPENDIX 2.

DIGITAL COMPUTATION OF WAVE SPECTRUM

A2.1 Data Sampling

The theoretical relationships described in Section 2 may be analysed using either digital or analogue methods. This section deals only with digital analysis since a large digital computing facility was available to process any wave records.

Wave records are generally represented by the measuring instrument as an analogue voltage. The method of recording this voltage determines to a large extent the ease with which it may be digitally analysed. Typical methods are chart recordings, magnetic tape recordings and punched paper tape. Each has disadvantages, for example, the punched tape, although readily digitised may be in the wrong code or the parity may be different from that of the computer used, thus requiring specialised interface equipment. Magnetic tape recordings of the voltage require digitisation before being presented to the computer, but this is generally no problem with the ready availability of high speed data loggers. Chart records are very tedious to digitise and cannot really be considered as realistic if large scale recordings are contemplated.

The matter of digitisation brings its own problems relating to the interval of digitisation and the number of digitisation levels. Obviously it is uneconomic to digitise at too great a rate since it increases both capital costs of analogue-to-digital converters and computing time without necessarily gaining any more information.

If samples are taken too far apart then the phenomenom of aliasing takes place. For example, if the time interval between samples is Δt then the highest frequency permissible in the time history is $1/2\Delta t$ since any higher frequencies will be confused with the corresponding low frequency. The cut-off frequency $1/2\Delta t$ is known as the Nyquist or folding frequency and is illustrated by considering the sine wave in Fig. A2.1. However, although this is often taken as the only criterion for selecting the interval of digitisation a further factor should be considered if wave heights are to be computed. If the time series has significant components with frequencies near f_c then any wave in this region may only be defined by two or three sample points and the risk of considerable error in wave height measurement is great. Consider Fig. A2.1 where a sine wave of frequency f and amplitude a is subjected to a sampling interval of Δt . Should a sample be taken at point 1 then no error in the amplitude results. For a sample taken at point 2, $\frac{\Delta t}{2}$ secs. after point 1 then the error is $a(1 - \cos \pi f \Delta t)$. If the sample point is assumed to be uniformly distributed between positions 1 and 2 in the amplitude domain then the mean error will be half the maximum. The error in the wave height measurement depends on the relationship between f and Δt since the nearest sample point to the minimum determines the amplitude. This had been determined empirically using a digital computer and relevant values of frequency and sampling rate have been used to calculate the maximum errors in wave amplitude and height estimation shown in Fig. A2.2. Thus, the sampling rate is governed not only by the Nyquist criterion

but by the accuracy with which the component wave heights are to be determined.

Bendat and Piersol (1966) show that the errors due to quantisation are unimportant if the signals are quantised at 256 levels or more, which is feasible with just about any analogue-to-digital converter.

Having a suitably digitised record it remains to calculate the spectral and statistical characteristics. The power spectral density function may be calculated by two methods, via the autocorrelation function or via the complex Fourier series. Both methods are important, although the latter is used mostly, the former illustrates several important effects inherent in the digital approach. By using a finite record of length T_R the true power spectrum cannot be computed since this would require an infinitely long record to evaluate the integral equations exactly. Thus, the computed spectrum $\hat{S}(f)$ is referred to as an estimate of the true spectrum $S(f)$, although in practice the distinction becomes somewhat blurred.

A2.2 Digital Estimation of the Power Spectral Density Function via the Autocorrelation Function.

It is usual to compute the spectral density function by means of a Fourier transform making use of the relationships expressed by Equations 2.1 and 2.6.

By using a finite record of length T_R secs. the true power spectrum cannot be computed, since this would require an infinitely long record

to evaluate Equation 2.6 exactly. The computed spectrum $\hat{S}(f)$ is an estimate of the true spectrum $S(f)$ and, in general, the longer the record the nearer is the estimate to the true value.

The autocorrelation function is also an approximation since the maximum lag time is restricted to a finite length of time and cannot practically be allowed to approach infinity as required by Equation 2.6. The autocorrelation function is estimated by

$$\hat{R}(\tau) = \frac{1}{N-r} \sum_{i=1}^{n-r} x_i \, x_{i+r} \qquad r = 0, 1, 2 \ldots . m \qquad \text{(A2.1)}$$

where n is the number of samples separated by $\Delta t = h$ seconds and m is the number of lags. Using the trapezoidal rule to compute a 'raw' estimate of the spectral density $\tilde{S}(f)$ at m distinct values of f thus:

$$\tilde{S}(f) = \tilde{S}(k, \Delta t) = 4\left[\hat{R}(0)\frac{\Delta t}{2} + \Delta t \sum_{r=1}^{m-1} \hat{R}(r\Delta t)\cos(2\pi f r \Delta t) + \frac{\Delta t}{2}\hat{R}(m\Delta t)\cos(2\pi f m \Delta t)\right] \qquad \text{(A2.2)}$$

$$k = 0, 1, 2 \ldots \ldots . m$$

Associated with these two calculations is the choice of the number of lags, m . Since the highest frequency to be computed is the Nyquist Frequency:

$$f_c = \frac{1}{2\Delta t} = k_{max} \Delta f \qquad \text{(A2.3)}$$

The equivalent resolution band width of the spectral density estimate is defined as:

$$B_e = \frac{1}{m \Delta t} \qquad \text{(A2.4)}$$

and may be regarded as a window or filter through which a frequency band may be observed. Consequently, the sampling interval Δt is constrained by both the required band widths and the maximum frequency encountered.

$$\frac{1}{2f_c} \geq \Delta t \geq \frac{1}{m B_e} \qquad \text{(A2.5)}$$

It is usual to compute up to m values of $S(f)$ at $\Delta f = \frac{1}{2m\Delta t}$ This will provide $\frac{m}{2}$ independent spectral estimates since estimates at points less than $\frac{2f_c}{m}$ will be correlated.

The spectral density function described by Equation A2.2 is called a 'raw' estimate because Equations 2.1 and 2.6 are only approximated in the calculations. For a continuous record of finite length the observation time may obviously not approach infinity, neither is it possible to estimate the autocorrelation function for arbitrary long lags. Usually the maximum length of lag is approximately 5 or 10 per cent of the length of the record.

The estimated autocorrelation function may be written as:

$$\hat{R}(\tau) = \lambda(\tau)\,\psi(\tau) \qquad \text{(A2.6)}$$

where

$$\psi(\tau) = \frac{1}{n-r} \sum_{i=1}^{n-r} x_i\, x_{i+r} \qquad \text{(A2.7)}$$

$\lambda(\tau)$ is referred to as the lag window and has values such that:

$$\lambda(\tau) = 1 \quad , \quad |\tau| < T_m$$
$$\lambda(\tau) = 0 \quad , \quad |\tau| > T_m \qquad \text{(A2.8)}$$

This particular lag window is known as the rectangular lag window.

Special lag windows have been designed to produce a 'better' estimate of the power spectral density function.

The Fourier transform of the lag window is the spectral window and is related to the spectral density function thus:

$$\tilde{S}(f) = W(f) * \Phi(f) \qquad \text{(A2.9)}$$

where $\Phi(f)$ is the Fourier transform of $\varphi(t)$, $W(f)$ is the spectral window and the asterisk denotes convaluation. The average value of the apparent autocorrelation function $\varphi(\tau)$ is the true autocorrelation function for $|\tau| < T_m$. Thus:

$$\text{ave}\{\hat{R}(\tau)\} = \lambda(\tau) \cdot R(\tau) \qquad \text{(A2.10)}$$

It follows that:

$$\text{ave}\{\hat{S}(f)\} = W(f) * S(f) \qquad \text{(A2.11)}$$

where $S(f)$ is the true power spectrum. This may be written explicitly as:

$$\text{ave}\left\{\hat{S}(f_1)\right\} = \int_{-\infty}^{\infty} W(f - f_1)\, S(f)\, df \qquad \text{(A2.12)}$$

This relation exhibits the average value of $S(f_1)$ as a smoothing of the true power spectrum over frequencies near f_1 with weights proportioned to $W(f - f_1)$. The name 'spectral window' arises because this may be interpreted as a collected impression of the true power spectrum $S(f)$ obtained through a window of variable transmission.

The problem of improving the raw estimate of power spectral density function obtained in Equation A2.2 may be tackled in two ways. A special lag window may be designed and applied in the time domain. The resulting Fourier transform will yield an estimate of $S(f)$ similar to that in Equation A2.12.

A typical smoothing procedure is that due to Julius van Hann and is generally known as Hanning smoothing. The smoothed estimates are given by:

$$\begin{aligned} \hat{S}_0 &= 0.5\,\tilde{S}_0 + 0.5\,\tilde{S}_1 \\ \hat{S}_k &= 0.25\,\tilde{S}_{k-1} + 0.5\,\tilde{S}_k + 0.25\,\tilde{S}_{k+1} \\ \hat{S}_m &= 0.5\,\tilde{S}_{m-1} + 0.5\,\tilde{S}_m \end{aligned} \qquad \text{(A2.13)}$$

The corresponding lag window is:

$$\begin{aligned} \lambda(\tau) &= \tfrac{1}{2}\left(1 + \cos\left(\frac{\pi\tau}{T_m}\right)\right), \quad |\tau| \le T_m \\ &= 0, \quad |\tau| > T_m \end{aligned} \qquad \text{(A2.14)}$$

A number of window pairs have been used to improve the final smoothed values of the spectral density function. Some of the more common

ones are listed below:

1. The Rectangular Window.

This yields the 'unsmoothed' or 'raw' estimate and is described thus:

$$\lambda_0(\tau) = 1 \quad , \quad |\tau| \leq T_m$$
$$= 0 \quad , \quad |\tau| > T_m$$
$$W_0(f) = 2T_m \left(\frac{\sin 2\pi f T_m}{2\pi f T_m} \right) \qquad \text{(A2.15)}$$

2. The Bartlett Window.

$$\lambda_1(\tau) = \left(1 - \frac{|\tau|}{T_m}\right) \quad , \quad |\tau| \leq T_m$$
$$= 0 \quad , \quad |\tau| > T_m \qquad \text{(A2.16)}$$
$$W_1(f) = T_m \left(\frac{\sin \pi f T_m}{\pi f T_m} \right)^2$$

3. The Hanning Window (or Tukey Window).

$$\lambda_2(\tau) = \frac{1}{2}\left(1 + \cos \frac{\pi \tau}{T_m}\right), \quad |\tau| \leq T_m$$
$$= 0 \quad , |\tau| > T_m \qquad \text{(A2.17)}$$
$$W_2(f) = \frac{1}{2} W_0(f) + \frac{1}{4}\left[W_0\left(f + \frac{1}{2T_m}\right) + W_0\left(f - \frac{1}{2T_m}\right)\right]$$

4. The Hamming Window.

$$\lambda_3(\tau) = 0.54 + 0.46 \frac{\pi \tau}{T_m} \quad , |\tau| \leq T_m$$
$$= 0 \quad , |\tau| > T_m \qquad \text{(A2.18)}$$
$$W_3(f) = 0.54\, W_0(f) + 0.23\left[W_0\left(f + \frac{1}{2T_m}\right) + W_0\left(f - \frac{1}{2T_m}\right)\right]$$

5. The Parzen Window is also well-known and is expressed as:

$$\lambda_4(\tau) = 1 - 6\left(\frac{\tau}{T_m}\right)^2 + 6\left(\frac{\tau}{T_m}\right)^3 , |\tau| \leq T_m$$
$$= 0 \quad , |\tau| > T_m \qquad \text{(A2.19)}$$
$$W_4(f) = \frac{3T_m}{4}\left[\frac{\sin(\pi f T_m/2)}{\pi f T_m/2}\right]$$

The various shapes of the windows are illustrated in Figs. A2.3 (a) and (b). The use of a particular window is largely a matter of personal preference and suitability to the spectrum being examined.

However, an ideal spectral window may be defined as being a rectangle in the frequency domain. This would give an unbiased estimate of the spectral density function for the band-width considered. Unfortunately, this situation is not physically realisable since the corresponding lag window is finite for $\tau > T_m$

Since the digitisation process takes a finite number of samples at a finite sampling interval, the final estimate of the spectrum will be subject to a statistical error.

The so-called 'confidence limits' are the values between which a given ordinate will be found for, say, 80 per cent of the time. These values are investigated through the chi-squared distribution.

It may be shown that if the random variables $x_1, x_2, \ldots\ldots x_k$ are independently distributed with zero mean and unit variance, then the sum of the squares $x_1^2 + x_2^2 + \ldots\ldots + x_k^2$ is by definition a chi-square distribution with k degrees of freedom.

Blackman and Tukey (1958) showed that repeated sampling of the process for the purpose of estimating the spectral density function is subject to the chi-square distribution of variance. The measure of variability of the estimated value of $S(f)$ is given by the number of degrees of freedom k . For a sampling procedure described previously this is given by:

$$k = 2 B_e T_R \qquad \text{(A2.20)}$$

A graphical representation of the confidence limits and degrees of freedom is given in Fig. A2.4. The correct interpretation of

these limits is given by Colonell (1966). In order to be 80 per cent certain that the true $S(f)$ value is within + 30 per cent and - 27 per cent of the estimate, then 40 degrees of freedom are required.

The mean square error is also defined as $\varepsilon = E[(\hat{S}(f) - S(f))^2]$ and is approximated by $1/B_e T_R$. It is also used when dealing with accuracy.

A2.3 Power Spectral Density Function via the Fast Fourier Transform.

The Fast Fourier Transform (FFT) provides a method of computing the discrete equivalent of Equations 1 and 2, usually known as the Discrete Fourier Transform (DFT) and the Inverse Discrete Fourier Transform (IDFT). The estimation of the power spectral density function makes use of the relationship in Equation 2.5. The time history is simply fast Fourier transformed, squared and time averaged.

The discrete versions of the Fourier relationships are:

$$X(n) = \Delta t \sum_{k=0}^{N-1} x(k) \exp(-j 2\pi n k/N)$$

$$x(k) = \Delta f \sum_{n=0}^{N-1} X(n) \exp(j 2\pi n k/N) \qquad \text{(A2.21)}$$

where $t_k = k\Delta t$ $\qquad \Delta t = T_R/N$

$f_n = n\Delta f$ $\qquad \Delta f = 1/T_R$

Consider the time series $x(t)$ sampled at intervals Δt to produce the N -point series $x(k)$. The sampling function may be represented by $b(t)$ (as shown in Fig. A2.5) and is, in fact, a series of Dirac functions Δt apart $\delta(t - k\Delta t)$.

The Fourier transform $B(f)$ of the sampling function may be shown to

be (see Papoulis (1962) page 44) a similar pulse train $\delta(f - n\Delta f)$ The sampling of $x(t)$ may be thought of as the multiplication of $x(t)$ by $b(t)$ in the time domain. Since, by the convolution theorum, multiplication in the time domain is equivalent to convolution in the frequency domain, the Fourier transform of $x(t)$ is repeated at intervals $1/\Delta T$. The discrete Fourier transform computes $X(f)$ at frequencies corresponding to zero to $1/\Delta T$. Thus, for a real time series the DFT will be the mirror image pair shown in Fig. A2.5.

The computation of the DFT by the fast Fourier transform method makes use of the cyclic nature of the exponential term. Instead of arranging the list of digitised data in one list it is possible to arrange the numbers in rows. The transform is then performed on the columns. Take, for example, the case of 2 columns and N/2 rows.

1st column $y(k) = x(2k)$

2nd column $z(k) = x(2k+1)$ $\quad k = 0, 1, 2 \ldots\ldots N/2 - 1$

The Fourier transforms of the two rows are given by:

$$Y(n) = \frac{2}{N} \sum_{k=0}^{N/2-1} y(k) \exp(-j4\pi nk/N)$$

$$Z(n) = \frac{2}{N} \sum_{k=0}^{N/2-1} z(k) \exp(-j4\pi nk/N) \qquad \text{(A2.22)}$$

The required transform is given by:

$$X(n) = \frac{2}{N} \sum_{k=0}^{N/2-1} \left[y(k) \exp(-j\pi nk/N) + z(k) \exp(-j2\pi n(2k+1)/N) \right] \qquad \text{(A2.23)}$$

$n = 0, 1, 2 \ldots\ldots N-1$

This may be written as:

$$X(n) = Y(n) + \exp(-j2\pi n/N) Z(n) \qquad \text{(A2.24)}$$

$0 \leq n \leq \frac{N}{2}$

For values of n greater than $N/2$ the DFT of $Y(k)$ and $Z(k)$ repeat periodically. Thus, substituting $n + N/2$ for n

$$X\left(n + \tfrac{N}{2}\right) = Y(n) + \exp\left(-j2\pi\left(n+\tfrac{N}{2}\right)/N\right)Z(n) \qquad n=0,1,\ldots,N/2-1 \qquad \text{(A2.25)}$$

$$= Y(n) - \exp(-j2\pi n/N)Z(n)$$

So, for the full transform:

$$X(n) = Y(n) + W^n Z(n)$$

$$X\left(n+\tfrac{N}{2}\right) = Y(n) - W^n Z(n) \qquad n=0,1,\ldots,N/2-1 \qquad \text{(A2.26)}$$

where $W^n = \exp(-j2\pi n/N)$

Thus, all N terms of the DFT of $x(k)$ may be obtained from the DFT's of $y(k)$ and $z(k)$, both sequences of $N/2$ samples. The transforms of $y(k)$ and $z(k)$ may be reduced to DFT's of sequences of $N/4$ samples, and so on, as long as each function has a number of samples which is divisible by 2. Thus, it is usual to make N equal to 2^n The result of this is that finally a number of transforms of a single point are required which is, of course, the sample itself. So the FFT of 2^n samples is reduced to a series of multiplication and additions. A similar factorisation is suitable for numbers which are not powers of 2 and will differ in that the transform of single points would be replaced by a transform of a number of points.

The actual computation of the FFT is a matter of computational convenience. Standard routines are available which generally fall into two categories. Those which compute the coefficients of the transform 'in place' at each stage which results in the final coefficients not being in the appropriate place but are, in fact, in

what is known as 'bit reversed' order. This method requires less storage. Alternatively, the method which sorts as it computes may be used, the disadvantage being that additional storage is required. However, it is simpler than the previous method. The differences may be illustrated by so-called treegraphs.

The advantage of the FFT may be seen by noting that to compute the DFT requires N^2 multiplications, whereas the FFT requires of the order of $N \log_2 N$ operations. Thus, for $N=2^{10}$ the FFT is of the order of 100 times faster.

Having computed $X(n)$ by the FFT the estimate of the power spectral density function is given by:

$$S(n) = \frac{2}{N\Delta t} |X(n)|^2 \qquad \text{(A2.27)}$$

However, once again the restriction imposed by only considering a record of finite length must be considered. Defining the data window $u(t)$ as:

$$u(\tau) = 0 \quad , |\tau| > T_R/2$$

$$u(\tau) = 0 \quad , |\tau| < T_R/2 \qquad \text{(A2.28)}$$

Again, by the convolution theorum, the estimated spectrum is a convolution of the spectral window (derived from the data window) and the actual spectrum. For the box-car function the spectral window is:

$$U(f) = T_R \left(\frac{\sin \pi f T_R}{\pi f T_R} \right) \qquad \text{(A2.29)}$$

To reduce the leakage due to the side lobes on this window other windows may be used. A common method is to cosine taper the one-tenth of each end of the record, resulting in a spectral window as shown in Fig. A2.6. Although this reduces the leakage, it also reduces the variance by a factor of 0.875 which must be corrected for after computing the spectrum.

Frequently the number of data points are not an exact power of 2. In this case, zeros may be added to supplement the record, although care should be taken as undesirable side lobes may occur.

Since the band-width B_e is equal to $1/T_R$ for the estimates computed as above, these estimates are governed by a χ^2 distribution with 2 degrees of freedom for each estimate. To improve this statistical accuracy, two methods are appropriate. Firstly, by averaging over adjacent estimates (reducing the resolution at the same time) the number of degrees of freedom is given by $2l$ where l is the number of estimates which are averaged. Alternatively, several data segments may be used to compute sets of estimates at the same frequency and these periodograms averaged to produce the final estimate which has $2q$ degrees of freedom where q is the number of segments which were averaged.

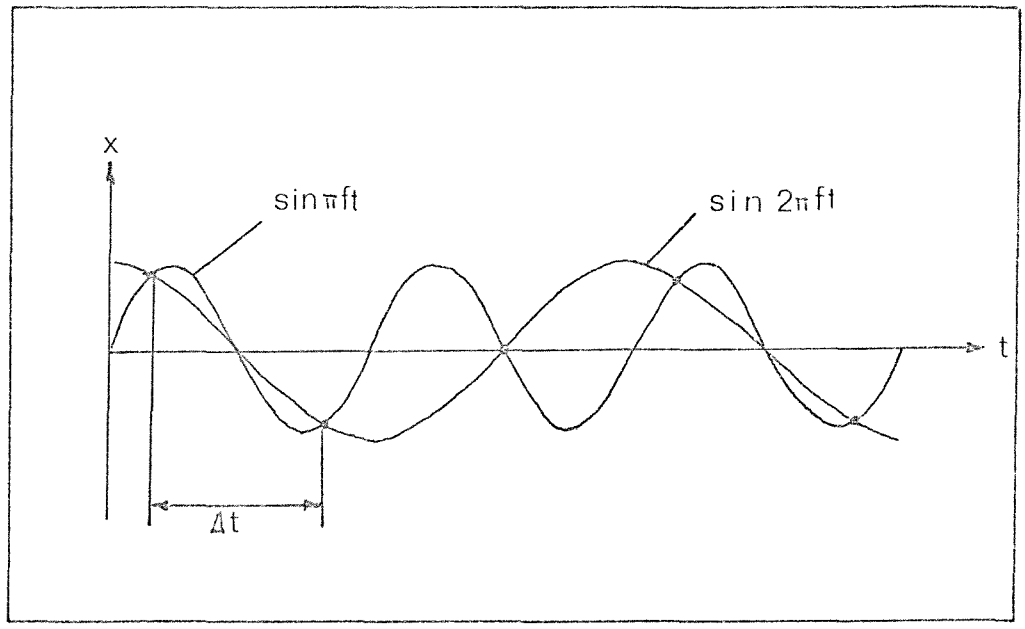

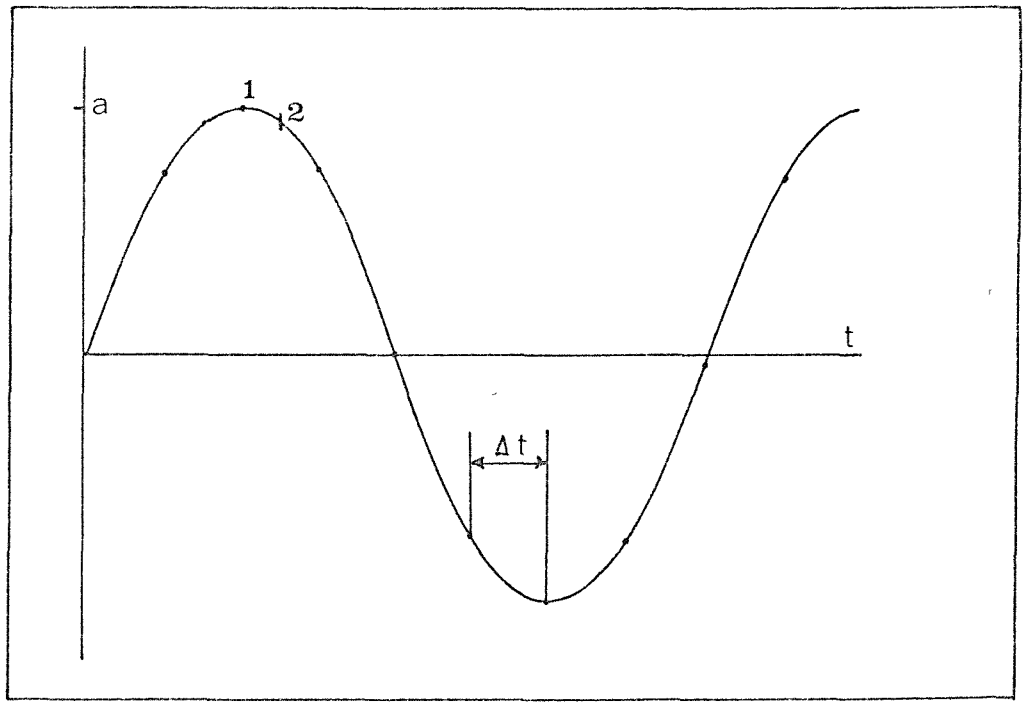

FIG. A2.1 Aliasing (upper) and Sampling (lower) of a Sine Wave

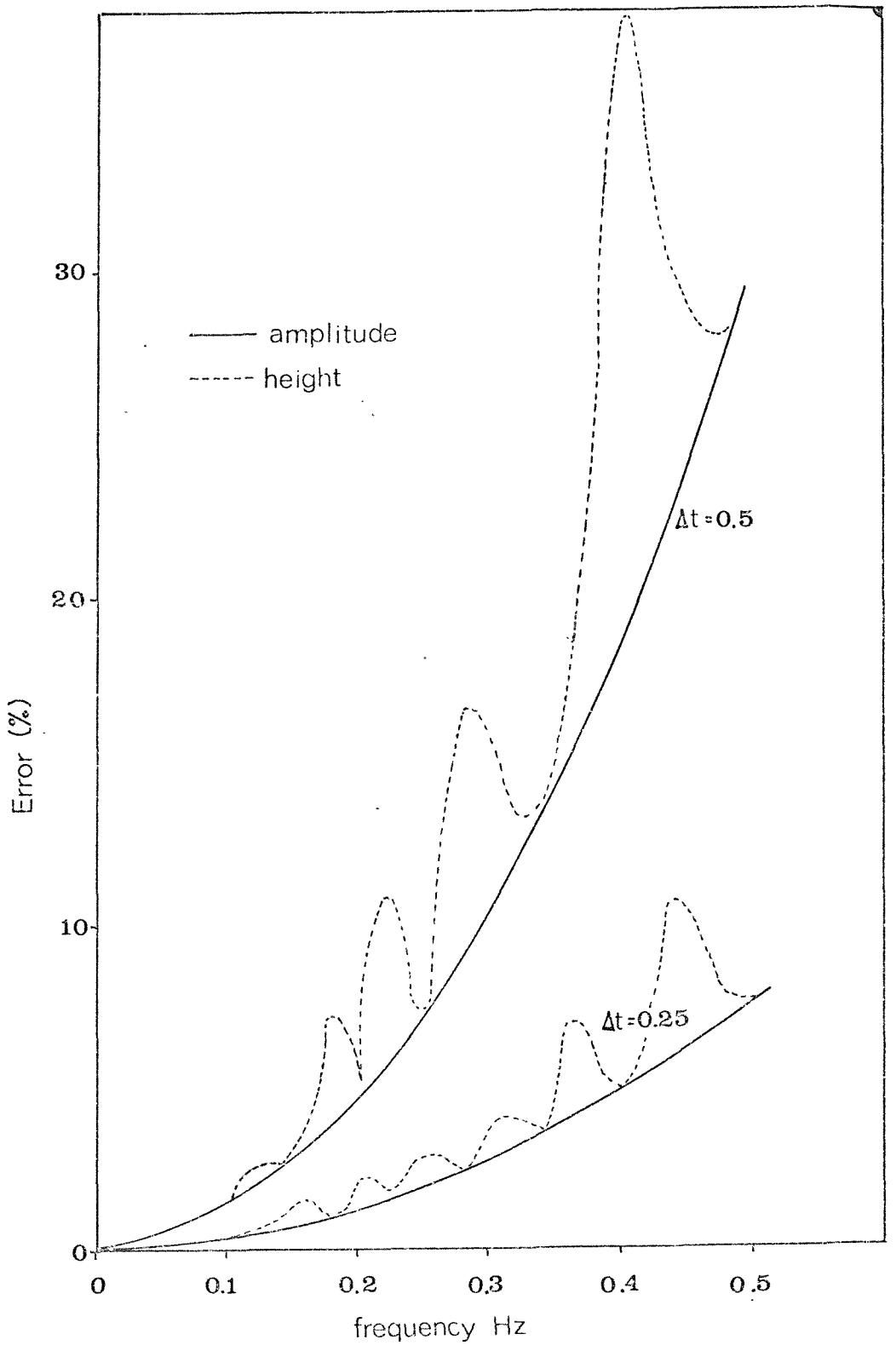

FIG. A2.2 Errors in Wave Height and Amplitude due to Sampling Process

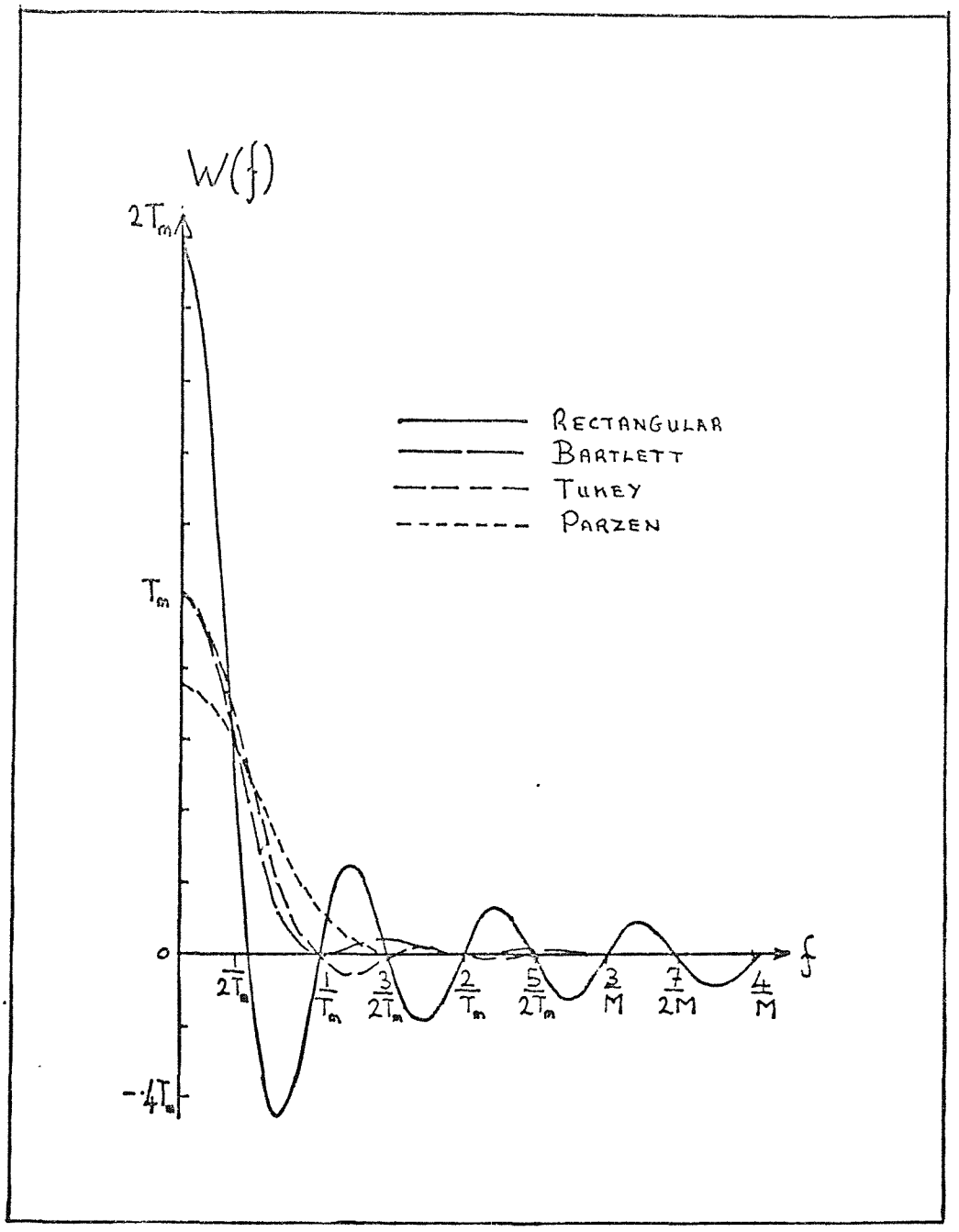

FIG. A2.3a Common Spectral Windows

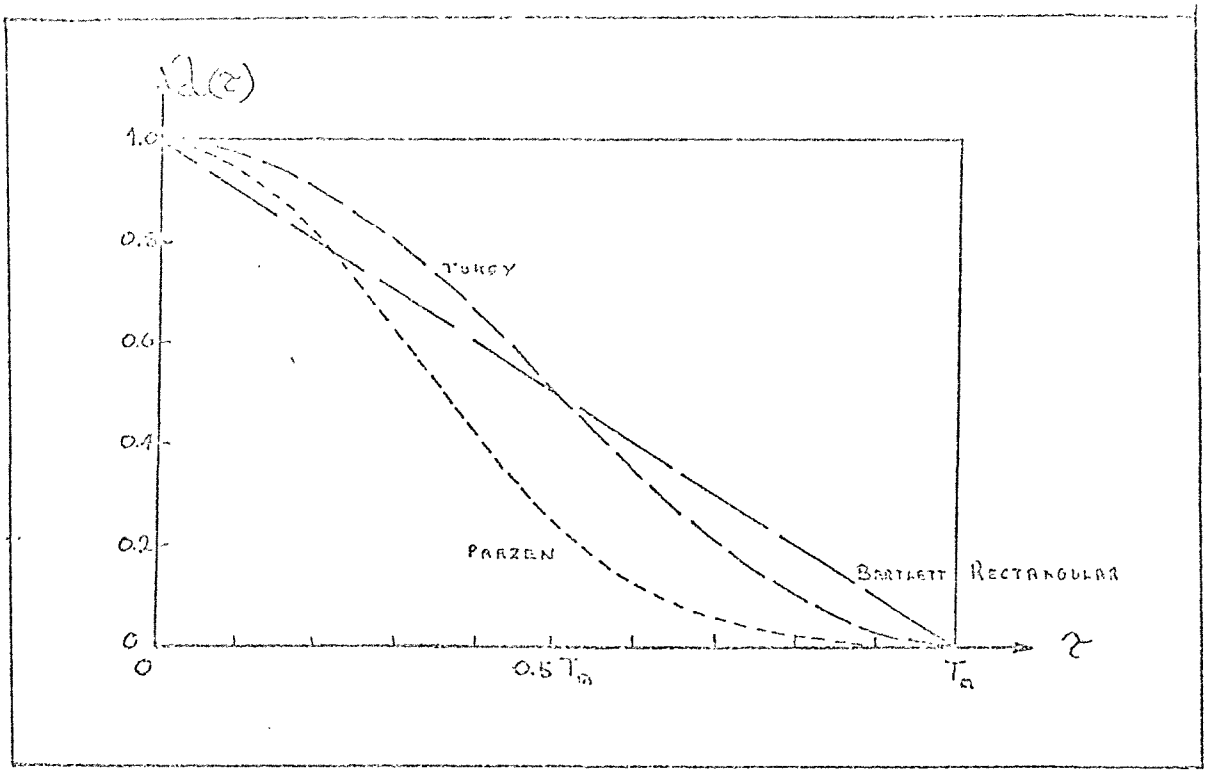

FIG. A2.3b Some Typical Lag Windows

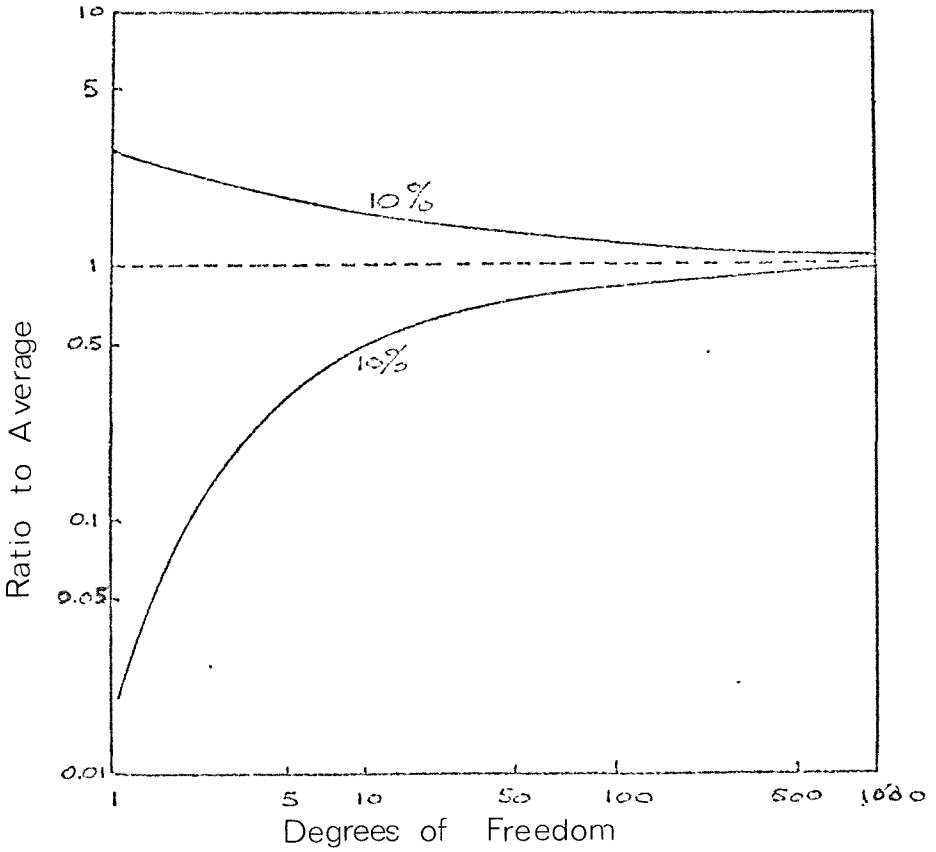

FIG. A2.4 Confidence Interval for Spectral Estimates

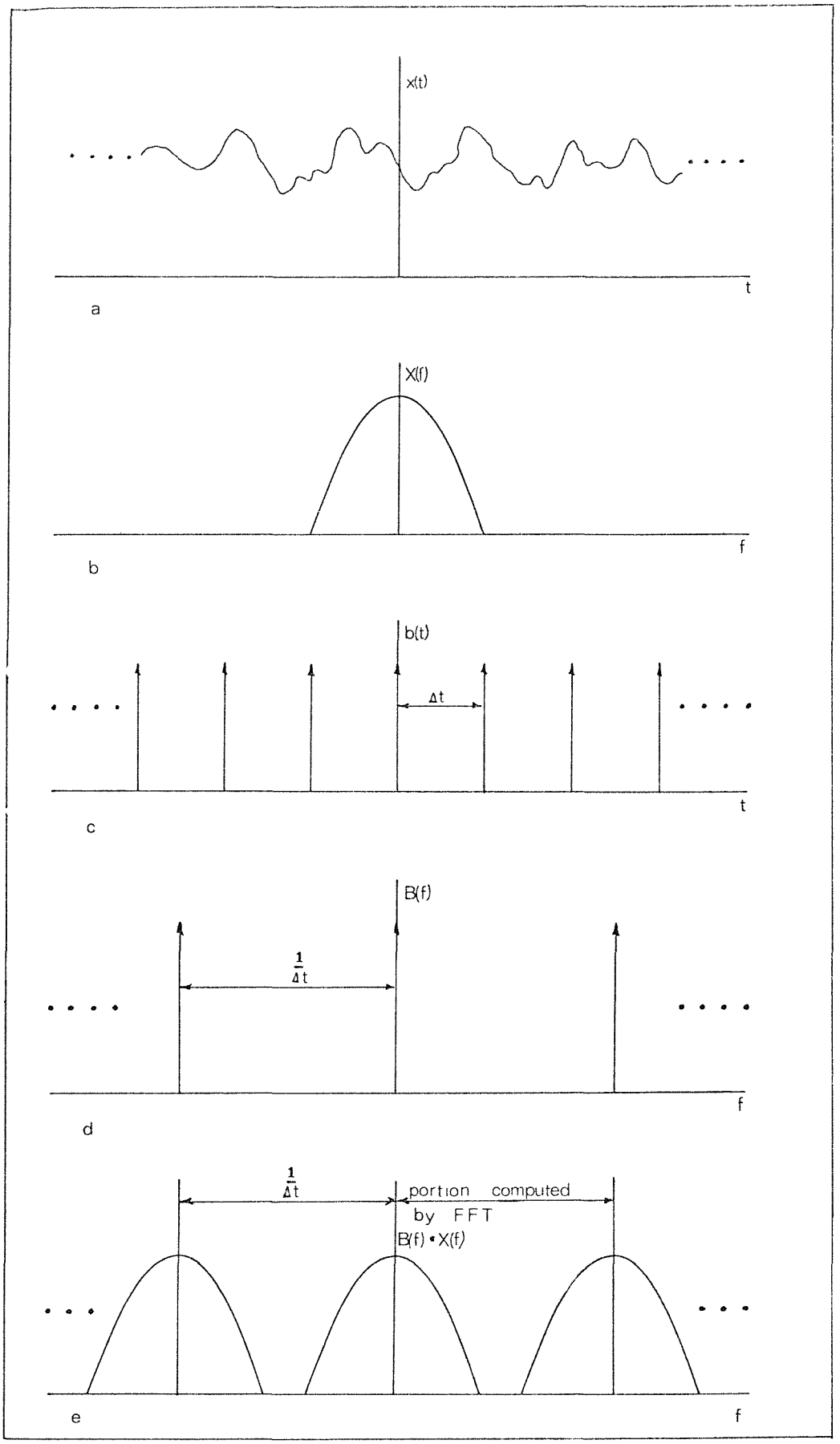

FIG. A2.5 The Fourier Sampling Process

APPENDIX 3.

NOTATION

$A^2(f)$ - Fourier energy spectrum

BCD - binary coded decimal

$B(f)$ - Fourier transform of $l(t)$

$B(s)$ - feedback signal

B_e - equivalent resolution bandwidth

$C(s)$ - controlled variable

$C_{xy}(f)$ - co-spectral density function

D_{rms} - root mean square of the water surface elevation

DAC - digital-to-analogue converter

$E(s)$ - actuating signal

FFT - fast Fourier transform

$G(f)$ - two-sided spectral density function

$G(s)$ - forward transfer function

$H(s)$ - feed-back transfer function

H - wave height defined by zero crossing method

H^* - wave height defined by peak-to-trough method as the average difference in elevation between a trough and two adjacent peaks

$\hat{H}$ - wave height defined by peak-to-trough method as the difference in elevation of a peak and the preceding trough

$H_{1/10}$ - average height of the highest tenth waves

H_s - significant wave height

H_{rms} - root mean square wave height

H_{mean} - mean wave height

H_{max} - maximum wave height

H_{mode} - most probable wave height

$H(f)$ - frequency response function

IFFT - inverse Fourier transform

K - overall system gain

L - wave length

LSB - least significant bit

MSB - most significant bit

N - number of sample points in a time series

N_c - number of crests in a record

N_z - number of zero upcrossings in a record

PSD - power spectral density

$P(x)$ - cumulative probability distribution function

Q_p - peakedness

$Q_{xy}(f)$ - quad spectral density function

$R(s)$ - reference input

$R(\tau)$ - autocorrelation function

$\hat{R}(\tau)$ - estimate of $R(\tau)$

$R_{xy}(\tau)$ - cross correlation function

$S(f)$ - power spectral density function

$\hat{S}(f)$ - estimate of $S(f)$

$\tilde{S}(f)$ - raw power spectral density function

$S_{xy}(f)$ - cross spectral density function

T - wave period

$\tilde{T}$ - apparent wave period

T_m - maximum lag time

T_z - zero crossing period

$U(f)$ - Fourier transform of $u(\tau)$

$W(f)$ - spectral window

$X(f)$ - Fourier transform of $x(t)$

$X(n)$ - discrete Fourier transform of $x(k)$

$b(t)$ - sampling function

d - water depth

f - frequency in

f_c - Nyquist or cut-off frequency

g - acceleration due to gravity

m - number of lags

m_n - n^{th} spectral moment

$p(x)$ - probability density of $x(t)$

$q(x)$ - cumulative probability distribution of $x(t)$

s - Laplace transform variable

t - time

$u(\tau)$ - data window

$x(t)$ - time dependent variable

$x(k)$ - sampled time series $x(t)$

x - normalised water surface elevation ℓ/σ

$\Phi(f)$ - Fourier transform of $\psi(\tau)$

β_1 - skewness

β_2 - kurtosis

ε - spectral width parameter

η - water surface elevation

η_{max} - maxima of water surface elevation

$\lambda(\tau)$ - lag window

μ_n - n^{th} moment about the origin of the probability distribution

μ_n' - n^{th} central moment of the probability distribution

σ^2 - variance

τ - time lag

ψ - mean lagged product

$\gamma_{xy}(f)$ - coherence function